Green Synthesis and Characterization of Alloy Nanoparticles Using Plant Extracts

By

Naledi Seatle (215242017)

This thesis is submitted in fulfilment of the requirements of the degree
Master of Applied Science: Chemistry
in the Faculty of Applied Science
at the Cape Peninsula University of Technology
Bellville Campus

Supervisor: Prof Ahmed Mohammed

Submitted in November 2023

Declaration of Authenticity

I, **NALEDI DORKUS SEATLE**, declare that the contents of this dissertation/thesis represent my own unaided work, and that the dissertation/thesis has not previously been submitted for academic examination towards any qualification. Furthermore, it represents my own opinions and not necessarily those of the Cape Peninsula University of Technology.

Signed **Date** **17 November 2023**

Abstract

Medicinal plant-mediated synthesis represents an environmentally friendly approach that is currently gaining increased attention due to its potential as an alternative to conventional toxic reducing agents, such as sodium borohydride and hydrazine, commonly employed in chemical and physical methods. Medicinal plants, rich in diverse bioactive phytochemicals, are especially intriguing for their potential role in bioreduction and stabilization of phytogenic nanoparticles with remarkable therapeutic properties. This pioneering study introduces the efficient synthesis of novel Au-Pd bimetallic nanoparticles alongside monometallic gold (Au) and palladium nanoparticles (PdNPs). The synthesis process utilizes *Aspalathus linearis* (Burm.f.) R. Dahlgren, commonly known as green rooibos, as well as its pure bioactive compound, Aspalathin (*C*-glucosyl dihydrochalcone). The biomolecules within the plant extract serve as both reducing and capping agents, facilitating the reduction of Au and Pd metals and resulting in the formation of distinct AuNPs, PdNPs, and Au-Pd bimetallic nanoparticles. Comprehensive characterization of the synthesized nanomaterials was conducted through Ultraviolet-Visible (UV-Vis) Spectroscopy, Dynamic Light Scattering (DLS) Analysis, High-Resolution Transmission Electron Microscopy (HRTEM), Selected Area Electron Diffraction (SAED), Scanning-Transmission Electron Microscopy-High Angle Annular Dark Field (STEM-HAADF) and Attenuated Total Reflection-Fourier-Transform Infrared Spectroscopy (ATR-FTIR). The initiation of Au nanoparticle formation was visually evident through a noticeable colour change in the solution from pale yellow to deep purple, further confirmed by UV-Vis spectroscopy. The UV-Vis spectra exhibited Surface Plasmon Resonance (SPR) peaks between 530 nm and 540 nm for AuNPs, while no SPR band was observed for PdNPs due to the absence of free electrons in the outer shell. However, a blue shift in the SPR peak of Au-Pd bimetallic nanoparticles was observed compared to that of AuNPs. DLS analysis revealed a hydrodynamic size range of 42 nm to 80 nm for the synthesized nanoparticles, with Zeta Potential ranging between -18.2 to -31.6 mV, indicating minimal to moderately stable nanoparticles. HRTEM coupled with SAED was employed to assess particle size, morphology, and crystallinity, revealing mostly spherical nanoparticles with occasional triangular shapes of varying sizes. STEM-HAADF mapping elucidated the structural configuration of the Au-Pd bimetallic nanoparticles. Cytotoxicity testing on cell lines, coupled with cellular uptake analysis, demonstrated that none of the tested samples exhibited significant cytotoxic effects; instead, they showcased cell proliferation against the selected cell lines. This green synthesis approach proves to be convenient and simple, with potential applications extending to the synthesis of various nanomaterials, promising new advancements in technological and biomedical fields.

Keywords: *Aspalathus linearis*; green synthesis; gold nanoparticles; palladium; bimetallic nanoparticles

Acknowledgements

I would like to express my heartfelt gratitude to a circle of incredible individuals who played a pivotal role in my thesis journey:

To my HEAVENLY FATHER, to whom the honour is due, and a firm foundation from whom I have drawn strength to finish this research work; thank you.

To my PARENTS, **Nthabiseng and Moeketsi Seatle** for their unwavering love, support, prayers, and belief in me throughout this challenging endeavour. Your encouragement and faith have been my driving force.

To my SISTER, **Thato Seatle** for being my confidant and a source of motivation. Your presence made this journey more meaningful.

To my dedicated SUPERVISOR, **Professor Ahmed Mohammed**, your guidance, and expertise have been instrumental in shaping my research. Thank you for the role you played which extended far beyond your title. Your mentorship has been invaluable.

To my MENTOR, **Professor Subelia Botha**, thank you for laying the foundation of research and for inspiring me to further my knowledge in the field nanoscience. Your wisdom, insights, prayers, and encouragement have been the guiding light of my research. Your belief in my potential pushed me to excel beyond limits.

Special thanks go out to **Dr Enas Ismail** for her thoughtful assistance in the lab, **Dr Abdulrahman Elbagory** for his brilliant insight, **Dr Rajan Sharma** for his generosity, **Dr Akeem O. Akinfenwa**, whose participation helped to bring this study to light, to **Eloge Wakwanyembo Lwamba**, **Bleck Romario Tanefo Tchiogoua, Kadidiatou Ndjoubi Ossamy**, **Ali Eltahir**, **Dr Masande Yalo** and **Dr Masixole Makhaba** your interaction at the lab and support is greatly appreciated.

To **Dr Jonas Sagbo**, I extend my gratitude for your exceptional assistance and contributions to the biological studies. Your invaluable insights have significantly enhanced my understanding of biochemistry.

I would like to express my sincere gratitude to **Mr. Ndumiso Mshicileli** from the Agrifood Technology Station (ATS), Food Technology Department and **Mr. Fanie Rautenbach** as well as **Oiva Viety Kamati** from the Oxidative Stress Unit (Health and Wellness Department) for providing the facility for freeze-drying plant extracts at the Cape Peninsula University of Technology.

To **Dr Nasheeta Hanief** at the University of Cape Town (UCT), Electron Microscope Unit (EMU), I extend my sincere gratitude for your invaluable support in the electron microscopy analysis. Your generous efforts in training me on STEM-HAADF analysis and processing have been truly enlightening, and I am grateful for the knowledge and skills you have shared.

To the exceptional LABORATORY STAFF, **Zandile Mthembu**, **and Gillian Fennessy-Yon**, thank you for your assistance, patience, and expertise in helping me navigate the intricacies of my experiments. Your support was indispensable.

To my close-knit circle, I express heartfelt appreciation for your unwavering support and prayers throughout this journey. Your encouragement has meant a great deal to me.

Each of you has left an indelible mark on my academic journey, and I am profoundly grateful for your contributions. This achievement is as much yours as it is mine.

The financial assistance of the CPUT Postgraduate Scholarship towards this research is acknowledged. Opinions expressed in this thesis and the conclusions arrived at, are those of the author, and are not necessarily to be attributed to the CPUT Postgraduate Scholarship.

Dedication

This thesis is dedicated to my loving and caring family.

Glossary

Ac	Acetone
ASP	Aspalathin
ATIR	Attenuated Total Reflection
Au	Gold
DLS	Dynamic Light Scattering
DMEM	Dulbecco's Modified Eagles Medium
DMSO	Dimethylsulfoxide
EDS	Energy Dispersive Spectroscopy
EDX	Energy Dispersive X-ray Spectroscopy
EtOAc	Ethyl acetate
FBS	Fatal Bovine Serum
FTIR	Fourier-Transform Infrared Spectroscopy
GR	Green Rooibos
HRTEM	High-Resolution Transmission Electron Microscopy
ICP-OES	Inductively Coupled Plasma-Optical Emission Spectroscopy
MeOH	Methanol
MTT Assay	3-(4, 5-dimethylthiazol-2-yl)-2, 5-diphenyltetrazolium bromide
NPs	Nanoparticles
Pd	Palladium
SAED	Selected Area Electron Diffraction
SPR	Surface Plasmon Resonance
STEM-HAADF	Scanning- Transmission Electron Microscopy- High Angle Annular Dark
TEM	Transmission Electron Microscopy
UV-VIS:	Ultraviolet-Visible Spectroscopy
XRD	X-ray Powder Diffraction

Table of Contents

List of Figures

List of Tables

List of Appendices

Chapter 1

1.1. Introduction

Nanotechnology has become a leading-edge technology that combines academic disciplines such as physics, biology, chemistry, medicine, and material science (Shaikh et al., 2021). Amongst its wide applications, nanotechnology has been applied in various fields, which include energy storage and production (Pomerantseva et al., 2019), medicine (Adithan et al., 2009), the food industry (Sozer & Kokini, 2009), etc. In recent years, there has been a burgeoning interest among global researchers in the utilization of nanoparticles, driven by their distinctive physical, chemical, and mechanical attributes (Akbari et al., 2011; Ikhmayies, 2014). Nanoparticles are characterized by a remarkable surface area to volume ratio, endowing them with heightened reactivity, mobility, and strength (Dikshit et al., 2021). Significant strides have been taken in advancing the customization of nanoparticle size and morphology, tailoring them precisely to specific requirements (Mirzaei & Darroudi, 2017; Sajjad et al., 2018). This progress has led to their widespread application across various fields, capitalizing on their myriad and unique characteristics (Rana et al., 2020). The primary objective now is to enhance the synthesis methods for noble nanoparticles, ensuring a defined size, shape, composition, and uniform distribution. This optimization aims to influence their properties, rendering them well-suited for diverse applications in different fields (Kim et al., 2003; Wei et al., 2005; Bar et al., 2009; Sajjad et al., 2018). Furthermore, there is a growing fascination among researchers worldwide for the synthesis of bio-functional nanoparticles, creating an immersive space for exploration and innovation (Ahmad et al., 2003; Sajjad et al., 2018).

Various physical, chemical, biological, and hybrid methodologies have been employed in the synthesis of nanoparticles with specific characteristics (Mohanpuria & Rana, 2008; Tiwari et al., 2008; Liu et al., 2011; Lee et al., 2015; Sajjad et al., 2018). Typically, the process of nanoparticle formation entails the reduction of metal salt by a reducing agent, followed by the safeguarding of the freshly formed nanoparticles through a capping agent to prevent agglomeration (Kumar et al., 2021; Rana et al., 2020). The attractive forces between nanoparticles during the synthesis process contribute to the agglomeration or aggregation phenomenon. The stabilizing or capping agents utilized in nanoparticle synthesis encompass polysaccharides (such as cellulose and starch), surfactants, small ligands, polymers, dendrimers, and cyclodextrins (Javed et al., 2020). Additionally, the interaction between the capping agent and the nanoparticle surface induces steric hindrance, ensuring the stability of the resulting nanocomposite (Amina & Guo, 2020; Javed et al., 2020). It is noteworthy that certain chemicals may exhibit toxicity and could contaminate the nanoparticle surface, rendering them unsuitable for specific applications like drug discovery (Khandel et al., 2018). In contrast, plant-based polysaccharide capping agents present advantages such as biocompatibility, biodegradability, non-toxicity, and cost-effectiveness (Su & Kang, 2020; Rai et al., 2020).

Meanwhile, commonly employed solvents in nanoparticle synthesis, including hydrazine, sodium borohydride, and hydrogen, are preferred due to their hydrophobic nature and toxicity. Careful consideration of the choice of solvents is crucial to maintain the desired characteristics of the synthesized nanoparticles (Rai et al., 2020).

Several drawbacks are associated with physical and chemical techniques, such as long-term processing, high cost and toxicity (Narayanan & Sakthivel, 2010; Thakkar et al., 2010; Sajjad et al., 2018). Due to unexpected energy consumption, the use of organic solvents, the fabrication of unstable intermediates, and the formation of hazardous substances that result in environmental damage and other biological dangers result in constrained development of these techniques for bulk production (Sajjad et al., 2018).

Other than environmental contamination, a number of drawbacks emerge from these methods, including poor production rates, inadequate growth, and deformed structures of synthesised nanoparticles (Kumari et al., 2021). Over time, the use of toxic and dangerous chemicals and other biological effects have limited the use of nanomaterials in biomedicine, especially in the clinical domains (Gan et al., 2012; Sajjad et al., 2018). Striving for a new and cheaper route for nanoparticle synthesis, scientists have committed to developing a relatively new and largely undiscovered region of research based on the green synthesis of nanoparticles (Mohanpuria & Rana, 2008).

Green synthesis involves the utilization of substances derived from nature, serving as both reducing and capping agents in the chemical process (Jain & Mehata, 2017). This one-pot procedure is straightforward, environmentally benign, and organically compatible (Soltys et al., 2021). Green synthesis has thus eliminated the need for high-pressure, energy, or toxic chemicals and is an area of research that is becoming quite popular (Sajjad et al., 2018).

Earlier research has highlighted the employment of microorganisms like bacteria (Lengke et al., 2007), algae, yeast (Kowshik et al., 2002), and fungi (Rautaray et al., 2003) in the environmentally friendly synthesis of nanoparticles. More recently, various sources, including plant extracts (Ajitha et al., 2014; Ibrahim, 2015), diatoms (Scarano & Morelli, 2002), and even human cells (Anshup et al., 2005) have demonstrated the potential to generate nanoparticles that are both safe and non-toxic, encompassing materials like gold, palladium, gold alloys, and more (Song & Kim, 2008; Vilchis-Nestor et al., 2008; Song et al., 2009; Sajjad et al., 2018).

Numerous researchers have employed phytochemicals extracted from plants, notably *Aspalathus linearis* (Rooibos), for the synthesis of diverse nanoparticles (Blom van Staden et al., 2021; Lyimo et al., 2022;

Ayyıldız et al., 2023) because the bio-components such as flavonoids, found in the roots and leaves of the plants, aid in the reduction and stabilisation process (Amina & Guo, 2020).

The Aspalathus genus belongs to the Leguminosae family of plants, which includes more than 270 different species of plants. Remarkably, the sole recognized edible species to date is *Aspalathus linearis* (Burm.f.) R. Dahlgren (Johnson et al., 2018; Fantoukh et al., 2019), a distinctive shrub indigenous to the Western Cape province in South Africa, particularly within certain regions of the Fynbos Biome within the Cape Floristic Region (Krafczyk & Glomb, 2008; Soltys et al., 2021). It thrives naturally in the Cederberg Mountains, specifically in the Citrusdal, Clanwilliam, and Nieuwoudtville districts, which serve as the primary hubs for the rooibos industry (Fantoukh et al., 2019). The leaves and stems of *Aspalathus linearis* are utilized in crafting the caffeine-free rooibos drink, known for its tannin content (Smith & Swart, 2016; Epure et al., 2019). Beyond its role in beverage production, *Aspalathus linearis* (Burm.f.) R. Dahlgren exhibits a spectrum of health-promoting properties. These include hypoglycaemic, anti-allergic, antispasmodic, photoprotective, anti-inflammatory, and estrogenic characteristics, complemented by antioxidant attributes (Gilani et al., 2006; Shimamura et al., 2006; Baba et al., 2009; Kawano et al., 2009; Son et al., 2013; Lee & Bae, 2015; Magcwebeba et al., 2016).

Rooibos stands as a globally acclaimed herbal tea, enjoying widespread popularity in over thirty-seven countries. It comes in two varieties: fermented (brown) and unfermented (green) (Marais et al., 2000; Joubert & de Beer, 2011; Johnson et al., 2018). The oxidation and browning of green rooibos (GR) alter tea's phenolic profile and biological characteristics during fermentation (Tobin, 2018). The primary flavonoids in rooibos leaves include Aspalathin (ASP), nothofagin, orientin, vitexin, quercetin, rutin, etc. (Fantoukh et al., 2019; Samodien et al., 2021). This study focuses on the recent research on the eco-friendly formation of AuNPs, PdNPs, and Au-Pd bimetallic nanoparticles, which has benefits above conventional approaches that use chemical products linked to pollution. The reduction and stabilisation of Au and Pd salts by a plant extract called *Aspalathus linearis* (green rooibos-GR) to form Au-Pd bimetallic nanoparticles will also be discussed. This study will further look into discussions of the applications of monometallic nanoparticles, including Au and PdNPs and Au-Pd bimetallic nanoparticles.

1.1. Justification

The limitations of traditional chemical methods for the synthesis of nanomaterials, including their high cost, environmental impact and complexity due to the use of chemicals, resulted in the emergence of green nanotechnology, focusing on environmentally friendly approaches and organic materials, to meet sustainability goals (Daruich De Souza et al., 2019; Devi et al., 2019). However, due to concerns raised about the safety and environmental impact of nanoparticles synthesised from plant extracts, a need exists for careful assessment, particularly in medical contexts. Plant extracts pose several challenges due to their

inherent variability, complex composition, and potential interactions with biological systems., leading to the suggestion of isolating specific compounds for targeted research (Ying et al., 2022). In addition, the potential toxicity of noble metal nanoparticles highlights the importance of safety assessment, even for metals such as gold and palladium (Barbafieri & Giorgetti, 2016; Zhu et al., 2019). Finally, bimetallic nanoparticles stand out for their remarkable versatility in combining the unique properties of multiple metals, thereby expanding their potential applications beyond what single-metal counterparts can achieve. They offer a wide range of advantages, including the ability to finely tune their properties, enhanced catalytic activity, enhance stability, and enable selective sensing. Their versatility finds application across various fields, encompassing catalysis, sensing, and more. (Velpula et al., 2021).

1.2. Statement of Research Problem

The synthesis of nanomaterials using chemical methods has been found to be time consuming and have drawbacks such as high cost , amongst others (Dikshit et al., 2021). Furthermore, these methods require complex steps leading to the absorption of toxic chemicals on the surface, which may adversely affect medical applications and are harmful to the environment (Hasan, 2014; Rehana et al., 2017; Yasothamani & Vivek, 2020). Consequently, traditional chemical methods can yield substantial environmental impacts, including chemical pollution, energy intensity, waste generation, water and air pollution, resource depletion, and health risks. In recent times, an intriguing alternative has emerged, centred around the utilization of organic materials—an idea commonly referred to as "green nanotechnology" (Nasrollahzadeh et al., 2019). As a result, nanotechnology is placing increasing emphasis on creating safe, biocompatible, non-toxic, and environmentally friendly methods that use plant extracts. Although total extracts are generally considered safe, there could still be concerns about the biocompatibility and potential toxicity of nanoparticles synthesized using plant extracts.

The complex composition of plant extracts poses a challenge in understanding the mechanisms governing nanoparticle formation and stabilisation (Rapachi et al., 2023). This inherent complexity can hinder the optimization and rational design of nanoparticles. Moreover, the diverse array of phytochemicals present in plant extracts may intricately shape the interactions between nanoparticles and biological systems, influencing their efficacy in applications such as drug delivery and imaging (Dauthal & Mukhopadhyay, 2016; Chahardoli et al., 2018; Pal et al., 2022). To overcome these challenges, the further isolation and purification of plant extracts become essential (Alirezalu et al., 2020). This method enables the identification of particular phytochemicals accountable for the reduction and stabilization of nanoparticles (Dauthal & Mukhopadhyay, 2016; Álvarez-Chimal & Arenas-Alatorre, 2023). By isolating these compounds, a focused investigation ensues, shedding light on the precise role of each compound in the synthesis process. The isolation and purification of plant extracts are essential for obtaining standardized, bioactive-rich sources of compounds, which not only enhance the efficacy and safety of plant-based products but also contribute to a

deeper understanding of the mechanisms governing nanoparticle formation and stabilization. By systematically studying purified plant extracts, researchers can uncover novel bioactive molecules, optimize extraction conditions, and elucidate the molecular mechanisms underlying nanoparticle synthesis. This focused approach contributes to a more comprehensive understanding of their individual contributions, thereby enhancing the overall comprehension of nanoparticle behaviour (Amini, 2019).

Nanoparticles can interact with biological systems in complex ways, potentially leading to adverse effects or unintended interactions. Monometallic nanoparticles, such as gold, exhibit strong plasmonic properties. The plasmonic properties of monometallic nanoparticles enable enhanced light-matter interactions, tunable optical properties, surface-enhanced spectroscopy, photothermal effects, and optical sensing/imaging capabilities, making them valuable tools for a wide range of applications in biomedical, environmental, and nanotechnology fields (Sarfraz & Khan, 2021). Bimetallic nanoparticles can combine plasmonic properties, thereby broadening their potential use (Sytwu et al., 2019). In the same context and to eliminate the use of harmful substances, this study opted for a purified and pharmacologically defined compound known as Aspalathin (ASP), a *C*-glucosyl dihydrochalcone found in South African *Aspalathus linearis* (green rooibos-GR). ASP has previously been used to form stable nanoparticles made from Au and PdNPs however, for the first time, a combination of both metals (Au-Pd bimetallic nanoparticles) will be investigated and assessed for potential anti-cancer properties.

1.3. Aim and Objectives

1.3.1. Aim

To synthesise and characterise Au-Pd bimetallic alloyed nanoparticles using *Aspalathus linearis* (green rooibos-GR) and its major pure compound, Aspalathin (ASP) for possible biomedical applications.

1.3.2. Objectives

The present study aims to synthesise and characterise Au-Pd bimetallic alloyed nanoparticles using GR plant extract with the following specific objectives:

a) To prepare two types of extracts (i.e., an organic extract and aqueous (water) extract) from GR.
b) To isolate the pure bioactive substances, such as ASP, that is present in the GR plant extract.
c) To synthesize AuNPs, PdNPs and Au-Pd bimetallic nanoparticles using both the total extract and the isolated compound.
d) To characterise the resulting AuNPs, PdNPs and Au-Pd bimetallic alloyed nanoparticles using UV-Vis Spectroscopy, DLS Analysis, HRTEM, SAED, STEM-HAADF, and ATR-FTIR.
e) To explore the biomedical potential of AuNPs, PdNPs, and Au-Pd bimetallic alloyed nanoparticles for assessing their efficacy in treating cancer cells.

1.4. Hypothesis

a) GR plant extract serves as a natural reducing and stabilizing agent due to its rich composition of phytochemicals. These phytochemicals have the capability to reduce metal ions and act as stabilizing agents to prevent nanoparticle aggregation.

b) The synergistic effects of the diverse phytochemicals present in the GR plant extract, including Aspalathin and other compounds, optimize the reduction and stabilization processes during nanoparticle synthesis, leading to nanoparticles with specific properties.

c) ASP, a specific compound in GR extract, is a key biomolecule in the green synthesis process. It acts as a reducing agent for metal ions, controls the reduction process, and contributes to the stabilization of resulting nanoparticles.

d) Green synthesis methods using GR plant extract and ASP as reducing and stabilizing agents offer several advantages, including eco-friendliness by avoiding hazardous chemicals, cost-effectiveness, and sustainability by utilizing natural resources efficiently.

1.5. Thesis Outline

The first chapter of this thesis delves into the background and importance of nanoparticles, the methods used for their synthesis, the objectives of the research, and the overall structure of the thesis.

Chapter Two delves into the literature, examining the importance of nanoparticles and investigating GR plant extract as a potential source for both reducing and stabilizing agents in nanoparticle synthesis. It provides insights into the benefits of employing plant extracts in contrast to conventional methods, citing earlier research on the eco-friendly synthesis of both monometallic and bimetallic nanoparticles utilizing specific plant extracts. By addressing gaps in the current literature and posing pertinent research questions, Chapter Two adds to the academic conversation.

Chapter Three details the collection and preparation of GR plant material, emphasizing the extraction, isolation, and characterization techniques employed to identify the major compound, ASP. The chapter also outlines the protocols for the green synthesis of monometallic Au and PdNPs, along with Au-Pd alloyed bimetallic nanoparticles, utilizing the selected plant extract and its isolate. Multiple characterization techniques are employed to assess the properties of the nanoparticles.

Chapter Four unveils the study's results and engages in a thorough discussion, interpreting the characterization outcomes of the nanoparticles and analysing the impact of synthesis parameters on their properties. This section also offers insights into the roles played by GR extract and ASP in the formation

and stabilization of nanoparticles. Ultimately, Chapter Four outlines the implications of these findings for green nanoparticle synthesis and explores potential applications in various fields.

Chapter Five provides an overview of the biological study of monometallic and bimetallic nanoparticles, including their use in biomedical applications with the selected plant extract and it's isolate.

Chapter Six concludes the research findings, their significance, and contributions to the field of green nanoparticle synthesis. It assessed the implications of research on sustainable nanotechnology. Finally, the chapter concludes with recommendations for further research and future directions.

Chapter 2

2. Literature Review

2.1. Introduction

The literature review examines the value that plants have on their own. This chapter begins by acknowledging the importance of plants, ecological roles as well as their potential as sources of bioactive compounds set the stage for our exploration. The processes of extracting and isolating compounds from plants will be studied against literature. Thus, the spotlight is cast upon *Aspalathus linearis* (green rooibos-GR), a plant of notable botanical and medicinal significance. Aspalathin (ASP), a chemical compound found in abundance in this plant, will also be investigated by highlighting its chemistry and pharmacological potential.

The narrative shifts to the synthesis and characterization of nanoparticles, both monometallic and bimetallic. Here, the emphasis was on the use of plant extracts in these processes, emphasizing the significance of green synthesis in reducing environmental impact. This transitioned into the field of nanoparticle stability within the complex biological environments. Understanding the behaviour of these nanomaterials in biological media is crucial for their successful integration into biomedical applications. The spotlight was then cast on the expanding role of nanoparticles in biomedicine. From targeted drug delivery to advanced diagnostics and therapeutic interventions, these nanoparticles hold promise for reshaping healthcare.

2.2. Plant Material Importance

Plant material encompasses substances derived from plants, such as leaves stems, roots, seeds, or extracts. Thus, a new horizon has opened to discovering new therapeutic agents through natural products such as plant extracts (Jadimurthy et al., 2023). In most developing countries, traditional medicine and medicinal plants have been discovered, and nearly 80% of the world's population relies on herbal medicine (Vaou et al., 2021).Various chemical substances found in plants can be used to treat a variety of human ailments (Mohan et al., 2021; Mohan et al., 2022). The vast array of secondary metabolic products found in plants is commonly referred to as “phytochemicals”. Plants produce compounds known as phytochemicals (Majrashi et al., 2023). Numerous phytochemicals have been linked to significant biological effects such as analgesia, anticancer, and wound healing (Yeshi et al., 2022).

Phytochemical-rich plants are beneficial for long-term health and illness prevention (Kumar et al., 2023). Plants are ingested due to containing essential compounds such as saccharides, coumarins, lignans, flavonoids, terpenoids, and steroids (Kiani et al., 2022). Because plant chemical contents are complicated, it is necessary to obtain pure phytochemicals through extraction and separation, followed by structural

identification, bioactivity screening, etc. There are new technical methods for accelerating the extraction and analysis of phytochemicals (Bitwell et al., 2023).

2.2.1. Phytochemical Screening

Phytochemicals, bioactive compounds found in plants, contribute health benefits despite not being classified as essential nutrients. These compounds, present in fruits, vegetables, grains, nuts, and seeds, play roles in enhancing taste, colour, and disease resistance in plants (Kumar et al., 2023). As highlighted by Koparde et al (2019), the initial step in phytochemistry research involves extraction before isolating specific compounds. The primary goal of extraction is to eliminate or minimize undesired chemical constituents while retaining the necessary chemical elements. Subsequently, to discern the types of phytochemicals within the extract combination or fraction obtained from the crude extract or active fraction of the plant material, phytochemical screening is conducted using appropriate tests (Sasidharan et al., 2011). This simple, rapid, and cost-effective screening procedure serves as a crucial tool in the analysis of bioactive compounds, providing researchers with prompt insights into the diverse types of phytochemicals present in a mixture (Jiang et al., 2019).

2.2.2. Isolation of Phytochemicals

Phytochemical separation involves the isolation and purification of each component within a plant extract, both physically and chemically (Gao et al., 2021). Various traditional isolation techniques, such as solvent extraction, precipitation, crystallization, fractional distillation, salting-out, and dialysis, are commonly employed in contemporary practices (Stéphane et al., 2021). However, cutting-edge separation methods, including high-performance liquid chromatography, ultrafiltration, and column chromatography, are indispensable for achieving enhanced precision in phytochemical separation. Determining the chemical structures of these phytochemicals is vital, laying the foundation for subsequent studies on bioactivities, structure-activity relationships, *in vivo* metabolisms, structural alterations, and the synthesis of active phytochemicals (Wang et al., 2019). Given the challenges associated with traditional methods for structural analysis, spectral analysis is frequently employed. This involves extracting minimal sample quantities and acquiring structural data by measuring and analysing various spectra, providing valuable insights into the intricate nature of phytochemical compounds (Bossier, 1962; Bitwell et al., 2023).

2.2.3. Phytochemical Composition in Plants

Phytochemicals, originating from the Greek word "phyton" denoting "plant," are inherent compounds present in grains, vegetables, and fruits. Predominantly consisting of non-nutrient substances, these compounds play a crucial role in enhancing overall health (Frank et al., 2020). Despite the identification of over ten thousand phytochemicals, many remain undiscovered and necessitate further exploration. The health benefits associated with phytochemicals primarily revolve around reducing the risk of various human

diseases (Iyer et al., 2023). These plant-based compounds offer easy accessibility, often with fewer toxic effects compared to synthetic molecules. They exhibit a broad spectrum of biological and pharmacological effects, including anti-microbial, anti-tumour, anti-mutagenic, and both anti-oxidant and pro-oxidant activities (Ullah et al., 2020). This diversity emphasises the potential of phytochemicals as valuable contributors to human health and well-being.

Phytochemicals, identified by the presence of a minimum of one aromatic ring, classify substantial and intricate tannins, along with the polyphenols originating from them, as phenolics (Vuolo et al., 2019). Within plants, diverse physiological processes yield a class of secondary metabolites termed phenols. These processes involve essential functions including growth, lignification, pigmentation, pollination, and protection against pathogens, predators, and environmental stressors. Significantly, plant tissues consist of two primary classes of naturally existing phenolic compounds: flavonoids and non-flavonoids (Crozier et al., 2009; Ajuwon et al., 2015).

Flavonoids encompass diverse subclasses, as elucidated by Nabavi et al (2020), which include flavones, flavanols, anthocyanins, isoflavones, flavanones, chalcones, and dihydrochalcones. Moreover, other recognized classes involve coumarins, aurones, dihydroflavonols, and flavan-3,4-diols. These compounds play a pivotal role in various aspects of plant biology, influencing growth and development (Khalid et al., 2019), interactions with insects (Simmonds, 2001), and radiation protection. Notably, flavonoids absorb ultraviolet B (UVB) radiation and scavenge reactive oxygen species (ROS) produced by UVB exposure, as demonstrated by studies by Davies et al (2020), Ferreyra et al (2021), and Zhang et al (2023). In contrast, essential non-flavonoids encompass lignans, stilbenes, phenolic acids, and phenolic alcohols.

All humans consume plant-based teas and drinks such as teas, fruits, vegetables, spices, cocoa, and wine, which are rich in flavonoids. When ingested, flavonoids have been found to enhance human health (Bondonno et al., 2020). According to research, flavonoids offer a range of beneficial health effects, comprising anti-inflammatory, oestrogenic, enzyme regulation system, antibacterial, as well as vascular (Mutha et al., 2021). The most researched flavonoid attribute is antioxidant activity, which is responsible for various biological processes where oxidative stress is advantageous (Ciumărnean et al., 2020; Dias et al., 2021).

Adding to their antioxidant and free-radical scavenging properties, flavonoids demonstrate anti-cancer activity through various mechanisms. These actions involve the control of gene expression associated with cell proliferation, oncogenes, and tumour suppressor genes. Furthermore, flavonoids induce cell cycle arrest and apoptosis, regulate detoxification enzyme activity, boost the immune system, and manage hormone metabolism (Ginwala et al., 2019; Maleki et al., 2019).

2.3. *Aspalathus linearis* (Rooibos)

2.3.1. Occurrence, History and Uses of *Aspalathus linearis*

The leguminous *Aspalathus linearis* (Burm. F.) R. Dahlgren (Fabaceae Family, tribe Crotalarieae) is as 2m tall shrub with little yellow blooms and green needle-like leaves (Ajuwon et al., 2015). Before drying, the needle-like leaves can be fermented after harvesting (Chaudhary et al., 2021; Joubert et al., 2023). As a result of the oxidation of polyphenols in the plant throughout the fermenting procedure, the green colour changes to red. The finished item is called “red tea” or “red bush tea”. The fermented substance was originally named "rooibos," meaning "red bush," until the introduction of an "unfermented" variation, commonly referred to as GR or "unfermented" rooibos, as noted by Damiani et al (2019) and Bednarska & Fecka (2022). The recent legal safeguarding of the term "rooibos" in South Africa, combined with its designation as a geographical indication (GI) in Europe, not only solidifies South Africa's exclusive right to the name but also guarantees its utilization exclusively for genuine rooibos products (Muller et al., 2018).

South Africa is home to 278 species of the *Aspalathus* genus (Figure 2-1), which have a high proportion of phenolic compounds (Johnson et al., 2018; Fantoukh et al., 2022). Rooibos has been consumed by South Africans for over three centuries and was not known outside of the country. In 1904, a Russian immigrant named Benjamin Ginsberg bought tea from Khoi descendants. He was the first person to export rooibos (Meyer & Naicker, 2023).

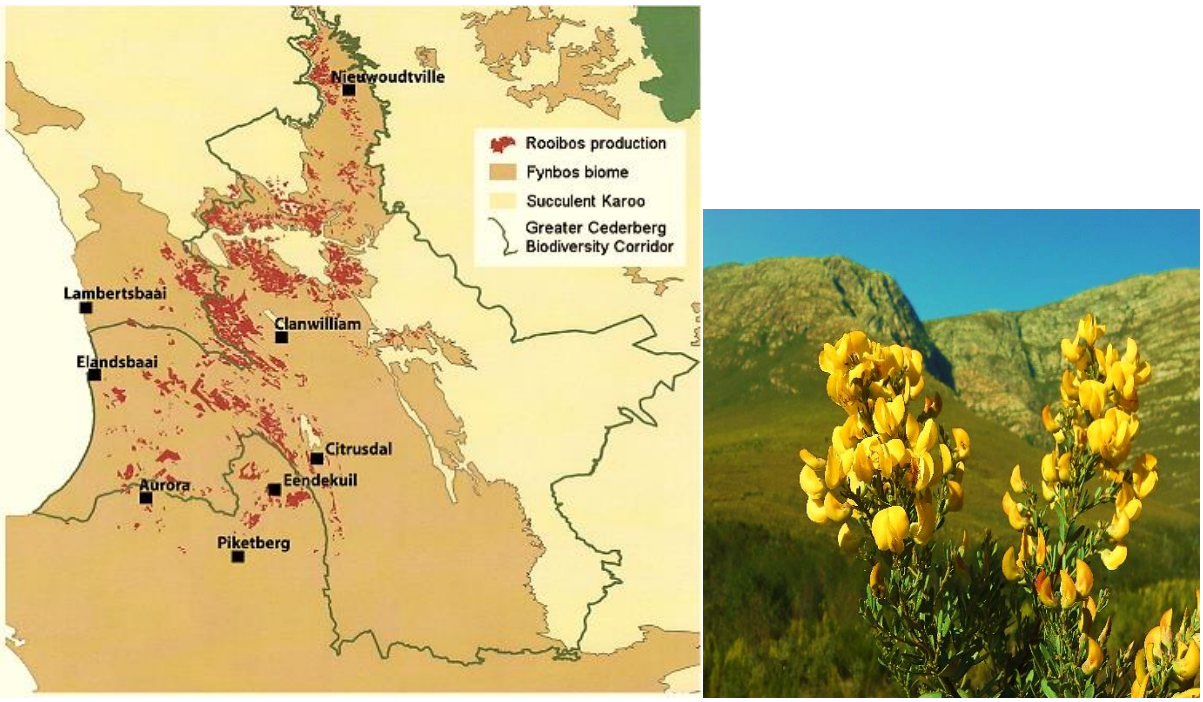

Figure 2-1: A map showing *Aspalathus linearis* location areas in and around the Greater Cederberg Biodiversity Corridor (Hawkins et al., 2011; Krafczyk and Glom, 2008)

The first economic potential of rooibos was acknowledged by doctor and botanist Dr P.F. Le Fras Nortier in the 1930s, and local farmers began cultivating plantations in his honour. The local market absorbed 70-75 percent of rooibos' annual production by the 1900s and 2000s, when production increased to 6000 tonnes. The cultivation has now reached more than 1200 tonnes, supplying both the domestic and international markets (Wilson, 2005; Ajuwon et al., 2015).

In the late 1960s, research findings indicated that rooibos had soothing effects on infantile colic, establishing the tea as a healthful beverage. Beyond its reputation as a delightful drink, rooibos is purported to have appetite-boosting properties and is believed to address conditions such as allergies, sleeplessness, and nervous ailments (Marnewick et al., 2005; Gilani et al., 2006; Muller et al., 2013; Johnson et al., 2018). Furthermore, a Japanese company developed an "anti-aging" solution based on rooibos, demonstrating successful outcomes in treating various illnesses. Notably, this solution was found to reduce serum lip peroxidase levels in patients.

Over the last two decades, accounts of its antioxidant properties, coupled with promotional claims about antioxidants serving as "anti-ageing" agents, have heightened its reputation as a healthful beverage. Research has indicated that antioxidants can slow down the ageing process (Joubert & de Beer, 2011; Muller et al., 2018). According to the findings of a study that was conducted in 1977 by the Imperial Institute of London, "It seems doubtful whether this material would be acceptable in the United Kingdom as a substitute for ordinary tea" because the substance in question does not contain caffeine or any other alkaloids and, as a result, would have the stimulating effect that tea does. According to data provided by the South African Rooibos Council (2022), Rooibos exports grew from 6552 in 2013 to 8789 tons in 2021. The top three importers of Rooibos are Germany, Japan, and the Netherlands, while the UK and USA follow closely behind. In 2016, African countries entered the top ten export markets for the first time and since then cross-border and intercontinental exports have increased exponentially. Zimbabwe, Botswana, and Zambia have consistently been among the top ten export market destinations for Rooibos (South African Rooibos Council, 2022).

Furthermore, various model systems showed that rooibos inhibited lipid peroxidation *in vivo* (Hoosen, 2019). There is a growing market for functional meals and nutraceutical goods made from unfermented rooibos because of the growing interest in these items among consumers (Zuñiga-Martínez et al., 2022). Rooibos extracts of food-grade quality can be found in a wide variety of foods and drinks, such as iced teas, yoghurt, "instant cappuccino", and even bread. Rooibos extract tinctures and dietary supplements can also be purchased (Joubert & de Beer, 2011; Muller et al., 2018).

2.3.2. Phytochemical Composition of *Aspalathus linearis*

The fermentation process in rooibos results in a reduction of its polyphenolic content. As indicated by recent studies (Nogueira Silva Lima et al., 2022; Wang et al., 2022) , unfermented rooibos, often referred to as GR, possesses a notably higher proportion of polyphenols, flavonoids, and non-flavonoids compared to its fermented counterpart. These variations arise from both (i) enzymatic and chemical changes occurring during fermentation and (ii) the specific processing techniques employed in the production of each variant (Fantoukh et al., 2022). Antioxidant properties are also affected by the fermentation and processing of rooibos, as demonstrated by *in vivo* studies indicating that antioxidant activity declines with fermentation. Fermentation reduces the total polyphenolic content, producing this effect (Elisha & Viljoen, 2021). According to various sources, rooibos leaves have a tannin concentration of 3.2-4.4% (Cheney & Scholtz, 1963; Morton, 1983; Marnewick et al., 2000; Ajuwon et al., 2015).

Moreover, rooibos stands out due to its unique composition, housing two rare compounds, aspalathin and aspalalinin, which are flavonoids according to research by Chaudhary et al (2021) and Bednarska & Fecka (2022). During the fermentation process, the conversion of aspalathin, found in unfermented rooibos, results in dihydroiso-orientin, as elucidated by de de Beer et al (2017). Rooibos claims a diverse range of flavonoids and flavones, encompassing C-C linked D-glucopyranosides, orientin, iso-orientin, analogues of nothofagin vitexin and iso-vitexin, chrysoeriol, luteolin, and luteolin-7-*O*-glucoside. Additionally, flavanols present in rooibos include quercetin, quercetin-3-*O*-arabinoside, hyperoside, iso-quercetin, and rutin, as meticulously outlined by Fantoukh et al (2019).

Table 1: Flavonoids found in *Aspalathus linearis* (Fantoukh et al., 2019)

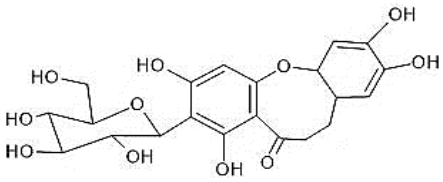 **aspalalinin**	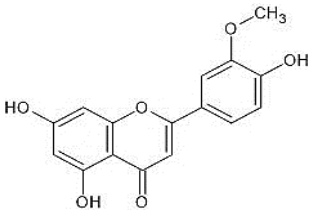 **chrysoeriol**
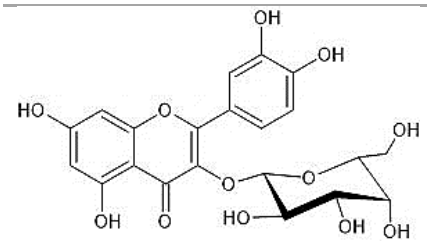 **hyperoside**	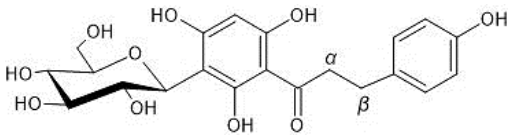 **nothofagin**
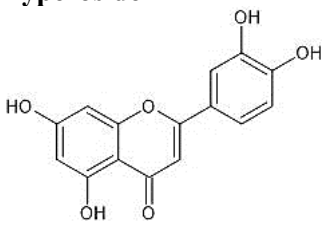 **luteolin**	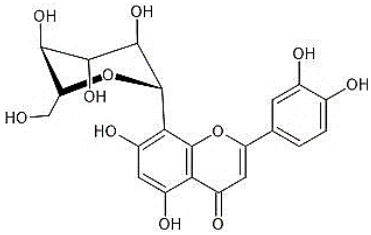 **orientin**
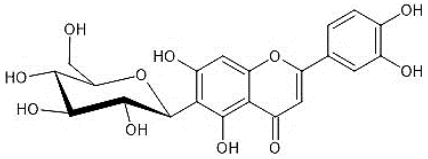 **iso-orientin**	
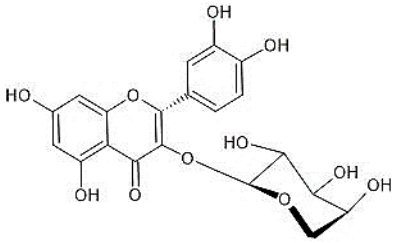 **quercetin-3-*O*-arabinoside**	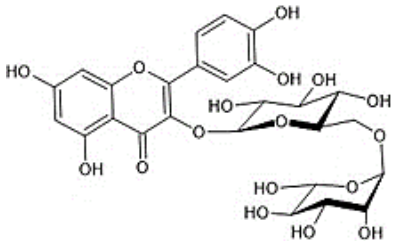 **rutin**
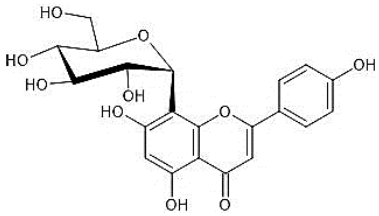 **vitexin**	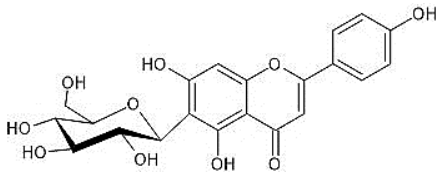 **iso-vitexin**

Rooibos is revealed to house an array of compounds, including phenolic acids, lignans, coumarin, esculetin, (+)-catechin, oligomeric flavan-3-ol, procyanidin B3, and bis-fisetindol-(4β, 6: 4β, 8)-catechin, as documented by Ajuwon et al (2018) and Fantoukh et al (2022). The presence of enolic phenylpyruvic acid

glucoside (PPAG; Z-2- (*β*-D-glucopyranosyloxy)-3-phenylpropenoic acid) in rooibos is noteworthy, serving as a precursor in flavonoid production, as discussed by Muller et al (2018) and Joubert et al (2023). Although not phenolic by strict definition due to the absence of a hydroxyl group on the phenyl ring, its identification in rooibos extracts and infusions warrants attention, particularly in light of recent findings pointing to its anti-diabetic activities.

2.3.3. Aspalathin

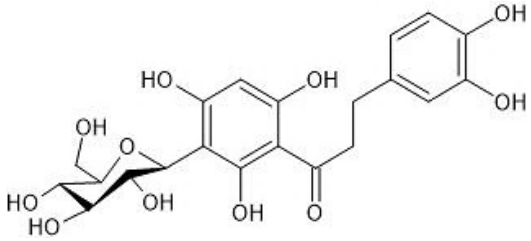

Figure 2-2: Chemical structure of Aspalathin (*C*-glucosyl dihydrochalcone)

Aspalathin (as shown in Figure 2-2) is a flavonoid compound found abundantly in *Aspalathus linearis*, a herbal infusion derived from the leaves of the *Aspalathus linearis* plant extract (Moosavi et al., 2018). Over the years, this natural compound has gained significant attention in the field of pharmacology due to its potential health benefits and diverse pharmacological properties. This discussion explores the pharmacological potential of aspalathin, shedding light on its various applications and mechanisms of action.

Pharmacological Properties of Aspalathin

Oxidative stress is associated with several chronic conditions, including cancer, cardiovascular diseases, and neurodegenerative disorders (Colon Hidalgo et al., 2022).

Antioxidant Properties: Aspalathin functions as a scavenger of free radicals, assisting in alleviating oxidative stress within the body (Schalkwyk et al., 2020). The antioxidative characteristics of aspalathin play a pivotal role in shielding cells and tissues from oxidative damage (Shabalala et al., 2019).

Anti-inflammatory and Cardiovascular Effects: Chronic inflammation is a hallmark of many diseases and compounds with anti-inflammatory properties are of great interest to researchers (Schilrreff & Alexiev, 2022). The ability of aspalathin to modulate inflammatory pathways makes it a potential candidate for managing conditions associated with excessive inflammation, such as arthritis and inflammatory bowel disease (Shabalala et al., 2019).

Additionally, studies have indicated that aspalathin may contribute to cardiovascular health (Chaudhary et al., 2021). Regulating blood pressure, reducing cholesterol levels, and improving lipid metabolism, as

highlighted by Mazibuko-Mbeje et al (2019), are pivotal effects for maintaining heart health and preventing cardiovascular diseases.

Anti-diabetic Properties: Aspalathin shows promise for diabetes management (Orlando et al., 2019). Research suggests that it enhances insulin sensitivity and reduces insulin resistance, potentially benefiting individuals with diabetes or those at a risk of developing this condition (Mthembu et al., 2021). Furthermore, the role of aspalathin in weight management was explored. This may influence appetite regulation and support healthy weight management by affecting hunger hormone levels (Mazibuko et al., 2015).

Neuroprotection: The neuroprotective potential of aspalathin is particularly fascinating. Research indicates its capability to defend brain cells against damage, hinting at a prospective role in reducing the exposure to neurodegenerative conditions, such as Alzheimer's and Parkinson's disease (Zhao et al., 2020; Omoruyi et al., 2023).

Potential Anticancer Effects: Although further research is warranted, some studies have suggested that aspalathin may possess anticancer properties (Huang et al., 2020). It can inhibit the proliferation of cancer cells and holds promise in reducing the risk of specific cancer types. A recent study revealed that aspalathin exhibits p53-dependent cyto-protective effects in H9c2 cardiomyocytes and Caov-3 ovarian cancer cells. Additionally, it mitigates doxorubicin-induced cytotoxicity by up regulating ATGs and AMPK, concurrently leading to a reduction in P53/mTOR/p62 signalling (Johnson et al., 2017).

2.4. Purification and Characterization of Secondary Metabolites

2.4.1. Chromatography Methods

Chromatography is the method most frequently used to separate the chemical components of natural products (Koparde et al., 2019; Abubakar & Haque, 2020). High separation efficiency, speed, and simplicity are all benefits of the approach. Numerous types of phytochemicals can be separated and purified utilizing various separation principles, operating modes, chromatographic pickings, or a combination of chromatographic techniques (Santhiya-Nair et al., 2022). This technique allows for compound purification (Sunkar et al., 2022). This section only focuses on the techniques used through the purification process in this thesis.

Adsorption Column Chromatography (Open Column)

According to (Shinde et al., 2023), the difference in the adsorptive properties of distinct adsorbents is what drives the effectiveness of Adsorption Column Chromatography. Various substances, such as silica gel, alumina, activated carbon, polyamide, and others, serve as adsorbents (Pourhakkak et al., 2021). Adsorption Column Chromatography relies on variations in the adsorptive capacities of these different adsorbents (Pal et al., 2022).

Silica gel, alumina, activated carbon, polyamide, and others are frequently used as adsorbents. Silica gel adsorption chromatography is the most highly utilized of the adsorbents described, and it is suitable for separating numerous chemical elements from plants (Shinde et al., 2023). Alkaloid, steroid, and terpene separation is the principal use of alumina adsorption chromatography (Stéphane et al., 2021). Polyamide is often used to separate chemicals by making different hydrogen bonds with phenols, quinones, flavonoids, anthraquinones, tannins, and other chemicals (Poole, 2018).

Factors such as resolution, sensitivity, and specificity play crucial roles in determining the effectiveness and applicability of this method. In adsorption chromatography, resolution relies on stationary phase selectivity, mobile phase polarity, and particle size (Spangenberg et al., 2011). Achieving higher resolution involves customized stationary phases and optimized mobile phase composition, which can be challenging with complex samples. Sensitivity is influenced by surface area, pore size distribution, and detection methods. Specificity is enhanced by tailoring stationary phases and employing selective detection techniques like MS/MS to accurately distinguish analytes (Peng et al., 2007). Adsorption chromatography is favoured for its simplicity, versatility, and cost-effectiveness in separating analytes with varying polarities or non-polar compounds, finding utility in pharmaceuticals, environmental monitoring, and food testing (Das & Dasgupta, 1998).

Thin Layer Chromatography (TLC)

In 1970, Stahl pioneered the practical application of Thin Layer Chromatography (TLC) (Stahl, 1970). In contrast to paper chromatography, TLC boasts advantages such as versatility, speed, and sensitivity. This technique, rooted in adsorption chromatography, segregates samples by leveraging the interactions within thin layers of adsorbent affixed to a plate. Notably, TLC is particularly adept at separating compounds with low molecular weight, as highlighted by Ingle et al (2017).

TLC is affected by resolution, sensitivity, and specificity. Resolution relies on factors like stationary phase type and mobile phase composition, with higher resolution achieved through optimization but challenging with complex mixtures. Sensitivity depends on detection methods, with techniques such as densitometry enhancing it, though varying with compounds (Ravikumar et al., 2022). Specificity is influenced by stationary and mobile phase selectivity, with tailoring improving it and complementary techniques aiding compound identification. TLC is favoured for simplicity and low cost, useful in preliminary screening and field settings, but challenges include limited resolution and sensitivity for complex analyses, difficulties in quantitative analysis, and subjective result interpretation (Kowalska & Sajewicz, 2022).

Partition Chromatography

This chromatography technique is employed to separate components by altering the coefficients between the immiscible stationary and mobile phases (Shinde et al., 2023). When classifying partition chromatography, a key distinction arises between normal-phase and reverse-phase chromatography (Grabenauer & Stafford, 2020). In normal-phase chromatography, the separation of polar and moderately polar molecular compounds is facilitated by the increased polarity of the stationary phase compared to the mobile phase. Carriers such as silica gel, diatomite, cellulose powder, and other materials find application in normal-phase distribution chromatography (Sunkar et al., 2022).

To mitigate adsorption loss, silica gel with 17% water content proves effective as a carrier in partition chromatography. Conversely, in reverse-phase partition chromatography, the mobile phase exhibits greater polarity than the stationary phase (Syed, 2023). Octadecyl-silylated silica, commonly referred to as ODS, serves as a prevalent type of stationary phase. The mobile phase typically comprises a mixture of acetonitrile and water or methanol. This method is frequently employed to differentiate molecules that lack polarity or possess only slight polarity (Atapattu et al., 2016; Poole, 2019).

Moreover, partition chromatography, utilizing differences in partitioning behaviour between mobile and stationary phases, hinges on resolution, sensitivity, and specificity. Resolution, pivotal for component separation, is influenced by stationary phase selectivity, mobile phase polarity, and analyte distribution coefficients, with tailored phases and optimized mobile phase composition enhancing resolution (Shinde et al., 2023). Sensitivity, critical for detecting low analyte concentrations, relies on detection methods and analyte distribution coefficients (Poole, 2018). Specificity, vital for accurate compound identification, is bolstered by stationary phase selectivity and mobile phase composition, with tailored phases and selective detection techniques such as MS/MS improving specificity (Cui et al., 2018).

High-Performance Liquid Chromatography (HPLC)

The separation analysis method known as HPLC (High-Performance Liquid Chromatography) is based on the traditional column chromatography principles, however, been greatly improved and optimized for speed, accuracy, and efficiency (Sorensen et al., 2020). This includes a variety of chromatography methods, including adsorption, gel, partition, and ion-exchange chromatography (Christian Ebere et al., 2019). High-pressure homogenate column loading and particle filters with diameters ranging from 5 to 20 μm are used to create HPLC columns. Eluents are injected into a column outfitted with detectors, automatic recording equipment, and high-pressure infusion pump collection equipment (LaCourse, 2023). As a result, it is faster and more effective than traditional column chromatography at separating samples. It is noteworthy for its high automation, speed, and efficiency (Ji et al., 2018).

Ji et al. (2018) revealed that preparative HPLC might be used to prepare many ultrapure samples. HPLC has substantially facilitated the separation of plant components, their qualitative identification, and their quantitative analysis (Tang et al., 2021). Removing trace elements or impurities from crude extracts is a critical step in the HPLC analysis of plant constituents (Mahato et al., 2019). In the final separation stage, high- or medium-pressure liquid chromatography is commonly employed to generate samples of exceptional purity (Fernandes et al., 2019). In preparative HPLC, constant concentration elutes are typically used, but gradient elution may also be employed for challenging separations (Nugroho et al., 2020).

HPLC retains benefits such as a broad range of applications and phase-change adaptability for the mobile phase (Haidar Ahmad et al., 2019; Shulyak et al., 2021), and it can also be applied to chemical ingredients that are hard to gasify, have a considerable molecular weight, or are thermally unstable. The most often used detectors in HPLC are differential refractive index and UV detectors (Al-sanea & Gamal, 2022). However, both have limitations.Differential refractive index detectors are sensitive to changes in temperature, detecting trace amounts of substances is not always ideal, and gradient elution cannot be used (Al-sanea & Gamal, 2022). Recently, a mass detector termed an ELSD has been created to detect materials without ultraviolet adsorption and gradient elution, making it perfect for detecting the majority of on-volatile components (Ji et al., 2018).

Additionally, HPLC is a distinct separation method influenced by various factors affecting resolution, sensitivity, and specificity. HPLC relies on parameters like column packing and mobile phase composition to achieve high resolution. HPLC generally offers superior resolution and sensitivity due to precise control over parameters and detector sensitivity (Shen et al., 2021). Specificity the techniques depends on factors such as selectivity of stationary phase and detection methods, with HPLC offering more method flexibility (Chen et al., 2018; W.-L. Li et al., 2019).

2.5. Structural identification of phytochemicals

Identification or elucidation the chemical structures of compounds establishes the foundation for further research into bioactivities, structure-activity relationships, *in vivo* metabolisms, structural modifications, and the synthesis of active phytochemicals (Nguyen et al., 2023). Often, only a few milligrams of compounds with physiological activity are of sufficient quality to be extracted from plants. Traditional chemical techniques, such as chemical degradation and derivative synthesis, can make structural research challenging (Tian & Liu, 2020). Consequently, spectral analysis is the method of choice for obtaining structural information by measuring distinct spectra using as few samples as possible. A complete analysis is conducted using data from the literature. If necessary, chemical methods would be added to previous approaches to determine the planar and even stereochemical structures of compounds (Feng et al., 2020).

2.5.1. Spectroscopic Techniques

Spectral analysis, particularly through the utilization of superconducting Nuclear Magnetic Resonance (NMR) and Mass Spectroscopic (MS) methods, has emerged as the primary methodology for elucidating chemical structures of plant compounds (Salem et al., 2020). The speed and precision of structure determination are substantially enhanced. In this section, we will briefly outline the applications of Infrared (IR), Ultraviolet (UV), and Nuclear Magnetic Resonance (NMR) techniques in structural identification. Beyond these methods, X-ray single crystals serve as a crucial tool for identifying both the chemical structure and absolute configuration (Valentín-Pérez et al., 2022).

Ultraviolet-Visible (UV-Vis) Spectroscopy

The UV-Vis spectrum manifests as an electron transition spectrum generated when molecules absorb electromagnetic radiation within the 200 to 800 nm wavelength range (Vogt et al., 2023). Valence electrons within molecules can absorb light at specific wavelengths, inducing electronic transitions from the ground state to the excited state. This phenomenon constitutes a fundamental principle in spectroscopy, particularly in UV-Vis spectroscopy (Feng et al., 2020). Substances containing double bonds, unsaturated carbonyl groups (including aldehydes, ketones, acids, and esters), and aromatic compounds can display significant UV absorption attributed $n \rightarrow \pi^*$ or $\pi \rightarrow n^*$ transitions. As a result, the UV spectrum is primarily employed for identifying conjugated systems within structures (Sajid & Akash, 2022).

UV spectra include the following details, according to (Kumar et al., 2020): (a) The absence of UV absorption at 220-800nm indicates that the chemicals are aliphatic hydrocarbons, aliphatic cyclic hydrocarbons, or simple derivatives of these hydrocarbons. (b) The compounds absorb strongly between 220-250nm, which indicates the existence of conjugated dienes, unsaturated aldehydes, or substructures of ketones. (c) The moderate absorption at 250-290nm demonstrates that the substances include benzene rings or aromatic heterocycles. Carbonyl groups are present when absorbance at 250-350nm is weak. Absorptions greater than 300nm suggest the presence of long conjugated chains in the structures. Additionally, the UV spectrum can only reveal a portion of a compound's structural information instead of the entire structure (Martirez et al., 2021). Therefore, it can only be a backup strategy for recognizing structures.

Fourier-Transform Infrared Spectroscopy (FTIR)

The alteration in the vibrational-rotational energy state of the molecule results in the generation of infrared radiation (IR) with wavelengths ranging from 4000 to 625 cm^{-1}. Above 1250cm^{-1} where the functional group region is located. Additionally, numerous functional groups are absorbed, including hydroxyl, amino, carbonyl, and aromatic rings. The fingerprint zone is between 1250 and 625cm^{-1}. The peaks are caused by stretching vibrations of single C-X (X=C, O, N) bonds and diverse bending vibrations (Feng et al., 2020).

Infrared spectroscopy, according to (Md Salim et al., 2021) is mostly used to determine functional groups and types of aromatic ring replacement. The chemical composition of plant components can occasionally be determined using infrared (IR) technology. For 25R and 25S spirospanol saponins, for instance, there is a significant variation between 960 and 900cm^{-1} (Pattasseril et al., 2022).

Nuclear Magnetic Resonance (NMR)

The advent of the Fourier Transform Spectrometer marked a significant stride in radionuclide research, encompassing isotopes such as ^{1}H, ^{13}C, ^{15}N, ^{19}F, and ^{31}P, along with advancements in two and three-dimensional nuclear magnetic technology (Koshani et al., 2020). NMR stands out as a fundamental spectroscopic technique for deciphering the chemical structures of substances, with hydrogen and carbon spectra being the most frequently employed (Rodríguez-Alonso et al., 2019). In NMR, the molecular compounds are subjected to electromagnetic waves within a magnetic field, inducing shifts in energy levels as atomic nuclei at a specific magnetic distance absorb a given amount of energy (Skoog et al., 2019). The NMR spectrum is constructed by associating the intensity with the frequencies of the absorption peaks. This spectral analysis provides detailed structural details concerning the identity and abundance of carbon and nitrogen atoms present in the molecule. It elucidates their specific surroundings and the chemical framework in which they are situated, thereby aiding in the examination, construction, and validation processes (Richards & Hollerton, 2023).

Mass Chromatography

Based on changes in their retention capacity or affinity for the stationary phase or mobile phase, the components of a sample are separated using liquid chromatography (LC) (Bouziani & Yahya, 2021). The separated components are identified based on their quality by means of a variety of analytical techniques, including UV, fluorescence, and electrical conductivity (Rouessac et al., 2022). Mass spectrometry (MS) uses a variety of ionisation processes, including rapid atom bombardment, electrospray ionisation, chemical ionisation, and laser desorption, to ionise sample components as part of its excessively sensitive detection process (Rajawat & Jhingan, 2019). In a vacuum, the resulting ions are divided into groups based on their mass-to-charge ratios, and their intensities are measured. As a result, LC-MS systems combine the outstanding separation resolution of liquid chromatography with the remarkable qualitative capabilities of mass spectrometry (Perez de Souza et al., 2021). Charged ions are formed and identified by MS. The molecular weight, structure, identification, and quantity of specific sample components can be determined using LC-MS data (Agrawal & Kulkarni, 2020).

2.6. Nanotechnology

Nanoscience includes a range of disciplines such as physics, chemistry, biology, medical science, and material science. The term "nano" is derived from the Greek word "nanos," meaning "dwarf," and it refers to objects that are one billionth in size. The concept of nanotechnology was brought forward in the 20th century. An American physicist named Richard Feynman was referred to as the "Father of nanotechnology". In 1959, Feynman's lecture sparked a scientific revolution as he outlined diverse processes capable of transforming individual atoms or molecules from one smaller form to another using various tools. The term "nanotechnology" was coined by Norio Taniguchi from the Tokyo University of Science (Sharma et al., 2019).

Eric Drexler's work in "Engines of Creation" introduced the concept of nanotechnology, which entails the manipulation of matter at the molecular level. This technology plays a crucial role across diverse technological sectors, enhancing health, safety, and environmental quality. Its applications span from efficient drug delivery and solar energy harvesting to cancer treatment, food packaging, and water purification (Sharma et al., 2019).

2.6.1. Nanoparticles

Nanoparticles are defined as nanoscale particles between 1 and 100nm designed at the atomic or molecular level to either form novel or superior physical qualities that cannot be achieved from traditional bulk materials (Bayda et al., 2020). Smaller-diameter particles than ordinary solids have unique characteristics. The foundation of nanotechnology is nanoparticles. These have a variety of uses, depending on the application (Sharma et al., 2019).

Nanoparticles find applications in a variety of fields, serving as delivery systems for medications, and being utilized in optical, magnetic, and biosensors, as well as in catalysis and electronics (Srinoi et al., 2018).Nanoparticles are used in many different applications, such as medication delivery systems, optical, magnetic, and biosensors, as well as catalysis and electronics (Bratovcic, 2019). Different criteria can be used to categorise nanoparticles, including origin, dimension, and structure. The classification of nanoparticles based on their originality states that they can be synthetic or natural. The dimension of nanoparticles might be zero, one, two, or three. Nanoparticles exhibit diverse structural compositions, encompassing liposomes, dendrimers, carbon-based, or metal-based configurations (Mazhar et al., 2017; Xu et al., 2019).

Moreover, to their size, composition, and shape, nanoparticle characteristics are influenced by their application in science and technology. Its tiny size results in the formation of structures, devices, and systems with at least one distinguishing quality (Joudeh & Linke, 2022). These characteristics could be distinct from those of its bulk constituents as well as from those of individual atoms and molecules (Sahiner et al., 2016;

Harish et al., 2022). The synthesis of nanomaterials involves two primary methods: the top-down technique and the bottom-up approach. (Figure 2-3) (Rawat, 2016; Sharma et al., 2019).

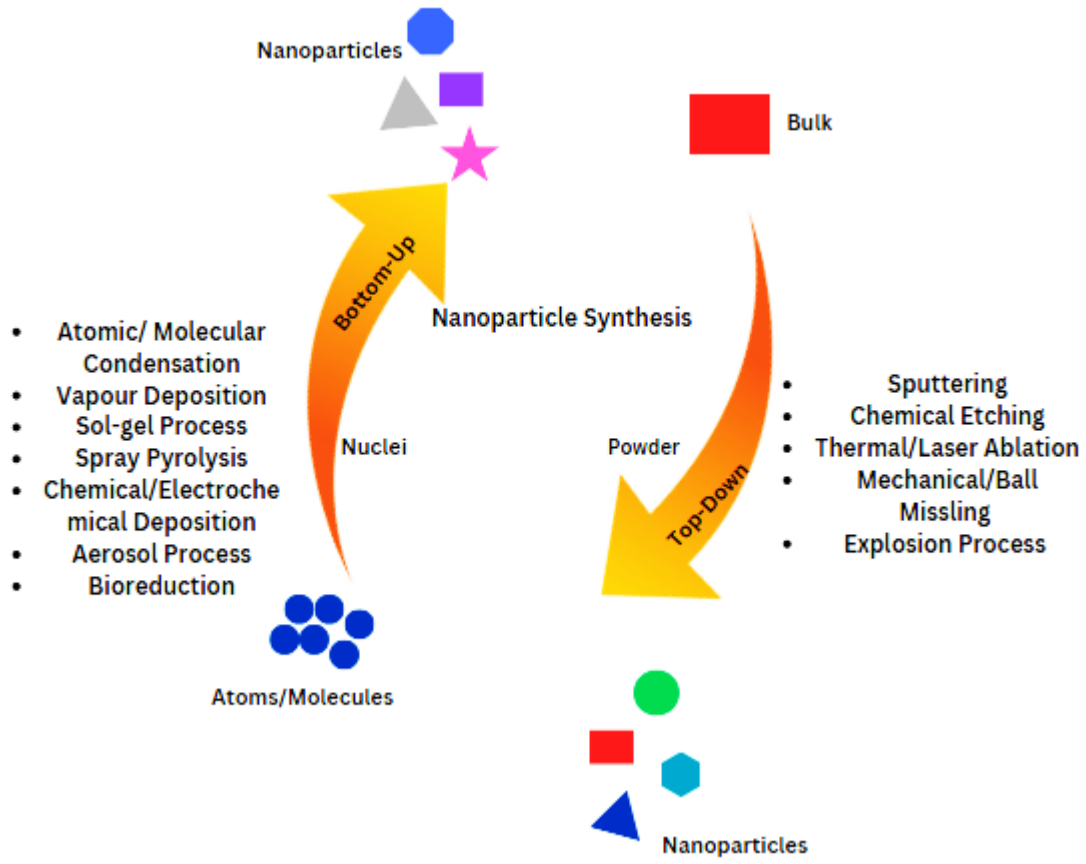

Figure 2-3: An illustration of the Top-Down versus Bottom-Up approach used in the synthesis of nanoparticles (Rawat, 2016; Sharma et al., 2019)

2.6.2. Synthesis of Nanoparticles

Top-Down Approach

In his description of the top-down strategy as a physical process, (Ebad-Sichani et al., 2023) makes reference to the microfabrication technique, in which materials are cut, milled, ad shaped using tools to get the desired shape and arrangement. Integrated circuits are one instance. It offers lithographic preparation methods, etching, ball mill, sputtering, etc.

Bottom-Up Approach

The bottom-up strategy entails creating devices out of smaller building blocks like atoms, molecules, or self-assembly. Tailoring precursor concentrations and adjusting reaction conditions such as temperature and

pH, alongside surface functionalization, template utilization, and similar strategies, remains viable for controlling the size and shape of nanoparticles, depending on the intended application. This particular approach ensures the production of highly accurate and precise products, exemplified by the creation of colloidal dispersions (Jamkhande et al., 2019).

Researchers have identified various methods for preparing bimetallic nanoparticles that are the correct size, composition, and form, as these aspects determine the qualities of a material (Absalan et al., 2019; Appa et al., 2021; Velpula et al., 2021). The following section discusses some methods for synthesizing nanoparticles.

(a) Successive Reduction Methods

Seeded-Mediated Growth

One of the common and established processes for creating bimetallic nanoparticles is the seed growth approach (Dahir Idris & Roy, 2023). Having two metal precursors results in bimetallic nanoparticles (Bhol et al., 2020). Consequently, the initial stage entails reducing one metal using a selected reducing agent and surfactant to generate seeds (Loza et al., 2020). Subsequently, an additional metal precursor, along with a surfactant and a reducing agent, is introduced to the seed stage. This facilitates the controlled growth of the second metal on the well-defined surface of the first metal. In the structural evolution of bimetallic nanoparticles, physical characteristics play a pivotal role (Duan et al., 2020). As a result, the lattice match, correlation of surface interfacial energies, electronegativity between metals, and reduction potentials are the factors that influence the nucleation and production of bimetallic nanocrystals (Sundarapandi et al., 2019).

Electrochemical Reduction

The leading force in this method is electricity. An electric current flows between two electrodes separated by an electrolyte (Katwal et al., 2015). The electrochemical approach was utilised to prepare metallic nanoparticles after first dissolving the anodic metallic sheet (Anandgaonker et al., 2019). The metal salt was then converted to metallic particles by the cathode. Tetraalkylammonium salts stabilised the metallic particles. This approach has resulted in the formation of bimetallic salts. The current density has the ability to influence the size of nanoparticles. As a result, increasing the current density leads to smaller nanoparticles (Su et al., 2019). The key benefits of this approach are its low cost, high yields, safe particle separation, and control over the final composition of bimetallic nanoparticles (Jamkhande et al., 2019).

(b) Simultaneous Methods

Co-Reduction

Two metal precursors are either reduced successively or simultaneously during the synthesis of bimetallic nanoparticles (Li et al., 2021). The co-reduction method is the less complicated of the two techniques used to form bimetallic nanoparticles (Bhol et al., 2020). A core-shell bimetallic nanomaterial is formed using

the co-reduction process, comparable to the synthesis of monometallic nanoparticles in which two metals are reduced one at a time (Appa et al., 2021). The formation of bimetallic nanoparticles via the co-reduction technique has also been mentioned as a standard technique. Researchers have undertaken several investigations and experiments for controlling the morphology and composition of bimetallic nanoparticles (Alruqi et al., 2019; Zhan et al., 2020; Liao et al., 2021). According to the literature, sodium citrate was used as a reducing agent in a study by (Bhol et al., 2020) to form bimetallic nanoparticles like Au-Pt and Pd-Pt.

Poly (N-vinyl-2pyrrolidone) (PVP), a stabilising agent, was also used to simultaneously reduce two metal precursors to produce Pd-Pt bimetallic nanoparticles in continuous reflux of ethanol-water (1:1 v/v) and water. Due to their low redox potentials, smaller atomic number transition metal nanoparticle synthesis can be complex. However, catalysis and magnetic materials benefit from transition metals with a lower atomic number. These are fabricated through a modified alcohol reduction technique, involving the treatment of various additional chemical constituents, such as alcohol, glucose, and tetraoctylammonium bromide, wherein a polymer plays a crucial part in influencing the formation of bimetallic nanoparticles (Bhol et al., 2020).

Thermal Decomposition Method

The temperature of the reaction and the surfactants have a significant impact on the reduction of metal ions (Guntlin et al., 2019). As a result, this approach entails the pyrolysis of precursors in boiling solvents at high temperatures. The main drawback of the strategy is how difficult it is to separate the reactive phase from the unstable nanocrystal phase at such high temperatures (Absalan et al., 2019). Because of the high energy required for bond breakdown, the thermal process is frequently endothermic (Sharma et al., 2019). The heat deposition rate governs the production of monodisperse nanoparticles with controlled composition, size, shape, and internal structure. The diameter of the nanoparticles is influenced by the nucleation rate and termination time. The method can be adapted to modulate reaction parameters, including time, temperature, concentration, reagent chemistry, and surfactants (Cele, 2020). Notably, these studies focused on thermal deposition in the presence of PVP. Heating palladium and copper acetates in a high-boiling-point solvent, such as ethoxyethanol, initiates the reaction, resulting in the formation of PVP-stabilised Pd-Cu nanoparticles (Bhol et al., 2020).

Sol-gel Method

The term "sol-gel" is a combination of two words: "sol" and "gel." Sol refers to a liquid colloidal suspension of stable particles where only van der Waals forces operate due to the minimal amount of sol in the dispersed phase (Jamkhande et al., 2019). In contrast, the gel comprises a semi-rigid mass with a solid concentration surpassing the liquid concentration, forming a continuous network from which particles or ions can evaporate (Zorkipli et al., 2016). Many gel systems exhibit apparent covalent connections.

The sol-gel approach involves the integration of these two substances and essentially consists of two reactions: hydrolysis and condensation. This method is commonly used for the production of diverse bimetallic nanoparticles, including but not limited to Au-Ag, Au-Pd, and Au-Pt combinations (Dlamini et al., 2023). The sol-gel method is favoured for its simplicity, cost-effectiveness, and practicality in producing high-quality nanoparticles (Sharma et al., 2016). Notably, it stands out as a low-temperature technique capable of precisely managing the composition of the final product.

Sonochemical

Ultrasound irradiation has been employed and validated in the synthesis of bulk materials. It is presently being applied to the production of nanoparticles. What distinguishes ultrasonic irradiation from microwave irradiation is that heating is generated indirectly through acoustic cavitation rather than directly. Under the impact of these acoustic waves, bubbles are formed and oscillated, growing as ultrasonic energy is gathered. The number of bubbles finally exceeds the threshold for stabilisation, resulting in the collapse and release of energy trapped inside. The hot spots created by a high temperature of 5000K and high pressure of 1000 bar are the inspiration for nanoparticle synthesis (Baig & Varma, 2012).

Under such severe conditions, ultrasound can produce nanoparticles with narrow size distribution and good phase purity. Mizukoshi et al. (1997) reported surfactant-assisted Au/Pd bimetallic nanoparticles via ultrasonic irradiation were later dubbed the sonochemical approach. In the synthesis, the reaction was stabilised using sodium dodecyl sulphate (SDS), and the Au (III) and Pd (II) ions in the aqueous medium were reduced with continuous ultrasonic irradiation.

Radiolysis

In the 1990s, radiolysis emerged as a significant approach, supported by multiple studies validating the synthesis of bimetallic nanoparticles. This method found application in synthesizing bimetallic nanoparticles of noble metals. For instance, the radiolysis of an aqueous mixture of Ag_2SO_4 and K_2PtCl_4 resulted in the formation of Ag-Pt bimetallic nanoparticles (Remita et al., 1996; Doudna et al., 2011). Furthermore, Ag-Au bimetallic nanoparticles, featuring an Au layer atop an Ag nanoparticle, were successfully produced through radiolysis (Dahir Sagir Idris & Roy, 2023).

Different reducing agents, such as trisodium citrate, hydrazine hydrate, ascorbic acid, alcohols, carbon monoxide, $LiAlH_4$, and $NaBH_4$, were utilized to reduce metal ions to nanoscale dimensions, promoting the creation of bimetallic nanoparticles (Heuer-Jungemann et al., 2019). The successful synthesis of these bimetallic nanoparticles has motivated researchers to delve into the fabrication of more complex multi-metallic nanoparticles. Consequently, the creation of multi-metallic nanoparticles has been achieved through processes such as selective element segregation, diffusion, and electrochemical etching of metals (Saleem et al., 2019).

2.6.3. Monometallic Nanoparticles

Monometallic nanoparticles, as their name suggests, are made up of just one metal. The metal atom that is employed to make these nanoparticles affects their characteristics. The type of metal atom present determines whether the monometallic nanoparticles are magnetic, metallic, or transition metal nanoparticles. The process that is most frequently employed to create monometallic nanoparticles is chemical. Utilizing a variety of functional groups, their structure can be stabilised (Sharma et al., 2019). Below is a summary of the synthesis of the monometallic Au and PdNPs used in this study.

Synthesis of Gold Nanoparticles

Typically, the chemical reduction of gold salt with an appropriate reducing agent is the first step in producing AuNPs (Souza et al., 2019). Particle stabilisation is accomplished by either employing an external capping agent or a reducing agent that also serves as a stabilising agent (Amina & Guo, 2023). AuNPs have been created using various reducing agents, including citric acid, sodium borohydride, and hydrazine (Tyagi et al., 2014).

Studies and procedures have been applied to synthesise AuNPs involving various physical and photochemical reduction, electrochemical reduction, heat evaporation, laser ablation, inert gas condensation, thermolysis, and radiolysis (Kharissova et al., 2019). However, the physical techniques that are now accessible have high prices and a limited production rate of AuNPs. In addition, hazardous substances used in chemical methods will adsorb on the surface of AuNPs (Sarfraz & Khan, 2021).

Synthesis of Palladium Nanoparticles

Historically, a variety of physical or chemical methods employing toxic and hazardous reducing and stabilising chemicals have been used to form PdNPs (Hazarika et al., 2017). Typically, a precursor for palladium that contains palladium in its ionic phase precipitates porous support, including amorphous carbons, alumina, silica, or other mesoporous oxides, before being reduced to Pd°. Moreover, producing PdNPs (Bugaev et al., 2018).

Methods attached to their disadvantages include physical and chemical processes (Roy et al., 2010; Alam et al., 2015; Thakkar et al., 2010). The chemical reduction process is frequently used to synthesise nanoparticles. The bulk of synthetic methods employ reactive reducing substances, including formaldehyde, hydrazine (H_2N_4), and sodium borohydride ($NaBH_4$). In experiments, more reducing agent by volume is introduced than is necessary to maintain stoichiometry due to the extremely reactive reducing agents left in the end products (Roy et al., 2010; Duan et al., 2015). Another downside of such procedures is the development of toxic by-products (Roy et al., 2010; Shankar et al., 2004; Alam et al., 2015; Thakkar et al., 2010). In the physical synthesis method, elevated temperatures and pressures are needed resulting in high

energy consumption (Thakkar et al., 2010). As a result, their usage in biological applications is constrained (Duan et al., 2015).

To correct the surface structure imperfections arising from both physical synthesis and the utilization of hazardous substances leading to detrimental by-products in the chemical synthesis of nanoparticles, a viable alternative is to employ a naturally biodegradable extract. This approach involves biological synthesis methods, which are environmentally sustainable and friendly (Pandit et al., 2022). In this case, an alternate synthetic approach has been developed recently based on Green Chemistry principles (Saleh & Koller, 2018; Kharissova et al., 2019).

Challenges, Limitations and Future Prospective of Nanoparticles

Given the variations in plant constituents across different species and genera, optimizing parameters such as pH, precursor and extract concentration, time, and other factors becomes imperative to achieve nanoparticles with desired size and shape. Stability is another critical aspect to consider in nanoparticle research. While chemically synthesized nanoparticles typically exhibit long-term colloidal stability, the stability of biologically synthesized nanoparticles relies on the presence of capping agents. For instance, in a comparative study where both chemical and biological methods were employed to synthesize silver nanoparticles, the zeta potential values were recorded as 17.8 mV for chemical AgNPs and 15.2 mV for biological AgNPs (Mousavi-Khattat et al., 2018). In biological nanoparticle synthesis, stability is attributed to the role of biomolecules in stabilizing the metal particles within the solution. Additionally, factors such as pH, surface capping agents, and functionalization techniques also influence nanoparticle stability.

2.6.4. Bimetallic Nanoparticles

The formation of bimetallic nanoparticles, encompassing various shapes, sizes, and compositions, brings about alterations in the optical, electrical, plasmonic, thermal, magnetic, and catalytic properties initially attributed to monometallic nanoparticles. The combination of two metal nanoparticles results in the formation of bimetallic nanoparticles that are smaller than their monometallic counterparts. This indicates a significant influence on the miscibility and ordering of bimetallic structures (Zhang & Zhang, 2018).

As the surface-to-volume ratio increases, the amount of active sites also grows, leading to a reduction in the energy barrier and an enhancement in the overall activity for applications. The interaction of two metals in bimetallic nanoparticles results in new properties that expand their functions and applications. A mixture of electronic, lattice, and bifunctionality effects and the ensemble are responsible for the synergism (Zhang & Zhang, 2018).

Types of Bimetallic Nanoparticles

Bimetallic nanoparticles fall into this classification due to their characteristics being influenced by factors such as size, shape, structure, architecture, or the relative arrangement of two distinct metals. The structure and order of mixing two metals are used to form major classes (depicted in Figure 2-4). Alloyed structures (random), intermetallic structures (ordered), core-shell, subcluster, multi-shell core-shell, and multiple core-single are some of the several types of nanostructures (Kumar et al., 2020).

The structure and order of two metals

Bimetallic nanoparticles are characterised as mixed or separated structures based on their structure. As previously stated, mixed structures are classified into random and ordered configurations based on the arrangement of atoms. An alloyed structure is an illustration of a hybrid structure with a random configuration (Velpula et al., 2021). An intermetallic structure is a hybrid structure with a well-organised pattern (Yu et al., 2023). A segregated structure consists of two metals interacting, forming a subcluster structure, or one metal surrounded by another, creating a core-shell structure (Behera et al., 2020).

A solid solution of bimetallic nanoparticles is formed by combining one metal with another in a solid state (Li et al., 2021). These nanoparticles are divided into two types: substitutional and interstitial. When the sizes of two metals are the same, a substitutional structure is generated when one metal is replaced by the other in a lattice structure (Chen et al., 2021). When one metal is smaller than the other, the smaller metal positions itself within the atoms of the larger metal, leading to the formation of interstitial structures (Chen et al., 2021). The arrangement of atoms from two metals can vary based on factors like bond energy, surface energy, atomic radius, charge transfer, and the size of the bimetallic nanoparticles (Srinoi et al., 2018; Yun et al., 2020).

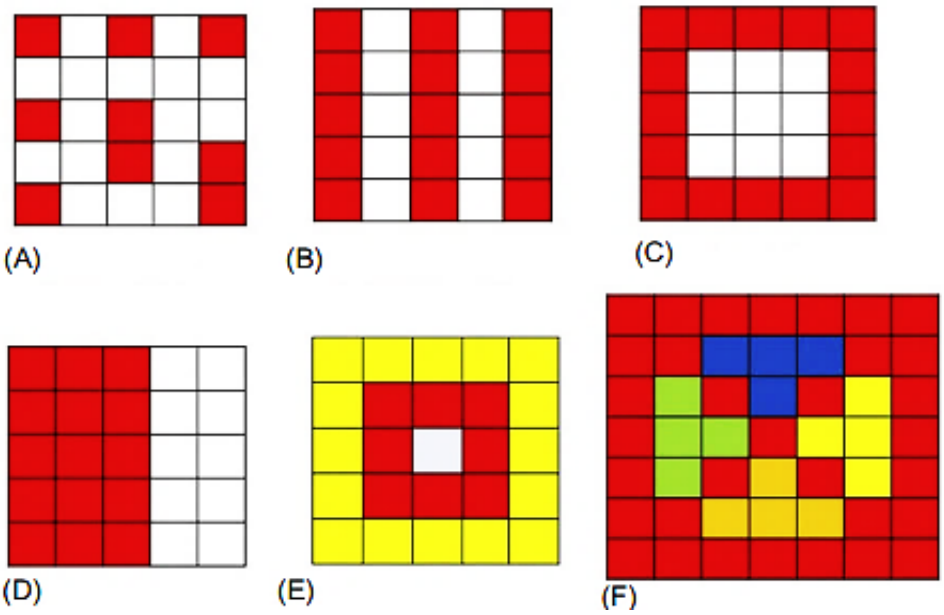

Figure 2-4: A depiction of various nanostructures: (A) random alloyed nanostructure, (B) ordered intermetallic nanostructure, (C) core-shell nanostructure, (D) subcluster nanostructure, (E) multi-shell core-shell nanostructure, and (F) nanostructures with multiple cores and a single shell (Behera et al., 2020)

Dimensions of Bimetallic Nanoparticles

Bimetallic nanoparticles are classed based on their geometry, with zero, one and two-dimensional nanoparticles being the most common (T. Li et al., 2019). Wet synthesis is used to produce zero-dimensional bimetallic nanoparticles (Joudeh & Linke, 2022). The most common varieties of zero-dimensional bimetallic nanoparticles are nanospheres, nanopolyhendrons, nanoframes, and concave and convex nanostructures (Kolahalam et al., 2019). Nanowires, nanorods, and nanotubes are one-dimensional bimetallic nanoparticles, whereas nanosheets, nanoplates, and nanoribbons are two-dimensional bimetallic nanoparticles. The chemical and physical properties differ depending on the number of active sites available (Zhang & Zhang, 2018; Behera et al., 2020).

Bimetallic Nanoparticles: Metal Types Involved

Bimetallic nanoparticles are formed by combining two distinct metals (Zhou et al., 2019). The proportions and mixing patterns of transition and noble metals vary. Various types of bimetallic nanoparticles exist, such as platinum-based ones, renowned for their remarkably efficient catalytic activity, and nickel-based counterparts, prized for their combined catalytic and magnetic properties (Fan et al., 2021). The nickel-based bimetallic nanoparticles are not only cost-effective but also exhibit remarkable stability and a high turnover rate. On the other hand, iron-based bimetallic nanoparticles exhibit better catalytic activity than iron monometallic nanoparticles (Li et al., 2021). Because of their inexpensive cost and availability,

palladium-based bimetallic nanoparticles are employed. Bimetallic nanoparticles made of gold are employed in catalysis, biosensors, and biomedicine (Sharma et al., 2019).

Mixing gold and palladium in a range of nanoparticle geometries has improved behaviour in a variety of industrially related reactions, as has the addition of palladium shells of different thicknesses to gold seed nanoparticles, which has increased surface-enhanced Raman effects (Heuer-Jungemann et al., 2019). It has also been established that the improved properties of Au-Pd nanoparticles may be controlled by modifying the particle composition (Velpula et al., 2021).

Challenges, Limitations and Future Prospective of Bimetallic Nanoparticles

Looking ahead, there are numerous prospects and future perspectives for bimetallic nanoparticles. The advancement of novel synthesis techniques holds the promise of enhancing the production of these nanoparticles with precise control over morphology. This, in turn, offers the opportunity to tailor their activity and selectivity, thus expanding their utility across a broader spectrum of applications. Moreover, bimetallic nanoparticles show promise in driving the development of sustainable and eco-friendly technologies, particularly as catalysts for various environmental endeavors such as water treatment, energy conversion/storage, and air pollution mitigation. For instance, they have been investigated as catalysts for biomass conversion to biofuels, contributing to greenhouse gas emission reduction (Gu et al., 2022). Similarly, their integration into biomedical applications could enhance treatment efficacy and specificity while minimizing side effects (Singh et al., 2016). Additionally, coupling bimetallic nanoparticles with emerging technologies like nanosensors and nanoelectronics holds potential for creating innovative and high-performance devices. However, it's essential to address safety concerns and regulatory aspects surrounding nanoparticle usage, considering the likelihood of intentional or unintentional release into the environment (T. Li et al., 2010; Formaggio et al., 2019). Despite toxicity assessments conducted using different models, uncertainties persist regarding the impact and potential hazards of bimetallic nanoparticles. Further research is imperative to ascertain their toxicological effects, and the establishment of guidelines for their safe handling and disposal is crucial. Overall, the future outlook for bimetallic nanoparticles appears promising, with vast potential applications across diverse fields. Continued interdisciplinary research efforts and collaboration among scientists, engineers, and policymakers will be essential to fully exploit their capabilities and realize their potential in shaping the future landscape of science and technology.

2.6.5. Green Synthesis of Nanoparticles

Researchers in the fields of nanoscience and nanotechnology have high aspirations for the design and development of energy-efficient yet simple, affordable, and environmentally friendly synthesis methods for nanoparticles with structures capable of serving particular tasks and biocompatibility (Alam et al., 2016).

These green synthesis methods are conducted at room temperature and pressure and simplified laboratory set-up. Natural sources provide a diverse range of building blocks that can be used as reducing and stabilising agents to synthesise bimetallic nanoparticles. The reducing and stabilising agents include bacteria, fungi, yeast, enzymes, and plant extracts, which are all bio-renewable (Pandit et al., 2022).

A current area of widespread research interest revolves around the use of plants or plant extracts for the synthesis of metal nanoparticles, gaining considerable acceptance in the scientific community (Ahmeda et al., 2020). This method, involving a single-step process, employs plant extracts to reduce metal salts into nanoparticles. The compounds or phytochemicals present in these extracts play a crucial role in reducing metal ions to nanoparticles and subsequently stabilizing them. The method offers stable nanoparticle dispersions with good oxidation resistance and resistance to agglomeration in biological conditions, which is crucial (Rane et al., 2018). This technique is known to be advantageous compared to physical and chemical methods. Thus, it can be scaled up easily. It has been verified that plant extracts rich in phytochemicals exhibit a faster initiation of bio-reduction compared to microbes and traditional chemical methods (Mittal & Roy, 2021; Nagore et al., 2021). Alkaloids, flavonoids, terpenoids, phenolic chemicals, proteins/enzymes, polysaccharides, vitamins, and other biomolecules found in plant extracts are involved in the reduction, formation, and stabilisation of metal nanoparticles (Ikram et al., 2021).

Reducing metal salts using plant extracts is a straightforward ambient process known for nanoparticle formation (Aboyewa et al., 2021). The procedure involves thoroughly combining the metal salt solution with the plant extract. The reaction concludes swiftly, initiating the bio-reduction of the salt immediately upon the combination of metal salt precursor solutions. The successful synthesis of nanoparticles can be monitored by observing the colour change in the reaction solution (Dikshit et al., 2021). The green synthesis of nanoparticles is broken down into three steps: activation phase, growth phase, and termination phase (Figure 2-5) (Sajjad et al., 2018).

The initial stage, known as the activation phase, involves the utilization of plant metabolites—biomolecules possessing reducing properties—to recover metal ions from their metal salt precursors (Ishak et al., 2019). Subsequently, nucleation occurs as the metal ions undergo a reduction process, transitioning from their mono- or divalent oxidation states to zero-valent states (Malik et al., 2014). This initiates the growth phase, where the biological reduction of metal ions induces the fusion of isolated metal atoms, resulting in the creation of metal nanoparticles. Throughout the growth phase, nanoparticles aggregate to take on various morphologies, such as cubes, spheres, triangles, rods, hexagons, pentagons, and wires (Md Ishak et al., 2019). The growth phase leads to nanoparticle thermodynamic stability, while nucleation results in the aggregation of nanoparticles, altering their morphologies. The termination phase is the last step in the green

synthesis of nanoparticles. When capped by plant metabolites, the nanoparticles obtain their promising and stable morphology (Sajjad et al., 2018).

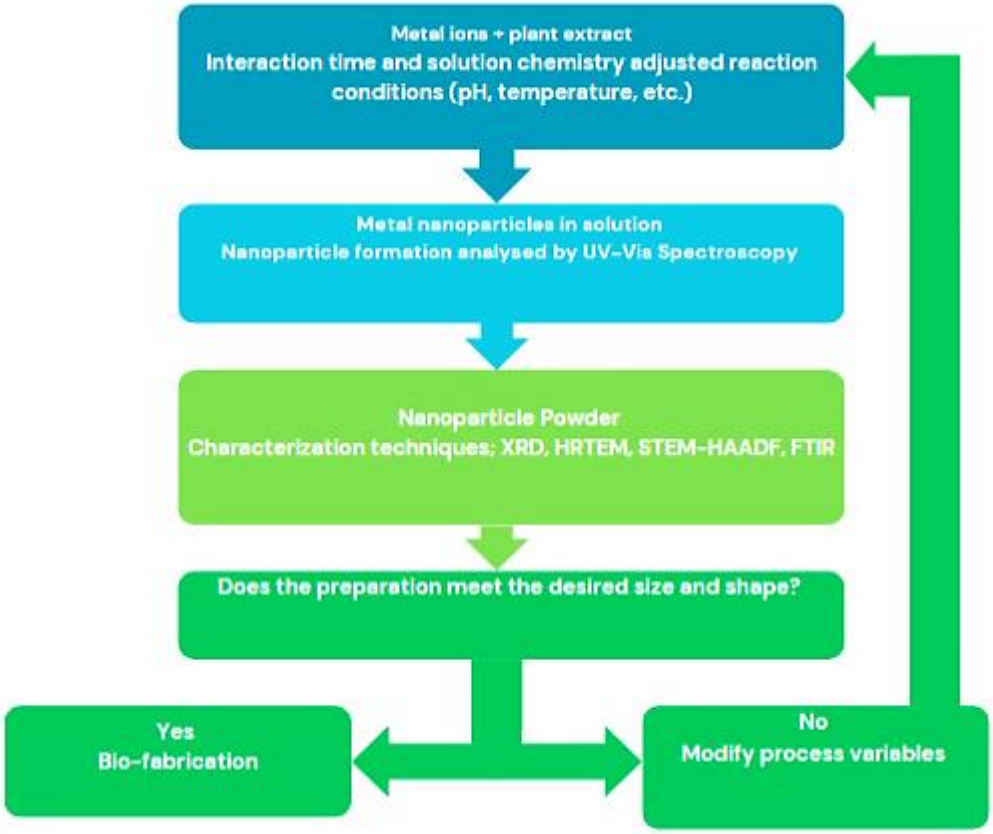

Figure 2-5: An elaborate flowchart illustrating the standard procedures in the eco-friendly synthesis of metal nanoparticles (Sajjad et al., 2018)

Hazarika et al. (2017) highlighted the utilization of plant extracts, bacteria, marine organisms, and similar entities as environmentally friendly reductants in the biological synthesis of PdNPs. Among these biological sources, plant extracts emerge as particularly promising due to their ready availability, rapid processing, cost-effectiveness, and the potential for large-scale biosynthesis. Banana peel extract and leaf extracts from *Pulicaria glutinosa*, *Perilla frutescens*, *Euphorbia granulate*, *Ocimum Sanctum*, and *Origanum vulgare* are a few examples.

On the other hand, the resulting colour of Au nanoparticle solutions depends on the plant extract concentration (Hammami et al., 2021). As outlined by Khan et al. (2020), the proposed reduction process of Au^{+} ions into metallic Au° nanoparticles in the presence of metabolites and enzymes is represented as follows: $HAu^{+}Cl_4 \cdot 4H_2O$ + plant extracts→ Au° nanoparticles + by-products. Moreover, the utilization of *Suaeda monoica* leaf extract facilitated the formation of AuNPs, revealing the involvement of biomolecules

containing carboxyl, amine, and hydroxyl functional groups in the reduction of gold ions. Additionally, stable Au-Pd bimetallic nanoparticles were synthesised using an accessible and environmentally sustainable approach by treating an aqueous tetrachlorogold (III) hydrate, palladium chloride ($PdCl_2$) solution using *Cacumen Platycladi* (CP) leaf extract as both a reductant and a stabiliser (Zhan et al., 2011).

Aspalathus linearis extract has been utilized in the synthesis of various metal nanoparticles, including gold (Akinfenwa et al., 2021; Blom van Staden et al., 2021) and palladium (Ismail et al., 2017; Mayedwa et al., 2018). However, there are currently no reports on the synthesis of Au-Pd bimetallic nanoparticles using Aspalathus linearis. This highlights a significant gap in the literature regarding the use of extract in the plant-mediated synthesis of Au-Pd bimetallic nanoparticles. Noticeably, there is an absence of reports on the utilization of aspalathin as the sole stabilizing and reducing agent in the synthesis of Au-Pd bimetallic nanoparticles. Phytochemical studies of rooibos have identified various flavonoids, including rutin, orientin, quercetin, luteolin, and aspalathin, among others (Stander et al., 2017).

Aspalathin, characterized by its *C*-glucoside dihydrochalcone skeleton, stands out as a distinctive bio-antioxidant, particularly abundant in green rooibos (Koeppen & Roux, 1965). The chemical structure of Aspalathin provides electron-rich and multi-binding sites, making it favourable as a reducing agent in the synthesis of metallic nanoparticles (Nakamura et al., 2003; Akinfenwa et al., 2021). This characteristic of Aspalathin, along with the elevated phenolic content found in rooibos extracts, has been investigated in various studies for potential biomedical applications.

2.7. Applications of Nanoparticles

Due to their special characteristics, such as a sizable portion of surface atoms, significant surface energy, spatial confinement, and decreased shape, metal nanoparticles set themselves apart from bulk materials. According to Rajitha et al. (2021), nanoparticles can be used for biomedical analysis, groundwater cleaning, agriculture, electronics, and catalysis due to their special features. Because of their broad range of antibacterial properties, metal nanoparticles such as gold (Au), palladium (Pd), silver (Ag), copper (Cu), iron (Fe), zinc (Zn), and others find application in various products, including food packaging, wound dressings, catheters for drug delivery, and similar items (Altammar, 2023). Green nanoparticles have a dual role, serving as the foundation for biosensors related to environmental variables and agriculture, as well as playing a crucial role in gene delivery and cell labelling for both plants and pharmaceuticals (Altammar, 2023).

Using bimetallic nanoparticles helps form new materials with desired properties that are impossible to obtain using a single metal atom (Sharma et al., 2019; Dlamini et al., 2023). Due to the composition and synergistic effects, bimetallic nanoparticle properties include electronic, chemical, mechanical, thermal, and biological properties (Berta et al., 2021). The elemental configuration of bimetallic nanoparticles is dictated by the

synthesis procedure, and the relationship between the two metals is not in thermodynamic equilibrium within the system (Loza et al., 2020). The collaboration between the two metals plays a crucial role in the formation of bimetallic nanoparticles (Sharma et al., 2017). Bimetallic nanoparticles such as Pt-Ag, Pt-Rh, Ag-Ni, Au-Pt, Pd-Au, Ni-Au, etc., have already been created. Many attempts have been undertaken to date to construct different Au-Pd nanostructures, such as spherical Au-Pd alloys, hallow Au-Pd nanostructures, and Au-Pd core-shell nanoparticles (Singh & Bhateria, 2021).

Bimetallic nanoparticles are also used in antibacterial and wound dressings. Medical applications of these particles, as reported by Sharma et al. (2019), aid in the easy diagnosis of illness and its treatment, while bimetallic nanoparticles are utilized to reduce the harmfulness and drug side effects in the pharmaceutical sciences. The following is the focus application field of Au-Pd alloy structured bimetallic nanoparticles for this present study.

2.7.1. Biomedical Applications of Nanoparticles

There is growing concern regarding the potential exposure and adverse effects of nanoparticles on both human health and the environment. Over recent years, numerous in vitro and in vivo studies have been conducted to explore the toxicological impacts and potential hazards associated with various nanoparticle exposures. However, there remains a significant gap in our understanding of the toxicity effects resulting from nanoparticle exposures (Sengul & Asmatulu, 2020).

Consequently, depending on how various types of metal nanoparticles interact with organisms, the biosynthesized metallic nanoparticles with non-toxic surface functional molecules still demonstrate differing levels of toxicity. Research examining the toxicity of noble metals such as Ag, Au, and Pd has revealed that silver nanoparticles are highly toxic, primarily due to the gradual oxidation and release of highly reactive Ag^{+} ions. (Adetunji, 2019; Gurunathan et al., 2019; Lee et al., 2019). Due to this, biomedical applications for less harmful Au and PdNPs have shown popularity. The monometallic nanoparticles are pesticide and larvicidal-resistant, antiplasmodial, and anti-cancer (Minal & Prakash, 2020).

. In a study conducted by Steckiewicz et al (2019), it was demonstrated that among the various types of gold nanoparticles examined, star-shaped nanoparticles with a size of approximately 215 nm exhibited the greatest anticancer efficacy but were also the most cytotoxic. Conversely, spherical gold nanoparticles, measuring approximately 6.3 nm, appeared to be the safest option albeit with limited anticancer potential. Moreover, the research highlighted that short-term exposure to gold nanoparticles did not impede cell growth, but prolonged exposure could potentially disrupt cellular metabolism and energy balance.

Additionally, AuNPs possess distinctive qualities, featuring a substantial surface area, stability, and thereby presenting novel possibilities for delivery methods. These nanoparticles are well-suited for anti-angiogenic

applications due to their ease of synthesis and characterization (Saeed et al., 2019). Angiogenesis is crucial in many disorders, including cancer, arthritis, and others, and therefore, AuNPs may help develop novel therapeutic approaches (Bhattacharya & Mukherjee, 2008). Similarly, the selective killing of target bacteria by irradiating AuNPs attached to the bacterial surface with a laser has also been carried out (Yaqoob et al., 2019).

Contrarily, palladium has a range of uses and has been employed as a drug precursor, a toxin degrader, and a monitor for detecting numerous analytes. Pd and Pd^{2+} ions are also required in a variety of biotechnological operations (Mondal et al., 2019). The multidrug resistance of PdNPs against Cronobacter sakazakii strain AMD04 was also investigated. Selecting a bio-source for synthesizing PdNPs with distinct functionalities is critical (Hazarika et al., 2017), and it's crucial to assess the toxicity of these nanoparticles while exploring their potential for antimicrobial applications.

The investigations examining eco-friendly extract-induced Au-Pd bimetallic nanoparticles are well known for their better catalytical activity compared to their monometallic forms, according to Minal & Prakash (2020). The new biosynthesised Au-Pd bimetallic nanoparticles have a number of potential uses, including the potential therapy of cancer, per the evidence on the usage of monometallic AuNPs and PdNPs in catalysis, protein microsensor function, imaging, and bioassay (McGrath et al., 2015; Chowdhury et al., 2018; Badeggi et al., 2020; Wang & Bai, 2020; Wicaksono et al., 2020).

2.8. Characterisation of Nanoparticles

The characterization of nanoparticles revolves around evaluating physicochemical attributes such as molecular weight, identity, composition, purity, stability, and solubility. Various techniques commonly employed for characterising conventional pharmaceuticals can also be applied to assess nanoparticles (Patri et al., 2005). To better understand how nanomaterials behave *in vivo*, it is vital to explore a number of their properties thoroughly. These attributes contain dimensions, surface composition, surface energy, surface charge, and morphology. The techniques employed to examine the specific physicochemical traits of nanomaterials, along with their primary advantages and drawbacks, are concisely outlined here.

2.8.1. X-Ray Diffraction (XRD)

Several X-ray spectroscopic methods depend on X-Ray Diffraction (XRD) as their primary instrument for thoroughly revealing the atomic-level tertiary structures of crystalline materials. (Wang et al., 2019; Sakthivel et al., 2020). Following Bragg's Law, X-ray diffraction entails directing a focused X-ray beam onto the crystalline planes of a sample, causing reflection (Li & Jin, 2020; Sharma et al., 2022). XRD proves to be an invaluable instrument for analysing crystalline dimensions, structure, and lattice deformities resulting from long-range order, although its effectiveness is somewhat constrained when applied to distorted materials. This technique is grounded in X-ray wide-angle elastic scattering. Furthermore, XRD

enables the study of monometallic nanoparticle phase shifts with increasing nanoparticle diameter (Unruh & Forbes, 2019; Rabiei et al., 2020).

XRD can also demonstrate the presence of bimetallic nanoparticles instead of a mixture of monometallic particles, where the mixture of physical combinations, differing from bimetallic nanoparticles, is composed of overlapping lines of two separate monometallic nanoparticles (Olmos et al., 2019). It can be difficult to determine the structural details of metals when they are broken down into tiny nanoparticles with fewer than hundreds of atoms, the interatomic lengths of small particles can fluctuate, and particles can occasionally take on an amorphous shape. To obtain the proper information in these cases, it is required to compare the diffractograms of the bimetallic nanoparticles with the comparable monometallic nanoparticles and their physical mixtures (Ijaz et al., 2020). By contrasting the XRD spectra with computer-simulated ones, the structural model of bimetallic nanoparticles can be provided (Khan et al., 2019).

2.8.2. Ultraviolet-Visible (UV-Vis) Spectroscopy

The most conspicuous characteristic of metal and alloy nanoparticle dispersions for certain metals is their colour. Group 1B metals like Au, Ag, and Cu nanoparticles exhibit distinct colours associated with their particle sizes. The distinctive colouration emerges due to the activation of Surface Plasmon Resonance (SPR) within the metal nanoparticles (Khan et al., 2019; Velpula et al., 2021). This phenomenon results from the interaction of electromagnetic fields with metallic nanoparticles, causing free-conduction electrons to oscillate collectively.

Bimetallic alloy nanoparticles display a single SPR peak typically situated between the SPR peaks of two individual pure metals (Ghosh et al., 2020). The intensity of the SPR band is dependent on factors such as nanoparticle types, morphology, composition, and the surrounding medium. Therefore, analysing UV-Vis spectra for these metals proves to be a valuable complement to other characterization techniques (Joudeh & Linke, 2022).

To validate the bimetallic structure of nanoparticles, a comparison is conducted between spectra of bimetallic nanoparticles and physical mixtures of the corresponding monometallic particle dispersions (Saha et al., 2019). Furthermore, the analysis of spectral UV-Vis alterations during the reduction process can offer valuable insights into illustrating the development of bimetallic nanoparticle processes, encompassing both reducing metal ions and the aggregation phase (Ahmed & Emam, 2019).

2.8.3. Dynamic Light Scattering (DLS)

Size characterization, an important aspect of nanoparticle quality control throughout manufacturing, application, and environmental release, has been effectively conducted through Dynamic Light Scattering (DLS), also referred to as photon correlation spectroscopy, across various disciplines (Raval et al., 2019).

This method is considered classical and has proven valuable in the study of smaller particles by assessing their Brownian motion, correlating it to an equivalent hydrodynamic diameter. The hydrodynamic size is influenced by both mass and shape. Essentially, DLS monitors changes in the amount of elastically scattered light, known as Rayleigh scattering, caused by particles undergoing Brownian motion with a wavelength shorter than the reflected light (Joudeh & Linke, 2022).

The combination of constructive and destructive interferences in the scattered light results in the formation of the intensity fluctuation trace (Alai, 2023). The determination of particle size can be achieved by employing the Stoke-Einstein equation to analyse the motion-dependent autocorrelation function. By using the autocorrelation function and experimental decay determination, the average particle size can be determined from time-dependent fluctuations in high light intensity (Kumar & Dixit, 2017).

The primary advantages of Dynamic Light Scattering (DLS) in characterizing nanomaterials lie in its non-invasive nature, rapid experiment duration (in minutes), precision in determining the hydrodynamic size of monodisperse samples, capability to analyse diluted samples, and its suitability for examining samples across a broad concentration range while detecting trace amounts of higher molecular weight species (Modena et al., 2019). DLS also has lower equipment costs and more repeatable measurements than other techniques (Filipe et al., 2010; Lim et al., 2013).

2.8.4. Zeta Potential

In an ionic solution, a charged particle surface establishes a strong association with oppositely charged ions, forming a thin liquid layer recognized as the Stern Layer, surrounded by a thinner outer layer of loosely connected ions (Kumar & Dixit, 2017). These two layers collectively constitute the "electrical double layer." The movement of charged particles, induced either by an external force or Brownian motion, shears ions as they migrate within a thin layer alongside the charged particle (Clogston & Patri, 2011). The electric potential at the shear surface is known as Zeta Potential. It is determined by gauging the velocity of charged species toward the electrode when an external electric field is applied across the sample solution (Leary, 2022). Particle stability is indicated by the Zeta Potential value, and a threshold of 30 mV is considered significant. A Zeta Potential surpassing 30 mV denotes stability, while a value below 30 mV suggests the potential for flocculation, aggregation, coagulation, or instability (Liu et al., 2022).

Furthermore, results obtained from Fourier Transform Infrared (FTIR) analysis are confirmed by the Zeta Potential measurement. For instance, a FTIR investigation revealed that the stability of green nanoparticles made by tansy fruit extract was influenced by carboxylate anions (Prabha et al., 2010). The finding agreed with the negative surface charge for green nanoparticles from the Zeta Potential analysis. The pH of the solution has a significant impact on this potential (Liu et al., 2022). By evaluating the Zeta Potential, Sathishkumar et al. (2009) examined the impact of pH on the stability of silver nanoparticles made with

cinnamon zeylanica extract. They discovered that increasing the pH levels resulted in improved stability in primary mediums because the absolute zeta potential value increased (Githala et al., 2022).

2.8.5. High-Resolution Transmission Electron Microscope (HRTEM) Imaging

Traditional Transmission Electron Microscopy (TEM) provides visual information on aggregation, size, size distribution, and shape (Khan et al., 2019). In TEM, an electron beam, produced by the electron gun, is accelerated towards an anode plate. Before entering the microscope column, electrons pass through a hole in the anode plate and the Wehnelt cylinder (Iqbal et al., 2019). Within the microscope column, as electrons move through a vacuum, lenses focus them into a concentrated beam above the specimen plane (Malatesta, 2021). The condenser system incorporates a small metallic physical aperture with a central hole, crucial for controlling both the strength and direction of the electron beam convergence (Perez-Campos & Esparza, 2017).

Three things can happen when electrons pass through a sample: they can pass through it unhindered, they can scatter without losing energy (this is known as elastic scattering), they can be inelastically scattered (which involves an energy exchange between the electron beam and the sample), or they can emit secondary electrons or X-rays from the sample (Perez-Campos & Esparza, 2017).

The objective lens, which encloses the specimen and somewhat enlarges the image of the sample, also alters the current passing through it via the microscope's focus adjustment (Malatesta, 2021). The projector lens, which has two additional lenses, magnifies the image even more. The final image of the specimen is created by electrons striking a fluorescent screen after they have exited the projector lenses (Perez-Campos & Esparza, 2017).

2.8.6. Selected Area Electron Diffraction (SAED)

In the characterization of nanoparticle crystal structures, Electron Diffraction (ED), specifically Selected Area Electron Diffraction (SAED), plays a pivotal role as a supporting microscopy method (Agrawal, 2022). While most Transmission Electron Microscopy (TEM) experiments utilize electron backscatter diffraction (Brodusch et al., 2021), ED relies on accelerating electrons through the electrostatic potential to reach the desired energy level and determine their wavelength before colliding with the sample under analysis. The scattering of electrons, induced by the periodic structure of crystalline materials, functions as a diffraction grating (Buffat, 2003).

2.8.7. Energy-Dispersive X-ray (EDX) Analysis

An electron probe with a sub-nm size is used in Scanning-Transmission Electron Microscopy (STEM) (Ortega et al., 2021). Spectra are produced in relation to the energy loss of photons and transmitted electrons using this method, while energy windows or slits are employed to measure the electron and photon

intensities that correlate to the characteristic emission loss. Elemental presence in specimens is indicated by intensity. A 2D map of the samples shows the distribution of the elements and associated electrical structures (Nord et al., 2020). The primary purpose of STEM-EDX is the elemental mapping of local areas by using a sub-nm-sized electron probe and detecting X-ray emissions from them. Energy- Dispersive X-ray (EDX) gives information on the initial transition (Tanaka, 2015). The core-shell structure of bimetallic Pd-Hg nanoparticles was analysed using STEM-EDX, and it was discovered to be a crystalline core-shell structure with a Pd core, and a Pd-Hg ordered alloy shell (Deiana et al., 2015).

2.8.8. Scanning- Transmission Electron Microscopy- High Angle Annular Dark Field (STEM-HAADF)

In Scanning-Transmission Electron Microscopy (STEM), a convergent electron beam is precisely focused on a small sample area. The electron probe traverses the material in a raster-scanning manner to capture an image (Peters et al., 2023). The interaction between electrons and the substance scatters the electron trajectory, resulting in the capture of various signals synchronized with the scanning of the electron probe. The spatial resolution of STEM is dictated by the size of the probe.

STEM offers distinct advantages over the conventional broad-beam illumination mode (Lin et al., 2021). A key advantage lies in the chemical sensitivity of the signal generated by electrons dispersed at high angles, detected by a HAADF detector. Importantly, a clear crystalline organization is not always necessary for effective sample analysis (Yang et al., 2022).

Its contrast in biological sample analysis is an additional benefit. The contrast of HAADF images of samples with a thickness of 100-120nm is superior to that of images made using other methods (Elbaum et al., 2021). The ability of STEM to produce these various contrast levels is referred to as Z-contrast. The contrast dependency roughly follows Z^2, where Z is the atomic weight of the element that generated the electron scattering (Lin et al., 2021). The STEM technique directly visualises the atomic structure and composition of nanostructures at a sub-angstrom resolution by combining the HAADF-STEM imaging with the new aberration correcting era. HAADF-STEM imaging thereby directly resolves alloying in metallic nanoparticles at a tiny scale (Duschek et al., 2019).

2.8.9. Fourier Transform Infrared (FT-IR) Spectroscopy

Infrared spectroscopy is a vital tool to characterise the structure of matter at the molecular scale. One can show its elements and bonding arrangement based on the single vibrational modes of the several branches or parts of a molecule (Bansal, 2023). Additionally, the reverse process is possible due to the unique infrared spectrograph a molecule has, equal to the fingerprint that can display its identity. FTIR is a method based on the infrared spectroscopy principle, and its area of application has been extended to study nano-scaled objects (Baudot et al., 2010).

Moreover, FTIR characteristic spectral bands are utilized for identifying biomolecule conjugation (such as proteins adhered to the surface of nanoparticles), organic functional groups (e.g., carbonyls, hydroxyls), and the conformational states of bound proteins (Jemilugba et al., 2019). In recent times, Attenuated Total Reflection (ATR-FTIR) spectroscopy has become increasingly popular. ATR-FTIR uses the total internal reflection characteristic in combination with IR spectroscopy to analyse the structure of a sample at the interface of solid/air or solid/liquid. As it overcomes the drawbacks of sample preparation and the challenges in reproducing spectral lines, it is considered superior to traditional IR methods (Hind et al., 2001; Johal & Johnson, 2018). An ATR-FTIR system involves total internal reflectance occurring inside the internal reflection element (IRE) crystal. When observed from a specific angle, the specimen penetrates into the sample at a depth of 0.5-5 μm. From the interface, there is an exponential decrease in the intensity of these waves (Johal & Johnson, 2018).

2.8.10. Nuclear Magnetic Resonance (NMR)

Metal isotope NMR spectroscopy provides valuable insights into the electronic environment of metal atoms within metallic particles through NMR shifts induced by free electrons, known as Knight Shifts. The NMR spectra of metal nanoparticles with Pauli paramagnetic properties are influenced by the density of energy levels at the Fermi energy and the corresponding wave function intensities at each site or the local density of states (LDOS) (Yun et al., 2020). Distinctions in s-like and d-like LDOS in Pt nanoparticles can be inferred from the 195Pt NMR spectra, offering insights into the coordination of metal atoms and the occurrence of bimetallic formation. Furthermore, understanding the electronic properties of metal nanoparticles is crucial for investigating their catalytic properties. Utilizing ^{13}C and ^{1}H NMR to comprehend the structures of organic molecules adsorbed on the surface of metal nanoparticles further enriches our understanding (Bansal, 2023).

2.9. Stabilisation of Nanoparticles

Metal nanoparticles are known to have the ability to agglomerate (Mousavi-Kouhi et al., 2021). Hence, the use of protective or passivating agents to prevent agglomeration is needed. Thus, the protective agent is essential for the metal salt reduction process. Polymers and surfactants are commonly used to protect or stabilise (Sultana et al., 2020). In order to prevent particle agglomeration, regulate particle development, and provide steric hindrance between nanoparticles, polymers are introduced during the reduction process (Javed et al., 2020). Surfactants create a layer of the molecular membrane around nanoparticles (Okoroh et al., 2019). Electrostatic repulsion and steric stabilisation are common methods for preventing nanoparticle aggregation.

Charged particles employ an electrical double layer to repel one another in electrostatic repulsion, which is dependent on the Zeta Potential and the Debye length (Karmakar, 2019). The chemisorption of charged

species at the surfaces of nanoparticles is the source of these repelling forces. The solution is diluted, and the pH is adjusted to accomplish this (Lunardi et al., 2021).

On the other hand, steric stabilisation is a more commonly applied method than electrostatic stabilisation because of the issues associated with the stability of nanoparticles at a high or low pH when electrostatic stabilisation is used (Chakraborty & Panigrahi, 2020). This is made possible by adding protective agents such as polymers, surfactants, and complexing agents (Chakraborty & Panigrahi, 2020). Furthermore, protective agents sometimes act as growth inhibitors and shape controllers besides preventing agglomeration.

2.9.1. Effect of Biological Media on the Stability of Nanoparticles

The stability of components in nanoparticles is a vital part of their biological function (Selvamani, 2019). Any component of the composite preparation that is released too soon may render it useless. For instance, if the targeting agent is cut or released too soon in a nano-delivery system containing a drug, the drug-containing nanoparticles cannot connect to the appropriate targeting location (Lu et al., 2016; Patra et al., 2018). If the medicine is administered too soon, there would no longer be a therapeutic advantage even if the nanoparticle successfully reaches its target (Chenthamara et al., 2019). This makes it essential to determine the functional component stability *in vitro* under physiological conditions.

The release profile should be evaluated at varied ionic strength, pH, and temperature conditions for nanomaterials that provide targeted or time-based drug delivery with an encapsulated drug (Patra et al., 2018). Examples of such conditions include the stability in biogenic media or buffers such as Phosphate Buffer Saline (PBS) and serum at 37°C. Several nanoparticle methodologies are being explored, including the selective release of components triggered by an external stimulus after targeted delivery (Castillo et al., 2019).

a) Phosphate-Buffered Saline (PBS)

Phosphate-buffered saline (PBS) is a water-based buffer solution comprising phosphate buffer, sodium chloride, and potassium chloride formulations (Janeiro et al., 2021). This buffer effectively stabilizes the solution's pH, while the inclusion of salts ensures ion concentrations and osmotic pressure akin to those in the human body. Renowned for its isotonicity with most human cells, PBS is extensively utilized in cell biology applications. Its versatility extends to cell culture tasks such as washing, transporting, and diluting cells (Dmitriev, 2017), preparing and maintaining live tissue (Barretto & Schnitzer, 2012) and bacteria (Nazemi et al., 2015). Additionally, PBS finds utility in DNA sensing (Layouni et al., 2020), and packaging of contact lenses (Kim & Ehrmann, 2020), as part of surface functionalization, and serving as a washing and transport medium.

b) Bovine Serum Albumin (BSA)

Serum albumin is among the most prevalent and well-studied universal proteins found in the plasma of animals (SA) (Javed et al., 2020). This protein's primary functions include maintaining the blood's pH balance, controlling colloidal osmotic pressure, and transporting diverse chemicals of several types, including ionic, hydrophilic, and hydrophobic compounds. Bovine serum albumin (BSA) has a molecular weight of 66 kDa and 582 amino acids, including 35 threonines and 32 serines (Javed et al., 2020). BSA exhibits multiple binding sites due to the presence of charged functional groups such as carboxyl, sulfhydryl, and amino. Furthermore, these sites facilitate the binding of various therapeutic entities, including medications, poly-conjugated dyes, and nanoparticles. BSA enhances the bioavailability of loaded nanoparticles by serving as a capping agent (Javed et al., 2020). Cells absorb it as an amino acid and nutrient source through specific receptors located on the surface of tumour cells. Similar to PVP, the mild reducing ability of BSA, attributed to its hydroxyl group, enables the formation of metal nanoplates from metals such as palladium (Pd), gold (Au), platinum (Pt), and silver (Ag) (Au et al., 2010; Bolaños et al., 2019).

In accordance with JyothiKumar et al. (2019), BSA was employed as a capping agent to stabilize AuNPs. BSA has exhibited remarkable properties in stabilizing and controlling the size of bio-conjugated AuNPs. In a separate investigation, a sensor based on the inner filter effect was developed using AuNPs and BSA-capped cadmium sulphide quantum dots (CdS QDs) for the detection of heparin and protamine (Li & Yang, 2015). Beyond its role as a structure-directing agent, BSA plays a regulatory role in nanoparticle assembly, nucleation, and growth. Studies have demonstrated that cuprous oxide (Cu_2O) nanoparticles coated with BSA can emulate biomineralization, leading to the formation of a hierarchical structure (Zhao et al., 2019; Javed et al., 2020).

c) Glycine (GLY)

Glycine, the smallest and most chemically neutral of all amino acids, is a non-essential, hydrophobic α-amino acid known for its non-polar nature. Many animal and insect cell culture mediums contain it as a component. Glycine serves various crucial roles in cell culture, including its involvement in the cellular production of proteins, earning its classification as a protein genic amino acid.

Additionally, glycine aids in purine production within the cell, provides protection to cells in culture from osmotic stress due to its buffering capability, and plays a crucial role in numerous anabolic reactions, including the synthesis of heme, creatine, and glutathione. In addition, it has been discovered that the glycine cleavage pathway is linked to cell proliferation in several human cancer cell lines (Kruer et al., 2016). The growth of mouse and cattle embryos is improved by the presence of glycine in conditioned media. Many neuropsychopharmacology drugs target glycine as their primary target because it functions as an inhibitory neurotransmitter in the brain and spinal cord (Marques et al., 2020).

d) Cysteine (CYS)

To find out whether 20 amino acids could reduce and stabilise metal ions, their effects on the environment were investigated (Tan et al., 2010). The carbonyl groups on the side chains of amino acids were later discovered to be the mechanism by which they attach to metal ions. Asparagine, glutamine, threonine, methionine, serine, thymine, and cysteine are just a few examples of amino acids that interact with metal ions by binding to them through their side chains (Alia et al., 2019). Cysteine is an essential amino acid that is often utilised in cell culture media and plays an important function in protein formation. It also acts as a precursor for essential compounds such as glutathione, taurine, and coenzyme (Chevallier et al., 2021; Stipanuk et al., 2006). Furthermore, cysteine is a thiol-containing molecule in their side chains that contributes to the intracellular redox state and functions as a reducing agent for the metal ions (Bin et al., 2017).

Cysteine is a promising molecule for bio-functioning AuNPs and mediating their assembly with gold surfaces (Sohrabi et al., 2021). The simplest imitators of protein surfaces are gold surfaces with amino acid coatings. Rodríguez-Zamora et al (2020) described the interactions of amino acids with metallic nanoparticles and the cysteine binding to AuNPs. Of all the amino acids, cysteine was employed as both a reducing and capping agent for the AuNPs. The S-Au interaction in cysteine-capped AuNPs was also studied, and cysteine binding to gold was compared to that of leucine and asparagine (Mahakal & Suse, 2020).

e) Dulbecco's Modified Eagle Medium (DMEM)

The most often utilized variation of Eagle's medium is Dulbecco's Modified Eagle Medium (DMEM). A modified version of Basal Medium Eagle (BME), DMEM, has four times the number of vitamins and amino acids that BME does (Mukherjee et al., 2023). The formulation also contains serine, ferric nitrate, and glycine. Originally used to cultivate embryonic mouse cell cultures, the original formulation contains 1000 mg/L of glucose. The original DMEM has been modified, and DMEM high glucose now includes 4500mg of glucose per litre. A number of other cell lines, including primary cultures of mouse and chicken cells, as well as many normal and altered cell lines, have shown promise in the cultivation of extra glucose (De Vriendt, 2020).

f) Sodium Chloride (NaCl)

Salt, commonly known as sodium chloride (NaCl), is a substance that the body needs for numerous processes to take place (Preuss, 2020). It helps maintain the proper conditions for muscle and neuron function, blood pressure control, fluid balance, and the absorption and transportation of nutrients across cell membranes. Additionally, the stability of nanoparticles is often evaluated against varying concentrations and volumes of NaCl. The addition of NaCl, a strong electrolyte, hides the negative charges of the colloidal

AuNPs and causes them to clump together to form bigger particles. Furthermore, agglomeration can happen when nanoparticles are exposed to high salt solutions, as found in most physiologically compatible media (Cen & Chen, 2021). Agglomeration can take place promptly or gradually over several days, contingent upon the nature of the substance, nanoparticle size, and surface characteristics (Carpen et al., 2023). Once the particles agglomerate, they behave like much larger particles and can settle quickly. On the other hand, Shahjahan et al (2023) reported that the size of AuNPs decreased with increasing NaCl concentration in an aqueous solution of auric chloride. Additionally, the AuNPs formed with the addition of NaCl solution ranged in size from 5 to 16nm, while the nanoparticles without NaCl ranged in size from 11 to 32nm (Fayaz et al., 2011).

g) Polyethylene Glycol (PEG)

Polyethylene glycol (PEG), with the structural formula H-(O-CH_2-CH_2)$_n$-OH, stands out as an excellent biocompatible polymer (Tohamy et al., 2021). In the production of PEG, ethylene glycol undergoes poly-condensation in the presence of an acidic or basic catalyst, leading to a product with a reduced molecular weight (Stefaniak & Masek, 2021). Employed in both aqueous and organic solutions, this substance's dissolution capability enhances its biocompatibility and process ability, making it non-immunogenic and less harmful, thus extensively used in surface modification with other substances, like biomaterials, micelles, and particles, facilitating the transportation of active molecules and the creation of physical and chemical hydrogels.

PEG is not hydrolytically separated *in vivo*, yet it possesses enhanced water affinity and biodegradability due to its hydrophilic properties, making it a popular choice in nanotechnology as a capping agent for diverse applications, such as sustained and targeted medication delivery in the biomedical industry, involving the wet-chemical synthesis of coating metal and metal oxide nanoparticles with PEG (Rajitha et al., 2021). PEG has been employed as a capping agent in studies involving metal nanoparticles, including Au (Zamora-Justo et al., 2019), Ag (Pinzaru et al., 2018), and Zn (Singletary et al., 2017). The aim of these investigations is to reduce cytotoxicity, enhance stability, and improve biocompatibility.

2.10. Biological Activity of Nanoparticles

The health and metabolism of a cell, as determined by its viability and proliferation rates, can be impacted by both physical and chemical agents (Buckner et al., 2019). These substances have the ability to damage cells in a variety of ways, including the rupturing of cell membranes, the inhibition of protein synthesis, irreversible binding receptors, the inhibition of oligodeoxynucleotide elongation, and enzymatic processes (Chenthamara et al., 2019). To detect the cell death of these processes, short-term cytotoxicity and cell viability assays must be inexpensive, dependable, and reproducible (Achparaki et al., 2018).

There are several methods for determining the vitality of adherent cell lines (Sigma-Aldrich Co. LLC, 2016) These methods can be broadly divided into four groups (Figure 2-6), or essays, that monitor four different phenomena: (a) loss of membrane integrity, (b) loss of metabolic activity, (c) loss of monolayer adhesion, and (d) cell cycle analysis (Buckner et al., 2019). It is possible to identify cell lines that are vulnerable to nanoparticle toxicity using the information from these repeated viability studies, which may also reveal details on the nature (i.e., cytostatic/cytotoxic) and location of cellular harm. Several of the cytotoxicity assays covered below are available for purchase (Achparaki et al., 2018).

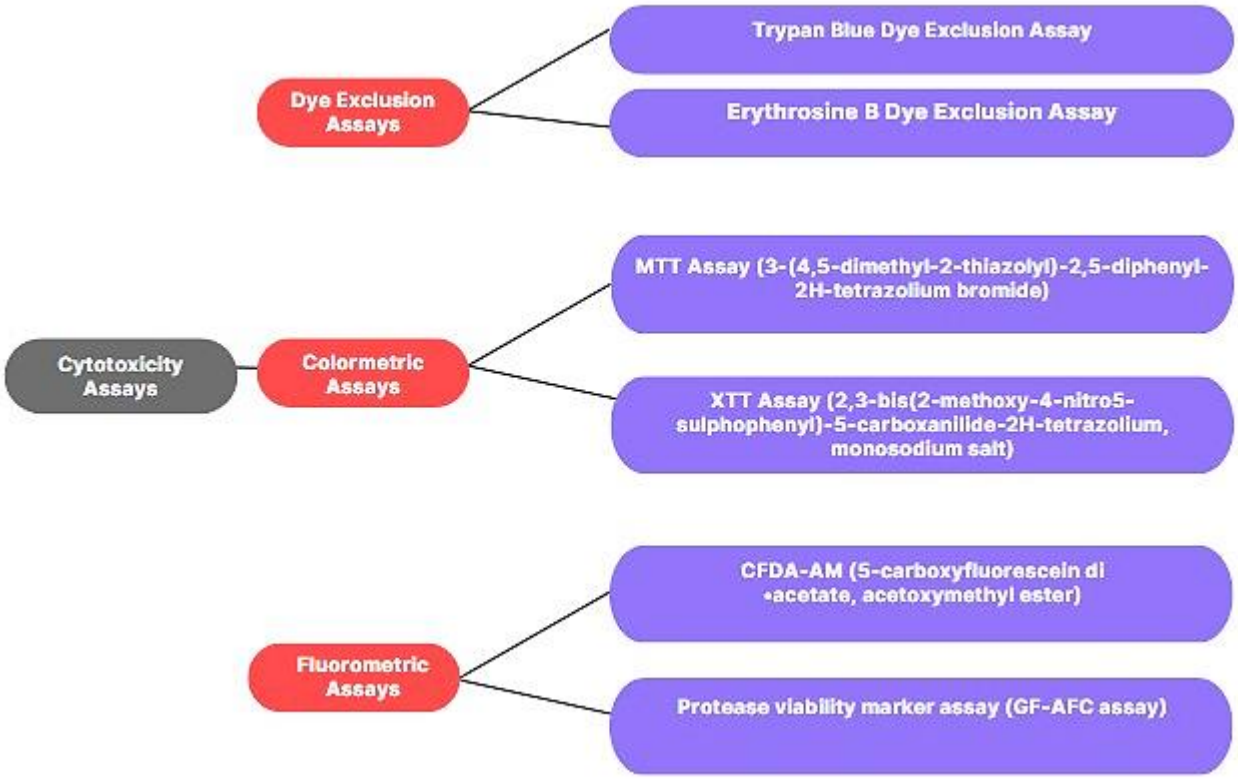

Figure 2-6: A schematic diagram of the several cytotoxicity assays (Achparaki et al., 2018)

a) Dye Exclusion Assays

There are numerous methods for calculating the percentage of viable cells in a cell population (Kamiloglu et al., 2020). The dye exclusion method, the most basic and widely used approach, involves live cells blocking colours, while dead cells do not. Despite the simplicity of the staining technique, conducting experiments on several samples using this method can be difficult and time-consuming. The dye exclusion method can be used to assess the integrity of the membrane. These dyes, including eosin, Congo red,

erythrosine B, and trypan blue, have already been utilized in various applications (Askin Celik & Aslantürk, 2013; Aslantürk & Celik, 2013; Eisenbrand et al., 2002).

Trypan blue has been used the most frequently of all the dyes described. The following considerations must be made when using dye exclusion tests: the surviving cells may continue to grow during this time; (i) lethally damaged cells may lose their membrane integrity over several days; (ii) lethally damaged cells may disintegrate too quickly; and (iii) some lethally damaged cells may not be stained with dye at the final stage of the culture period (Pandey et al., 2023). Factors (ii) and (iii) may cause an underestimation of cell death when the assay results are based on the expression of %viability (Lee et al., 2005; Son et al., 2003).

The use of dye exclusion assays for chemosensitivity evaluation has a number of benefits (Du Puch et al., 2021). They can detect cell death in populations of non-dividing cells, are quick and simple, and only a modest number of cells are required (Nozhat et al., 2021). The potential application of these assays in chemosensitivity assessment needs more investigation. None of these colours, however, are suggested for monolayer cell cultures; rather, they are made for suspended cell cultures. Therefore, trypsinization of monolayer cells is required first (Achparaki et al., 2018).

b) Colorimetric Assays

The core component of colorimetric assays is measuring a biochemical marker to determine cell metabolic activity (Kamiloglu et al., 2020). A spectrophotometer can assess cell viability by employing reagents used in colorimetric tests that change colour in response to cell viability (Aslantürk, 2018). Colorimetric assays, which are simple to perform and inexpensive, can use adherent or suspended cell lines (Präbst et al., 2017). Several companies sell commercial kits for colorimetric assays, and kit packages frequently include practical instructions for these experiments. The following are the most frequently used colorimetric assays:

MTT, a water-soluble yellow tetrazolium dye, is degraded by living cells to yield formazan, a purple, water-insoluble crystal (Setiawati et al., 2022). Formazan dissolved in DMSO can be evaluated by measuring the solution's absorbance at 570nm. When the spectra of the samples from cells treated with nanoparticles are compared to those of cells not treated with nanoparticles, a relative estimate of cytotoxicity is obtained (Patri et al., 2019; Kamiloglu et al., 2020).

Modern tetrazolium dyes that generate water-soluble formazans are excluded from the solubilization step of the MTT experiment (e.g., XTT) (Vasiljevic et al., 2020). However, the frequently unstable intermediate electron acceptor requirement in these analogues increases assay variability (Ghasemi et al., 2021). In addition, the extracellular reduction resulting from the net charge of these more recent compounds restricts cellular uptake (Berridge et al., 2005). MTT has a net positive charge, so it quickly passes through cell membranes and is mostly gone from the mitochondria.

The conventional MTT assay seems to be the preferable method for determining cellular viability in nanoparticle cytotoxicity experiments because it has been shown that nanoparticles interact with cell membranes and may potentially interfere with the reduction of the newer generation analogue via trans-plasma membrane electron transport (Ghasemi et al., 2021). It has been established that substances that are antioxidants, substrates for, or inhibitors of drug efflux pumps affect the MTT assay (Yun et al., 2020). Functionalized fullerenes mess up MTT assays, which leads to more MTT reduction and an overestimation of cell viability (Buckner et al., 2019), even though they are neither efflux pump inhibitors nor substrates and have intense antioxidant activity.

c) Fluorometric Assays

Conducting fluorometric studies of cell viability and cytotoxicity is made simple by using a fluorescence microscope, fluorometer, microplate reader, or flow cytometer (Aslantürk, 2018). Numerous benefits distinguish these tests from conventional dye exclusion and colorimetric techniques (Mani & Swargiary, 2023) Fluorometric tests are easy to execute and are relevant to adherent and suspended cell lines. These tests have higher sensitivity than colorimetric tests (Riss et al., 2004). Numerous firms sell commercial fluorometric assay kits. Typically, these kits include instructions on how to perform the respective treatments (Nolan et al., 2019).

According to Achparaki et al. (2018), CFDA-AM, a fluorescent dye (5-carboxyfluorescein diacetate, acetoxymethyl ester), is used to assess cytotoxicity, serving as a measurement of the stability of the plasma membrane. The dye CFDA-AM being a non-toxic esterase substrate that, when employed by non-specific esterase of living cells, converts a membrane-permeable, non-polar, non-fluorescent substance into carboxyfluorescein (CF), a polar fluorescent dye. Since an esterase-friendly environment inside the cell can only be kept by an intact membrane, and the fact that the cells can change CFDA-AM to CF shows that the plasma membrane is in good shape (Flampouri et al., 2019).

d) Luminometric Assays

Mammalian cells can be measured for cytotoxicity and cell proliferation using luminometric assays in a quick and straightforward manner (Mazumdar & Chowdhury, 2021). A luminometric microplate reader can be used to detect the outcomes of these studies, which can be performed in a 96-well or 384-well micrometre plate format that is simple to use (Tamang et al., 2023). After adding the reagent, luminometric tests produce a signal that is both persistent and steady. Utilizing this feature permits the generation of cytotoxicity and viability values from the same well (Aslantürk, 2018). Numerous businesses sell luminometric test kits that often contain practical instructions.

The luminometric assay for adenosine triphosphate (ATP) is the primary chemical energy source for cellular synthesis, signalling, transport, and movement. Therefore, ATP is one of the most sensitive cell viability

measurements (Gilbert et al., 2019). Cells that have suffered fatal damage and lost the ability to make ATP exhibit a dramatic drop in ATP levels, which is contingent upon the conversion of luciferin to oxyluciferin. This reaction is catalysed by the enzyme luciferase in the presence of Mg^{2+} ions and ATP, resulting in the emission of a luminous signal.

The luminous signal strength is proportional to the ATP concentration or cell count (Ley-Ngardigal & Bertolin, 2022). The ATP test reagent is often used in 1536-well plates because it can often find less than ten cells per well.

Chapter 3

3. Methodology

3.1. Introduction

Through careful selection from a variety of plant extracts, *Aspalathus linearis*, commonly known as unfermented green rooibos (GR), emerged as the preferred choice due to its rich polyphenol content. This selection played a pivotal role in establishing the foundation for the extraction, isolation, purification, and analytical procedures employed to verify the purity and structure of aspalathin (ASP), a C-glucosyl dihydrochalcone abundantly present in GR plant extract. In the quest for sustainable and environmentally friendly nanoparticle synthesis methods, this chapter offers a comprehensive overview of the methodologies used in the synthesis of gold (Au), palladium (Pd), and Au-Pd bimetallic nanoparticles (NPs). Furthermore, it sheds light on the techniques applied to use their distinctive properties in crafting nanomaterials with a wide range of applications. Subsequently, the chapter delves into *in vitro* stability studies of the nanoparticles in biological media. The chapter ends off by subjecting the nanoparticles to cytotoxicity tests against various cell lines, including human melanoma, human epidermal keratinocytes, human fibroblasts, and liver hepatocellular carcinoma cells. Additionally, cellular uptake analysis is conducted.

3.2. Materials and Chemicals

Standardized reagents were used for all solvents involved in extraction and column chromatography. The resin column, supplied by Merck in Gauteng, Modderfontein, South Africa, and Sephadex LH-20 from Sigma-Aldrich in Cape Town, WC, South Africa, served as stationary phases and were accommodated by glass columns of varying diameters. Polystyrene 96-well microlitre plates were sourced from Greiner bio-one GmbH in Franken Hauser, Baden-Württemberg, Germany.

Chemicals, such as sodium tetrachloroaurate (III) dihydrate $NaCl_4 \cdot 2H_2O$, palladium (II) chloride ($PdCl_2$), hydrochloric acid (HCl), sodium hydroxide (NaOH), sodium chloride (NaCl), and glycine (GLY), were procured from Sigma-Aldrich in Cape Town, Western Cape, South Africa. L-cysteine (CYS) and Folin-Ciocalteu's (FC) phenol reagent originated from Boehringer Mannheim GmbH in Mannheim, Baden-Wurttemberg, Germany. Dulbecco's Modified Eagle Medium (DMEM), Fetal Bovine Serum (FBS), Trypsin/Ethyl Diamine Tetra Acetic Acid (EDTA) were obtained from Gibco Invitrogen in Karlsruhe, Germany. Phosphate-Buffered Saline (PBS) was purchased from Lonza in Cape Town, Western Cape, South Africa. Bovine Serum Albumin (BSA) was sourced from Miles Laboratories in Pittsburgh, PA, USA. Additionally, Dimethylsulphoxide (DMSO), Penicillin, Streptomycin, 3-(4, 5-dimethylthiazolyl-2)-2, 5-diphenyltetrazolium bromine (MTT), and Trypan Blue (TB) were acquired from Sigma-Aldrich in Steinheim, Germany.

Cell lines, namely SKMEL-1 (human melanoma cell line), HaCAT (human epidermal keratinocyte cell line), KMST-6 (human fibroblast cell line), and HepG2 (liver hepatocellular carcinoma cell line), were procured from the American Type Cell Culture (ATCC) in Manassas, USA.

3.3. Isolation and characterization of Aspalathin

3.3.1. Collection and extraction of plant materials

The GR plant extract was received as a gift from the Rooibos Limited Company.

One kilogram of GR plant extract underwent extraction using four litres of acetone without exposure to light for 24 hours at room temperature. Following this, the sample was subjected to a three-hour heating period at 50°C in a water bath, succeeded by a 24-hour standing period. Following concentration, the resultant total extract (27 g) was transferred to vials and stored in a dry environment for subsequent use. It is worth mentioning that the solvent recovered from the rotary evaporators was effectively recycled.

3.3.2. Extraction and Isolation of *Aspalathus linearis*

A fraction of the total extract (27 g) underwent resin column chromatography (75 × 10 cm) with a gradient elution system (H_2O: MeOH), and 500 mL fractions were systematically collected. The concentrated fractions were monitored using TLC and then consolidated into 12 primary fractions, designated as 1-12. From the primary fraction N1-13-5, a semi-pure compound was obtained, subsequently subjected to further purification on a Sephadex column using a gradient mode ranging from 100% H_2O to 100% MeOH, resulting in the isolation of the major compound, Aspalathin (ASP).

Table 2: Chromatographic extraction of *Aspalathus linearis* plant extract (main fraction)

No	H_2O	MeOH	Ac	Total Volume (mL)
1	100%	-	-	500
2	90%	10%	-	500
3	80%	20%	-	500
4	70%	30%	-	500
5	60%	40%	-	500
6	50%	50%	-	500
7	40%	60%	-	500
8	30%	70%	-	500
9	20%	80%	-	500
10	10%	90%	-	500
11	-	100%	-	500
12	-	-	100	500
13	-	-	100	500
14	-	-	100	500

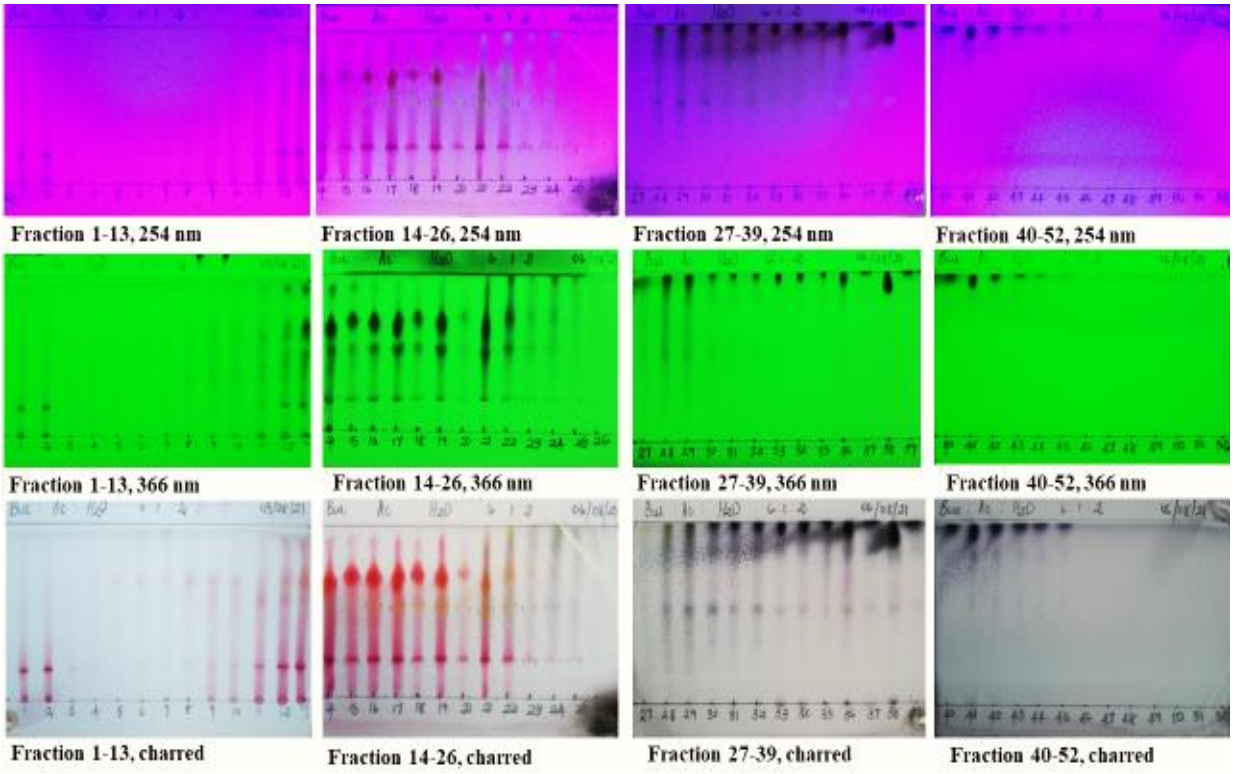

Figure 3-1: Preliminary chromatographic column fraction's TLC fractions under UV (254nm, 366nm, and heated plate with vanillin)

Table 3: Fractions collected from the main resin column

Code	Combinations	Weight Recovered (mg)
N1-13-1	1-2	12349.9
N1-13-2	3-8	12867.8
N1-13-3	9-10	12512.9
N1-13-4	11-13	12468.2
N1-13-5	14-15	12547.3
N1-13-6	16-18	12266.6
N1-13-7	19-23	12417.5
N1-13-8	24-27	11551.6
N1-13-9	28-30	12634.6
N1-13-10	31-35	12366.9
N1-13-11	36-40	12394.1
N1-13-12	40-45	12319.1

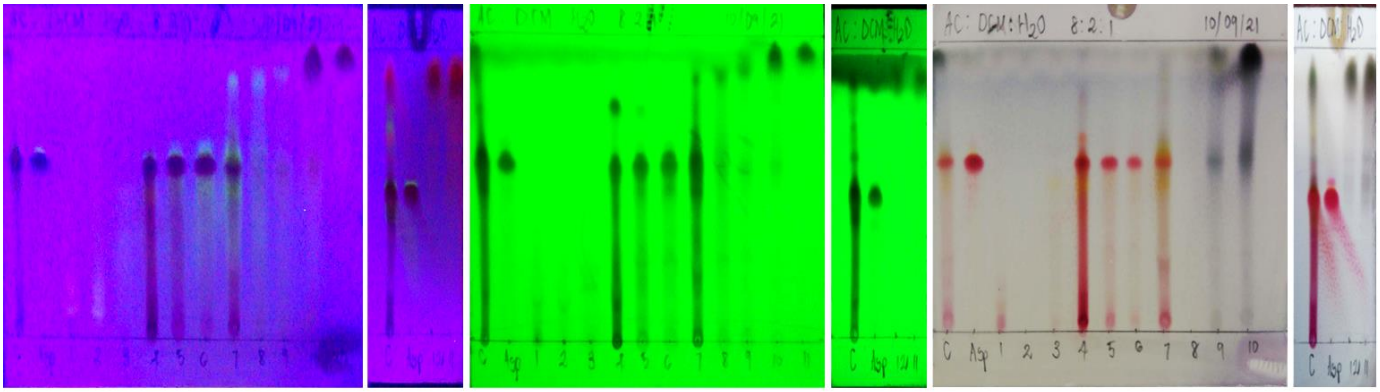

Combined Fraction, 254 nm Combined Fraction, 366 nm Combined Fraction, Vanillin

Figure 3-2: TLC of combined fraction leading to sub-fractions 1 to 12 at 254 nm (A), 366 nm (B), and (C) vanillin charred plate

3.3.3. Characterization of the Isolated Compound(s)

The isolated compound underwent characterization through infrared spectroscopy (Perkin Elmer 100 model in transmission mode) and Nuclear Magnetic Resonance (NMR) spectroscopy. NMR spectra were meticulously recorded at 20°C using deuterated DMSO-d6 on a Bruker Advance 400 MHz NMR spectrometer (Germany). Chemical shifts in ppm of ^{1}H (δH) and ^{13}C (δC) were precisely determined with dimethyl sulfoxide (DMSO) serving as an internal reference.

3.4. Synthesis of Nanoparticles

Both the water extract of GR and ASP were used separately to synthesize the nanoparticles.

3.4.1. Extraction of *Aspalathus linearis*

About 300 g of the plant extract was precisely measured, and 1500 mL of distilled water brought to a boil was added. The plant extract solution was allowed to cool to room temperature. Subsequently, the solution underwent filtration using a funnel and cotton before being transferred into falcon tubes. The extract within the falcon tubes then underwent centrifugation for 60 minutes at 5000 rpm. The resulting centrifuged product was further filtered through a 0.45 microliter filter attached to a syringe and deposited into clean, sterile 50 mL falcon tubes. The 1500 mL solution was recovered and filtered again before the lyophilisation process.

3.4.2. Lyophilisation of *Aspalathus linearis*

Lyophilisation, commonly known as freeze-drying, finds extensive application across diverse industries, including pharmaceuticals, cosmeceuticals, nutraceuticals, chemicals, and food (Elnaker et al., 2021). This process effectively eliminates water content while preserving crucial bioactive ingredients, particularly antioxidant compounds (Krakowska-Sieprawska et al., 2022). For instance, plant or biological materials are frequently subjected to lyophilisation at reduced temperatures to prevent the decomposition of essential metabolites (Villate et al., 2021). The method involves pre-freezing the samples, and under reduced pressure, frozen moisture sublimes from the sample, simultaneously alleviating oxidative changes to metabolites due to the applied vacuum (Nakbanpote et al., 2019; Sanfilippo et al., 2019).

The frozen plant extract material was placed into a low-pressure machine at -80°C for 24 hours for lyophilisation immediately after being removed from the fridge. The instrument was used at a pressure of -117 mT and a temperature of -54 °C. The dried lyophilised materials were collected as a powder and used in subsequent synthesis to evaluate their nanoparticle-forming abilities.

The investigation was conducted on 96-well plates to assess these characteristics at various concentrations through a serial dilution approach. UV-Vis Spectroscopy was employed to examine the formation of monometallic nanoparticles (specifically, Au and PdNPs) and bimetallic nanoparticles in the presence of 2.5 mM $NaAuCl_4 \cdot 2H_2O$ (Au salt). The reducing agent was diluted by two from one cell to its consecutive one when the synthesis of the nanoparticles showed that only specific concentrations formed nanoparticles; determining an optimal concentration was necessary for the next steps of the synthesis.

3.4.3. Synthesis of gold nanoparticles

The GR extract and ASP were initially screened for the synthesis of AuNPs, PdNPs, and Au-Pd bimetallic nanoparticles in a 96-well micro plate, employing a method described in a previous study with slight modifications.

A 50 µL portion of 10 mM Au salt, combined with 200 µL of distilled water to maintain a concentration of 2 mM, was added to 50.0 µL of the plant extract in a 96-well microliter plate. The plant extract concentrations ranged from 20 to 0.625 mg/300 µL. The plate underwent incubation in a water bath at 70°C for 1 hour. The synthesis of AuNPs was monitored by monitoring the UV-Vis spectra. After identifying the optimal concentrations of plant extracts that produce desirable AuNPs (10 mg/300 µL for GR/ASP), the volume of the mixture containing Au salt and GR/ASP was increased.

An amount of 85 mg of GR/ASP was dissolved in 8.5 mL of deionized water. This solution was then filtered using a 0.45-µm syringe filter. In parallel, 10 mM of Au salt was measured to 8.5 mL using a measuring cylinder and carefully transferred into a beaker containing 34 mL of deionized water, maintaining an optimal

concentration of 2 mM. While monitoring the temperature with a thermometer, the Au solution was added dropwise to 8.5 mL of the prepared GR/ASP under vigorous stirring and then heated at 70°C using a hot plate magnetic stirrer combination. The time taken for the colour transformation from pale yellow (Au solution) to deep purple was recorded, and the sample was allowed to stir for 1 hour. Following the centrifugation of the AuNPs, the pellets were washed three to four times with distilled water before being re-suspended in distilled water.

3.4.4. Synthesis of palladium nanoparticles

A mixture of 50 µL of 10 mM palladium (II) chloride ($PdCl_2$) and 200 µL of distilled water was used maintaining a concentration of 2 mM. In a 96-well microlitre plate, this mixture was added to 50µL of plant extract. The plant extract concentrations ranged from 20 to 0.625 mg/300 µL. The plate was incubated for 1 hour at 70°C in a water bath. The formation of PdNPs was monitored using UV-Vis spectra. Following the identification of the optimal concentrations of plant extracts yielding desirable PdNPs (1.25 mg/300 µL for GR/ASP), the volume of the Pd salt and GR/ASP mixture was scaled up.

85 mg of GR/ASP was dissolved in 8.5mL of deionised water. An amount of 34 mL of deionised water was measured. Then, using a measuring cylinder, 10 mM of palladium (II) chloride ($PdCl_2$) was measured to 8.5 mL and carefully transferred into a beaker containing the deionised water maintaining a concentration of 2 mM. The now 2 mM Pd solution was then added dropwise under vigorous stirring to the plant extract and heated at 70°C while monitoring the temperature with a thermometer. The time it took for the colour to shift from yellow-brownish to deep brown was recorded, and the sample was stirred for an hour.

3.4.5. Synthesis of Au-Pd bimetallic nanoparticles

A total of 100 µL of 2 mM $PdCl_2$ was introduced to 200 µL of AuNPs (prepared through the aforementioned method) in a 96-well microlitre plate. Subsequently, the plate was incubated in a water bath for 2 hours at 70 °C. The formation of Au–Pd bimetallic nanoparticles was observed through UV-Vis spectroscopy. The scaling up of the volume of AuNPs and the Pd salt solution was achieved using the following procedure:

The Au-Pd bimetallic nanoparticles were formed by transferring an aliquot of the prepared AuNPs into a beaker, and a solution of 2 mM $PdCl_2$ was added under constant and vigorous stirring at 70°C for 2 hours. A brown solution observed indicated that the Au-Pd bimetallic nanoparticles were successfully synthesised.

The solutions containing colloidal particles were allowed to cool down to the temperature of the room. Then, the nanoparticles were subjected to multiple rounds of centrifugal washing at 10 000 rpm for 20 minutes to prepare them for biological research. This process aimed to eliminate any remaining unreacted substances in the solution. A preliminary evaluation of the successful nanoparticle formation was conducted using UV-Vis analysis, followed by additional characterization techniques.

3.5. Characterisation of Nanoparticles

3.5.1. Ultraviolet-Visible (UV-Vis) Spectroscopy

The syntheses of AuNPs, PdNPs, and Au-Pd bimetallic nanoparticles were examined utilizing Ultraviolet-Visible (UV-Vis) Spectroscopy, specifically employing the BMG LABTECH-SPECTROstar-Nano instrument. The objective of this analysis was to verify the peak Surface Plasmon Resonance (SPR) of AuNPs at λ=536nm and the PdNPs. Spectra were meticulously recorded at room temperature, with the wavelength ranging from 220nm to 800nm and a resolution of 1nm, utilizing a double-beam spectrophotometer. To achieve this, the synthesized samples of AuNPs, PdNPs, and Au-Pd bimetallic nanoparticles were appropriately diluted at a 1:1 ratio of the base solvent and the nanoparticles.

3.5.2. Dynamic Light Scattering (DLS)

The Zeta-Sizer Nano-Series (Nano-zs90), equipped with both Zetasizer and Zeta Potential functionalities, was utilized to analyse AuNPs, PdNPs, and Au-Pd bimetallic nanoparticles. This instrument facilitates the measurement of approximate average sizes for colloids, nanoparticles, and molecules without requiring sample agitation. The analysis involved studying a 1 mL (1000 µL) diluted sample in quartz glass cuvettes (similar to those used for UV-Vis analysis). Key parameters, such as temperature (set at 25°C), the base solvent (water), and cuvette settings (disposable cell for Zeta Sizer and disposable folded capillary cell for Zeta Potential), were carefully configured, aligning with a greener methodological approach.

3.5.3. X-Ray Diffraction (XRD)

The XRD method was utilized to analyse the crystal structures of crystalline materials. The XRD patterns for lyophilized samples of AuNPs, Pd NPs, and Au-Pd bimetallic nanoparticles, supported on the plant extract, were obtained using a Bruker AXS (Germany) D8 Advance diffractometer at a voltage and current of 40 KV and 40 mA. The XRD patterns/spectra were meticulously recorded within the range of 30-90º (2θ), utilizing a CuKα (λ=0.154 nm) monochromatic radiation X-ray source and employing a step-scan of Δ2θ= 0.05°.

3.5.4. High-Resolution Transmission Electron Microscopy (HRTEM)

The size, shape, crystallinity, and elemental composition of the AuNPs and PdNPs formed in the solution underwent comprehensive characterization using HRTEM combined with EDX Spectroscopy. In this research, TEM micrographs were captured using the TECNAI F20 HRTEM, operating at 200kV and equipped with an X-ray analysis detector. Samples of AuNPs, PdNPs, and Au-Pd bimetallic nanoparticles were meticulously prepared by depositing a single, solution drop onto a copper carbon-coated grid, followed by drying under the illumination of an electric bulb.

3.5.5. Fourier-Transform Infrared (FTIR) Spectroscopic Analysis

ATR-FTIR analysis was employed to identify the biomolecules responsible for synthesizing and capping AuNPs, PdNPs, and Au-Pd bimetallic nanoparticles using *Aspalathus linearis* plant extract. The analysis was conducted using the Perkin Elmer Spectrum (Version 10.4.2) ATR-FTIR spectrometer. A drop of distilled water served as a blank, and the sample scan was adjusted to remove the background. The instrument was then loaded with a drop of the sample, and a scan covering the percentage range of wavenumbers from 400 to 4000 cm^{-1} was conducted.

3.6. Biological Studies

3.6.1. Stability Study of nanoparticles

The *in vitro* stability study involved combining 200 µL of solutions containing AuNPs, PdNPs, and Au-Pd NPs with 100 µL of biogenic amino acids such as 0.5% glycine, Phosphate-Buffered Saline (PBS at pH 7 and pH 9), and a 0.5% NaCl solution. This procedure was conducted in a 96-well plate. Subsequently, the mixture underwent incubation at a temperature of 37 °C for various durations. UV–Vis spectroscopy was employed for the evaluation of the stability of AuNPs, PdNPs, and Au-Pd bimetallic nanoparticles in these media, with a focus on observing the preservation of their absorbance maxima at 6-hour intervals over a 24-hour period.

3.6.2. Cell Culture

This research involved the use of SKMEL-1, HaCAT, KMST-6 and HepG2 cell lines. These cells were grown in a controlled environment at 37°C with a mixture of 95% air and 5% CO_2 following sterile procedures. HaCAT, KMST 6 and HepG2 cells were cultured separately in DMEM growth medium. This medium was supplemented with 10% Fetal Bovine Serum (FBS) along with penicillin (100 µg/mL). Streptomycin (100 µg/mL) at a concentration of 1%. The SKMEL-1 cells, on the other hand were cultured in complete RPMI growth medium supplemented with 10% FBS and penicillin/streptomycin at the same concentration as mentioned before.

3.6.3. Cytotoxicity assay

The cytotoxicity was evaluated using an assay called MTT, which involved 3-[4, 5-dimethylthiazol-2-yl]-2, 5-diphenyltetrazolium bromide. Briefly, SKMEL-1, HaCAT, KMST-6 and HepG2 cell lines were individually placed in 96-well cell culture plates with a density of 5000 cells per well. They were left to attach. Subsequently, the medium was replaced with the fresh medium containing increasing concentrations (12.5, 25, 50, 100, and 200 µg/mL) of the samples tested; GR- AuNPs, GR-PdNPs, GR-Au-Pd bimetallic nanoparticles, ASP-AuNPs ASP-Pd and ASP-Au-Pd bimetallic nanoparticles. This was maintained for duration of 24 hours. As for control samples used, cells were incubated with the medium. After the

incubation period of 24 hours, MTT solution (5 mg/mL) was in each well (10 µL) and was incubated for an additional 4 hours at a temperature of 37 °C. Therefore, the resulting MTT crystals were solubilized in DMSO, and the absorbance was measured at a wavelength of 570 nm for each well. The calculation of percentage cell viability was determined using the following formula:

$$\%\text{Cell Viability} = \frac{\text{Absorbance of treated well}}{\text{Absorbance of untreated well}} \times 100$$

3.6.4. Statistical Analysis

Information from the present study was accurately documented and underwent statistical analysis using GraphPad Prism for Windows, version 8.4.3, developed by GraphPad Software in San Diego, USA. To ensure reliability, the experiments were carried out in triplicate. After analysing the summary statistics, which included conducting the Kolmogorov-Smirnov test for a normal distribution, the data underwent analysis using the independent t-test in instances where normal distribution was observed. Statistical significance was established at $p < 0.05$.

3.6.5. Cellular Uptake of biosynthesized nanoparticles

In 6-well plates, 1×10^5 SKMEL-1, HaCAT, KMST-6, and HepG2 cells treated with biosynthesized GR-AuNPs, GR-PdNPs, GR-Au-Pd bimetallic nanoparticles, ASP-AuNPs, ASP-PdNPs, and ASP-Au-Pd bimetallic nanoparticles were individually seeded and incubated for 24-hour period. After the incubation period, the medium was aspirated, and PBS was used to rinse the cells. In 15 mL tubes, the cells were trypsinized, centrifuged at 3000 rpm, re-washed with PBS, and centrifuged again. After discarding the PBS, aqua regia (14 mL) was used to digest the nanoparticles at 80 °C briefly, resulting in the release of metal ions. The released metal ions from the cells were quantified using ICP-OES (Inductively Coupled Plasma-Optical Emission Spectroscopy) analysis. For ICP-OES analysis, Au and Pd standard solutions were each prepared at a concentration of 100 ppm, followed by subsequent serial dilutions yielding concentrations of 1 ppm, 2.5 ppm, 5 ppm, 10 ppm, 15 ppm, and 20 ppm for standard calibrations. The cellular uptake of nanoparticles was correlated with the Au and Pd ion concentrations in the cells.

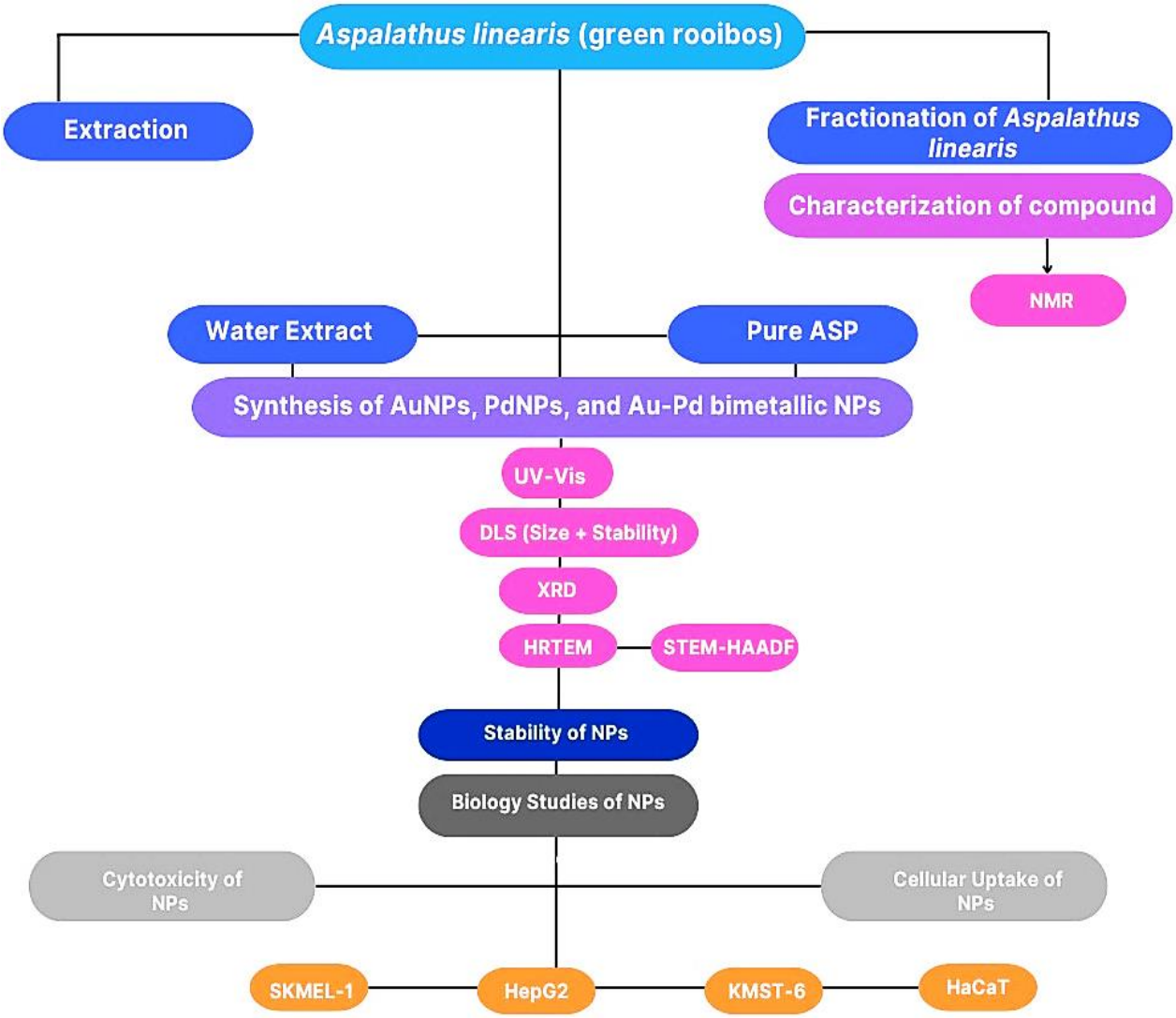

Figure 3-3: Schematic representation of the extraction, isolation, synthesis of nanoparticles and the biological evaluation of nanoparticles against cell lines

Chapter 4

4. Results and Discussion

4.1. Introduction

Nanoparticles, especially those created from noble metals like Au and Pd, have attracted considerable interest across diverse scientific fields due to their distinctive physicochemical characteristics and versatile applications. In recent years, there has been a growing emphasis on green and sustainable approaches to nanoparticle synthesis with the objective of decreasing the environmental impact of traditional chemical methods (Behera et al., 2020; Singh et al., 2020). Among these methodologies, employing plant extracts and natural compounds has surfaced as a promising avenue for producing nanoparticles with regulated properties (Kharissova et al., 2019).

This chapter explores the formation of AuNPs, PdNPs, and Au-Pd bimetallic nanoparticles, utilizing the unfermented *Aspalathus linearis* (GR) as a primary plant source. GR has gained recognition for its rich phytochemical composition, particularly aspalathin (ASP), a *C*-glucosyl dihydrochalcone compound found abundantly within its leaves. ASP, with its intriguing chemical structure and potential reducing capabilities, serves as a vital component in the green synthesis of the nanoparticles explored in this chapter (Gebretnsae & Gebretnsae 2021).

The primary aim of this chapter is to elucidate the intricate process of synthesizing Au, Pd, and Au-Pd bimetallic nanoparticles using the GR extract, as well as the characterization of the synthesized nanoparticles. A comparative analysis between nanoparticles synthesized with plant extract and those utilizing pure ASP are presented. This study explores the fundamental chemistry interactions that underlie this green synthetic approach. Furthermore, the distinct properties of Au-Pd bimetallic nanoparticles synthesized using this eco-friendly methodology are explored.

The introduction of GR extract and ASP as viable resources for nanoparticle synthesis gives emphasis to the significance of sustainable nanotechnology. This research leverages the properties of natural compounds and plant extracts, contributing to the principles of green chemistry and presenting a viable alternative to conventional methods of nanoparticle synthesis. Through a detailed examination of the synthesis and isolation procedures, this chapter seeks to offer valuable insights into the evolving field of green nanotechnology and its potential ramifications across diverse scientific domains.

The succeeding sections of this chapter will delve into the results, and discussions that elucidate the synthesis, characterization techniques, and properties of AuNPs, PdNPs, and Au-Pd bimetallic nanoparticles synthesized using GR extract and ASP.

4.2. Isolation and characterization of Aspalathin from *Aspalathus linearis*

The use of pure precursor provided a meaningful way to improve the understanding of the synthesis of the monometallic nanoparticles (i.e., AuNPs and PdNPs) and Au-Pd bimetallic nanoparticles at such a level of purity whereby the effect of the other compounds was removed in this way.

4.3. Characterization of major compound

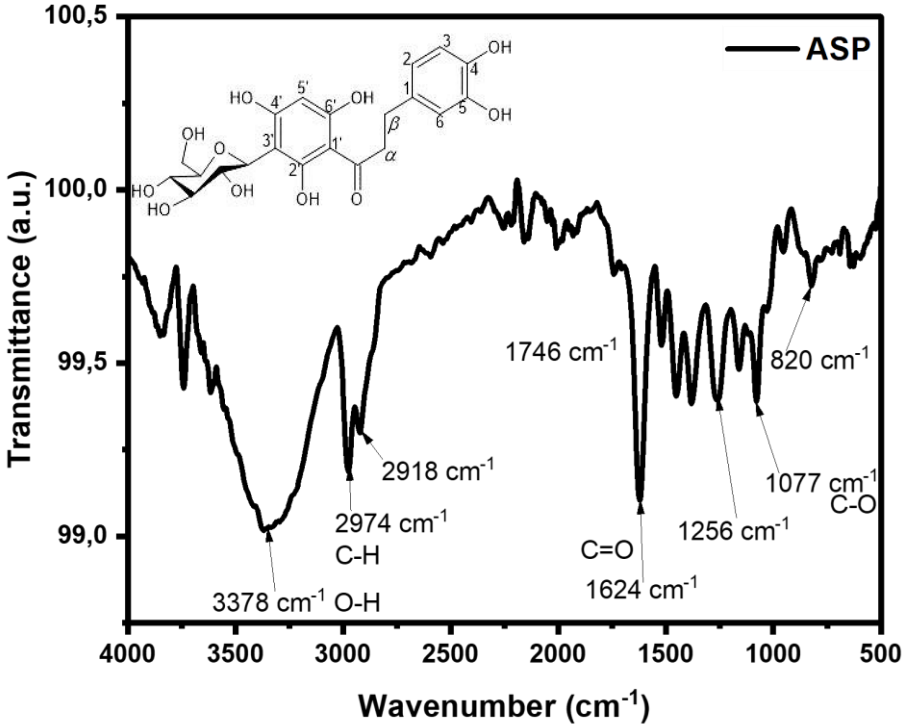

Figure 4-1: The infrared spectrum of ASP pure compound

Figure 4-1 exhibits the FTIR spectrum of the isolated compound, ASP, which depicted all the major peaks located at 3378, 2974, 2918, 1746, 1624, 1256, 1077, and 820 cm^{-1}, validating the existence of all the functional groups in its structure.

The peaks represent free O-H in the molecule and O-H group forming hydrogen bonds, carbonyl group (C-O), aromatic ring (C=C) stretching and C–OH stretching vibrations, respectively. The vibration frequency bands of 3378cm^{-1} confirmed the existence of O-H stretching band of alcohols, while the 2918 cm^{-1} stretching confirmed the presence of the sp^3 C-H band, typical of alkanes, the C=O bond of the carbonyl group at 1746 – 1624 cm^{-1}, and the C-O bond was accounted for at 1077 cm^{-1}.

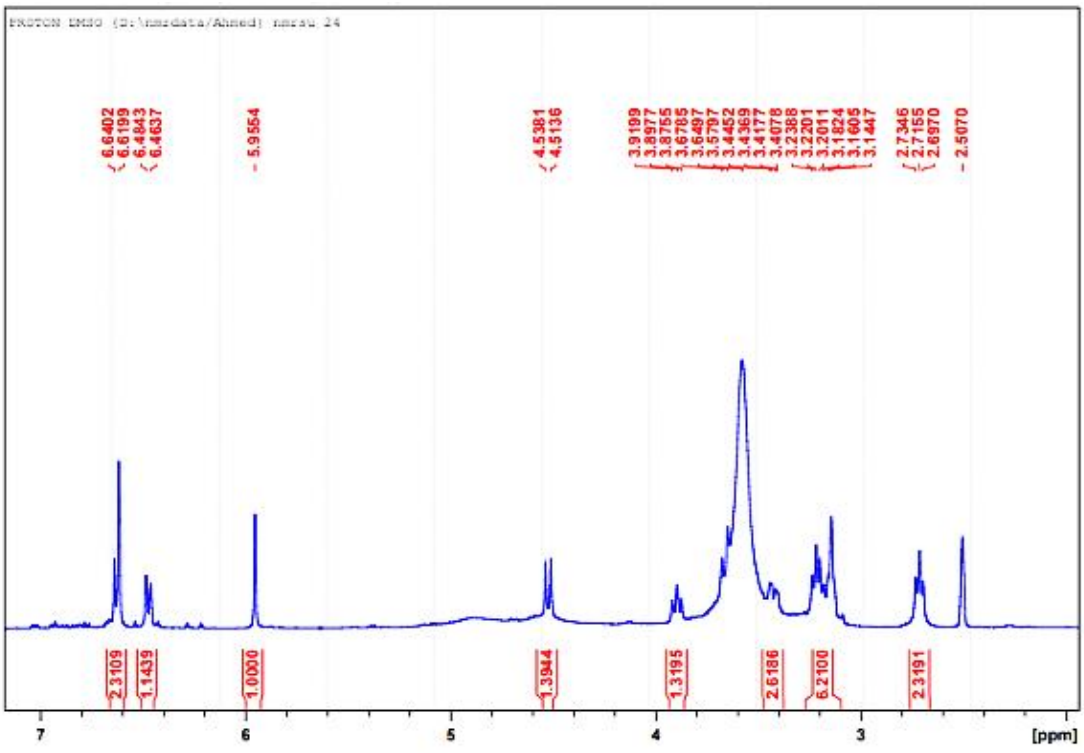

Figure 4-2: ^{1}H-NMR (400 MHz, DMSO) spectrum of ASP

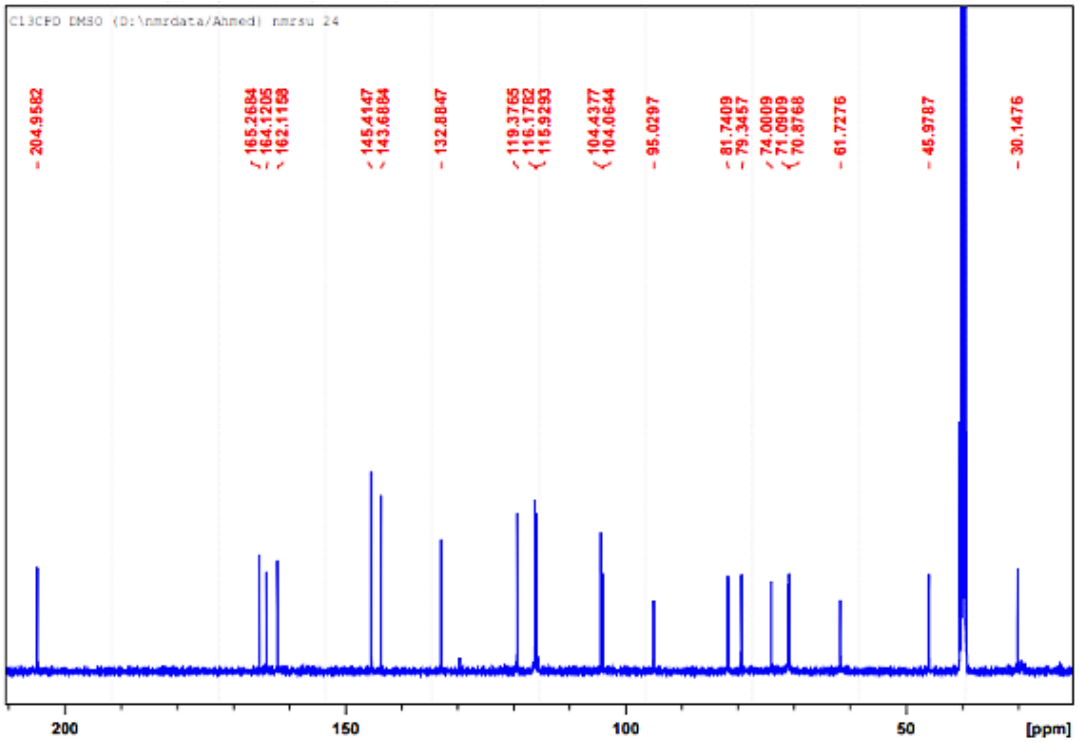

Figure 4-3: ^{13}C-NMR (400 MHz, DMSO) spectrum of ASP

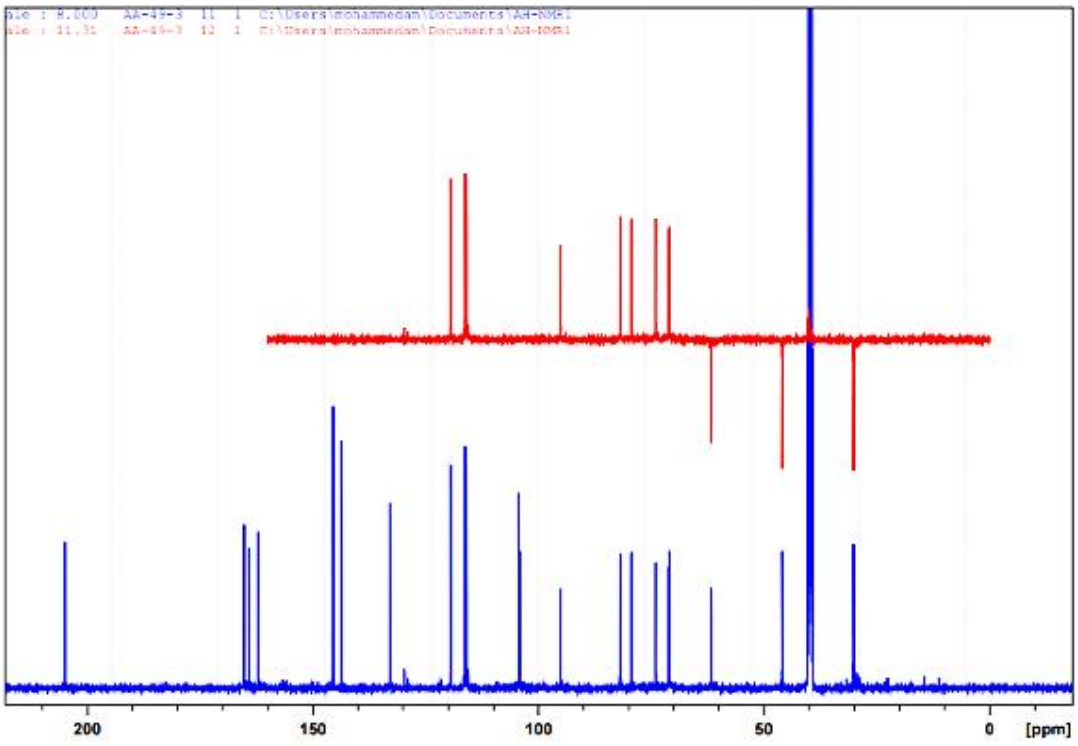

Figure 4-4: DEPT-135-NMR (400 MHz, DMSO) spectrum of ASP

Aspalathin (2500 mg), isolated as an amorphous white-yellowish powder, exhibited a characteristic dihydrochalcone skeleton according to NMR spectra (refer to Table 4 and Figures 4-2, 4-3, and 4-4). The ^{1}H-NMR spectrum revealed a singlet at 5.95 (H-5`) for the penta-substituted ring A, along with aromatic signals of the 1,3,4-trisubstituted ring B at 6.63 (H-6), 6.47 (H-5), and 6.61 (H-2), accompanied by two methylene groups at 3.32 (CH_2-*α*) / 2.83 (CH_2-*β*). Additionally, *C*-glucose signals at 4.52 (H-1``), 3.89 (H-2``), 3.22 (H-3``), 3.14 (H-4``), 3.15 (H-5``), and 3.42/3.66 (H-6``) were observed.

The ^{13}C and DEPT-135 (refer to Figure 4-3 and Figure 4-4) spectra illustrated a total of 21 carbons, with 15 belonging to the dihydrochalcone skeleton, specifically at δ_C: 132.9 (C-1), 116.2 (C-2), 145.4 (C-3), 143.7 (C-4), 115.9 (C-5), 119.4 (C-6), 104.4 (C-1`), 161.1 (C-2`), 104.1 (C-3`), 164.1 (C-4`), 95.0 (C-5`), 165.3 (C-6`), 45.9 (C-*α*), 30.1 (C-*β*), and 205.0 (carbonyl group). The remaining six carbons at δ_C: 74.0 (C-1``), 70.9 (C-2``), 79.3 (C-3``), 71.1 (C-4``), 81.7 (C-5``), and 61.7 (C-6``) were attributed to the glucose unit. Co-spotting the compound with the isolated aspalathin in the lab confirmed the same R_f value.

Table 4: ^{1}H and ^{13}C NMR data for aspalathin in DMSO-d_6

Position	^{13}C-NMR (ppm, J, Hz)	^{1}H-NMR (ppm, J, Hz)
1	132.9	
2	116.2	6.61 *(br s)*
3	145.4	
4	143.7	
5	115.9	6.47 *(d, 8.0)*
6	119.4	6.63 *(br d, 8.0)*
1`	104.4	
2`	161.1	
3`	104.1	
4`	164.1	
5`	95.0	5.95 *(s)*
6`	165.3	
α	45.9	3.32 *(2H, m)*
β	30.1	2.83 *(2H, t, 7, 9)*
CO	205.0	
1``	74.0	4.52 *(d, 9.9)*
2``	70.9	3.89 *(t, 8.7)*
3``	79.3	3.22 *(t, 7.6)*
4``	71.1	3.14 *(br t, 7.3)*
5``	81.7	3.18*
6``	61.7	3.42 *(dd, 3.6, 11.6)*
		3.66 *(d, 11.6)*

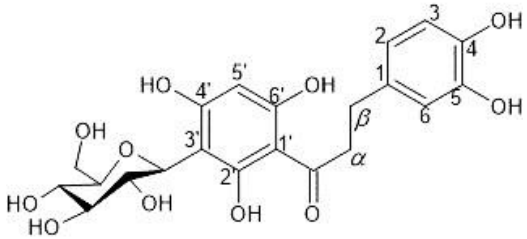

Figure 4-5: Chemical structure of ASP

4.4. Synthesis of gold nanoparticles using *Aspalathus linearis* (total extract)

With the aid of the distinctive bands and rings present in the biological macromolecules of the selected GR plant extract, the absorbance spectrum of the entire extract samples in this study reveals a unique photon absorption pattern. After one hour of incubation, a noticeable colour changes from yellow to ruby red signifies the formation of AuNPs arising from plant extract and Au salt interaction. This change substantiates the capacity of the extracts to reduce Au^{3+} ions to Au° through the involvement of secondary metabolites (Yuan et al., 2017). Alongside ASP, other phenolic constituents of interest in GR include orientin, iso-orientin, and nothofagin (Heinrich et al., 2012).

4.5. Characterization of gold nanoparticles using *Aspalathus linearis*

4.5.1. Ultraviolet-Visible (UV-Vis) Spectroscopy

Surface Plasmon Resonance (SPR), characterized by the oscillation of unbound conduction electrons, gives rise to the distinctive red colouration in colloidal Au nanoparticle solutions, a phenomenon not evident in bulk material or individual atoms (Ramalingam, 2019; Sarfraz & Khan, 2021). The specific position and profile of the SPR in the UV-Vis spectrum are influenced by various factors, such as nanoparticle size, shape, the refractive index of the medium, and interparticle distances (Majoumouo et al., 2020; Aldawsari et al., 2021). The presence of AuNPs is therefore confirmed through UV-Vis spectroscopy when a peak absorption falls within the range of 500 to 600 nm (Kumar et al., 2019).

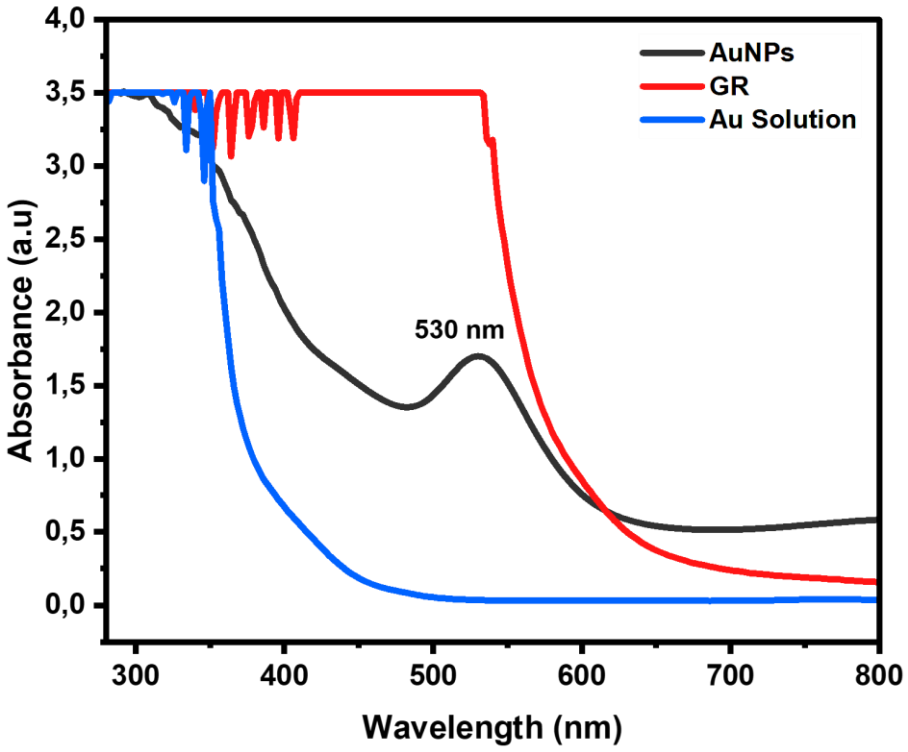

Figure 4-6: UV-Vis absorbance spectra of synthesized AuNPs using GR extract

Figure4-6 displays the UV-Vis spectrum of the formed AuNPs.

The absorbance peak at 530 nm was observed in the UV-Vis spectra of AuNPs derived from the GR plant extract. These finding imply the existence of the effective reducing and stabilizing agents found in the GR extract, effectively inhibiting Au nanoparticle aggregation and promoting their uniformity.

4.5.2. Dynamic Light Scattering (DLS)

The DLS technique is utilized for hydrodynamic size distribution determination and Polydispersity Index (PDI) of nanoparticles. Additionally, it can provide insight into the homogeneity and diffusion coefficient of nanoparticle dispersion. Through the DLS, information pertaining to physiochemical features of metal nanoparticles is obtained, including size, shape and surface functional groups (Minal & Prakash, 2020).

			Size (d.nm):	% Intensity:	St Dev (d.nm):
Z-Average (d.nm):	47.91	Peak 1:	78.40	93.5	43.55
PdI:	0.383	Peak 2:	4.767	5.7	1.761
Intercept:	0.878	Peak 3:	1.556	0.7	0.3525
Result quality :	Refer to quality report				

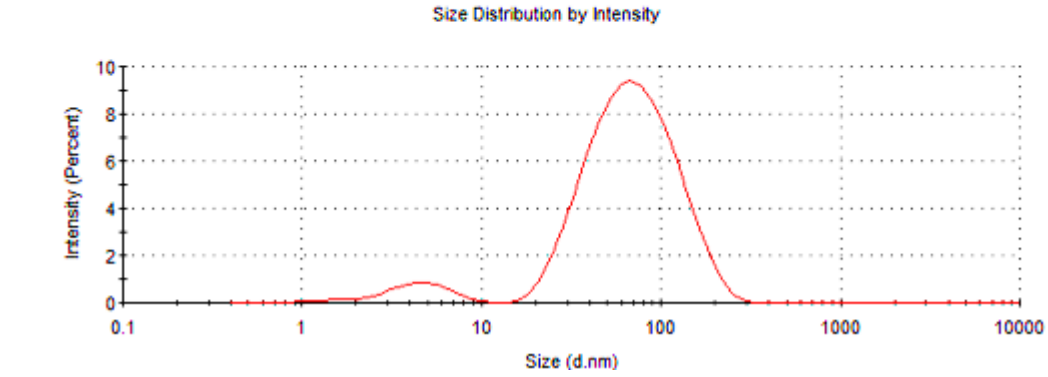

Figure 4-7: The size distribution graph of AuNPs, synthesized from GR extract, reveals a distribution below 100 nm, with an average hydrodynamic size of 47.91 nm

The recorded size measurement was 47.91 nm, and Figure 4-7 illustrates the size distribution graph, featuring two peaks ranging from 4.77 to 78.40 nm.

Compared to the GR matrix, the PDI value of the AuNPs was 0.383. Thus, the hydrodynamic size of 47.91 nm and PDI value of 0.383 suggested that the AuNPs formed from GR extract had a relatively narrow size distribution with a moderate level of uniformity in particle sizes.

4.5.3. Zeta Potential

The zeta potential is related to the particle surface charge, that is, the electrostatic repulsive forces. Zeta potential, expressed in ± mV, signifies the extent of inter-particle repulsion in the dispersion. Zeta potential analysis determines the electrokinetic potential of the Au nanoparticle sample, which allows conclusions to be drawn about the stability of the AuNPs in a suspension (Payne et al., 2018).

In accordance with prior studies, nanoparticles exhibiting a zeta potential falling in the range of -30 to +30 mV are considered stable and tend to avoid aggregation in a solution (Franco-Ulloa et al., 2020; Aboyewa et al., 2021). It is noteworthy that the stability assessment of any nano-formulation involves the interplay of both electrostatic repulsive and van der Waals attractive forces. In scenarios where particles possess weak van der Waals attractive forces, the evaluation of mild electrostatic repulsive forces becomes crucial in determining colloid stability, often resulting in a lower zeta potential (±10 to ±15mV) (Rahdar et al., 2019).

The zeta potential value (-24.3 mV) of the GR AuNPs were analysed using this instrument, as demonstrated in Figure 4-8.

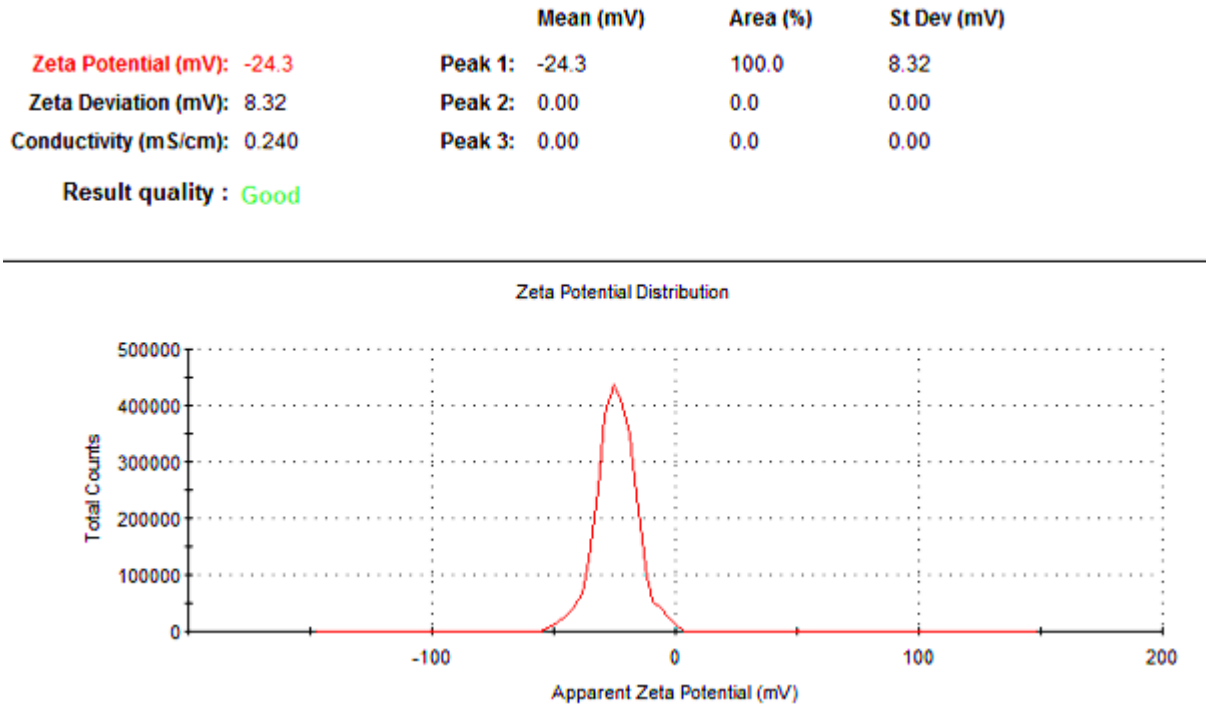

Figure 4-8: Zeta potential distribution graph of GR extract AuNPs

Therefore, the outcomes suggested the formation of an electrical double layer on the surface of the particle within the supporting matrix. The negative zeta potential value of -24.3 mV points to a prevalent negative charge on the surface of the nanoparticles when dispersed in the medium. This negative charge could be attributed to various factors, including the presence of biomolecules or phytochemicals derived from the plant extract used during synthesis. Thus, it indicates an abundance of negatively charged species or functional groups on the nanoparticle surface. As demonstrated in previous studies (Patra et al., 2015; Ali et al., 2016a; Elbagory et al., 2017; Badeggi et al., 2020), this negative zeta potential value suggests that the AuNPs maintain stability in colloidal dispersions, remaining uniformly dispersed within the liquid medium.

4.5.4. X-Ray Diffraction (XRD)

The XRD analysis is a facile and vital technique for determining the crystallinity of a material (Zheng et al., 2014). XRD patterns of the monometallic and bimetallic nanoparticles were compared to verify the formation of the Au nanoparticle structures. Derived from face-centred cubic (fcc) metallic Au, Bragg's reflections were compared to reported standards (JCPDSS card no. 89-3697) (Boomi et al., 2019).

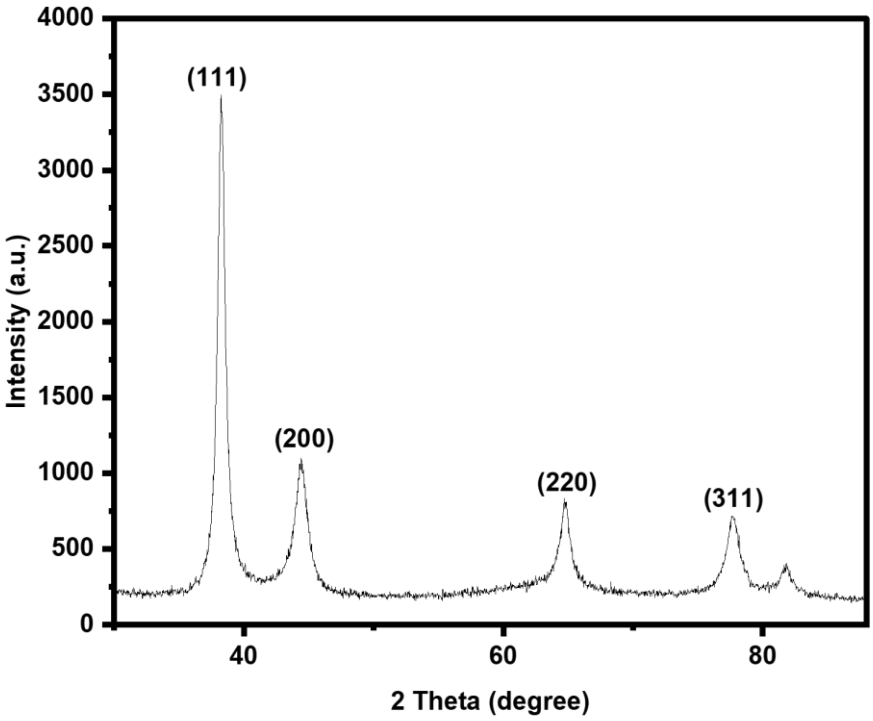

Figure 4-9: XRD pattern of Au-synthesized NPs using GR extract

Figure 4-9 shows the existence of peaks for 2θ values at 38.21°, 44.36°, 64.77°, 77.77°, 81.61° in the XRD patterns corresponding to the (1 1 1), (2 0 0), (2 2 0), and (3 1 1) planes of fcc Au (Milaneze et al., 2016).

4.5.5. High-Resolution Transmission Electron Microscopy (HRTEM)

Due to the broad spectrum of phytochemicals within the total extract, with the capability to reduce Au salt, it is expected that AuNPs generated by these plant phytochemicals will exhibit a variety of geometric shapes (Elbagory et al., 2017; Majoumouo et al., 2020; Sargazi et al., 2022). Figures 4-10 A and B present HRTEM micrographs, offering additional insights into the morphology, variations within a spectrum of shapes and sizes of the synthesized AuNPs.

Therefore, the formation of sphere-shaped particles in this study implies that the capping agents within the GR extract establish strong interactions with the freshly formed AuNPs, inhibiting them from adopting alternative shapes (Sujitha & Kannan, 2013). However, specific deviations from sphere-shaped particles were monitored in the HRTEM micrographs. The coexistence of various shapes is a distinctive feature of AuNPs and is associated with a variety of phytochemicals involved in the formation of AuNPs (Sosa et al., 2003; Elbagory et al., 2016). The small-sized nanoparticles obtained from the plant extract may suggest the effectiveness of the reducing agents.

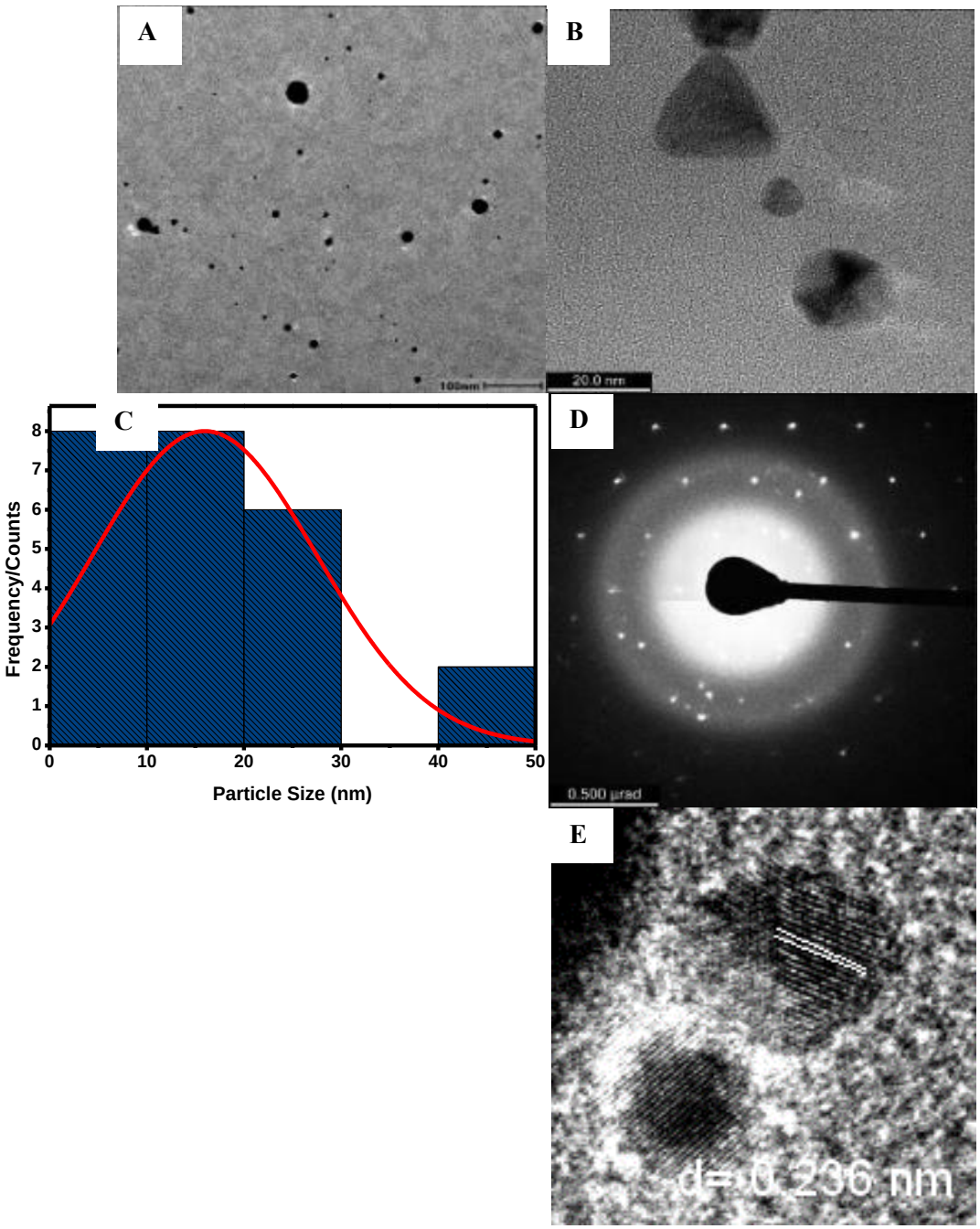

Figure 4-10: a) & b) HRTEM micrographs of AuNPs synthesized using GR extract; (c) particle size distribution corresponding to micrograph A; d) coupled with the SAED pattern and e) HRTEM lattice fringes of AuNPs.

Through DLS, information pertaining to the physicochemical features of metal nanoparticles is obtained, including size, shape, and surface functional groups, which are often compared to HRTEM results (Minal & Prakash, 2020). While there are notable differences between the visual results obtained from DLS and

HRTEM, the latter provides the actual size and configuration of the electron-dense metal nanoparticles. Conversely, the former indicates a larger size, accounting for the hydrodynamics of the particles within the liquid medium. DLS measures the hydrodynamic radius of a nanoparticle, encompassing the coating on its surface, whereas HRTEM measures the nanoparticle core size (Regmi et al., 2011; Foo et al., 2017). Hence, the hydrodynamic diameter of the Au NPs was larger than the core size determined by HRTEM.

Figures 4-10 C and D present particle size distribution analyses and the SAED pattern, respectively. Moreover, the particle size distribution (10.62 ± 8.34 nm) suggests that the nanoparticles exhibit a broad size distribution with a mean size of 10.62 nm, aligning with the broad maximum absorption band observed in Figure 4-6. The SAED patterns depicted in Figure 4-10 D for the synthesized AuNPs, specifically in the (1 1 1), (2 0 0), (2 2 0), and (3 1 1) planes, signify fcc lattice structure, aligning with the findings from the reported XRD analysis.

Figure 4-10 E is a high-resolution image of the particles. Lattice fringes are visible, providing additional confirmation of the crystalline nature of the nanoparticles. The measured interplanar/d-spacing of 0.236 nm agrees with the (111) plane of fcc Au (Zhan et al., 2011; Geng et al., 2017; Silva et al., 2023).

4.5.6. Fourier-Transform Infrared (FTIR) Spectroscopy

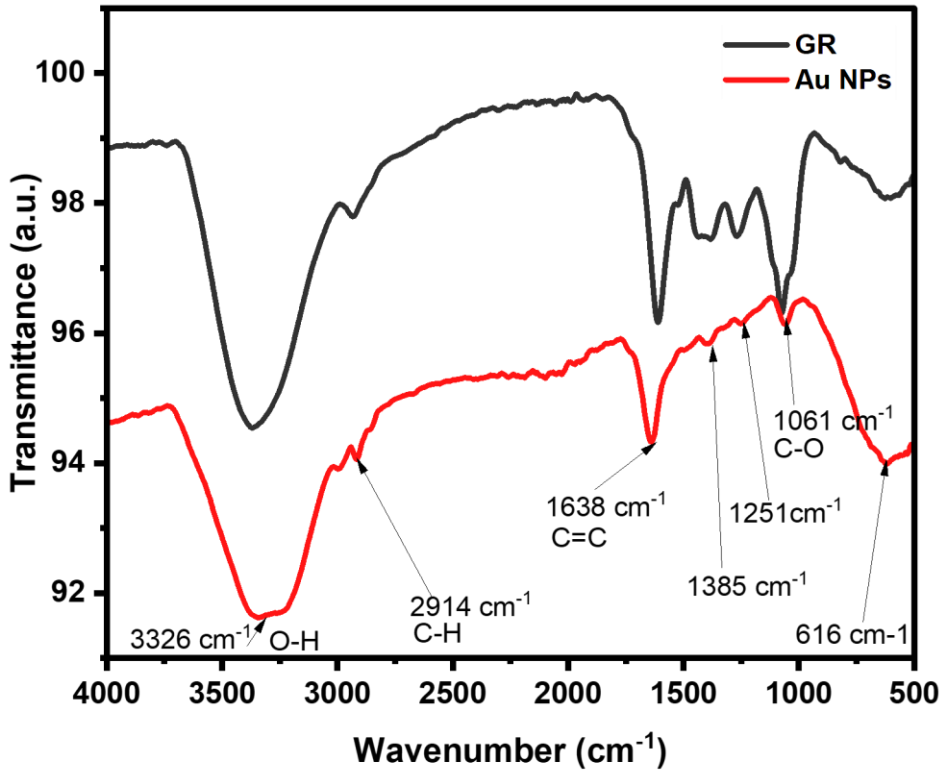

Figure 4-11: FTIR spectra of GR total extract and AuNPs formed using the total extract

The FTIR spectrum obtained from the plant extract (depicted in Figure 4-11) revealed distinct peaks at 3360, 2929, 1616, 1410, and 1080 cm^{-1}. In contrast, the Au nanoparticle FTIR spectrum (Figure 4-11) displayed peaks at 3326, 2914, 1638, 1385, 1251, 1061, and 616 cm^{-1}. These observed peaks provide evidence for the existence of phenolic compounds in the plant extract.

The peaks seen at 2929 and 2914 cm^{-1} in the GR plant extract and AuNPs, respectively, can be attributed to the aromatic compounds C-H stretching. This data reinforces the evidence for the existence of poly-hydroxy aromatic compounds (Biswal & Misra, 2020). The vibrational frequency bands observed between 1410 and 1385 cm^{-1} in both the extract and AuNPs spectra can be attributed to the bending vibrations resulting from sp^2 hybridization. This characteristic feature is indicative of the presence of alkenes and aromatic carbons. (Ahmeda et al., 2020). It may be assumed that the polyphenols in the GR plant extract may function as reducing and capping agents (Omolaja et al., 2021). In addition, peaks at 1061 - 1080 cm^{-1} are associated with the C-OH stretching of primary alcohols or the C–stretching ether group and C-O-C vibrations of proteins and polysaccharides, respectively. Hydroxyl groups (OH^-) were abundant in the constituents. Phenolics abundant in hydroxyl groups could have played a role in the reduction of AuNPs.

4.6. Synthesis of palladium nanoparticles using *Aspalathus linearis* (total extract)

This section evaluates the outcomes of the synthesis of PdNPs using GR plant extract, highlighting the key characterization steps involved. By conducting these analyses, valuable information regarding the size, shape, crystalline structure, composition, and optical properties of the synthesized nanoparticles was obtained.

4.7. Characterization of palladium nanoparticles using *Aspalathus linearis*

4.7.1. Ultraviolet-Visible (UV-Vis) Spectroscopy

The generation of PdNPs was evidenced by a colour change from yellow-brownish to brown, a change further verified through UV-Vis analysis. The existence of Pd ions (Pd^{2+}) was affirmed by the identified band at 418nm (Momeni & Nabipour, 2015; Kora & Rastogi, 2018).

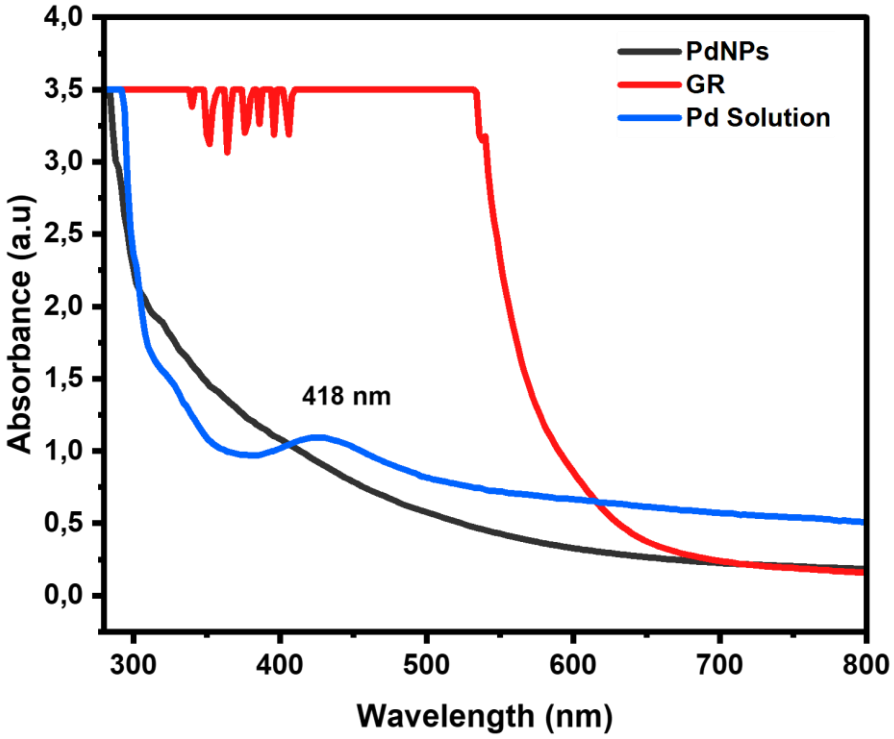

Figure 4-12: UV-Vis spectra of PdNPs synthesized using GR extract coupled with palladium chloride salt solution and total extract controls

In Figure 4-12, no SPR band was observed for PdNPs. This is due to the lack of surface plasmons (free electrons) in the outer shell (Minal & Prakash, 2018; Sivamaruthi et al., 2019).

The absence of the 418 nm absorption band indicates the existence of PdNPs. It is plausible that the phytochemical constituents reduced Pd^{2+} to Pd° without the use of any external reducing agent, as suggested by Hazarika et al. (2017).

4.7.2. Dynamic Light Scattering (DLS)

The intensity graph in Figure 4-13 displays the size distribution of GR PdNPs. The results show a bimodal graph, with smaller particles measuring approximately 214 nm and larger particles averaging around 797.2 nm. The reaction conditions generated PdNPs with a mean size of 272.9 nm.

			Size (d.nm):	% Intensity:	St Dev (d.nm):
Z-Average (d.nm):	272.9	Peak 1:	328.2	94.4	214.6
PdI:	0.385	Peak 2:	4783	5.6	797.2
Intercept:	0.949	Peak 3:	0.000	0.0	0.000
Result quality :	Good				

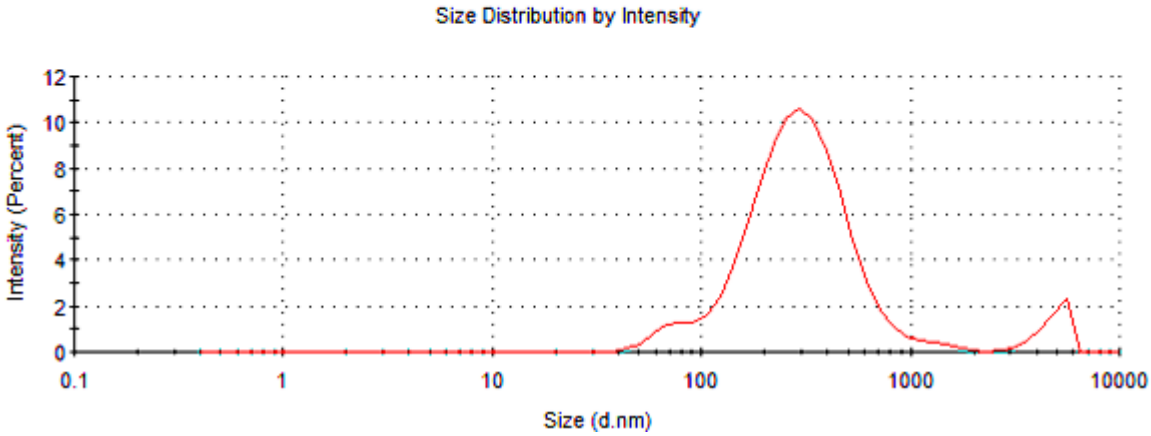

Figure 4-13: Hydrodynamic size distribution of PdNPs synthesized from GR extract

The PDI value was 0.385, demonstrating that the nanoparticles were nearly monodispersed (Clayton et al., 2016; Aljohani et al., 2022). Furthermore, the PDI value of 0.385 suggests a large size distribution and a moderate degree of heterogeneity in the PdNPs formed from GR extract. To summarise, the hydrodynamic size of 272 nm and PDI value of 0.385 indicate that the PdNPs formed from GR plant extract have a relatively large size distribution with significant variation in particle size.

4.7.3. Zeta Potential

The zeta potential measurement depicted in Figure 4-14 reveals that PdNPs possessed a negative zeta potential, averaging at -19.6 mV.

		Mean (mV)	Area (%)	St Dev (mV)
Zeta Potential (mV): -19.6	Peak 1:	-19.6	100.0	3.84
Zeta Deviation (mV): 3.84	Peak 2:	0.00	0.0	0.00
Conductivity (mS/cm): 1.17	Peak 3:	0.00	0.0	0.00

Result quality : Good

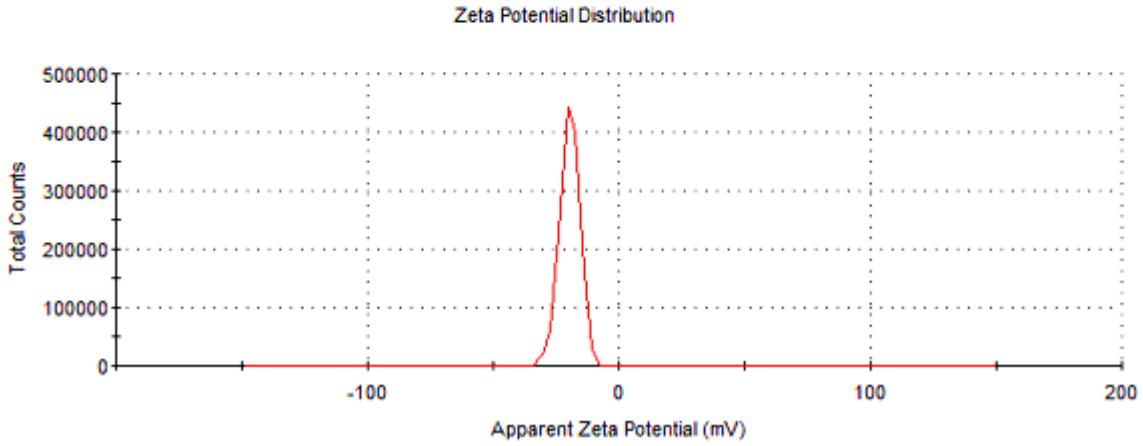

Figure 4-14: Zeta potential distribution graph of Pd NPs synthesized using GR extract

Higher negative values, exceeding -25mV, typically indicate a greater stability (Patra et al., 2015; Ali et al., 2016). The attained stability value of -19.6 mV is consistent with the standard range for stable and non-agglomerated nanomaterials. Furthermore, the magnitude of the zeta potential (-19.6 mV) is indicative of a moderately negative charge, which promotes electrostatic repulsion between the nanoparticles. Moreover, the PDI, gathered DLS, indicates the uniformity of particle size distribution in relation to the total number of particles.

4.7.4. X-Ray Diffraction (XRD)

The XRD pattern for the PdNPs synthesized using GR extract offers valuable information about the crystalline structure and the crystallographic planes existing in the nanoparticles, as depicted in Figure 4-15.

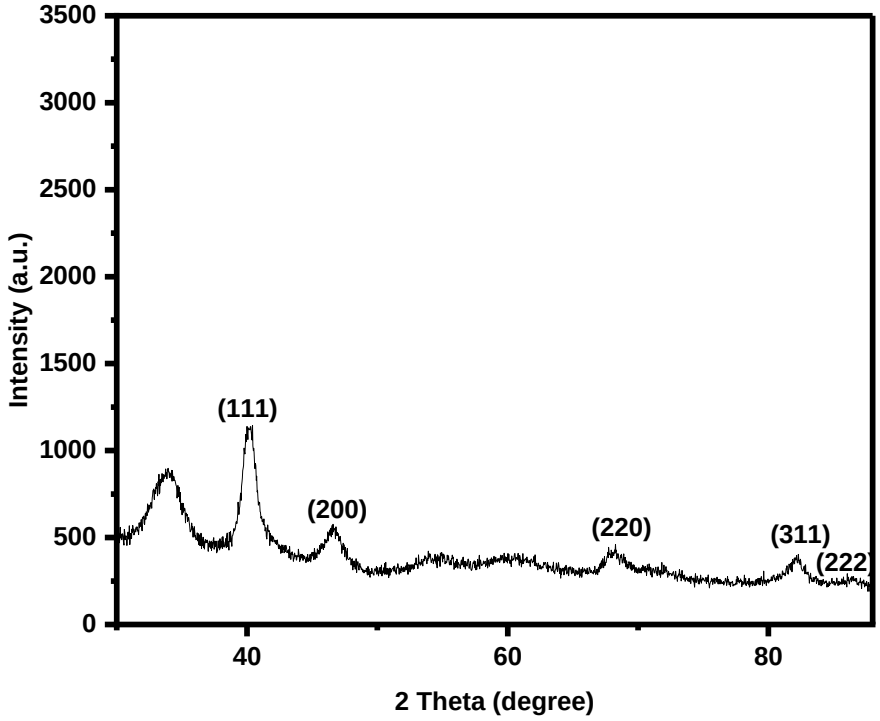

Figure 4-15: XRD pattern of PdNPs formed using GR extract

The Pd nanoparticle XRD pattern displayed five peaks at 33.95°, 40.32°, 46.66°, 68.04°, and 82.17°, corresponding to the (1 1 1), (2 0 0), (2 2 0), (3 1 1), and (2 2 2) planes of PdNPs respectively, with JCPDS card number 87-0645 (Turunc et al., 2017). This further indicated that the diffraction peaks displayed a fcc Pd crystal structure. Overall, the XRD pattern displaying these five peaks at specific 2θ angles confirms that the synthesized PdNPs are crystalline and have a well-defined crystal structure (Veisi et al., 2019). The broad peak at 33.95 is the characteristics peak of the (1 1 1) indices of Pd (0) which is an fcc structure.

4.7.5. High-Resolution Transmission Electron Microscopy (HRTEM)

Pd nanoparticle morphologies were confirmed by HRTEM analysis.

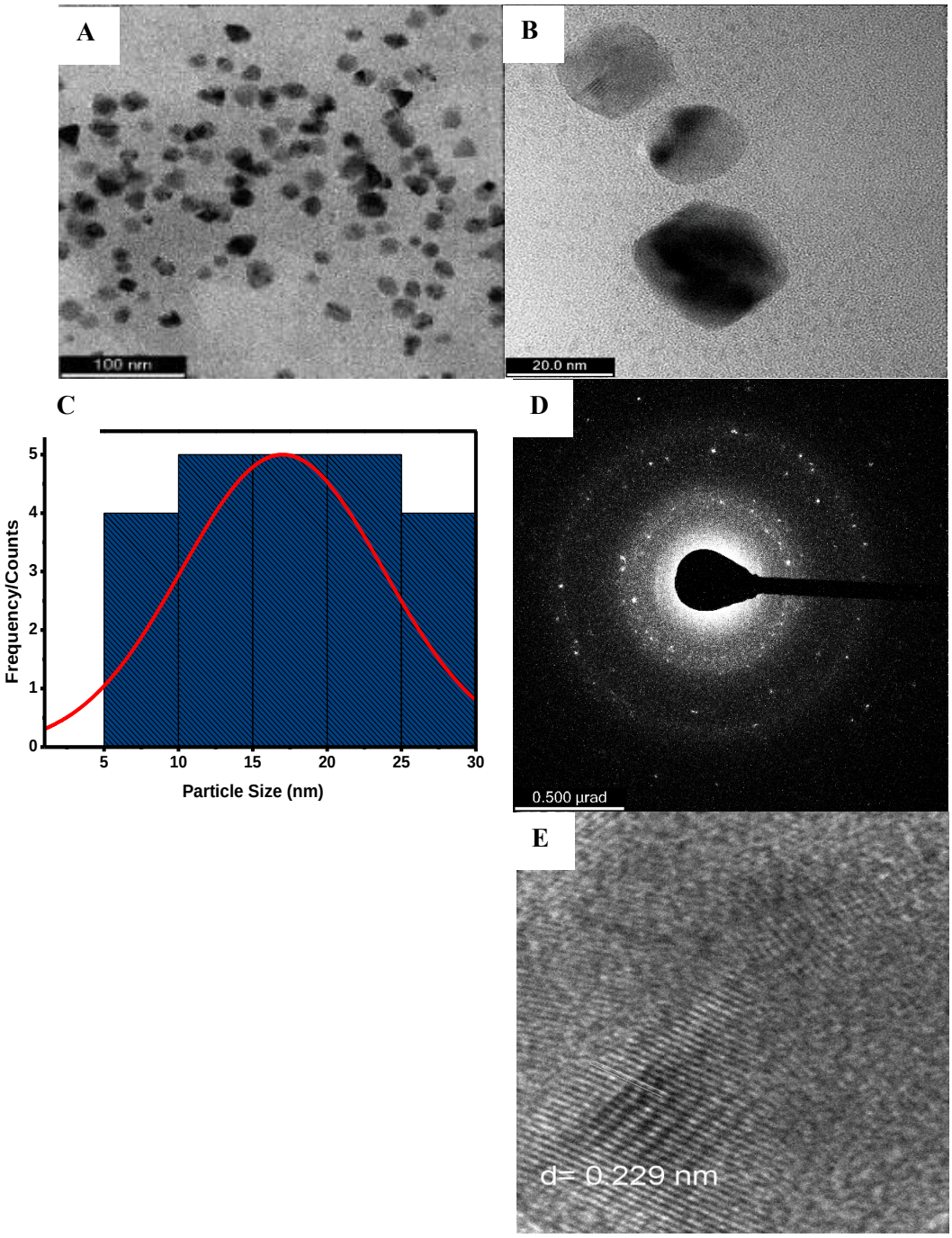

Figure 4-16: a) & b) HRTEM images of PdNPs synthesized from GR extract; c) particle size distribution curve corresponding to micrograph A; d) with its SAED pattern and e) d-spacing of PdNPs

Based on Figure 4-16 A, the PdNPs presented a homogeneous distribution and predominantly spherical nanostructures within a range of 6 to 28 nm. Moreover, the nanoparticles exhibited a mean core size of 16 nm with a size distribution of 16.25 ± 4.29 nm, as illustrated in Figure 4-16 C.

The 16.25 ± 4.29 nm particle size distribution indicates that these nanoparticles have a moderately narrow size distribution, with an average size of roughly 16.25 nm. According to Jiménez et al.'s research, higher levels of phytochemical compounds in the extract lead to a greater likelihood of forming nanoparticles with a standard shape, i.e. spherical (Jiménez Pérez et al., 2017). The GR total extract's ability to reduce was confirmed by the successful synthesis of PdNPs. Previous research investigating the use of GR by Ismail revealed PdNPs varying in size between 3.8 to 22 nm which were in agreement with the current results (Ismail et al., 2017). The reported difference in size compared to the DLS technique could possibly be attributed to factors such as the reducing agent or the matrix (Kora & Rastogi, 2018). The materials implemented in this study underwent filtration and lyophilisation to eliminate any interference from the plant extract. Compared to the other two techniques, this study presents a comprehensive set of steps involved in the production of PdNPs. Figures 4-16 D and E depict the d-spacing and the SAED patterns of the nanoparticles.

The SAED pattern (Figure 4-16 D) corresponds to (111), (200), (220), and (311) reflections of fcc structure that demonstrate the crystalline nature of the Pd nanoparticles. Moreover, these findings confirm the results of prior studies (Yang et al., 2010; Petla et al., 2012; Ismail et al., 2017). The d-spacing of 0.229 nm (Figure 4-16 C) for PdNPs indicates a precise arrangement of Pd atoms within their crystal lattice. Similar to Au, Pd also has an fcc structure. The d-spacing of 0.229 nm may correspond to a specific crystallographic plane, for example, (111) or (200), indicating the arrangement of the Pd atoms in the nanoparticles (Sonbol et al., 2021).

4.7.6. Fourier-Transform Infrared (FTIR) Spectroscopy

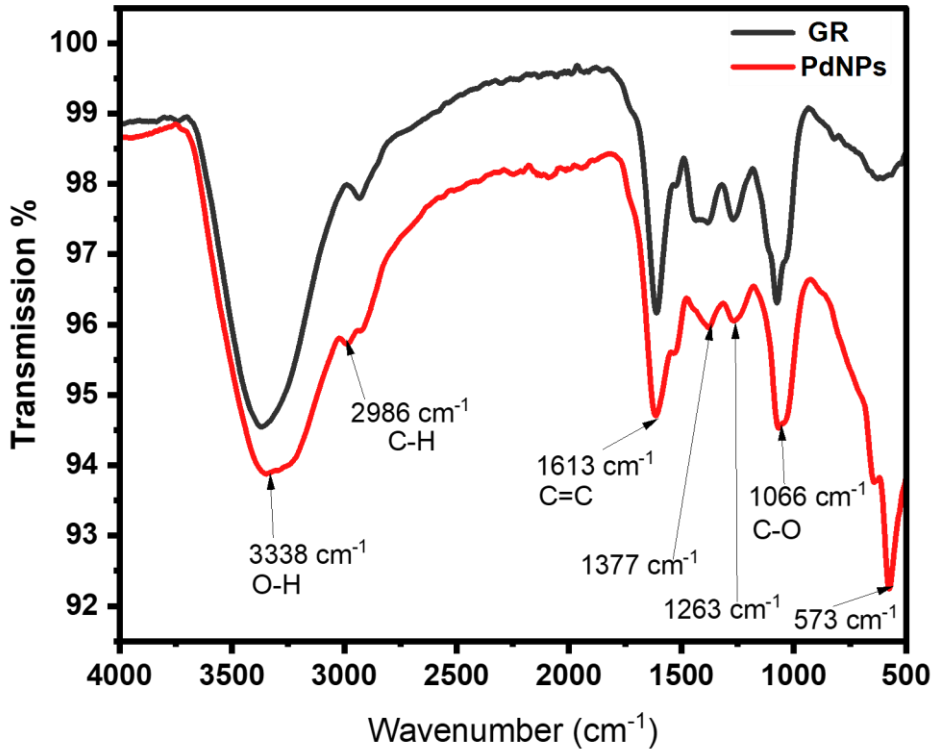

Figure 4-17: FTIR spectra of synthesized Pd NPs with the GR plant extract

Figure 4-17 shows the specific peaks and patterns observed in the FTIR spectrum of PdNPs were formed using the GR total extract, revealing the presence of various biomolecules and secondary metabolites that contribute to the reduction and stabilization processes. Thus, a comparison of the GR plant extract and its synthesized PdNPs illustrated vibrational bands at 3360 – 3338, 2929 – 2986, 1616 – 1613, 1410 – 1377, 1080 – 1066 cm^{-1}.

The hydroxyl (OH) groups present in polyphenols and flavonoids contribute to the reduction of Pd ions. This could be due to the presence of broad absorption peaks at 3338 - 3360 cm^{-1} in the FTIR spectrum (Rabiee et al., 2020; Sonbol et al., 2021). Additionally, there was an evident shift in the C-H vibrational stretching of the GR extract PdNPs from 2929 to 2986 cm^{-1}. The C=C stretching vibrations from alkene groups in the extract may also contribute to the reduction process and can be observed at approximately 1613 - 1616 cm^{-1}. Furthermore, aromatic groups (C=C) from flavonoids and phenolic compounds may have contributed to the stabilization and functionalization of PdNPs (Rabiee et al., 2020). Additionally, there was a noticeable decrease in intensity in the vibrational stretching for PdNPs within the range of 1377 – 1263 cm^{-1}.

4.8. Synthesis of Au-Pd bimetallic nanoparticles using *Aspalathus linearis*

This section provides a comprehensive analysis of the synthesized nanoparticles, their properties, and their potential implications. This section is organized into subsections to address specific aspects of the study, such as nanoparticle synthesis, characterization techniques employed, and discussions on the observed results.

4.9. Characterization of Au-Pd bimetallic nanoparticles using *Aspalathus linearis*

4.9.1. Ultraviolet-Visible (UV-Vis) Spectroscopy

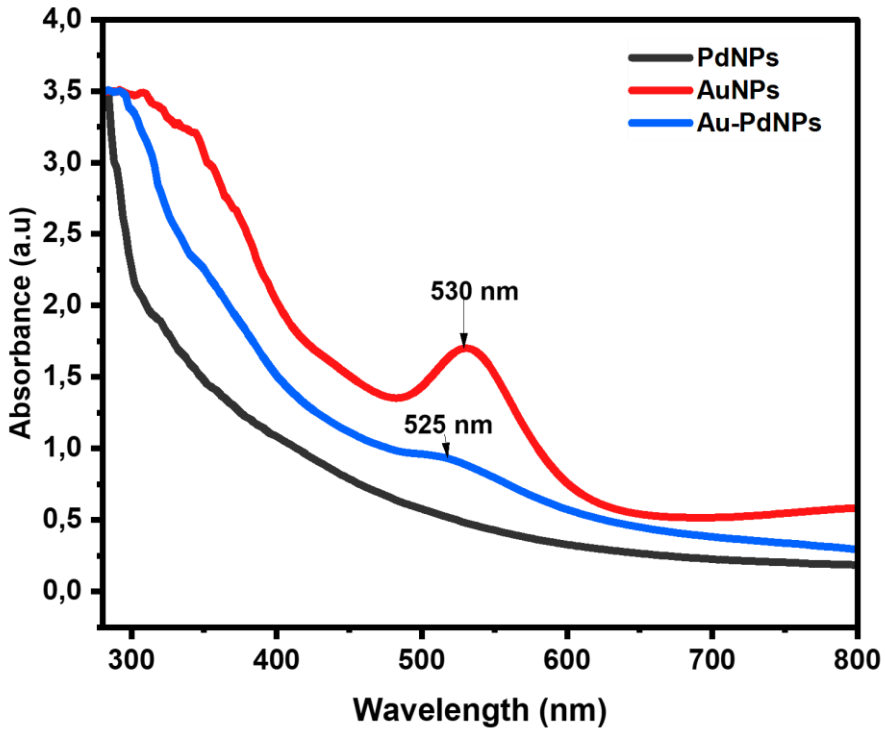

Figure 4-18: UV-Vis spectra of Au-Pd bimetallic nanoparticles and monometallic NPs (i.e., AuNPs and PdNPs)

As noted above, the Au core displayed a single SPR peak positioned at 530 nm, whereas the PdNPs had no detectable peak. The introduction of Pd alters the optical properties and could cause a shift in the SPR peak. This is in contrast to the pure AuNPs.

Figure 4-18 illustrates the spectral characteristics of Au-Pd bimetallic nanoparticles, exhibiting an absorption peak in the visible range with a maximum at 525 nm, similar to the absorption spectrum of AuNPs.

However, a blue shift in the SPR peak of Au-Pd bimetallic nanoparticles was observed in comparison to that of AuNPs. This shift is ascribed to the change in the composition and electronic structure of the nanoparticles

due to the presence of Pd (Wu et al., 2001; Cortie & McDonagh, 2011; Feng et al., 2013). The addition of Pd to AuNPs lead to a slight red-shift in the SPR peak compared to pure AuNPs, as Pd alters the optical properties. The shift in the SPR peak of the Au-Pd bimetallic nanoparticles formed using GR extract was attributed to the alloying effect between Au and Pd, changes in nanoparticle size, and alterations in the local electromagnetic environment. Similar to previous studies, the spectrum of the $Au_5Pd_{2.5}$ sample showed a comparable absorption band when prepared with a Au/Pd ratio of 2:1. Interestingly, when the concentration ratio was altered in samples Au_5Pd_5 and $Au_5Pd_{7.5}$, the maximum absorption peak was further red-shifted to 550 and 575 nm respectively, made with a concentration ratio of Au/Pd of 1:1 and 1:1.5 correspondingly (Chowdhury et al., 2018). Based on the primary analysis of the UV-Vis data, the Au-Pd bimetallic nanoparticles were formed in an alloyed configuration.

4.9.2. Dynamic Light Scattering (DLS)

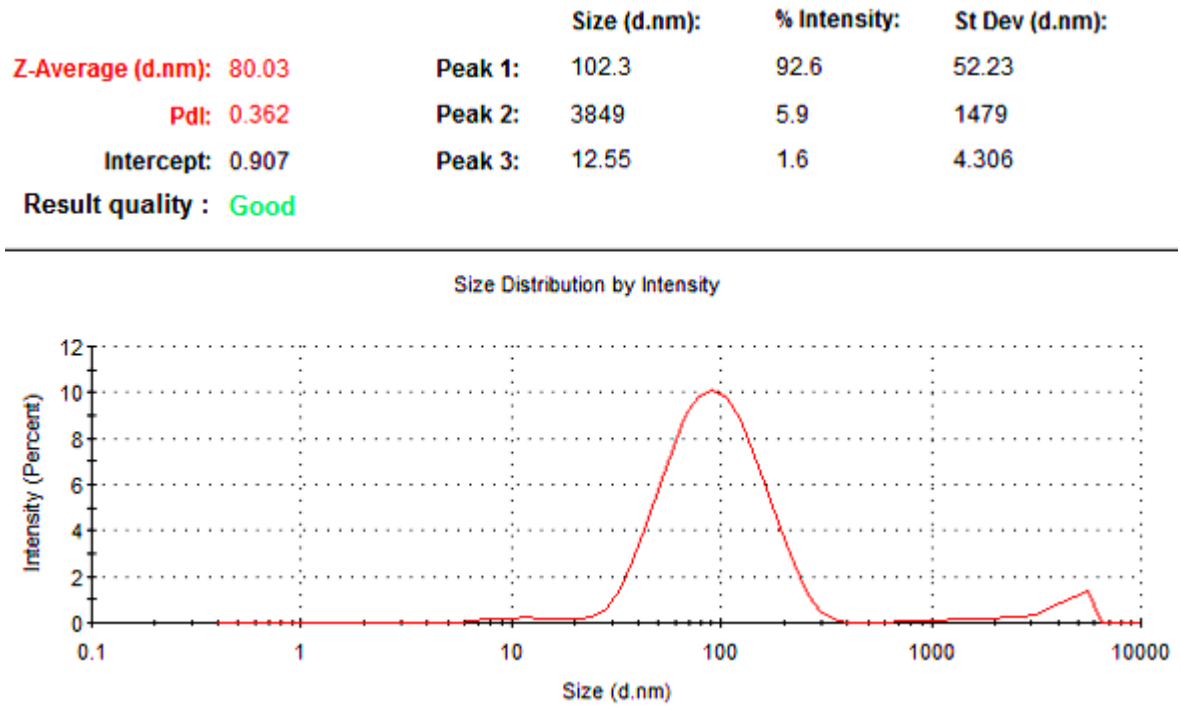

Figure 4-19: Size distribution graph of Au-Pd bimetallic nanoparticles as a function of intensity from the DLS technique

The intensity-based size distribution depicted in Figure 4-19 demonstrated a bimodal pattern (Elbagory et al., 2019), with one set of particles ranging from 12 nm to over 100 nm and a mean size of 80 nm.

Furthermore, DLS scattering plots tend to favour detecting data with frequent high-intensity scatterings, leading to skewed results. In samples with polydispersion, the low-intensity scattering from small nanoparticle sizes might be overshadowed by the high-intensity scattering from large-sized nanoparticles

(Tomaszewska et al., 2013; Minal & Prakash, 2020). The obtained PDI value of 0.362 indicates a nearly uniform and monodisperse structure.

4.9.3. Zeta Potential

		Mean (mV)	Area (%)	St Dev (mV)
Zeta Potential (mV): -18.2	Peak 1:	-18.2	100.0	3.55
Zeta Deviation (mV): 3.29	Peak 2:	0.00	0.0	0.00
Conductivity (mS/cm): 0.865	Peak 3:	0.00	0.0	0.00
Result quality : Good				

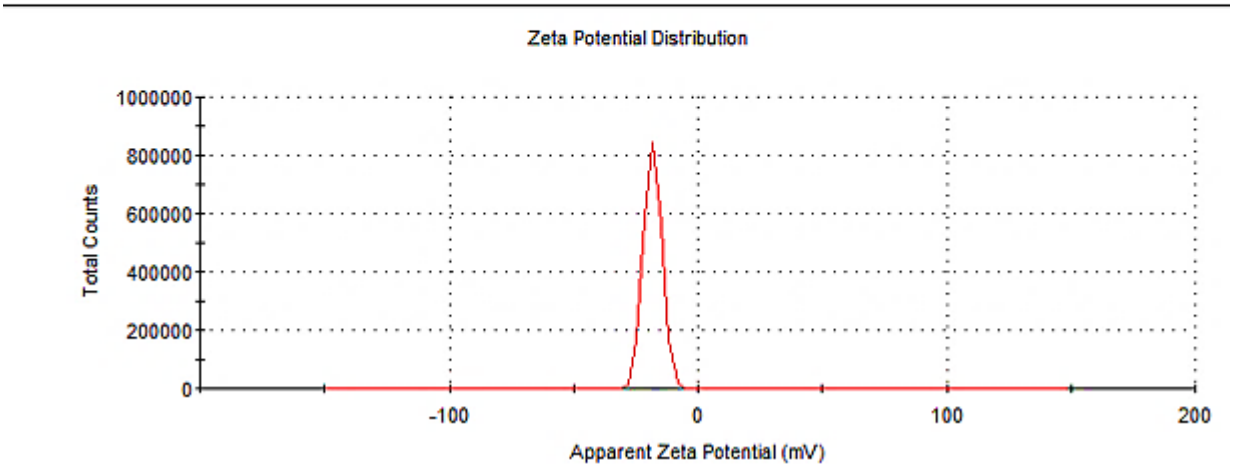

Figure 4-20: Zeta potential distribution of Au-Pd bimetallic nanoparticles by DLS

Figure 4-20 illustrates the zeta potential distribution graph of Au-Pd bimetallic nanoparticles.

The zeta potential value of -18.2 mV for Au-Pd alloy bimetallic nanoparticles, when used together with GR extract, depicts the surface electrostatic charge of the nanoparticles in suspension. The nanoparticles exhibit good dispersion stability as a result of the electrostatic repulsion between nanoparticles, as evident from their negatively charged zeta potential (Pochapski et al., 2021). This helps prevent their aggregation or flocculation. Upon interacting with GR extract, the nanoparticles may undergo interaction with the phytochemicals found in the plant, leading to changes in their zeta potential. The zeta potential value of -18.2 mV indicates that the components of GR extract adsorbed onto the surface of the nanoparticles, providing them with a negative charge (Danaei et al., 2018). This phenomenon creates an electrostatic barrier that renders the nanoparticles stable and prevents agglomeration, thereby maintaining their dispersed state.

4.9.4. X-Ray Diffraction (XRD)

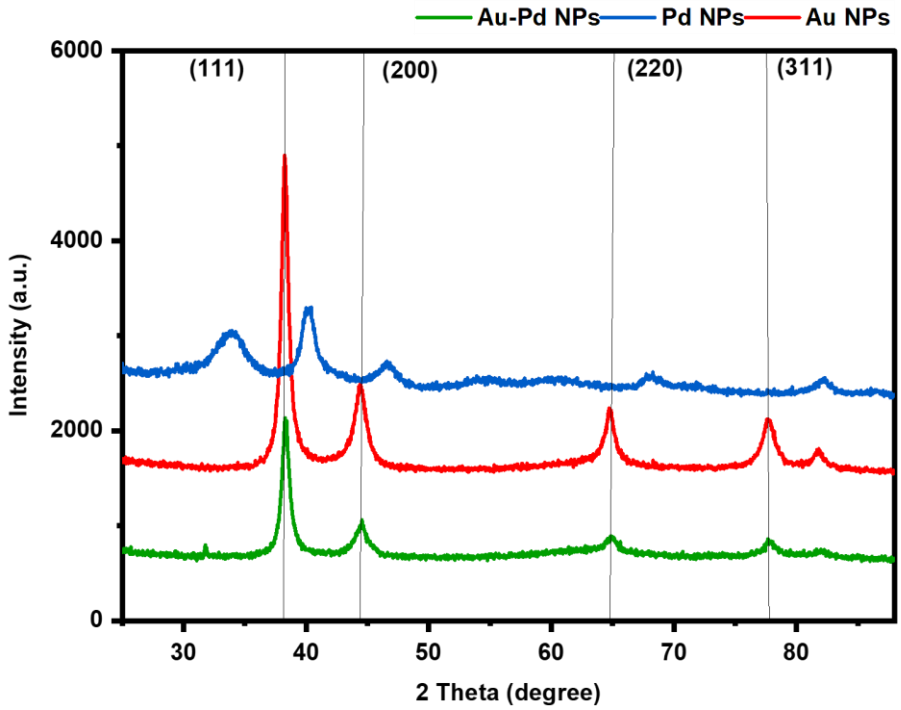

Figure 4-21: XRD pattern of AuNPs and PdNPs and Au-Pd bimetallic nanoparticles obtained using GR extract

The X-ray diffraction pattern of the Au-Pd NPs (refer to Figure 4-21) revealed 2θ peaks at 38.37, 44.49, 64.77, 77.83, and 81.97°. These peaks correspond to the (1 1 1), (2 0 0), (2 2 0), and (3 1 1) crystal planes, suggesting the fcc of Au and Pd (Mallikarjuna et al., 2019).

Notably, the diffraction peaks of the Au-Pd bimetallic nanoparticles fall between those of Pd and AuNPs. Additionally, the results show that the alloyed samples were slightly shifted to higher 2θ values compared to those of monometallic AuNPs due to the interactions with Pd atoms after the synthesis of the bimetallic Au-Pd alloy structure (Fageria et al., 2016). These findings confirm the formed Au-Pd alloyed bimetallic nanoparticles rather than a mixture of mono-metals or core-shell nanoparticles. A comparable occurrence was also documented by (Song et al., 2012; Wicaksono et al., 2020).

4.9.5. High-Resolution Transmission Electron Microscopy (HRTEM)

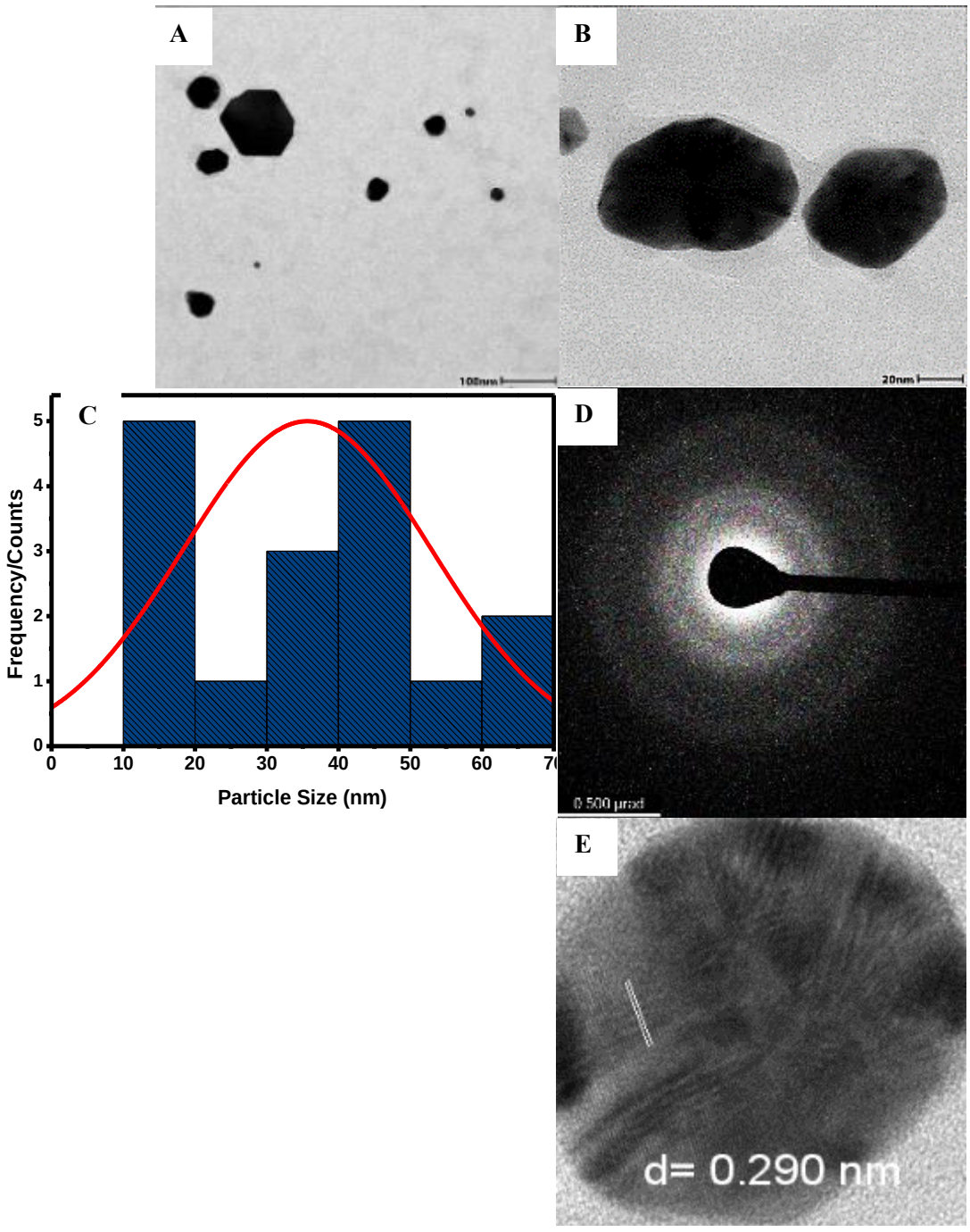

Figure 4-22: a) & b) HRTEM images c) particle size distribution corresponding to micrograph A; d) coupled with the SAED pattern of Au-Pd bimetallic nanoparticles synthesized using GR extract and e) lattice fringes of AuNPs

The HRTEM image, as presented in Figure 4-22 A, illustrates that the bimetallic nanoparticles were predominantly widely scattered, featuring both isolated particles and nanoparticles with a mean core size of 34 nm.

The core size of the bimetallic nanoparticles varied from 10 to 63 nm, with a particle size distribution of 33.78 ± 16.90 nm. This suggests that the nanoparticles have a broad size range, with some particles being relatively small (10 nm) and others being relatively large (63 nm). HRTEM analysis revealed that GR plant extract, provided good stability and dispersing effects on the bimetallic nanoparticles. This means that when the nanoparticles were exposed to GR extract, they exhibited enhanced stability by preventing agglomeration. Agglomeration of nanoparticles can have a negative impact on their performance and hinder their application. The stabilising effect of GR extract suggests that this plant extract may function as a potential stabiliser for bimetallic nanoparticles, thus helping them to maintain their dispersed state and improving their functionality.

It's noteworthy to highlight that the sizes of the Au-Pd bimetallic alloyed NPs differed when determined by the DLS method as compared to those obtained through HRTEM (Fang et al., 2019). This is due to the fact that size is related to the metal core of the nanoparticle. The dimensions of the nanoparticle are influenced by the thickness of the solvate shell that accompanies the particle, as well as any substances surrounding its surface, including capping agents. The solvate shell and the impact it has on the measured nanoparticle size rely on the material characteristics of the colloidal suspension and the nanoparticle surface. Consequently, the size of the nanoparticle as determined by DLS is larger than the size determined by HRTEM (Sekowski et al., 2017; Badeggi et al., 2022).

The Au-Pd bimetallic nanoparticle SAED pattern (Figure 4-22 D) revealed diffraction rings corresponding to crystal planes in the fcc structure (Velpula et al., 2021). The-phase segregated metals may therefore be described as polycrystalline bimetallic nanoparticles (Li et al., 2015). In addition, the distance between the crystallographic planes of Au-Pd bimetallic nanoparticles synthesised from Au and Pd is shown by the d-spacing of 0.290 nm in Figure 4-22 E. Bimetallic nanoparticles incorporate the characteristics of two different metals, and their d-spacing values may be different from those of the individual metals due to alloying effects (Zhan et al., 2011). This crystallographic plane is indicative of the arrangement of both the Au and Pd atoms. The participation of GR extract introduces an intriguing variable that may affect the alloying process and the resultant d spacing.

4.9.6. Scanning-Transmission Electron Microscopy-High Angle Annular Dark Field (STEM-HAADF)

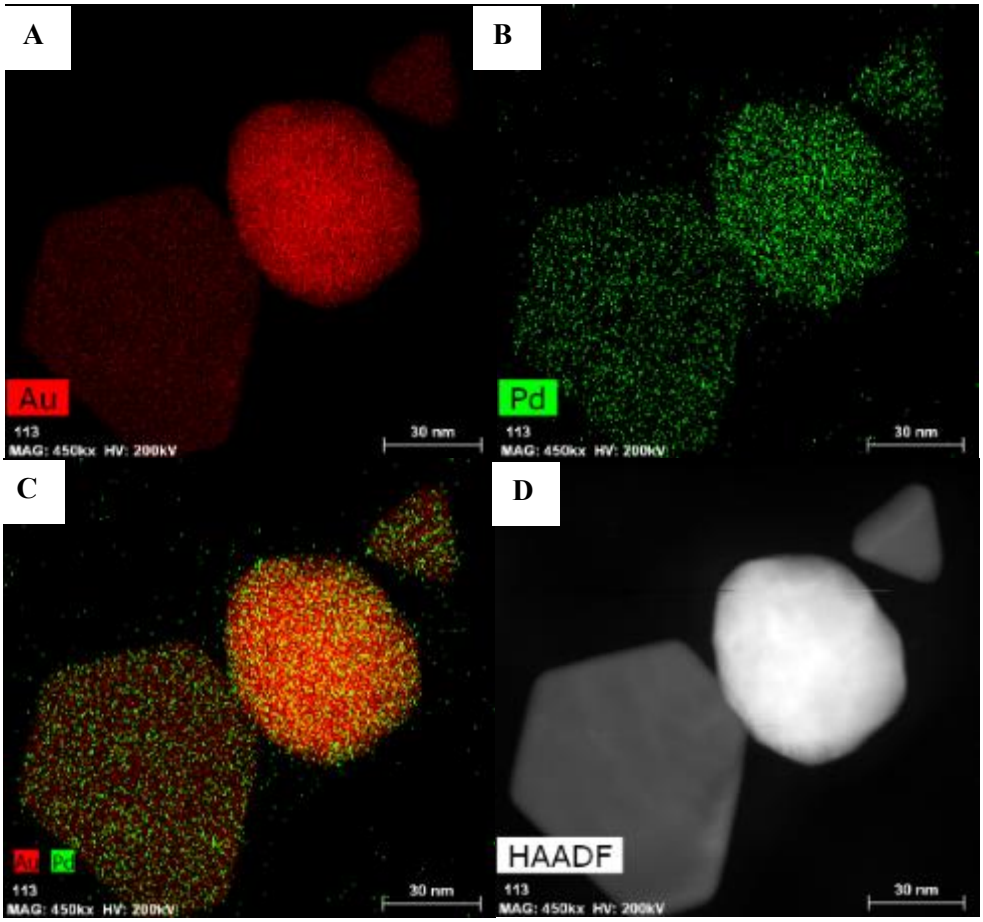

Figure 4-23: (a and b) Mapping images of individual Au (red) and Pd (green) atoms; (c) the overlaid image of Au and Pd atoms, (d) STEM-HAADF Au-Pd bimetallic nanoparticles, and the EDX spectrum is included in Appendix 2

In Figures 4-23, the STEM-EDX mapping method was employed to scrutinise the composition of the Au-Pd bimetallic nanoparticles (Slater et al., 2016). The analysis aimed to examine the Au and Pd atoms distribution. The coloured mapping images obtained exhibited an even dispersion of the Au (red) and Pd (green) atoms within the nanoparticle structure. The findings indicate an even Au and Pd atoms distribution within the nanoparticles, implying a well-formed alloy structure rather than phase separation. Figure 4-23 D shows a HAADF image of well-mixed Au-Pd alloy nanoparticles with uniformly dispersed bright spots that correspond to Au and Pd atoms, supporting the formation of an alloy with even dispersion of both elements (Zhan et al., 2011).

The EDX spectrum, as illustrated in Appendix 2, validated the existence of both Au and Pd in the solution. Any additional peaks observed are likely attributed to sample preparation or the glass substrate employed in the sample preparation for analysis.

4.9.7. Fourier-Transform Infrared (FTIR) Spectroscopy

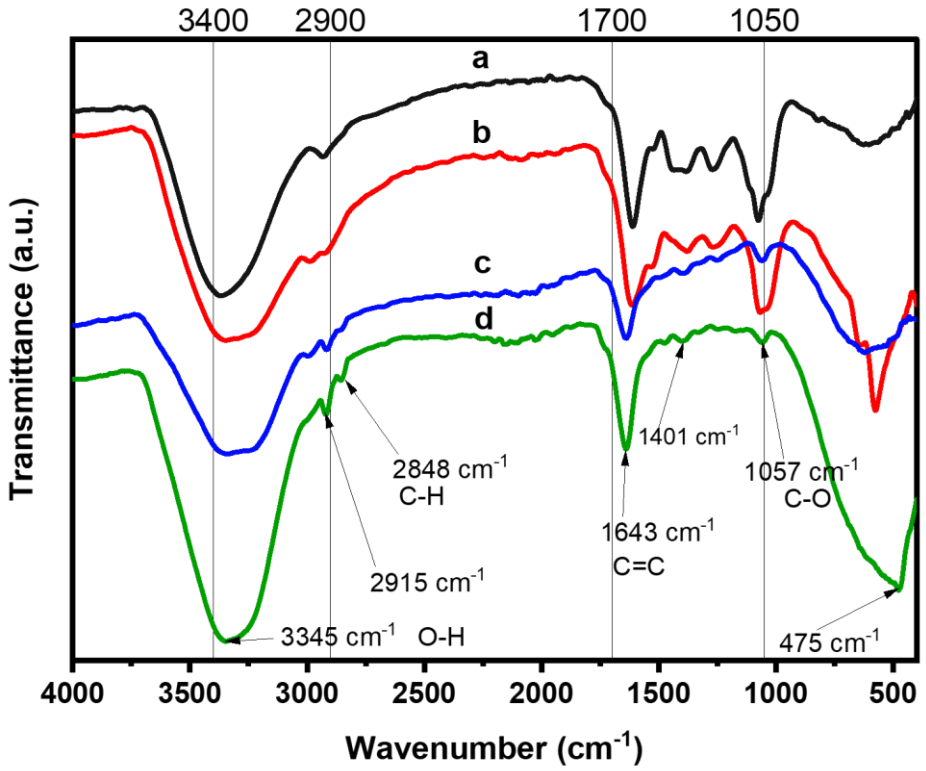

Figure 4-24: The FTIR spectra of the (a) GR extract, (b) and (c) monometallic Au and PdNPs with the (d) Au-Pd bimetallic nanoparticles

As Ovais et al. (2018) have highlighted, polyphenols play a pivotal role as primary reducing and stabilising agents in the environmentally friendly formation of metallic nanoparticles. Therefore, FTIR analysis was employed to identify the functional groups of phytochemicals that are involved in the reduction of metal ions to their zero-valent state (Aboyewa et al., 2021). The synthesized AuNPs, PdNPs, and Au-Pd bimetallic nanoparticles using the GR plant extract were subjected to FTIR analysis within the 400–4000 cm^{-1} range.

The FTIR spectrum of the plant extract (Figure 4-24 A) exhibited peaks at 3360, 2929, 1616, 1410, and 1080 cm^{-1}. Notably, the C=C vibration stretching at 1616 cm^{-1} and 3360 cm^{-1} for the O-H group of phenolic molecules was observed in the FTIR spectrum of the GR plant extract (Wicaksono et al., 2020; Samodien et al., 2021). The peaks at 1410 and 1080 cm^{-1} corresponded to -C-O and -C-O-C stretching modes, respectively. Additionally, the bands at 2929 cm^{-1} represented the asymmetric and symmetric C-H vibration

stretching (Blom van Staden et al., 2021). These vibrational bands indicated the existence of phenolics in the GR extract. A comparison of the extract spectrum with the synthesized AuNPs revealed a bonded stretch of the O-H group at 3326 cm^{-1} and C=C at 1638 cm^{-1}, closely resembling those of the extract. In contrast, the spectrum of PdNPs displayed O-H and C=C vibration stretching at 3338 cm^{-1} and 1613 cm^{-1}, respectively.

In Figure 4-24 D, the FTIR spectrum of Au-Pd bimetallic alloyed nanoparticles displayed vibrational peaks at 3345, 2915, 2848, 1643, 1401, and 1057 cm^{-1}. The spectrum displayed a peak at 3345 cm^{-1} representing O-H stretching vibrations, while another at 2915 cm^{-1} indicated the C-H stretching vibrations from the $-CH_3$ groups. The vibration of C=C in benzene was observed at 1643 cm^{-1} (Han et al., 2017; Mallikarjuna et al., 2019). Moreover, a small band at 1057 cm^{-1} associated to the C-H stretching vibrations of the aromatic rings. The FTIR profile suggested that the formation of Au–Pd bimetallic alloy nanoparticles corresponded to phenolic compounds.

The results confirmed that some of the phytochemicals present in the GR extract are bound to the surface of monometallic or bimetallic alloy nanoparticles, contributing to the stability of the nanoparticles.

4.11. Synthesis of nanoparticles using Aspalathin

In the context of nanoparticle synthesis, ASP acts as a reducing agent, providing electrons to reduce metal ions into metallic nanoparticles. The reducing strength of ASP can be attributed to its chemical structure, which contains functional groups capable of electron donation. Flavonoids, including ASP, often have hydroxyl (-OH) groups and carbonyl (C=O) groups, which can participate in redox reactions. During the synthesis of nanoparticles, ASP can donate electrons to metal ions, leading to their reduction and subsequent formation of nanoparticles. The specific mechanism of reduction can vary depending on the metal ions and reaction conditions employed. The electron donation by ASP helps stabilize the metal ions in a reduced state, preventing their re-oxidation and allowing for the formation of stable nanoparticles.

4.11.1. Synthesis of gold nanoparticles using Aspalathin

The previous sections examined the formation of AuNPs employing the GR total extract as a reducing and stabilizing agent. In this section, the pure compound ASP was used as a reducing and stabilizing agent in the formation of AuNPs to evaluate its effectiveness in producing AuNPs.

4.12. Characterization of gold nanoparticles using Aspalathin

4.12.1. Ultraviolet-Visible (UV-Vis) Spectroscopy

The transition from yellow to red-violet colouration primarily indicates the formation of AuNPs. The red-violet colour observed is attributed to the occurrence of SPR in AuNPs (Aldawsari et al., 2021), as mentioned above (Section 4.5.1).

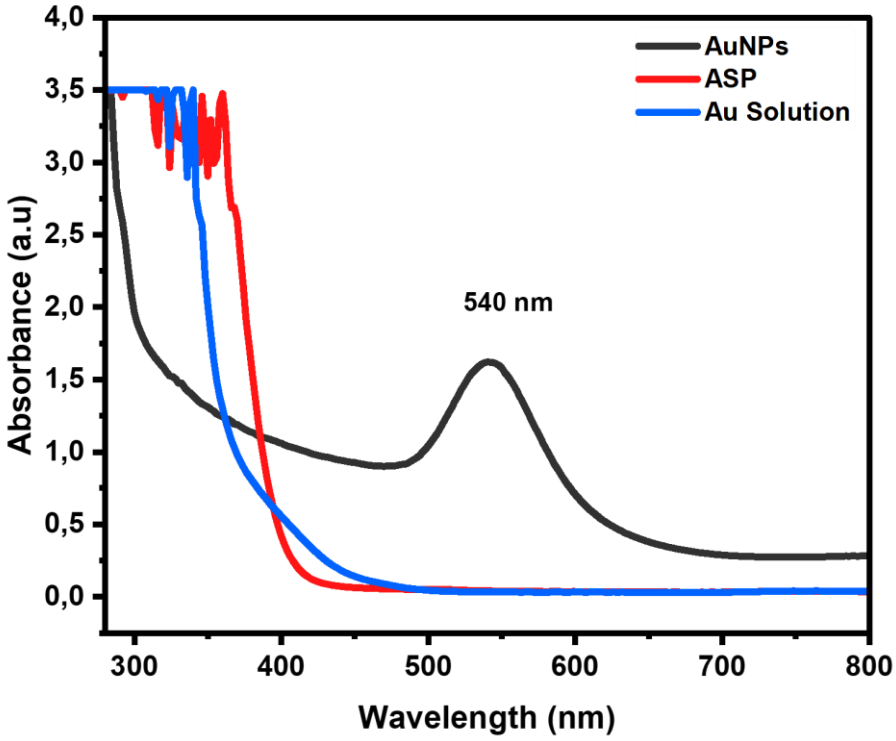

Figure 4-25: UV-Vis absorbance spectra of synthesized Au NPs using the major compound (ASP)

An absorption peak (shown in Figure 4-25) at 540 nm wavelength was observed after an hour of incubation, corresponding to the SPR band of AuNPs.

4.12.2. Dynamic Light Scattering (DLS)

The mean size of ASP Au NPs was 53.94 nm, as determined from the intensity distribution graph in Figure 4-26.

			Size (d.nm):	% Intensity:	St Dev (d.nm):
Z-Average (d.nm):	53.94	Peak 1:	76.48	94.6	31.83
PdI:	0.296	Peak 2:	5.613	5.4	1.357
Intercept:	0.899	Peak 3:	0.000	0.0	0.000
Result quality :	Refer to quality report				

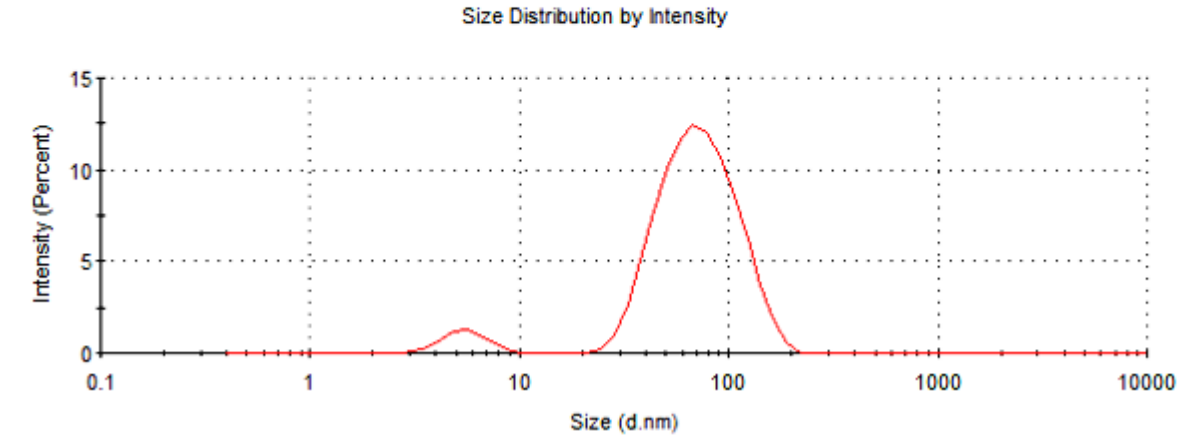

Figure 4-26: The hydrodynamic size distribution graph by the intensity of AuNPs formed from ASP

Additionally, the data on PDI acquired through the DLS technique reflects the uniformity of various particle sizes within the total particle population (Pedroso-Santana & Fleitas-Salasar, 2020; Sarfraz & Khan, 2021). The PDI value recorded was 0.296, signifying a nearly homogeneous and monodisperse distribution of particle sizes.

4.12.3. Zeta Potential

The AuNPs produced zeta-potential values that indicated stable colloidal dispersions. The corresponding zeta potential value of -27.1 mV, presented in Figure 4-27, confirmed this for the Au nanoparticles.

		Mean (mV)	Area (%)	St Dev (mV)
Zeta Potential (mV): -27.1	Peak 1:	-27.2	100.0	10.2
Zeta Deviation (mV): 10.2	Peak 2:	0.00	0.0	0.00
Conductivity (mS/cm): 1.29	Peak 3:	0.00	0.0	0.00

Result quality : See result quality report

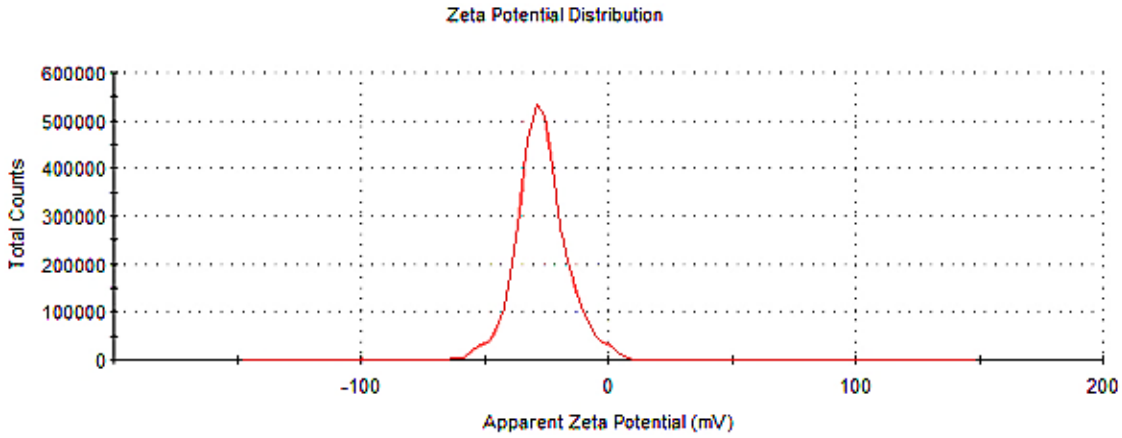

Figure 4-27: Zeta potential distribution graph of AuNPs formed using ASP

This value, using ASP, indicated a highly negative charge on the nanoparticle surface, suggesting a stable nanoparticle suspension with low potential for aggregation. The zeta potential of AuNPs was impacted by the presence of ASP.

Furthermore, ASP adsorbed onto the nanoparticle surface, causing a change in charge distribution, and resulting in a negative zeta potential value. The value of -27.1 mV indicated a strong stabilising effect of aspalathin on the AuNPs. Nanoparticles exhibiting zeta potential values of -30 mV or less are anticipated to be predominantly surrounded by negatively charged ions. A strong negative charge promotes repulsion between nanoparticles, ensuring their dispersion in the solution.

4.12.4. X-Ray Diffraction (XRD)

The X-ray diffraction spectrum presented in Figure 4-28 provides evidence of the crystalline properties of the Au NPs.

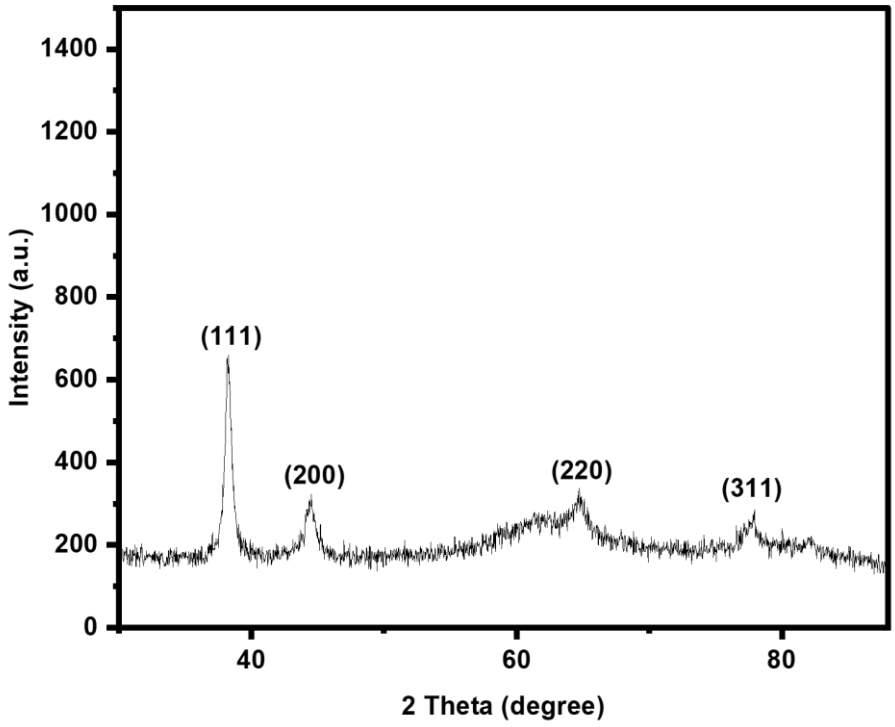

Figure 4-28: XRD pattern of AuNPs produced using ASP

The corresponding XRD pattern displays four peaks at 2θ values of 38.25°, 44.55°, 64.80°, and 77.61°, indicating the standard Bragg's reflections corresponding to the (1 1 1), (2 0 0), (2 2 0), (3 1 1) and (2 2 2) planes of the fcc lattice for AuNPs. The most prominent peak corresponds to the (1 1 1) plane. The (1 1 1) crystallographic plane peak of AuNPs, confirming the densely packed planes within the fcc lattice structure, is strong and intense in XRD patterns, and characteristic of the fcc arrangement (Apte et al., 2013; Cherian et al., 2022). Additionally, the existence of four peaks corresponding to the standard Bragg's reflections of the fcc lattice in the XRD pattern confirms the crystalline nature and well-defined crystal structure of the AuNPs. The fcc arrangement is widely acknowledged as one of the most stable and popular structural formations for bulk Au, and it is also sustained in numerous AuNPs of different shapes and sizes (Stanciu et al., 2022).

4.12.5. High-Resolution Transmission Electron Microscopy (HRTEM)

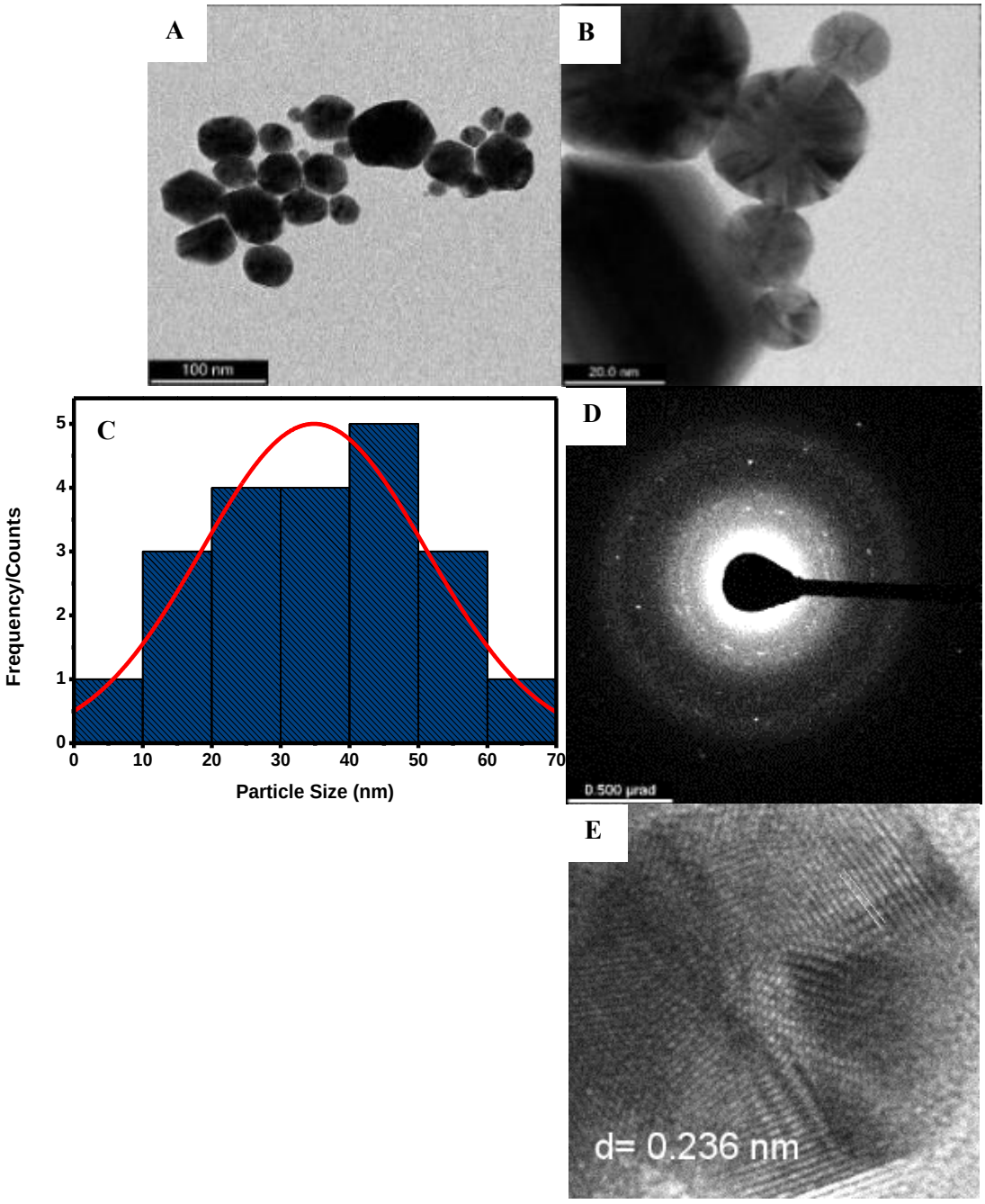

Figure 4-29: a & b) HREM micrographs of AuNPs synthesized using ASP; c) particle size distribution graph corresponding to micrograph A; d) coupled with its SAED pattern and e) d-spacing value of adjacent fringes

The morphologies of Au -synthesized NPs from ASP were characterized by HRTEM, as shown in Figure 4-29 A and B. The HRTEM analysis disclosed that the AuNPs derived from ASP exhibited a size spectrum ranging from 4 to 57 nm. The previously observed narrow UV-Vis peak (Figure 4-25) suggests a relatively uniform size distribution for the majority of nanoparticles contributing to the absorption signal, while HRTEM analysis indicate a considerable variation in size with some being very small (4 nm) and others being relatively larger (57 nm).

The histogram showing the relative size distribution of nanoparticles is displayed in Figure 4-29 C. Accordingly, the resulting size distribution was 34.36 ± 15.12 nm. The HRTEM micrograph of the AuNPs formed from the major compound indicated mainly spherical particles. The presence of a pure compound acting as a reducing and stabilizing agent might have contributed to the formed shape because the already discussed nanoparticles formed from the total extract appeared to have a mixture of shapes owing to the phytochemicals found in the plant (Pu et al., 2019). Furthermore, the micrographs indicate nanoparticles with a narrow size distribution, and were nearly monodispersed.

It is noteworthy that DLS analysis typically yields larger sizes than those obtained through HRTEM. The differences between DLS and HRTEM measurements may be attributed to the sample volume used during analysis, as the physical nature of the measurement and the average weight determined in some cases means DLS measurements are not always equivalent to those obtained using an electron microscope (Fang et al., 2019; Badeggi et al., 2020). Furthermore, it was noted that employing a pure compound led to the formation of nanoparticles with smaller sizes. This indicates the importance of synthesizing AuNPs utilizing a pure substance that serves as both a stabilizing and reducing agent.

Figures 4-29 D and E illustrate the SAED pattern of the nanoparticles, and the high-resolution image showing the lattice fringes and measured d-spacing, respectively. The HRTEM micrographs are coupled with the SAED pattern of the synthesized AuNPs which revealed the appearance of rings and bright spots in a circular pattern. The SAED pattern provided additional confirmation on the polycrystallinity of the sample. On the other hand, the d-spacing value of 0.236 nm for the AuNPs indicate the distance between specific crystallographic planes (i.e., (1 1 1)) within the lattice structure of the nanoparticles (Janecek & Kral, 2016; Anadozie et al., 2023).

4.12.6. Fourier-Transform Infrared (FTIR) Spectroscopy

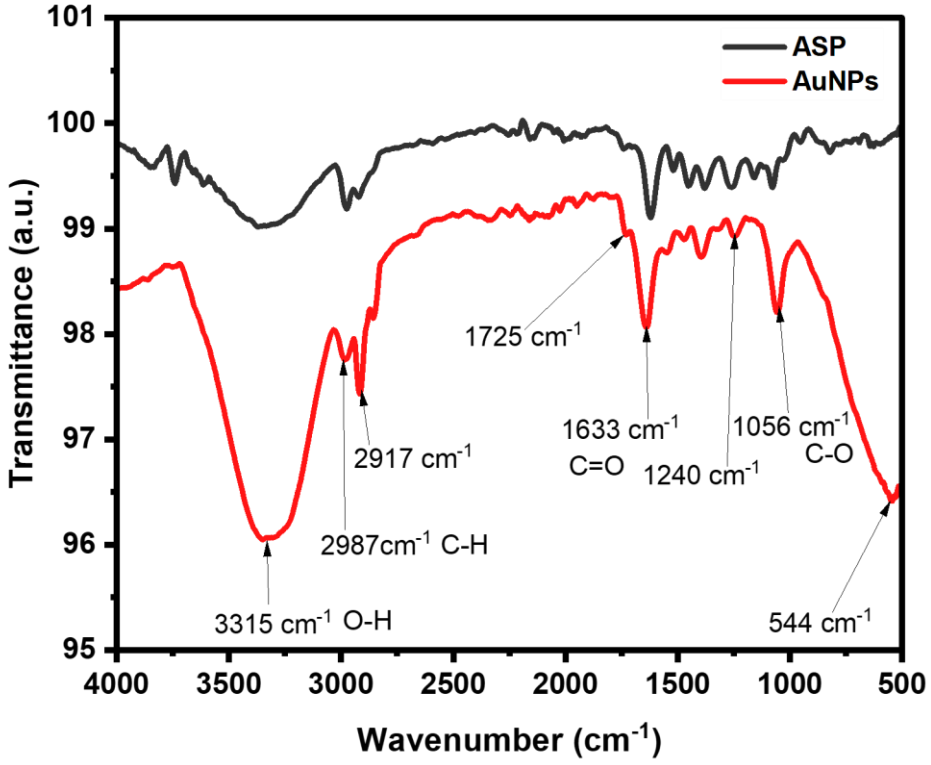

Figure 4-30: The FTIR spectrum of AuNPs synthesized using ASP with the ASP spectrum

FTIR is a powerful analytical technique that can be used to study the interactions between ASP and AuNPs. To analyse the synthesis of AuNPs using ASP, FTIR was utilised for the detection of the existence of capping agents within the frame of the prepared nanoparticles. This also can help to identify possible interactions between ASP and Au metal, as well as the stabilisation mechanism of the resulting Au NPs.

Typically, the FTIR spectrum of ASP (as shown in Figure 4-1 and Figure 4-30) showed characteristic peaks corresponding to different functional groups such as hydroxyl (-OH, 3338 cm^{-1}), carbonyl (C=O, 1624 cm^{-1}) and aromatic rings (as seen in Section 4.3). A comparison of the FTIR spectrum with that of the produced AuNPs confirmed a bonded stretch of the O-H group at 3315 cm^{-1} and C=C at 1633 cm^{-1}, which is shifted to that of the compound. Other vibrational frequency bands for AuNPs included 2987 cm^{-1}, 2917 cm^{-1} of C-H alkane stretching and 1056 cm^{-1}.

4.13. Synthesis of palladium nanoparticles using Aspalathin

The following section provides further insight into the reducing strength of the isolated pure ASP by employing it as both a reducing and stabilizing agent in the production of PdNPs to evaluate its ability to form PdNPs. Due to limited specific research on the synthesis and reducing the strength of ASP for Pd nanoparticle synthesis, this section will be regarded as a novel contribution to research.

4.14. Characterization of palladium nanoparticles using Aspalathin

4.14.1. Ultraviolet-Visible (UV-Vis) Spectroscopy

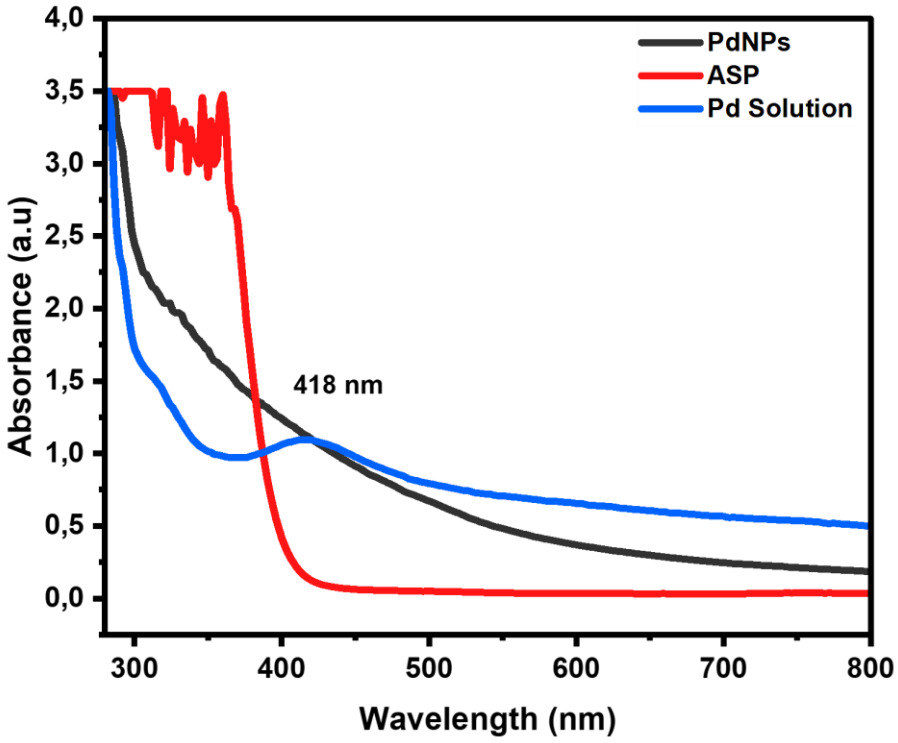

Figure 4-31: UV-Vis spectra of PdNPs synthesized using Aspalathin coupled with the Pd chloride salt solution and the major compound control

The optical properties of the synthesised PdNPs solution showed significantly different absorption spectra (Figure 4-31) from the main compound, suggesting complete reduction over time.

The yellow-brownish coloured reaction mixture was converted to the characteristic brown colour. The appearance of the brown colour is associated with the formation of PdNPs. The observed results are very consistent with recent reports. The exact mechanism is still unclear, but the phenolic/hydroxyl groups occupy a vital role in the reduction reaction. Here the λ_{max} of $PdCl_2$ was observed at 418 nm. UV-vis spectra were recorded with a notable change with the disappearance of the $PdCl_2$ peak at around 418 nm. No extinct

peak was observed for PdNPs, indicating the reduction of Pd^{2+} to Pd° metal ion. Literature has reported comparable findings in UV-Vis analysis regarding the environmentally friendly production of PdNPs (Ismail et al., 2017; Vaghela et al., 2019; Soltys et al., 2021). At the end of the reaction, a brown colour was observed after one hour, confirming that ASP had strong reducing properties.

4.14.2. Dynamic Light Scattering (DLS)

Employing DLS analysis facilitated the determination of the hydrodynamic size distribution of the PdNPs. The size distribution intensity graph of PdNPs is illustrated in Figure 4-32. The hydrodynamic size was quantified at 72.11 nm.

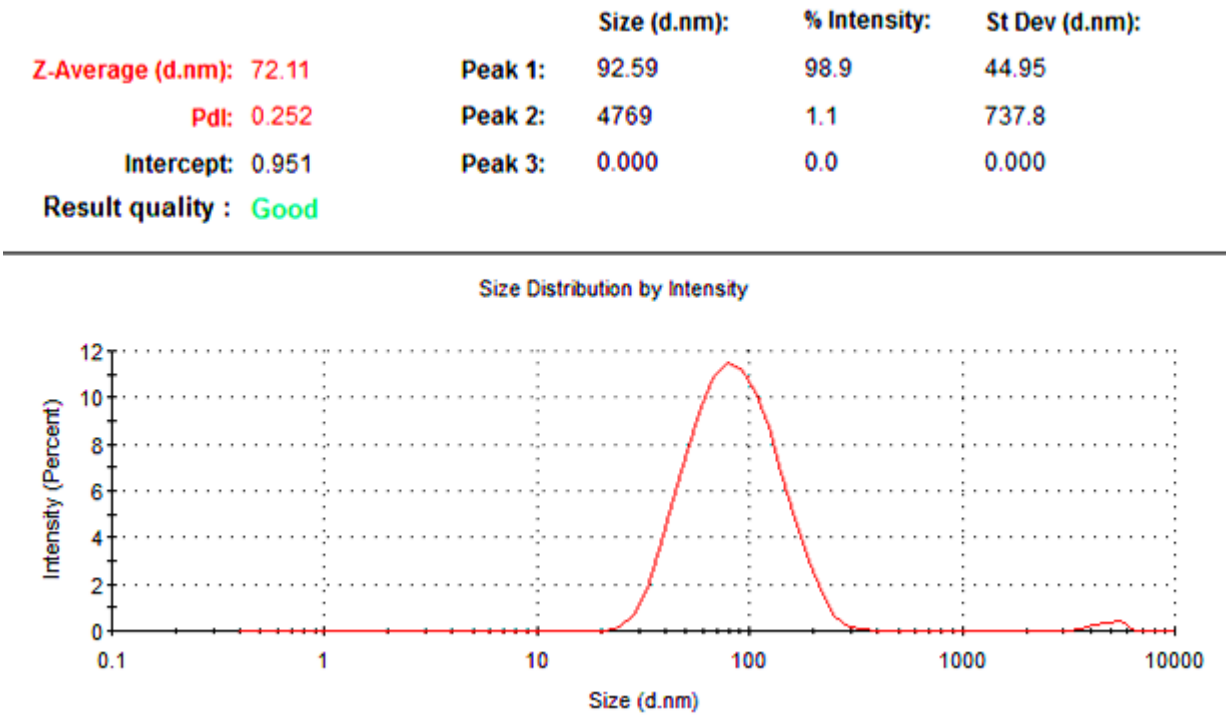

Figure 4-32: The size distribution graph of PdNPs obtained from ASP displaying a hydrodynamic size below 100 nm

Additionally, the PdNPs demonstrated a high degree of uniformity, as evidenced by a PDI value of 0.252, highlighting the consistency in the nanoparticle size distribution. Utilizing ASP yielded PdNPs with a reduced size compared to GR-PdNPs, suggesting the significance of using a pure material or compound as a reducing agent for Pd nanoparticle formation.

4.14.3. Zeta Potential

DLS analysis of all the nanoparticles yielded crucial insights not just into their size but also their stability. The stability of the synthesized PdNPs was evaluated through the measurement of their zeta potential. The determined zeta potential value of -24 mV is illustrated in Figure 4-33.

		Mean (mV)	Area (%)	St Dev (mV)
Zeta Potential (mV): -24.0	Peak 1:	-24.0	100.0	4.81
Zeta Deviation (mV): 4.62	Peak 2:	-38.4	3.6	2.28
Conductivity (mS/cm): 0.820	Peak 3:	0.00	0.0	0.00
Result quality : Good				

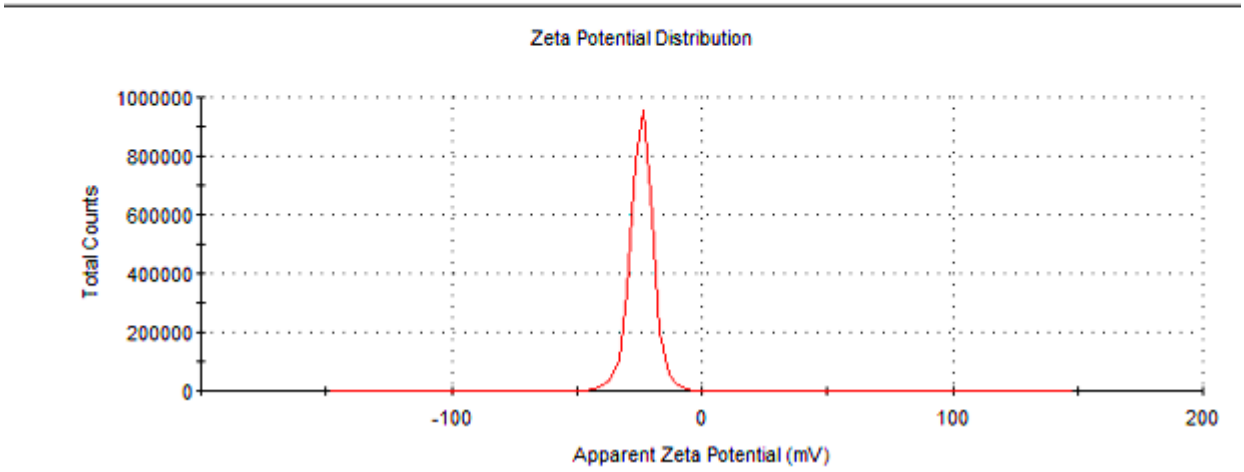

Figure 4-33: Zeta potential distribution graph of PdNPs synthesized using ASP

The significant magnitude of the zeta potential at -24.0 mV signifies a relatively strong negative charge, fostering electrostatic repulsion among nanoparticles. This repulsion plays a vital role in preventing aggregation, thereby enhancing the nanoparticle stability and dispersion in the surrounding medium.

4.14.4. X-Ray Diffraction (XRD)

Conversely, the XRD pattern after the synthesis of PdNPs displays the crystalline nature of all the peaks distinguishable. The XRD pattern, in Figure 4-34, corresponding to the pure crystalline nature of the biosynthesised PdNPs exhibits Bragg reflections manifested on fcc PdNPs.

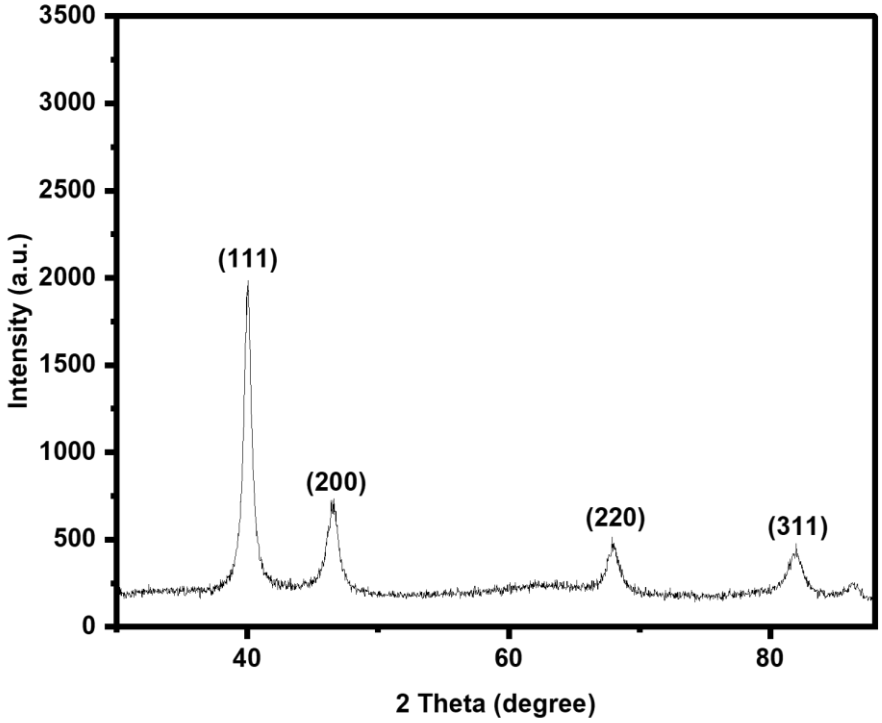

Figure 4-34: XRD pattern of PdNPs synthesized using ASP

The spectrum displayed five diffraction peaks at 39.99°, 46.39°, 68.04°, 81.94°, and 86.44° corresponding to the (1 1 1), (2 0 0), (2 2 0), (3 1 1), and (2 2 2) crystal planes of Pd observed which matched the standard powder diffraction card of JCPDS Pd file no.87-0643 (Shu et al., 2022). The XRD data were extensively reliable with the previous studies using plants as a reducing agent (Nadagouda & Varma, 2008; Vaghela et al., 2019; Fahmy et al., 2021).

4.14.5. High-Resolution Transmission Electron Microscopy (HRTEM)

The PdNPs generated from the compound are depicted in Figure 4-35 A and B, along with the corresponding presentation of particle size distribution illustrated in Figure 4-35 C. The crystallinity results were obtained from the SAED pattern and the d-spacing of the adjacent lattice fringes in Figure 4-35 D and E respectively.

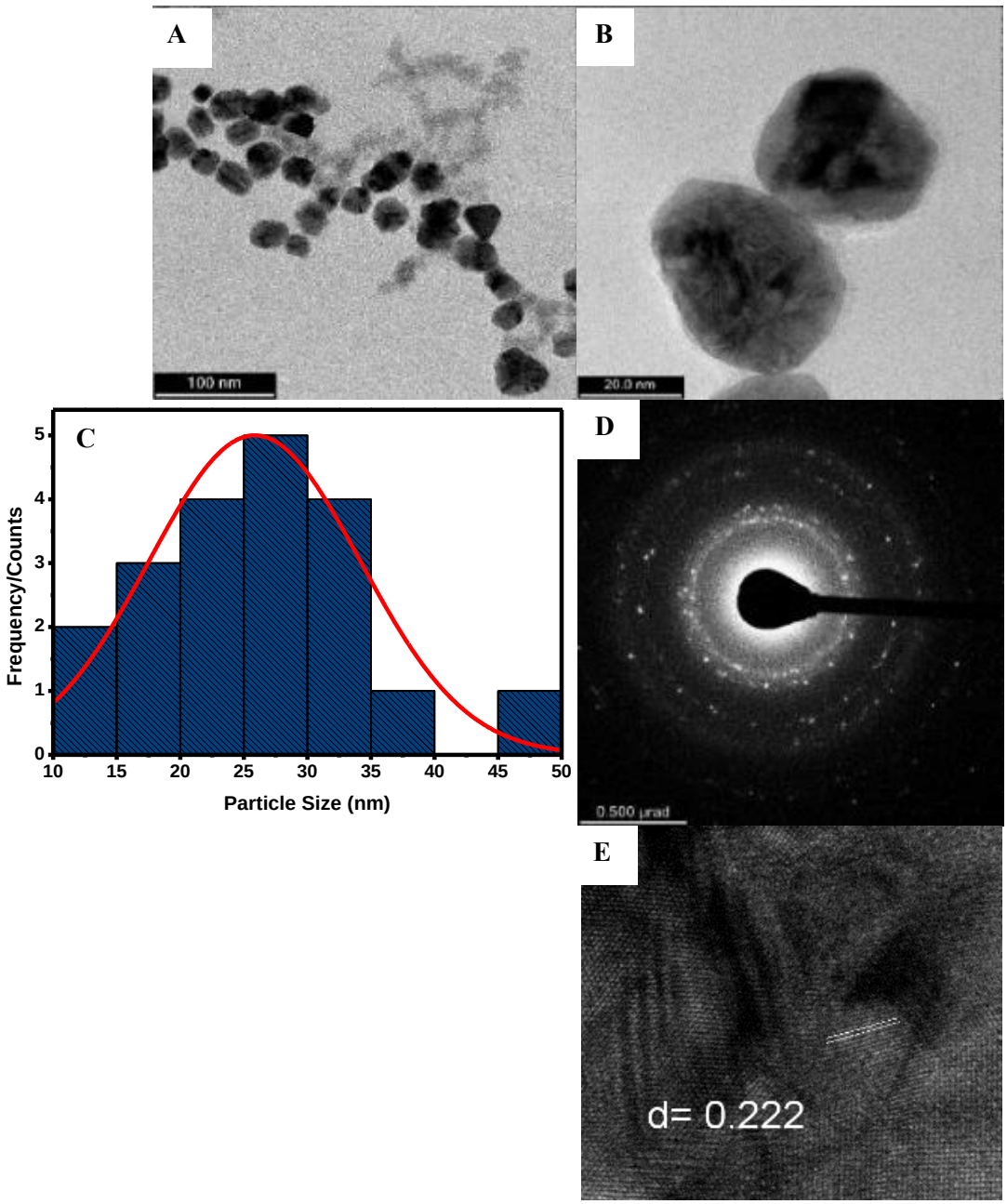

Figure 4-35: a) & b) HRTEM micrographs pattern of PdNPs using ASP; c) particle size distribution; SAED pattern and e) d-spacing value of lattice fringes

The PdNPs generated from the compound are depicted in Figure 4-35 A and B. The HRTEM analysis showed that the PdNPs formed from ASP exhibited different shapes, namely spherical and irregular shapes. Spherical nanoparticles are well defined and symmetrical, resembling tiny spheres. The PdNPs exhibited a size spectrum within a range of 13 to 47 nm, with a mean core size measured at 26 nm and a particle size distribution recorded as 26.18 ± 6.77 nm, as displayed in Figure 4-35 C. The nanoparticles appeared to be almost monodispersed and uniformly distributed. Uniform distribution means that the nanoparticles were

evenly distributed throughout the sample without significant clustering or agglomeration. Hence, ASP emerges as a crucial pure compound, serving as both a reducing and capping agent, attributing to the achievement of PdNPs with reduced dimensions.

The crystallinity results were obtained from the SAED pattern and the d-spacing of the adjacent lattice fringes in Figure 4-35 D and E respectively. Furthermore, the SAED patterns of the PdNPs confirmed the presence of the appearance of ring-like peaks, which are consistent with the XRD fcc corresponding to (1 1 1), (2 0 0), (3 1 1) and (2 2 2). Furthermore, the obtained d-spacing value of 0.222 nm for PdNPs was remarkably close to the d-spacing value of the (1 1 1) plane in bulk Pd. This similarity indicates that the nanoparticles have a well-defined crystallographic structure and are predominantly oriented along the (1 1 1) plane (Lee et al., 2009; Zhan et al., 2011; Ismail et al., 2017).

4.14.6. Fourier-Transform Infrared (FTIR) Spectroscopy

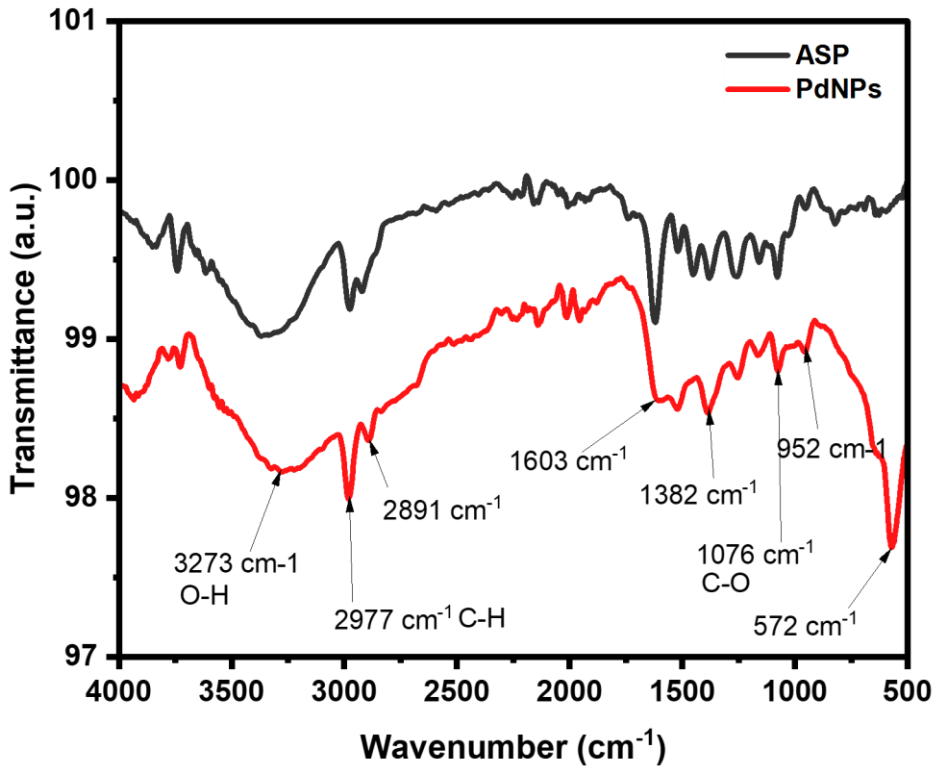

Figure 4-36: FTIR spectrum of PdNPs formed using ASP with the ASP spectrum

Figure 4-36 exhibits the FTIR spectrum of the pure compound, ASP, depicted some peaks (as shown in Section 4.3). On the other hand, the main FTIR peaks of PdNPs were noticeable at 3273 cm^{-1}, 2977 cm^{-1}, 2891 cm^{-1}, 1603 cm^{-1}, 1382 cm^{-1}, 1076 cm^{-1} and 572 cm^{-1}.

The interaction of ASP with the surface of the monometallic nanoparticle spectrum of PdNPs confirmed the existence of the O-H stretching of intermolecular bonded alcohols and C=O stretching of ketones at 3378 cm^{-1} and 1746 cm^{-1}. The band at 3378 cm^{-1} shifted to 3273 cm^{-1} in the presence of PdNPs. These observations clearly show the interaction of Pd with the O-H group of ASP. Both O-H and C=O vibration frequencies slightly dropped in intensity compared to the vibration transmission intensity of ASP. The medium band at 1603 cm^{-1} corresponded to the C=C stretching of the conjugated alkene compound. The variations in the shape and peak positions of the O-H stretching vibration, C=O group and –O-H bending vibration are due to the contribution of ASP towards the reduction and stabilization process (Venkatesham et al., 2012; Santoshi kumari et al., 2015; Olajire & Mohammed, 2019).

4.15. Synthesis of Au-Pd bimetallic nanoparticles Aspalathin

The production of Au-Pd alloyed bimetallic nanoparticles through the utilization of ASP represents a captivating aspect of this research, given the distinctive characteristics and possible applications, particularly in fields such as biomedicine. Below, are the discussions surrounding the formation of Au-Pd alloyed bimetallic nanoparticles employing ASP:

4.16. Characterization of Au-Pd bimetallic nanoparticles using Aspalathin

4.16.1. Ultraviolet-Visible (UV-Vis) Spectroscopy

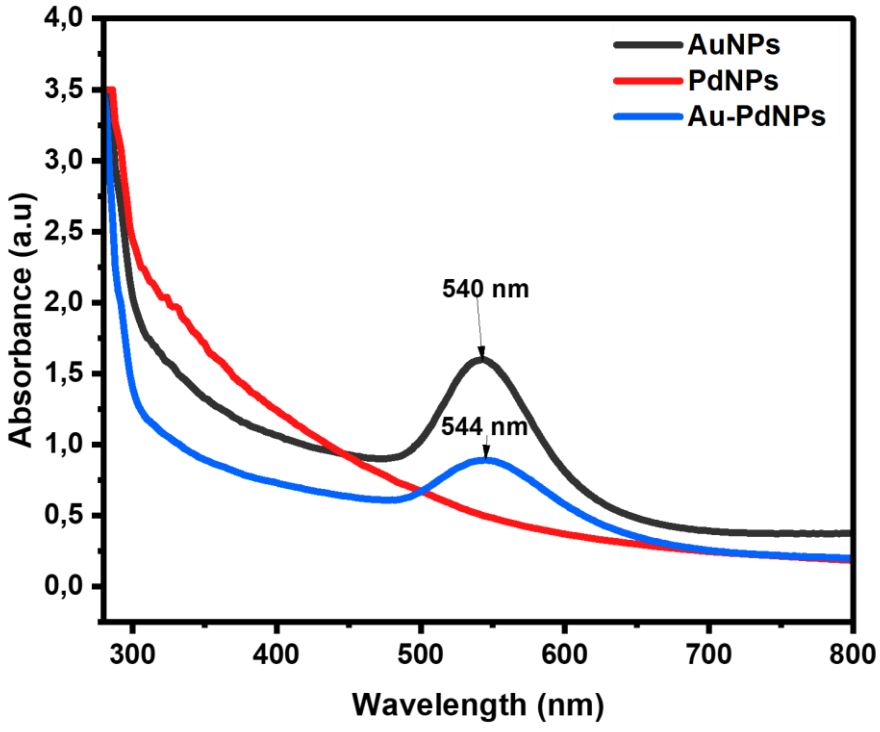

Figure 4-37: UV-Vis spectra of Au-Pd bimetallic nanoparticles synthesized from ASP overlaid with its monometallic nanoparticle spectra

Figure 4-37 shows that a similar absorption band (544 nm) to that of the Au NPs was observed in the spectral sample of the Au-Pd bimetallic nanoparticles, which was prepared with a concentration ratio of 2:1.

Chowdhury et al. (2018) achieved results consistent with those reported in another study. This observation is also consistent with a prior investigation where the existence of metal from group 10 (d^8s^2) in bimetallic nanoparticles was found to suppress the surface plasma energy of group 11 ($d^{10}s^1$) metal (Sahoo et al., 2019). Consequently, this indicates the formation of Au-Pd bimetallic nanoparticles in our samples. Additionally, a slight decrease in the absorbance of the Au SPR band was noted. This reduction in the intensity of the SPR peak serves as evidence for the creation of alloyed bimetallic nanoparticles (Cortie & McDonagh, 2011; Feng et al., 2013; Han et al., 2017). Moreover, there was minimal alloying between Au and Pd, as the SPR peak position of the alloyed nanoparticles closely aligned with the weighted average of the SPR peak positions of pure Au and PdNPs. This suggests that the two metals retained their individuality within the nanoparticles, forming a core-shell or heterogeneous structure.

4.16.2. Dynamic Light Scattering (DLS)

		Size (d.nm):	% Intensity:	St Dev (d.nm):
Z-Average (d.nm): 42.28	Peak 1:	61.15	96.4	35.70
PdI: 0.381	Peak 2:	4044	3.6	1085
Intercept: 0.867	Peak 3:	0.000	0.0	0.000
Result quality : Good				

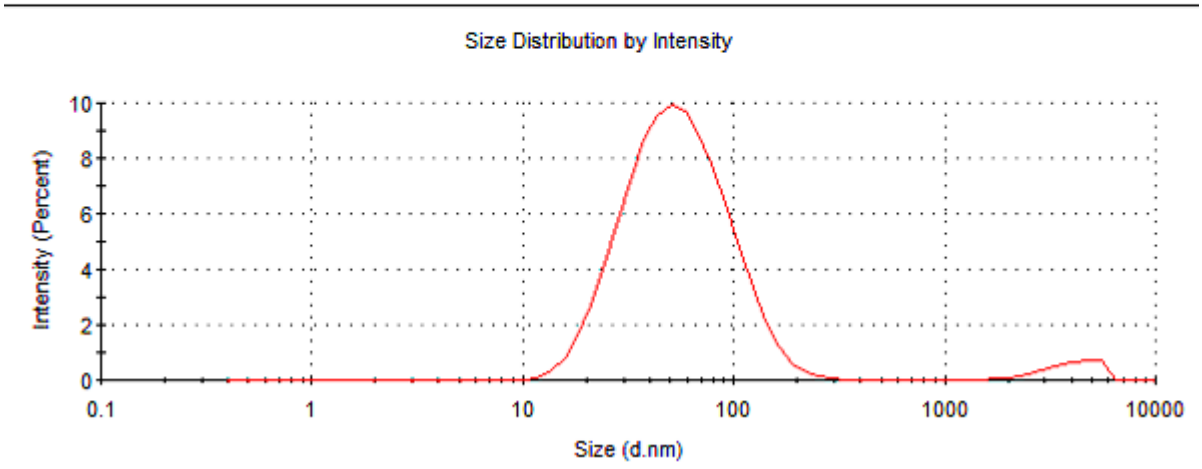

Figure 4-38: The graph illustrating the hydrodynamic size distribution in relation to intensity generated using the DLS technique for the Au-Pd bimetallic nanoparticles

The average hydrodynamic size of the Au-Pd bimetallic nanoparticles was 42.28 nm as determined from the intensity size distribution plot in Figure 4-38.

The hydrodynamic size, measured at 42.28 nm, coupled with a PDI value of 0.381, indicates that the Au-Pd alloyed bimetallic nanoparticles produced from ASP exhibit a moderately narrow size distribution with some level of size variability. Moreover, the PDI value indicates an almost uniform and monodisperse particle size distribution.

4.16.3. Zeta Potential

		Mean (mV)	Area (%)	St Dev (mV)
Zeta Potential (mV): -21.7	Peak 1:	-21.8	100.0	5.50
Zeta Deviation (mV): 5.23	Peak 2:	0.00	0.0	0.00
Conductivity (mS/cm): 1.11	Peak 3:	0.00	0.0	0.00

Result quality : Good

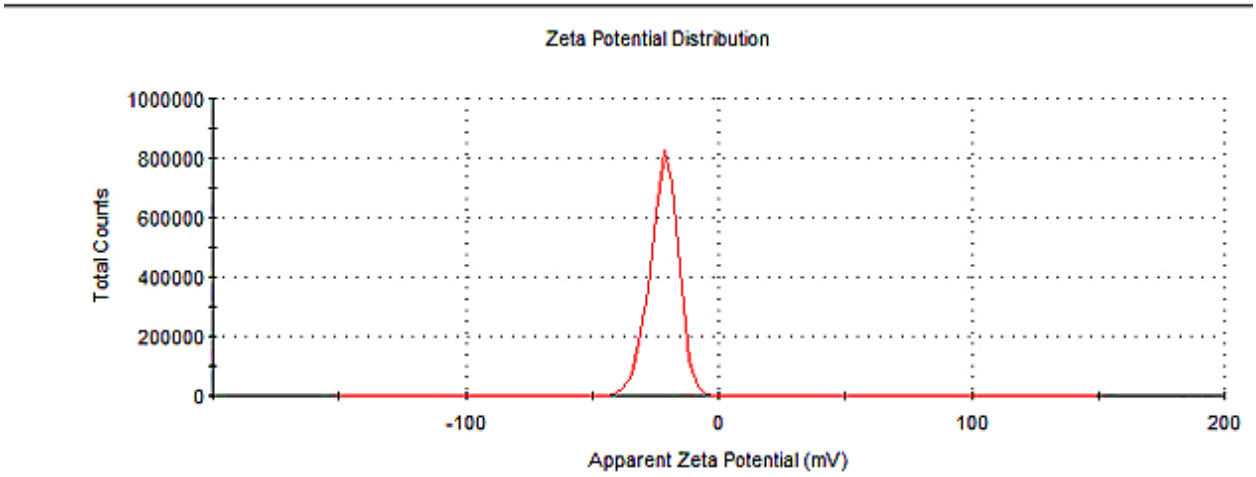

Figure 4-39: Zeta potential graph distribution of Au-Pd bimetallic nanoparticles using ASP

The zeta potential of the Au-PdNPs was confirmed to be -21.7 mV in Figure 4-39.

A negative zeta potential, such as -21.7 mV, indicates that the surface of the Au-PdNPs carries a negative charge. The negative charge arises from the existence of negatively charged functional groups or stabilizing agents on the surface of the nanoparticle. The degree of the negative zeta potential reflects the intensity of the surface charge and can offer crucial insights about the stability of nanoparticles in a particular medium. A higher negative zeta potential generally indicates stronger repulsive forces between nanoparticles, which helps to prevent agglomeration or flocculation. Therefore, the negative zeta potential of -21.7 mV indicates that the Au-PdNPs are likely to be well dispersed and stable in the surrounding medium. This property is advantageous for various applications that require stable and well dispersed nanoparticles. It is important to

note that the zeta potential can be affected by various factors including pH, ionic strength and the presence of other ions or molecules in the medium (Samari-kermani et al., 2021).

4.16.4. X-Ray Diffraction (XRD)

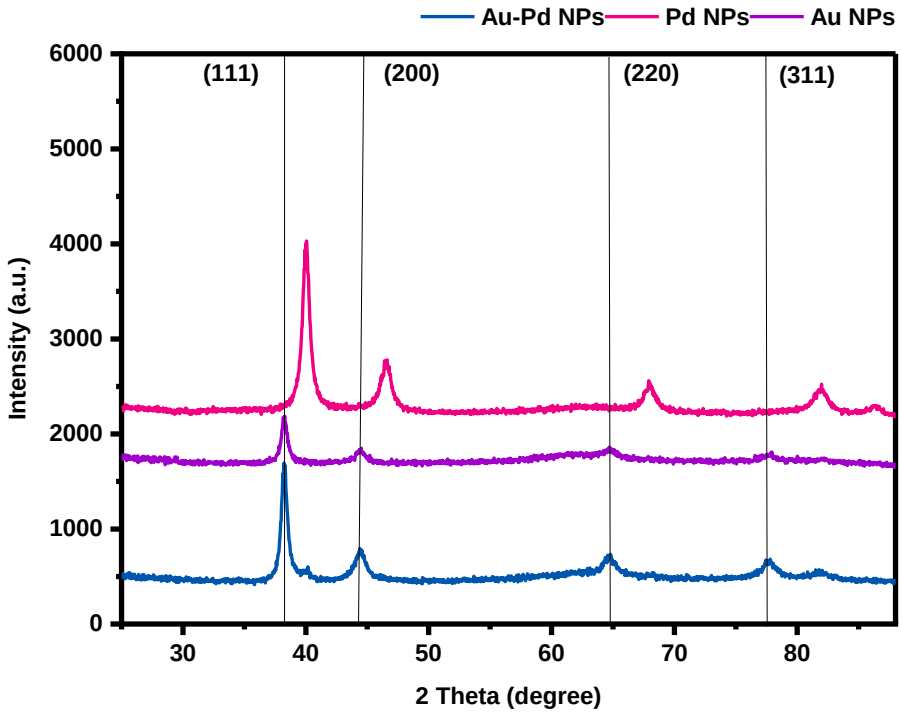

Figure 4-40: XRD pattern of Au and PdNPs and Au-Pd bimetallic nanoparticles using ASP

The Au-Pd bimetallic nanoparticles showed 2θ values at 38.28°, 40.06°, 44.42°, 64.61°, 77.67°, and 81.65° corresponding to the (1 1 1), (2 0 0), (2 2 0), and (3 1 1) crystal planes. In addition, as the Pd content increased, the Au-Pd bimetallic nanoparticles exhibited shifted Bragg peaks, shown in Figure 4-40, from pure Au to pure Pd.

The observed peak shift and broadening can be attributed to the interaction between Au and Pd atoms, causing lattice strain, thus affirming the creation of alloyed bimetallic nanoparticles (Ding et al., 2010; Chai et al., 2011; Xiao et al., 2014; Fageria et al., 2016). This indicates that the synthesized nanoparticles indeed constitute Au-Pd bimetallic alloys. Applying Vegard's law (Evstigneeva & Pchelkin, 2003) enables the determination of Au and Pd molar compositions in the alloy nanoparticles. This is achieved by analysing the shifts in lattice parameter derived from the angular positions of (1 1 1), (2 0 0), and (2 2 0) diffractions.

4.16.5. High-Resolution Transmission Electron Microscopy (HRTEM)

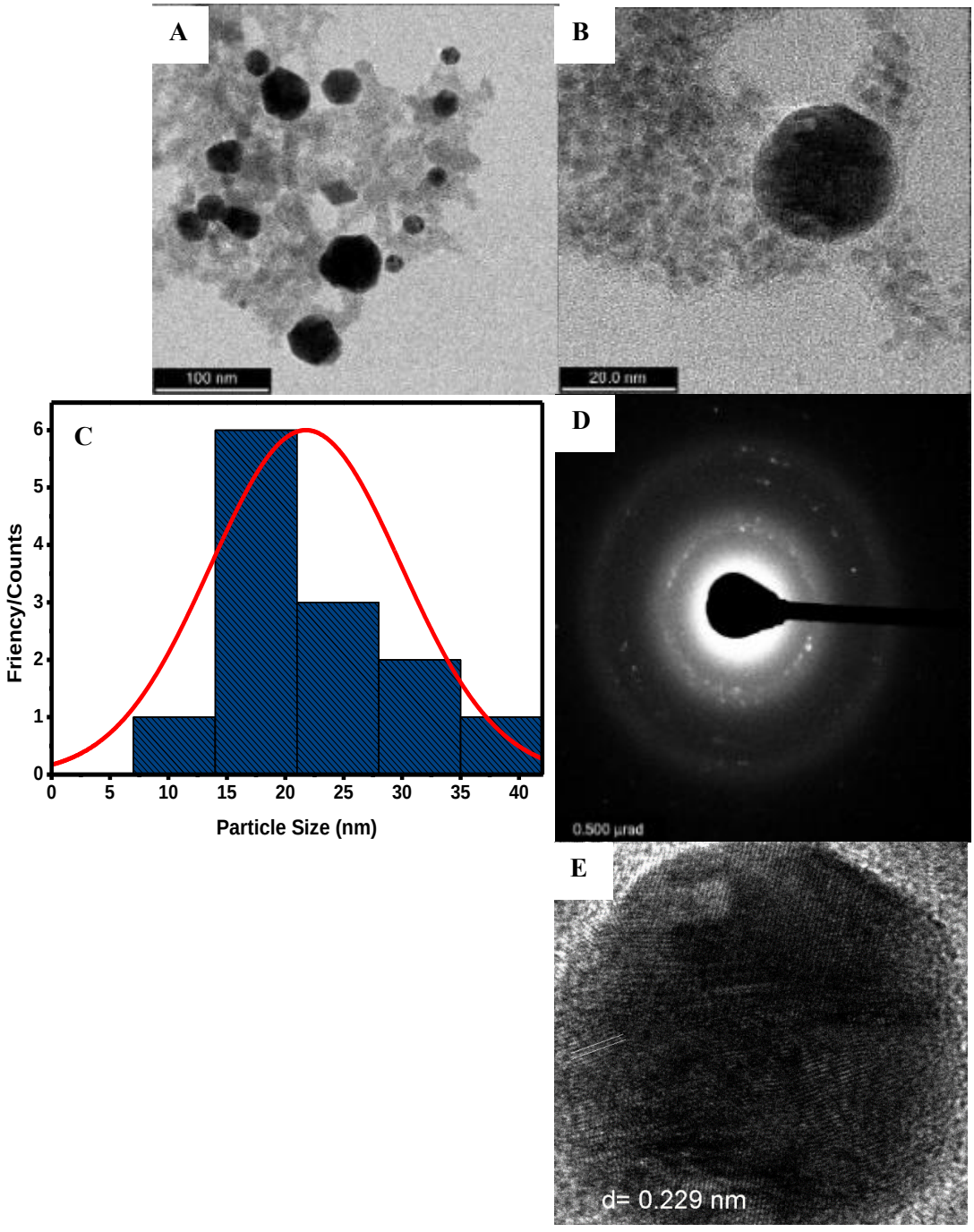

Figure 4-41: a) & b) HRTEM images of Au-Pd bimetallic nanoparticles synthesized using ASP; c) histogram depicting the particle distribution of nanoparticles corresponding to micrograph A; d) coupled with the SAED pattern and e) d-spacing value of lattice fringes

HRTEM is particularly useful for obtaining information on the morphology and Ångström level of bimetallic nanoparticles (Ferrando et al., 2008; Han et al., 2017). As illustrated in Figure 4-41 A, the

morphology of the Au-Pd nanoparticles exhibited a uniform dispersion in water, attributed to the stabilizing influence of the pure compound, ASP.

The size of the Au-Pd bimetallic nanoparticles ranged from 8 to 47 nm, indicating that they had varying sizes within this range and a resulting particle size distribution of 21.31± 8.67 nm. This size range is important because it allows for versatility in tailoring the properties of nanoparticles to meet specific application requirements. Smaller nanoparticles tend to have different properties than larger ones, and this variation in size can be advantageous for optimizing their behaviour in different environments. Additionally, the irregular shapes of the alloyed nanoparticles may have been caused by the use of the major compound as the reducing agent and the uncritical synthesis conditions. In the HRTEM micrograph of Au-Pd alloyed bimetallic nanoparticles, the dark interiors are electron dense AuNPs, surrounded by lighter entities (i.e., PdNPs). It can be argued that the apparent contrast between the Au cores and Pd shells indicates the core-shell configuration of the Au-Pd bimetallic nanoparticles, which is in agreement with the literature (Han et al., 2017). The pure compound ASP played a significant role in stabilizing the Au-Pd alloyed bimetallic nanoparticles in water. Stabilizing agents are often used during nanoparticle synthesis to prevent aggregation and to improve their stability in solution. ASP was likely adsorbed onto the surface of the bimetallic nanoparticles, forming a protective layer that hindered their agglomeration. This stabilization effect is essential for maintaining the dispensability of the nanoparticles and ensuring their uniform distribution in the medium.

The HRTEM micrograph in Figure 4-41 D displays the SAED pattern of the synthesized Au-Pd bimetallic nanoparticles. The bright spots that appear in a circular pattern correspond to the (1 1 1), (2 0 0), (2 2 0), and (3 1 1) reflections of the fcc Au-Pd bimetallic planes, which clearly indicates that the nanoparticles are poly-crystalline. The d-spacing of 0.229 nm (Figure 4-41 E) for bimetallic nanoparticles indicates separation between their crystallographic planes. This specific d-spacing is related to the crystallographic plane that signifies the arrangement of both Au and Pd atoms (Zhan et al., 2011; Wang et al., 2018). The involvement of ASP adds an interesting factor that might influence the alloying process and the resulting d-spacing. These results corroborate the XRD patterns of the respective Au-Pd bimetallic nanoparticles.

4.16.6. Scanning-Transmission Electron Microscopy-High Angle Annular Dark Field (STEM-HAADF)

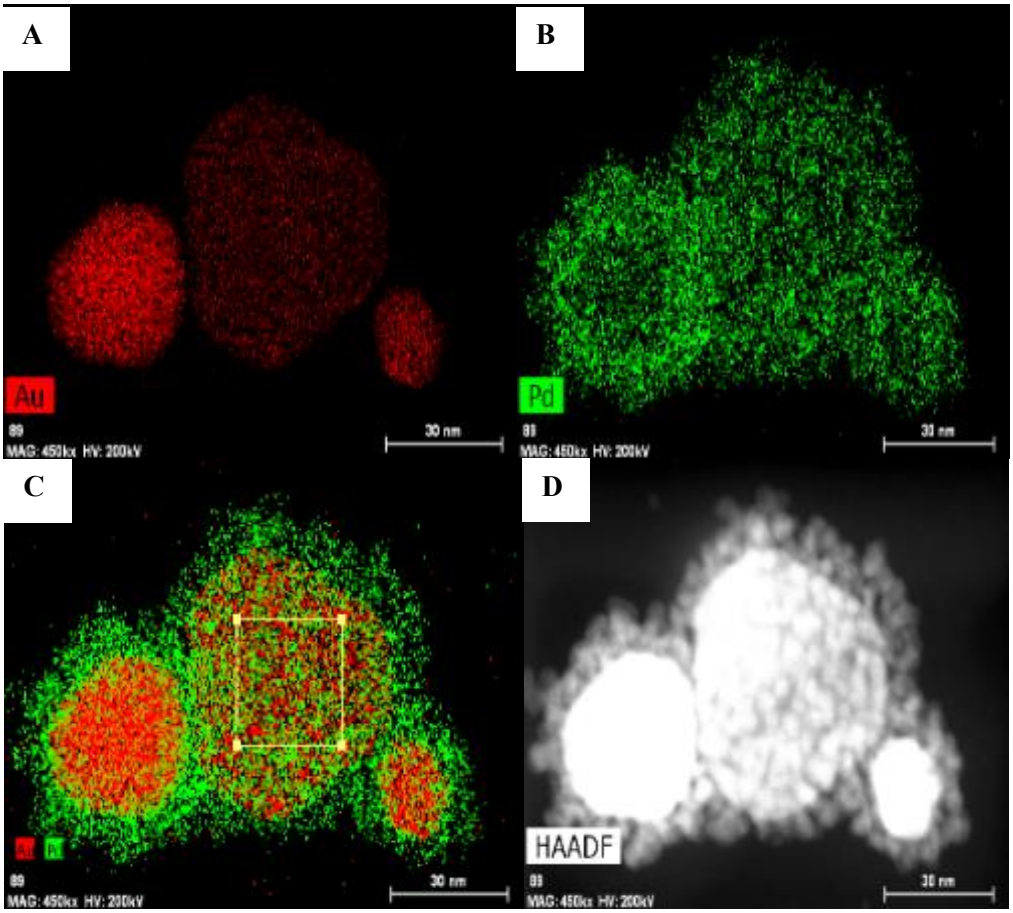

Figure 4-42: (a and b) Mapping images of individual Au (red) and Pd (green) atoms; (c) the overlaid image of Au and Pd atoms, (d) STEM-HAADF Au-Pd bimetallic nanoparticles, and the EDX spectrum of the bimetallic nanoparticles is included in Appendix 3

Figure 4-42 displays the elemental mapping images of the bimetallic nanoparticles obtained using the STEM-HAADF mode.

The red and green images are associated with Au and Pd, respectively. Mapping images were acquired using the L-line spectra of the elements. An overlapping image is shown in Figure 4-42, C. It can be observed that the elements have an inhomogeneous distribution in the nanoparticles, with zones with a high content of Pd (i.e., surface) and similar zones with a high content of Au (i.e., core) (Yang et al., 2016; Han et al., 2017). Furthermore, the overlaid image displays a Au centre coated or surrounded by Pd on the surface, as revealed by the HAADF STEM analyses. Moreover, Figure 4-42 D, displays the HAADF image, where bright areas correspond to regions with higher average atomic numbers, suggesting the presence of heavy or electron-dense elements (in this case, Au), while the dull areas reflect elements of lower atomic number (Pd) (Han

et al., 2017). This result is consistent with the HRTEM (Figure 4-41 A & B). Moreover, the EDX analysis substantiated the existence of both Au and Pd in the sample, as depicted in Appendix 3.

4.16.7. Fourier-Transform Infrared (FTIR) Spectroscopy

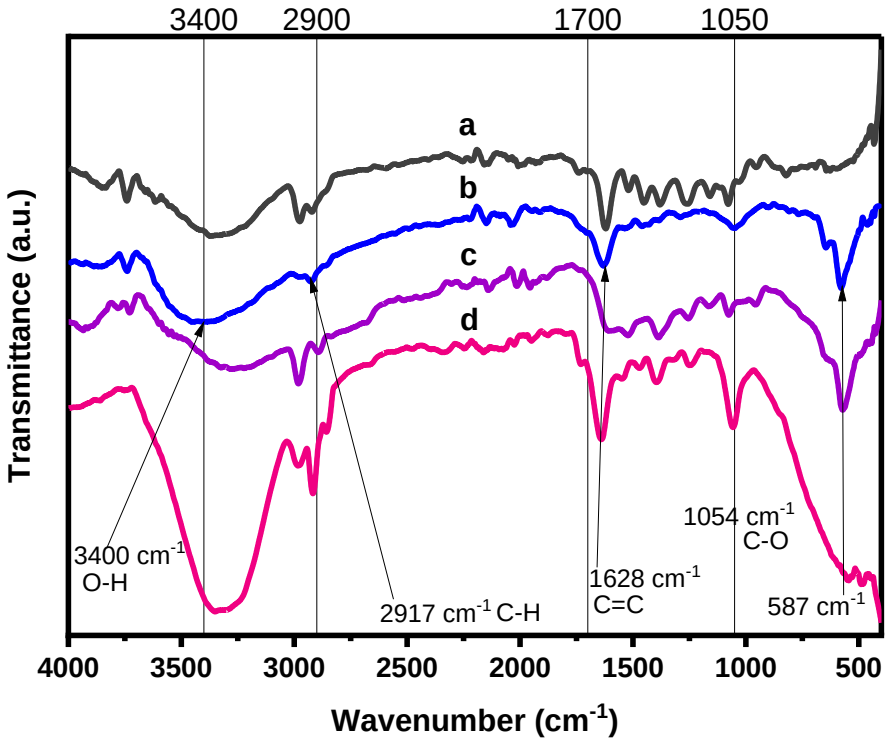

Figure 4-43: FTIR spectra of (a) Aspalathin, (b) Au-Pd bimetallic nanoparticles, (c) and (d) monometallic nanoparticles (i.e., Au and PdNPs synthesized using ASP

Furthermore, the vibrational frequencies of 3404 cm^{-1} and 1736 cm^{-1}, indicating the O-H stretching of alcohols and the C=O stretching of carboxylic acids, respectively, were observed in the Au-Pd bimetallic nanoparticle spectrum in Figure 4-43.

This spectrum was studied against the monometallic Au and PdNPs spectra. The alcohol band was slightly shifted to a higher wavenumber with a slightly lower intensity than that of the previously discussed spectra (ASP, Au, and PdNPs). Other vibrational frequencies included C-H stretching at 2853 cm^{-1}, 2917 cm^{-1} C-H stretching, and 1054 cm^{-1} C-O stretching. The sharp, intense peak at 1054 cm^{-1} is a result of the stretching vibrations associated with C-O-C and -C-OH of secondary alcohols. Furthermore, upon comparing the spectra of ASP and bimetallic nanoparticles, it was observed that majority of the absorption bands present in ASP also appear in the FTIR spectrum of Au-Pd bimetallic nanoparticles with a slight alteration in peak

position. The shift is particularly noticeable in the band related to O-H stretching modes, transitioning from 3378 cm^{-1} in the extract to 3400 cm^{-1} in bimetallic nanoparticles.

The FTIR peaks can be used as markers to assess the interactions between ASP and mono- and bimetallic nanoparticle surface. Moreover, the aforementioned slight shifts could result from the interaction between Au^{3+} and Pd^{2+} with the functional groups of ASP, providing confirmation of the coating of metal nanoparticles. For example, the appearance of new peaks or shifts in the carbonyl region of the FTIR spectrum suggested the coordination of carbonyl groups with the metal. In addition, shifts in the hydroxyl region indicated the adsorption and binding of hydroxyl groups to the nanoparticle surface, contributing to their stabilization (Sardar et al., 2009; Amina & Guo, 2020).

Chapter 5

5. Biological Studies

5.1. Introduction

Building on the foundation of controlled synthesis discussed in previous chapters, this section delves into the intricate realm of biological evaluation. Stability studies were performed using various biological media (Dulbecco's Modified Eagle Medium (DMEM), glycine (GLY), sodium chloride (NaCl), cysteine (CYS)), phosphate buffers at pH 7 and 9. In addition, the cytotoxicity and cellular uptake of these nanoparticles were investigated across various human cell lines (melanoma, epidermal keratinocytes, fibroblasts, and liver hepatocellular carcinoma), providing valuable insights into their biocompatibility and potential for therapeutic interventions.

The goal was to elucidate how these nanoparticles interact with diverse cell types and to understand how efficiently and selectively these nanomaterials are internalized by different cell lines, shedding light on their biocompatibility and potential as cytotoxic agents against specific cancer cell lines.

5.2. Stability Studies

The efficacy of nanoparticles in medical applications relies on their stability in biological solutions over a reasonable duration. As depicted in Figure 5-1 to Figure 5-6, the assessment of stability was conducted at 0, 6, 12, 18, and 24 hours of incubation in various biological media and buffers.

These included Dulbecco's Modified Eagle Medium (DMEM), glycine (GLY), sodium chloride (NaCl), cysteine (CYS), and phosphate buffers at pH 7 and 9, mixed with GR extract and ASP. Although the pH 9 solution exceeds the pH of human body fluids, investigating whether nanoparticles remain stable at such a high pH was deemed essential. These experiments were conducted both before and after incubation at 37 °C within the 0 to 24-hour timeframe. The selected 24-hour duration aims to accurately reflect the time required for complete medication bio-distribution within physiological systems. The expectation was that nanoparticles with stability would retain nearly identical wavelengths as the control samples over a defined time period before exhibiting any signs of instability.

The findings indicated consistent SPR across all formulations. However, notable shifts, particularly observed in the behaviour of certain proteins, were evident, especially from the 6th hour, particularly by CYS. In Figure 5-1, stable absorption bands at 530 nm for GR-AuNPs were maintained within the specified time interval. However, ASP-PdNPs, ASP-AuNPs, and GR-AuNPs displayed instability, demonstrating varying absorption maxima within these time intervals. These alterations suggested potential interactions of nanoparticles, particularly ASP-AuNPs, with components within the media and buffers, notably BSA and

DMEM, resulting in an enhanced dispersion quality of the AuNPs and the observed changes. Similarly, the variation in GR-AuNPs (Figure 5-1 A) in DMEM (544 nm) compared to the GR-AuNPs control (530 nm) likely arises from a combination of factors, including temperature-induced agglomeration, interactions with DMEM components (i.e., serum albumin), fluctuations in pH, protein interactions, ionic strength effects, and alterations in nanoparticle surface properties.

The shift and reduction in intensity observed in ASP-AuNPs in cysteine after the 12th hour result from the interaction of the thiol (-SH) group with the surface of ASP-AuNPs. Binding of cysteine to the ASP-AuNPs surface induces changes in the dielectric environment of the nanoparticles, influencing the SPR wavelength and causing a red shift in the absorption spectrum. This red shift signifies a displacement of the SPR peak to longer wavelengths.

Figure 5-5 and Figure 5-6 shows a decline in the absorption band intensity of ASP-Au-Pd and GR-Au-Pd bimetallic nanoparticles, which suggests it, may be linked to elevated ionic levels present in NaCl, PBS 7, and PBS 9 solutions. A high concentration of ions can potentially screen electrostatic repulsion between nanoparticles, rendering them more prone to aggregation. Additionally, higher pH values, particularly in PBS 7 and 9, might impact the stability and surface charge of the nanoparticles. While glycine is known to interact with nanoparticles and serve as a stabilizing agent, it may not be sufficiently effective in preventing aggregation in this specific system, as indicated by the observed reduction in intensity. It's plausible that the interaction between glycine and nanoparticles in this scenario doesn't provide adequate steric or electrostatic stabilization (Xue et al., 2011; Vilela et al., 2012).

Furthermore, the fact that the absorption band intensity has decreased over time implies that aggregation is a dynamic process. Due to steric or electrostatic repulsion, the nanoparticles may initially be well-dispersed. However, as time goes on, these stabilising forces could decrease or lose their effectiveness, allowing the nanoparticles to come together and eventually aggregate. Additionally, the presence of amine groups may have an impact on how the particles aggregate. Proteins have strong binding sites (-COOH and -NH_2) that might make this kind of coordination with Au-Pd bimetallic nanoparticles possible (Li et al., 2010; Badeggi et al., 2020).

In GR extract, numerous phytochemicals contribute to the formation nanoparticles and function as capping agents. As a result, how they interact with one another may have an impact on how they interact with the proteins and the environment. Therefore, GR-AuNPs and GR-PdNPs were found to be the most stable.

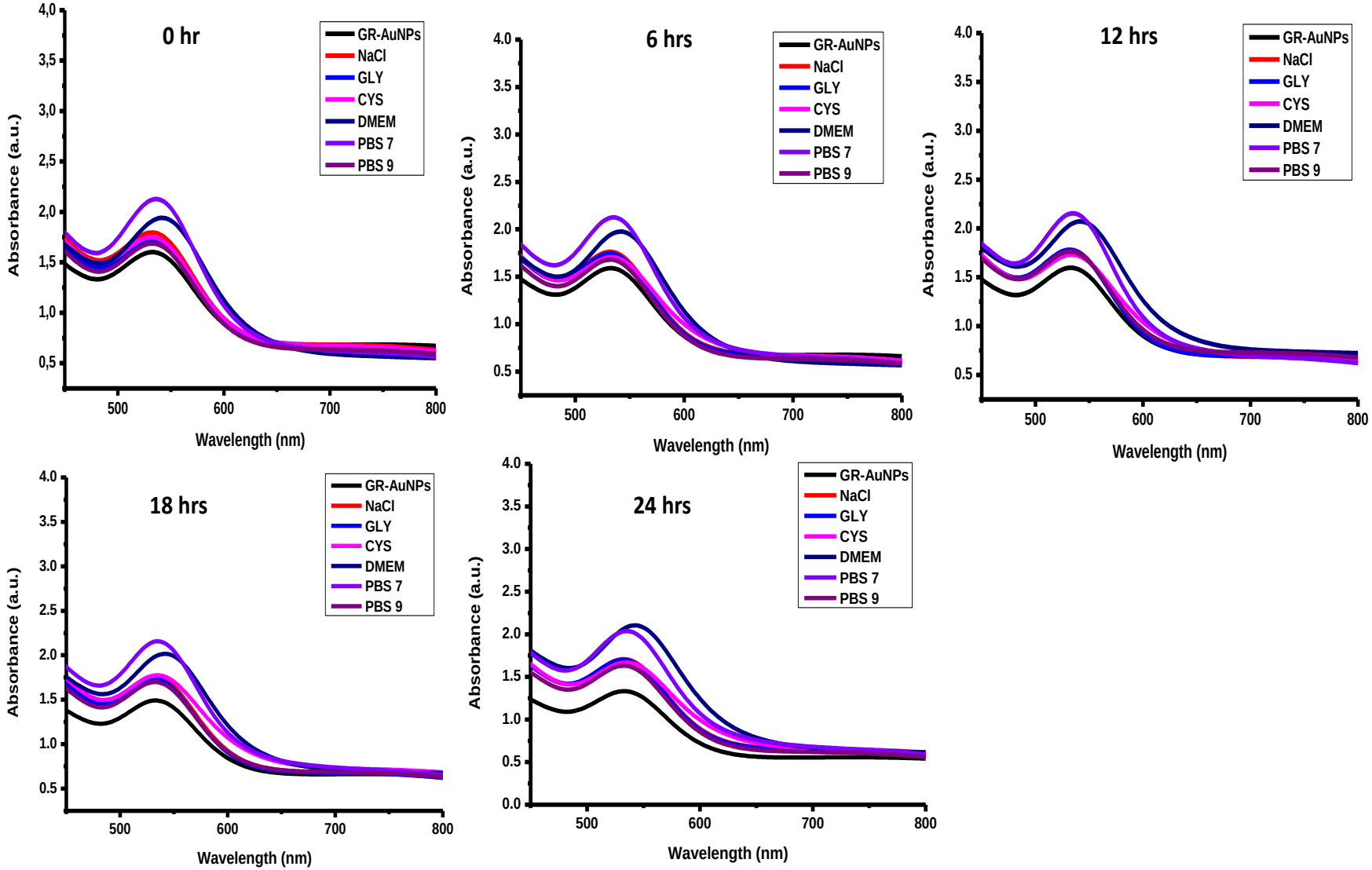

Figure 5-1: ***In vitro*** **examination of the stability of GR-AuNPs at specified time intervals within biogenic media**

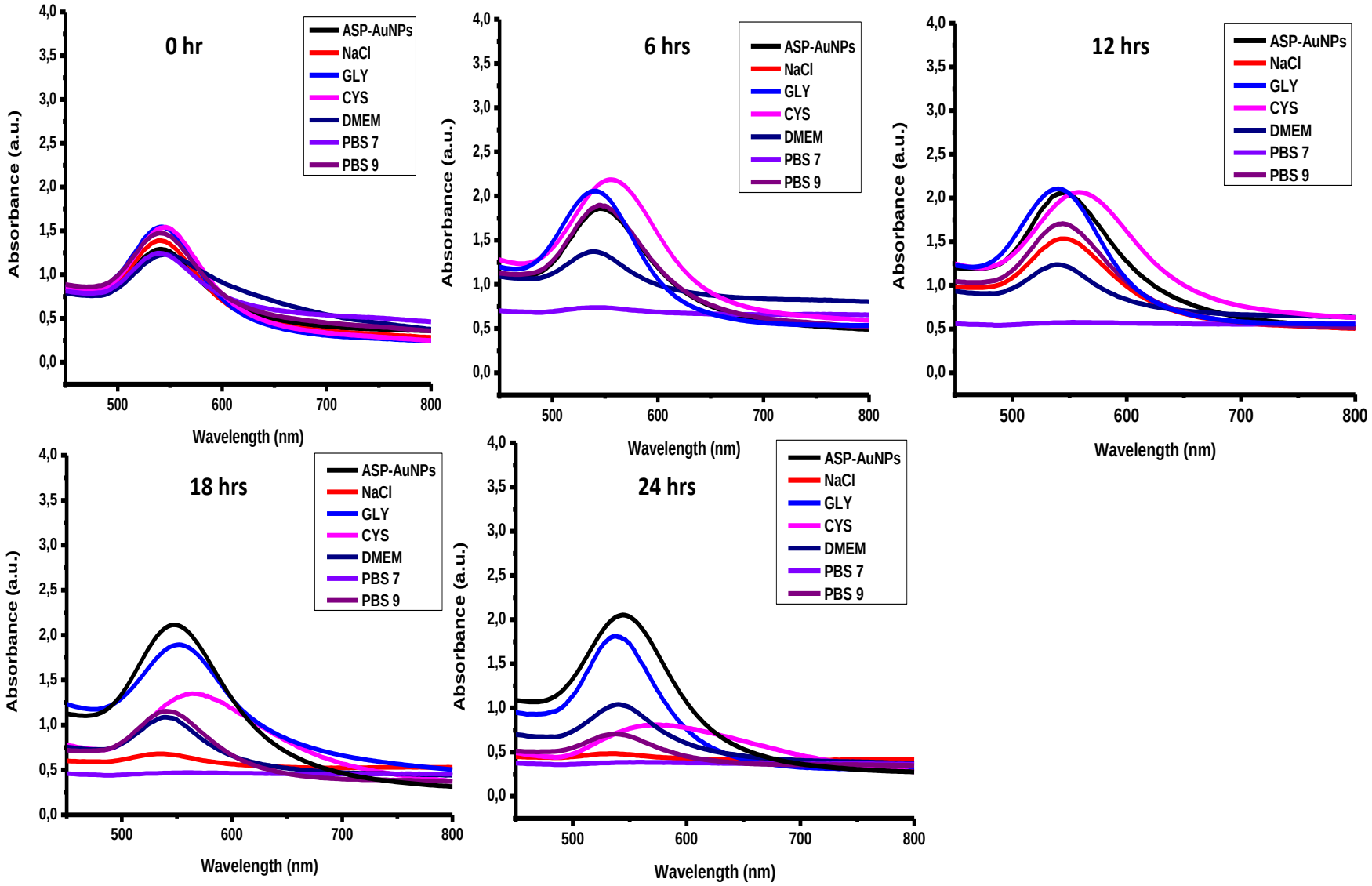

Figure 5-2: ***In vitro*** **evaluation of the stability of ASP-AuNPs at designated time intervals within biogenic media**

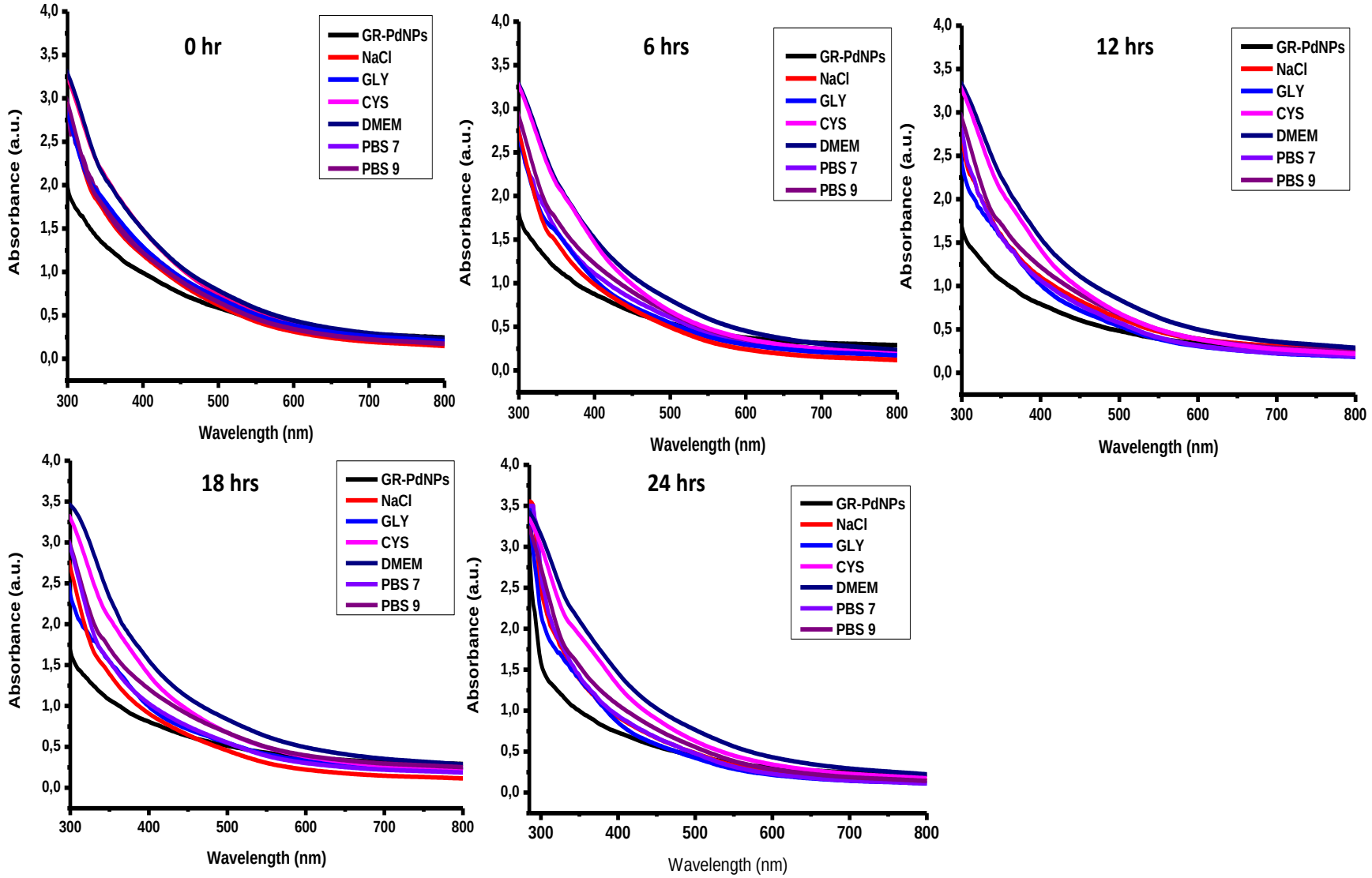

Figure 5-3: ***In vitro*** **assessment of the stability of GR-PdNPs at specified time intervals within biogenic media**

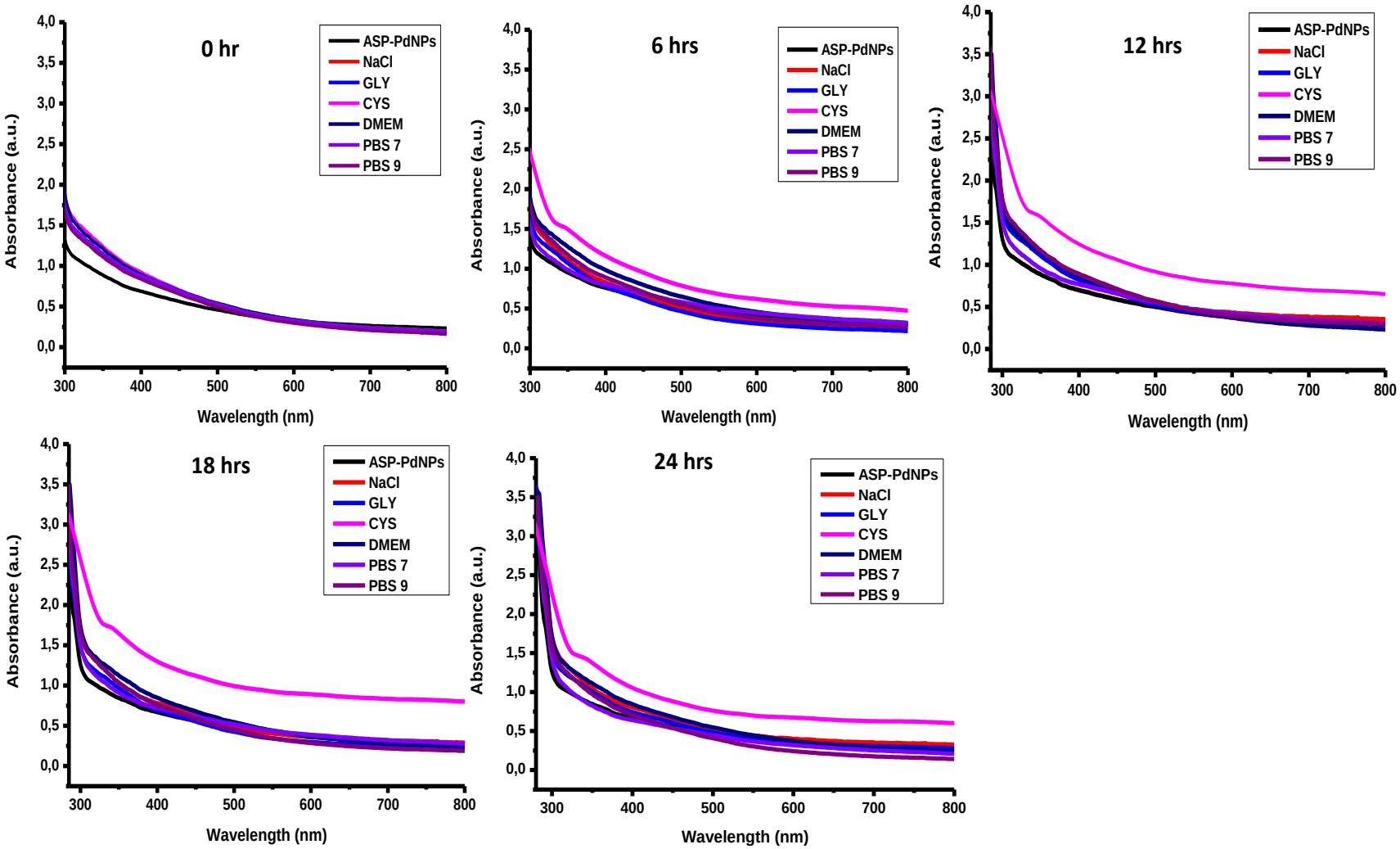

Figure 5-4: ***In vitro*** **evaluation of the stability of ASP-PdNPs at given time intervals within biogenic media**

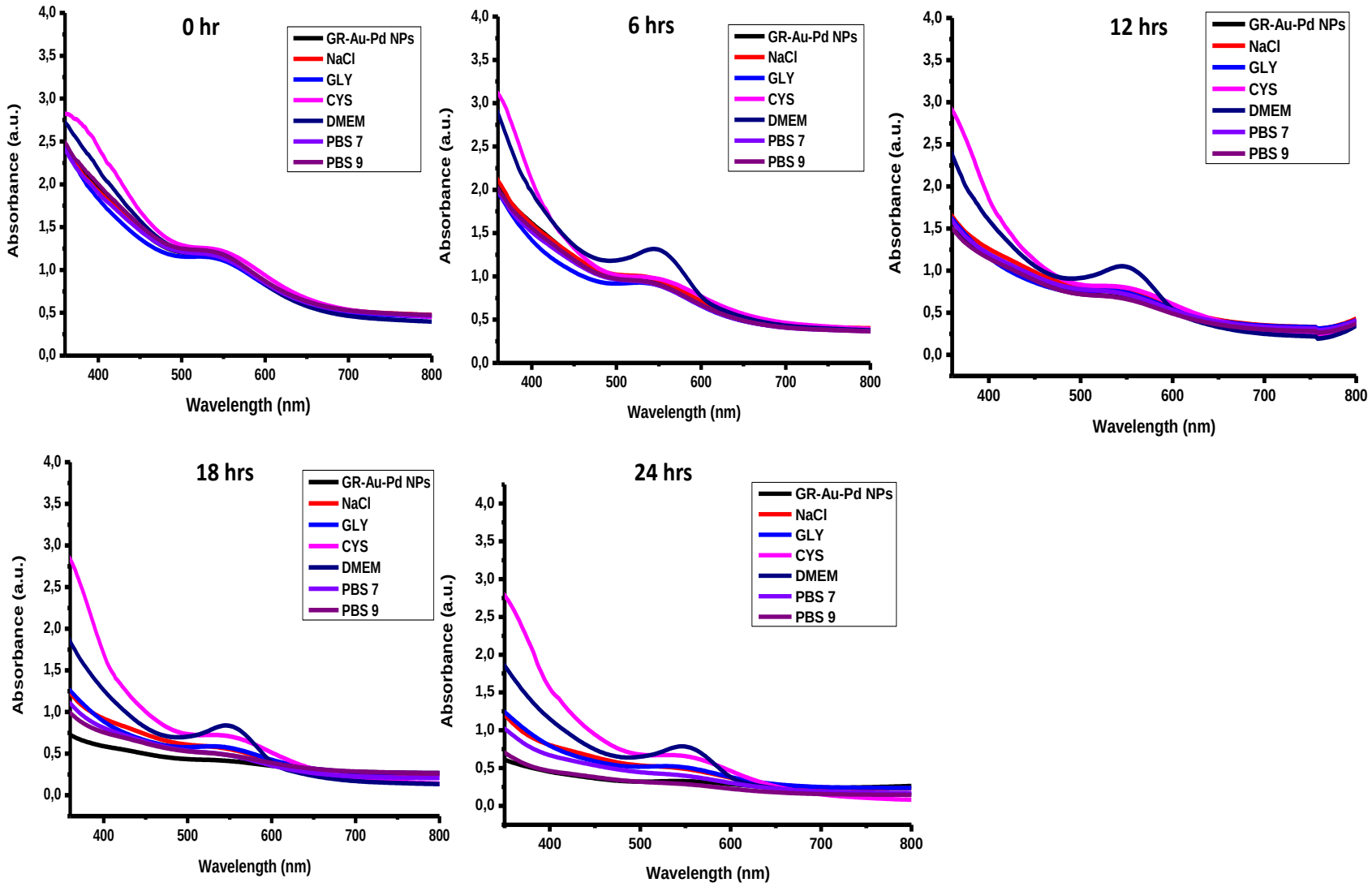

Figure 5-5: In vitro assessment of the stability of GR-Au-PdNPs at specified time intervals within biogenic media

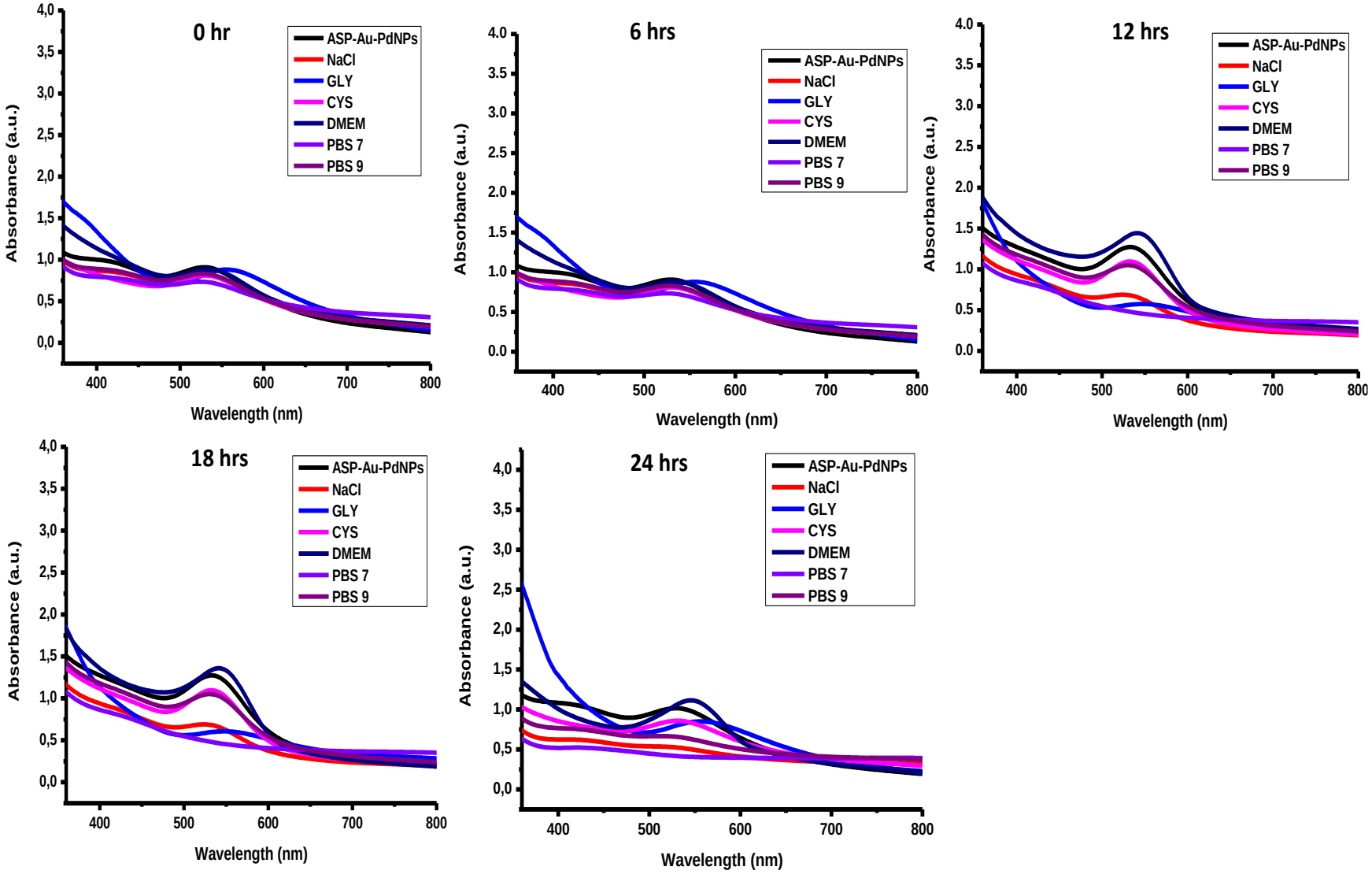

Figure 5-6: Assessing the in vitro stability of ASP-Au-Pd nanoparticles (NPs) over given time intervals in biogenic media

5.3. Cytotoxicity Assays of Monometallic and Bimetallic Nanoparticles

Investigating the cytotoxicity of nanomaterials is crucial to predict their effects on cells, whether intended or accidental. Nevertheless, there is a scarcity of research focusing on the synthesis of nanoparticles utilizing GR extract or its constituent ASP, along with the assessment of their cytotoxic effects. Various approaches have been employed for cytotoxicity analysis, with tetrazolium-based assays, such as the MTT assay, being the most widely used (Clichici & Filip, 2015). These assays measure the enzymatic activities associated with cellular metabolism in living cells, rather than counting the exact number of viable cells present (Alkilany & Murphy, 2010; Sharma et al., 2023). Following 24 hours of exposure to the tested samples, including green-synthesized Au, Pd, and Au-Pd bimetallic nanoparticles derived from GR and ASP, the MTT assay was conducted on SKMEL-1, HaCAT, KMST-6, and HepG2 cells, as depicted in Figures 5-7 to 5-10.

Most of the tested samples did not demonstrate significant reductions in cell viability at the tested concentrations compared to the control ($P > 0.05$). Specifically, SKMEL-1 cells exhibited no significant cytotoxic effects across all tested concentrations (12.5, 25, 50, 100, and 200 µg/ml), as illustrated in Figure 5-7. Similarly, the assessment of cytotoxicity in HaCaT and KMST-6 cells, shown in Figure 5-8 and Figure 5-9 respectively, revealed no significant cytotoxic effects with any of the samples tested.

Moreover, none of the investigated samples induced 50% cell death at any of the tested concentrations. This observation aligns with the findings of Akinfenwa et al. (2021), who reported similar results for the cytotoxicity studies of GR-AuNPs and ASP-AuNPs against SH-SY5Y and HepG2 cell lines.

Furthermore, it is noteworthy that none of the biosynthesized AuNPs, PdNPs, and Au-Pd bimetallic nanoparticles samples exhibited significant cytotoxicity when compared to their corresponding extract or compound. This consistent lack of cytotoxicity suggests the biocompatibility and potential safety of these green-synthesized nanoparticles for biomedical applications.

This comparative analysis with relevant studies underscores the reliability and reproducibility of the findings, while also providing valuable context for interpreting the cytotoxicity results. Additionally, it highlights the potential of green synthesis methods in producing nanoparticles with minimal cytotoxic effects, thus contributing to the growing body of literature on sustainable and biocompatible nanoparticle fabrication.

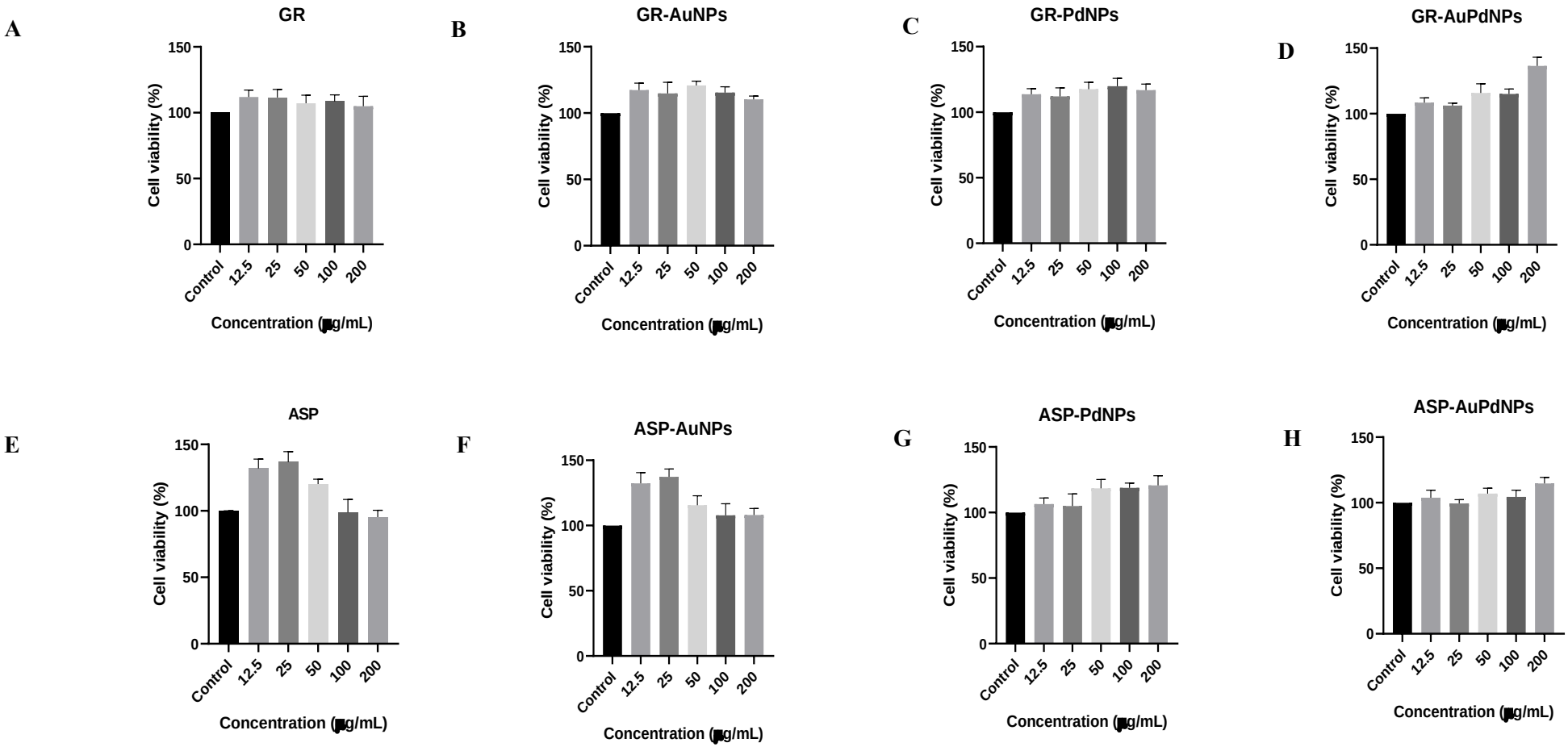

Figure 5-7: Cell viability of SKMEL-1 cells was assessed using the MTT assay during a 24-hour exposure to different samples, including GR (A), GR-AuNPs (B), GR-PdNPs (C), GR-AuPdNPs (D), ASP (E), ASP-AuNPs (F), ASP-PdNPs (G), and ASP-AuPdNPs (H)

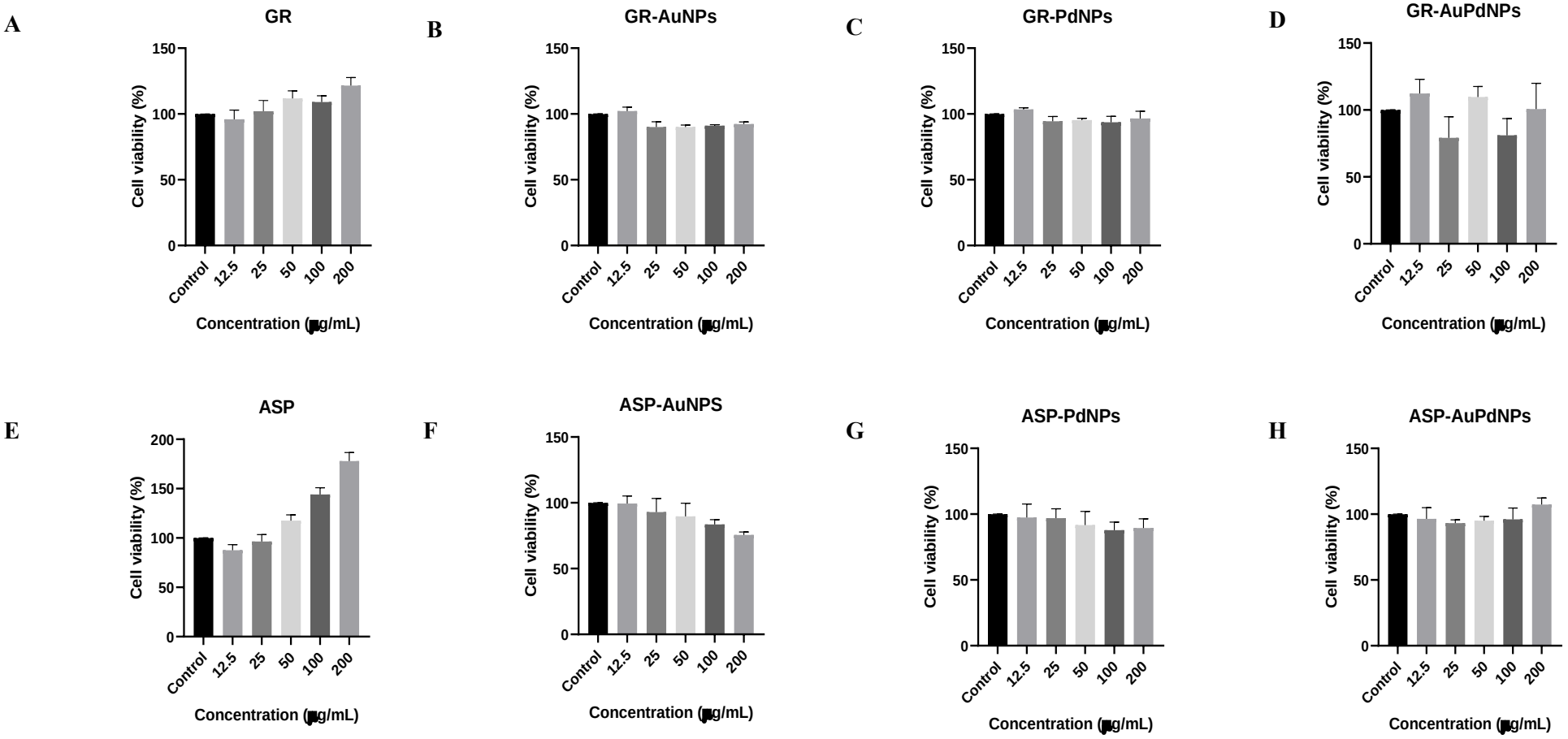

Figure 5-8: The viability of HaCAT cells was assessed using the MTT assay during a 24-hour exposure to various samples, including GR (A), GR-AuNPs (B), GR-PdNPs (C), GR-AuPdNPs (D), ASP (E), ASP-AuNPs (F), ASP-PdNPs (G), and ASP-AuPdNPs (H)

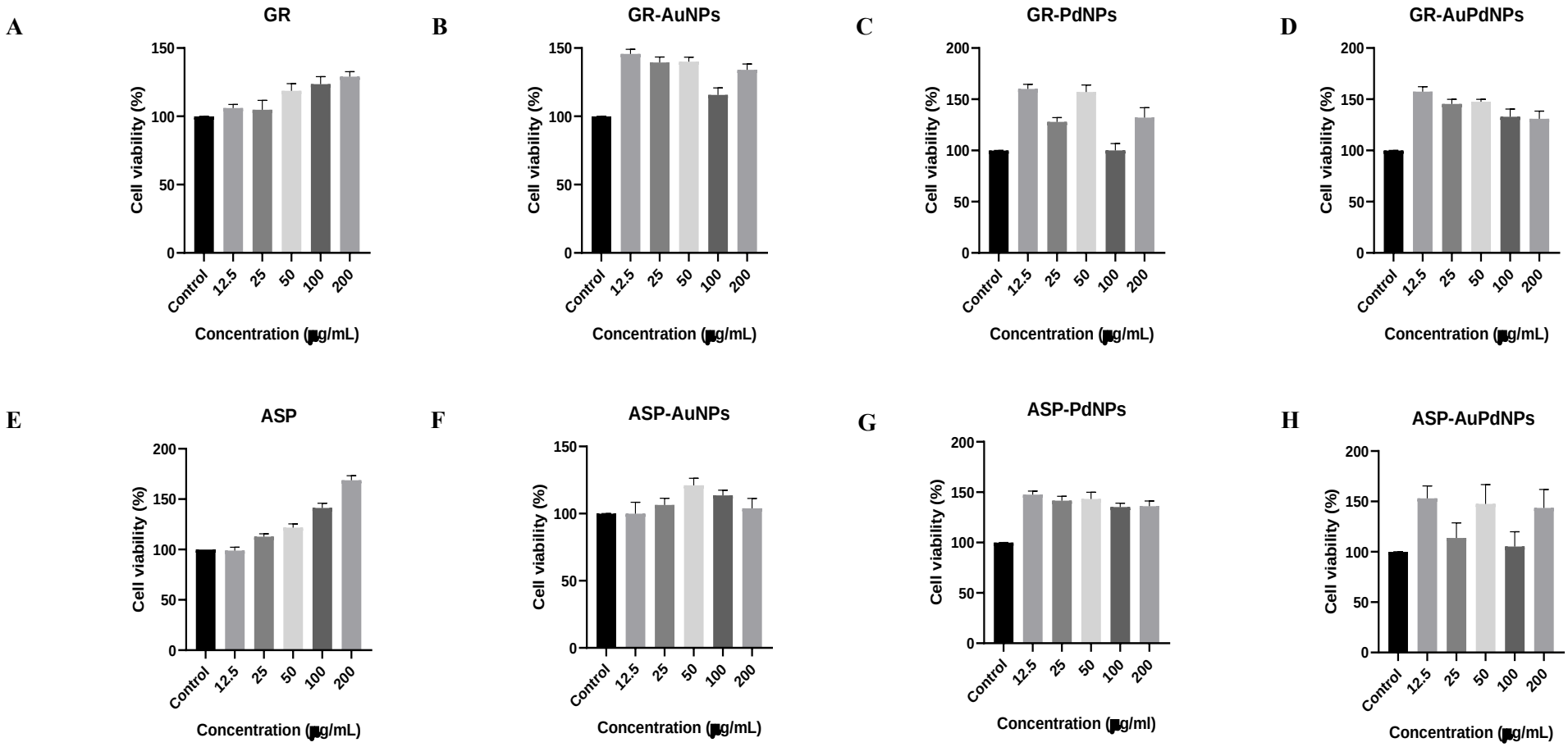

Figure 5-9: The MTT assay was employed to assess KMST-6 cell viability over a 24-hour exposure to various samples, including GR (A), GR-AuNPs (B), GR-PdNPs (C), GR-AuPdNPs (D), ASP (E), ASP-AuNPs (F), ASP-PdNPs (G), and ASP-AuPdNPs (H)

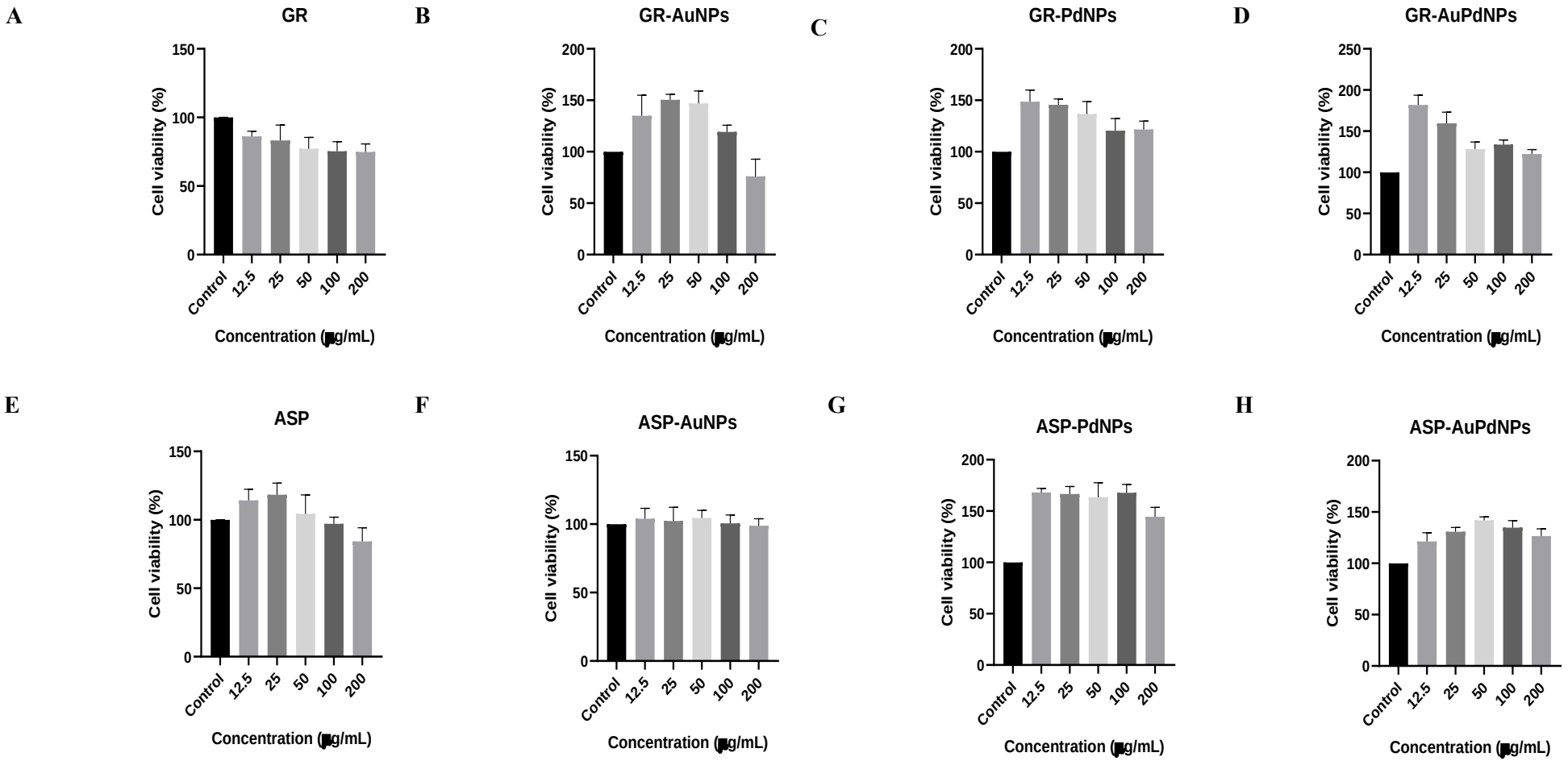

Figure 5-10: Cell viability in HepG2 liver cells was evaluated through the MTT assay following a 24-hour exposure to GR (A), GR-AuNPs (B), GR-PdNPs (C), GR-AuPdNPs (D), ASP (E), ASP-AuNPs (F), ASP-PdNPs (G), and ASP-AuPdNPs (H)

5.4. Cellular Uptake of Green Synthesized Nanoparticles

The cellular uptake of metal nanoparticles used as carriers for therapeutic drugs is a crucial aspect being explored in the domain of nanomedicine (De Jong & Borm, 2008). These nanoparticles, often functionalized with drugs or therapeutic agents, are designed to be taken up by cells, and deliver their cargo to specific targets within the body (Srinoi et al., 2018; Yusuf et al., 2023). The uptake of Au, Pd and Au-Pd bimetallic nanoparticle uptake confirmation was done through the ICP-MS analysis on each cell treated with the standard solutions of each metal to determine the concentration of each metal.

Figures 5-11 A-D depict the concentrations of Au, Pd, and Au-Pd bimetallic nanoparticles taken up by various cancer cells. The absorption of GR-AuNPs and PdNPs by HaCAT and SKMEL-1 cells respectively was notably greater compared to their respective monometallic counterparts. It's worth mentioning that the Au-Pd bimetallic nanoparticles evaluated with HepG2 cells featured a well-balanced composition, comprising equal proportions of Au and Pd, precisely set at a concentration of 0.191 µg/mL for both elements. Additionally, the uptake of ASP-Au-PdNPs by KMST-2 (0.316 µg/mL -Pd and 0.732 µg/mL-Au) and SKMEL-1 (0.371 µg/mL -Pd and 0.831 µg/mL -Au) cells demonstrated significantly higher levels compared to the uptake of the metallic nanoparticles. This suggests a potential synergistic effect or enhanced cellular uptake efficiency of the bimetallic nanoparticles compared to their monometallic counterparts. This heightened uptake suggests enhanced cellular interaction and potential therapeutic efficacy of the bimetallic nanoparticles.

Interestingly, the absorption of lower concentrations of GR and ASP-AuNPs, as well as PdNPs, by HepG2 and SKMEL-6 cells, respectively, aligns with the demonstrated anticancer effects observed in the MTT assay at lower doses. This correlation underscores the importance of nanoparticle uptake in mediating their biological effects and reinforces the potential therapeutic benefits of these nanoparticles at lower concentrations.

The uptake of AuNPs is influenced by both their functionalization and the type of cell (Thota & Crans, 2018). While AuNPs are typically eliminated when absorbed by healthy cells, their absorption by cancer cells often leads to cell death (Arnida et al., 2010; Dykman & Khlebtsov, 2014). This phenomenon highlights the potential of AuNPs as effective anticancer agents, with extensive research supporting their ability to penetrate cancer cells. However, concerns arise regarding the extensive penetration of gold, particularly in neuroblastoma cells, warranting further investigation to fully understand its implications.

Moreover, the findings suggest that increased nanoparticle dosage on cancer cells may hinder the interface between cells and reactive sites, leading to reduced permeation into the cells (Kalyane et al., 2019). This observation underscores the importance of optimizing nanoparticle dosage to maximize therapeutic efficacy while minimizing potential adverse effects.

Further research is warranted to elucidate the specific mechanisms of cellular uptake for GR- and ASP-Au-Pd nanoparticles, as this area remains largely unexplored. Understanding the intricacies of nanoparticle-cell interactions will not only enhance our knowledge of their therapeutic potential but also pave the way for the development of novel nanoparticle-based therapies for cancer treatment.

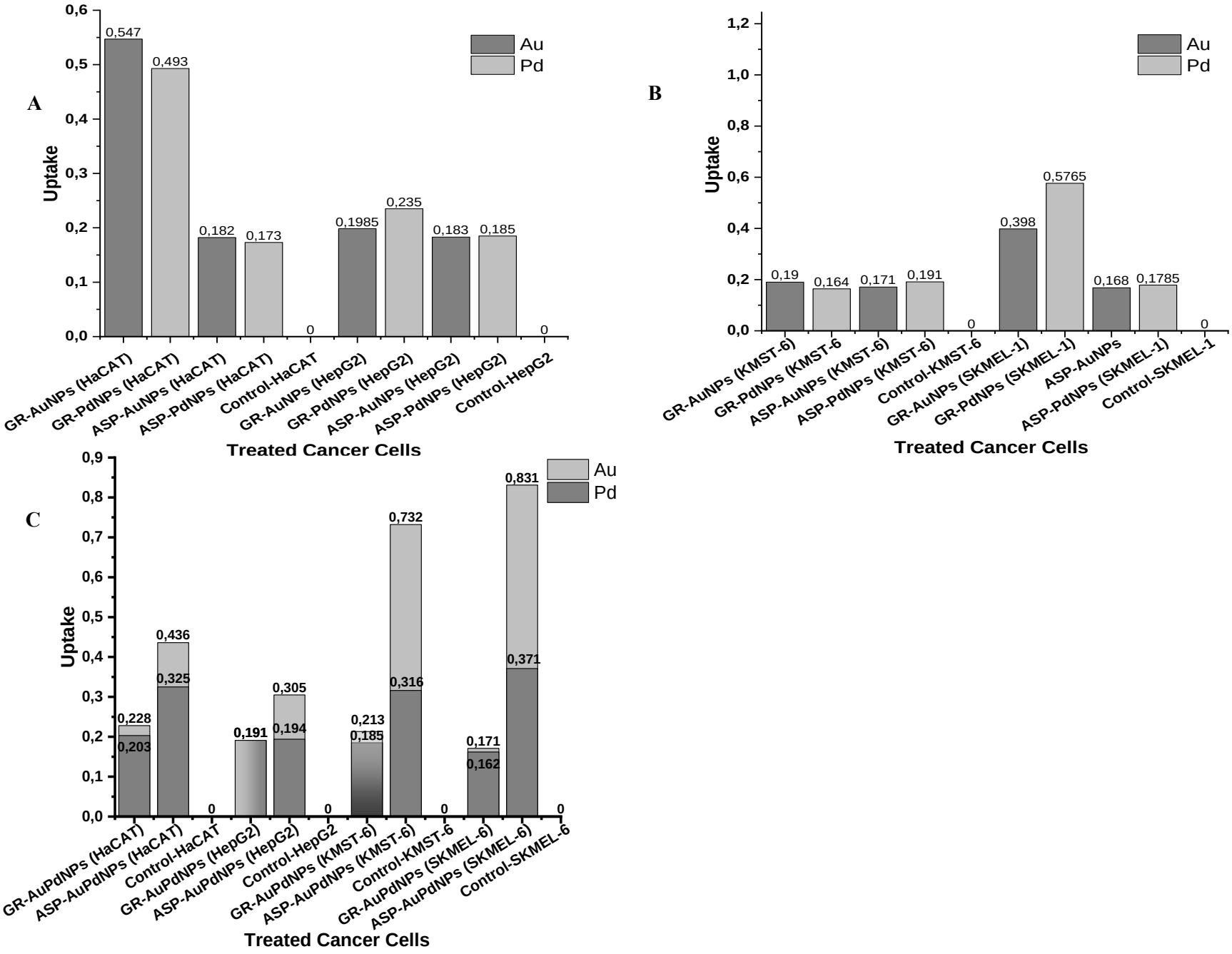

Figure 5-11: Cellular uptake results determined from ICP-OES measurements of Au, PdNPs and Au-Pd bimetallic nanoparticles.

Several factors, including size, shape, capping agents, target ligands, uptake mechanisms, cell type, biocompatibility, and toxicity, can influence the cellular uptake of nanoparticles (Kevadiya et al., 2020; Mukadam et al., 2020). The successful interaction of the cell membrane with the nanoparticles can result in the penetration through mechanisms like phagocytosis, micropinocytosis, endocytosis, diffusion, or adhesion (Kapara et al., 2020). Reports suggest that smaller nanoparticles exhibit better penetration of the cell membrane compared to larger counterparts (Barua & Mitragotri, 2014; Shang et al., 2014; Augustine et al., 2020). Quantitative analysis using ICP-OES indicates that the membrane permeation of GR and ASP nanoparticles was not influenced by size, aligning with recent discoveries (Akinfenwa et al., 2021).

The coexistence of both Au and Pd in the bimetallic nanoparticles may have induced a synergistic effect, contributing to an enhanced cellular uptake (He et al., 2021). This increased uptake could be attributed to the distinctive physicochemical characteristics, including size, shape, and surface chemistry, exhibited by the bimetallic nanoparticles in contrast to their monometallic counterparts (Dutta et al., 2016; Enea et al., 2021). In spite of the smaller size of the PdNPs within the samples in comparison to the Au-Pd bimetallic nanoparticles, cancer cells absorbed a greater concentration of the latter (as illustrated in Figure 5-11). The observed uptake of Au-Pd bimetallic nanoparticles can be ascribed to its optical properties, inert nature, biocompatibility, bio-conjugation potential, and low toxicity in biomolecules. The uptake order, based on decreasing magnitude, was ASP-Au-Pd NPs (SKMEL-1) > ASP-Au-PdNPs (KMST-6) > ASP-Au-PdNPs (HaCAT) > GR-PdNPs (SKMEL-1) > GR-AuNPs (HaCAT) > GR-PdNPs (HaCAT) > ASP-Au-PdNPs (HepG2) > GR-Au-PdNPs (SKMEL-1) > GR-AuNPs (SKMEL-1) > GR-AuNPs (KMST-6).

Chapter 6

6. Conclusions and Recommendations

6.1. Conclusions

The extract from *Aspalathus linearis* (GR) was prepared successfully. The main compound, Aspalathin (ASP), was extracted, isolated, and purified from *Aspalathus linearis* (GR) by the efforts of this study. Infrared (IR) and Nuclear Magnetic Resonance (NMR) Spectroscopy confirmed its structure.

AuNPs, PdNPs, and Au-Pd bimetallic nanoparticles were successfully produced using both the entire extract of GR and isolated compound, ASP.

High-Resolution Transmission Electron Microscopy (HRTEM) analysis unveiled a diverse array of AuNPs, showcasing various forms and configurations, including spheres and triangles. Shapes such as triangles may exhibit enhanced binding affinity to specific targets or cellular receptors, offering improved targeting efficiency and therapeutic efficacy compared to spherical nanoparticles. Furthermore, the obtained Polydispersity Index (PDI) values for AuNPs derived from GR and those associated with ASP, respectively, indicated a remarkably uniform and monodisperse distribution of particle sizes. X-Ray Diffraction (XRD) and Selected Area Electron Diffraction (SAED) outcomes confirmed the crystalline nature of the particles. The Zeta Potential measurements were highly negative with values indicated stable Au dispersions. Fourier-Transform Infrared (FTIR) spectroscopic analysis validated the existence of reducing components, including flavonoids, phenolic compounds, and carboxylic groups within the GR plant extract. The presence of lignans rich in hydroxyl groups is probable in facilitating the reduction process of Au...

. No SPR band was observed for PdNPs, in agreement with literature. The HRTEM results revealed that the PdNPs were monodisperse, with nanoparticles having predominantly spherical shapes. PDI values signified a particle size distribution that is nearly uniform and monodisperse for the AuNPs. The Zeta Potential values obtained fell within the acceptable stability range. FTIR spectroscopy showed the presence of phenolic compounds and soluble components found in GR plant extract, which possibly functioned as a surface capping and reducing agent for the reduction of PdNPs.

The blue shifted and red shifted absorption bands with a maximum at 525 nm and 544 nm were observed in the UV-Vis spectrum of the Au-Pd bimetallic nanoparticles when GR and ASP were used, respectively. The size of nanoparticles is crucial for their behaviour in biological systems because it influences various aspects such as their cellular uptake, distribution within tissues, interaction with biomolecules, and ultimately their therapeutic or diagnostic efficacy.. The pure compound provided nanoparticles that occurred at a lower size (8 to 47 nm) , suggesting that using a pure material or compound as a reducing agent was essential for the formation of Pd and Au-Pd alloyed bimetallic nanoparticles. Consequently, the Au-Pd bimetallic

nanoparticles demonstrated a stable and non-agglomerated nanomaterial within the acceptable range. Crystallinity of the bimetallic nanoparticles was validated through XRD and SAED analyses. The results indicated the successful formation of an alloy with even dispersion of both elements, attributed to complex interactions within the GR extract favouring alloyed bimetallic nanoparticles over distinct core-shell structures. Conversely, ASP-Au-Pd bimetallic nanoparticles exhibited a core-shell configuration, driven by the specific interactions and functionalities of the isolated compound.

The stability of AuNPs, PdNPs, and Au-Pd bimetallic nanoparticles was carried out in specific biological media. Nanoparticles used for biomedical assessment in context with cancer treatment must maintain their stability under physiological conditions to ensure their efficacy and safety. Thus, the findings revealed GR-AuNPs and GR-PdNPs to be the most stable. This is due to the fact that numerous phytochemicals in the GR extract contribute to the formation nanoparticles and function as capping agents. This means how the phytochemicals interacted had a positive impact on how they interacted with the biogenic media.

Additionally, the tetrazolium-based MTT assay demonstrated that GR, ASP, AuNPs, PdNPs, and Au-Pd bimetallic nanoparticles did not significantly diminish cell viability in SKMEL-1, HaCAT, KMST-6, and HepG2 cells at varying concentrations, indicating a lack of notable cytotoxic effects. The fact that these substances did not significantly diminish cell viability across the cell lines suggests a high level of biocompatibility and safety. In biomedical applications, especially in areas like drug delivery or tissue engineering, ensuring that materials do not induce cytotoxic effects is crucial for their clinical translation. Additionally, the lack of notable cytotoxic effects opens up the possibility of utilizing these materials in various therapeutic applications.

Furthermore, the coexistence of Au and Pd in bimetallic nanoparticles exhibited a synergistic effect, enhancing cellular uptake. Moreover, smaller nanoparticles possess the capability to penetrate deeper into tissues and undergo enhanced cellular uptake. This phenomenon was observed notably with ASP-Au-Pd bimetallic nanoparticles. Cancer cells absorbed higher concentrations of Au-Pd bimetallic nanoparticles, attributed to their optical properties, inert nature, biocompatibility, bio-conjugation potential, and low toxicity.

Overall, the comprehensive characterization of the synthesized nanoparticles and their constituents establishes a foundation for understanding their potential applications, especially in biomedical research, where their unique properties can be harnessed for various purposes such as drug delivery, imaging, and therapeutics.

6.2. Recommendations

The green synthesis of metal nanoparticles holds significant promise, yet it encounters challenges in material selection, synthesis conditions, product quality control, and practical application. These factors pose obstacles to the widespread adoption of industrially produced and large-scale applications of green-synthesized nanoscale metals. To overcome these challenges, it is crucial to address material selection, optimize synthesis conditions, implement stringent product quality control measures, and explore diverse applications.

Achieving precise control over reaction parameters is instrumental in influencing the quality of the nanoparticles produced. In various synthesis methods, adjusting parameters like the quantity of the reducing agent, temperature, and pH allows for a systematic investigation into their impact on the shapes and sizes of nanoparticles. Additionally, the stability of ASP can be enhanced through the incorporation of a green stabilizing agent, contributing to its varied stability.

The selection of optimal plant extracts, independent of temporal or seasonal constraints, offers practical advantages for green synthesis in terms of availability. Thoroughly studying the properties of the plant extract before application in synthesis ensures its suitability for a specific field. Utilizing agricultural waste aligns with the environmental protection concept of resource utilization.

Considering the storage of nanoparticles is crucial. If nanoparticles can be stored under ambient conditions, it significantly reduces storage or preservation costs. The stability of nanoparticles directly affects their storage feasibility and economic viability. The recommendation is to conduct a comprehensive examination of the economic factors linked to large-scale nanoparticle production, encompassing considerations of cost-effectiveness and scalability. Future research should therefore continue to focus on optimizing nanoparticles stability, ensuring their non-toxic nature, and enhancing their cellular uptake mechanisms.

Promoting collaboration among multidisciplinary teams and industries has the potential to significantly enhance the real-world application of green-synthesized nanoparticles. To maximize the effectiveness of such collaborations, it is recommended to foster partnerships between researchers, industry experts, and environmental scientists. By working together, these diverse teams can collectively address challenges and leverage their respective expertise to advance the development and implementation of sustainable nanoparticle technologies.

7. References

Aboyewa, J.A., Sibuyi, N.R.S. & Meyer, M. 2021. Gold Nanoparticles Synthesized Using Extracts of Cyclopia intermedia, Commonly Known as Honeybush, Amplify the Cytotoxic Effects of Doxorubicin. *Nanomaterials*, 11: 1–16.

Absalan, Y., Ryabov, M.A. & Kovalchukova, O. V. 2019. Thermal decomposition of bimetallic titanium complexes: A new method for synthesizing doped titanium nano-sized catalysts and photocatalytic application. *Materials Science and Engineering: C*, 97: 813–826.

Abubakar, A.R. & Haque, M. 2020. Preparation of Medicinal Plants: Basic Extraction and Fractionation Procedures for Experimental Purposes. *Journal of pharmacy & bioallied sciences*, 12(1): 1–10.

Achparaki, M., Thessalonikeos, E., Tsoukali, H., Mastrogianni, O., Zaggelidou, E., Chatzinikolaou, F., Vasilliades, N., Raikos, N., Isabirye, M., Raju, D.V.., Kitutu, M., Yemeline, V., Deckers, J. & J. Poesen Additional. 2018. In Vitro Cytotoxicity and Cell Viability Assays: Principles, Advantages, and Disadvantages. *Intech*: 1–19.

Adetunji, C.O. 2019. Environmental Impact and Ecotoxicological Influence of Biofabricated and Inorganic Nanoparticle on Soil Activity BT - Nanotechnology for Agriculture: Advances for Sustainable Agriculture. In D. G. Panpatte & Y. K. Jhala, eds. Singapore: Springer Singapore: 221–239.

Adithan, S., Sandhiya, S. & Pradhan, S. 2009. Novel applications of nanotechnology in medicine. *The Indian journal of medical research*, 130: 689–701.

Agrawal, O.D. & Kulkarni, Y.A. 2020. Mini-review of analytical methods used in quantification of ellagic acid. *Reviews in Analytical Chemistry*, 39(1): 31–44.

Agrawal, S. 2022. Spectroscopy techniques for rare-earth-activated phosphors. In V. Dubey, N. Dubey, M. M. Domańska, M. Jayasimhadri, & S. J. B. T.-R.-E.-A. P. Dhoble, eds. Elsevier: 147–175.

Ahmad, A., Senapati, S., Khan, M.I., Kumar, R., Ramani, R., Srinivas, V. & Sastry, M. 2003. Intracellular synthesis of gold nanoparticles by a novel alkalotolerant actinomycete,Rhodococcusspecies. *Nanotechnology*, 14(7): 824–828. http://dx.doi.org/10.1088/0957-4484/14/7/323.

Ahmed, H.B. & Emam, H.E. 2019. Synergistic catalysis of monometallic (Ag, Au, Pd) and bimetallic (AgAu, AuPd) versus trimetallic (Ag-Au-Pd) nanostructures effloresced via analogical techniques. *Journal of Molecular Liquids*, 287: 110975. https://www.sciencedirect.com/science/article/pii/S0167732219317945.

Ahmeda, A., Zangeneh, A. & Zangeneh, M.M. 2020. Green synthesis and chemical characterization of gold nanoparticle synthesized using Camellia sinensis leaf aqueous extract for the treatment of acute myeloid leukemia in comparison to daunorubicin in a leukemic mouse model. *Applied Organometallic Chemistry*, 34(3): e5290.

Ajitha, B., Ashok Kumar Reddy, Y. & Reddy, P.S. 2014. Biogenic nano-scale silver particles by Tephrosia purpurea leaf extract and their inborn antimicrobial activity. *Spectrochimica Acta Part A: Molecular and Biomolecular Spectroscopy*, 121: 164–172. https://www.sciencedirect.com/science/article/pii/S1386142513012341.

Ajuwon, O.R., Ayeleso, A.O. & Adefolaju, G.A. 2018. The Potential of South African Herbal Tisanes, Rooibos and Honeybush in the Management of Type 2 Diabetes Mellitus. *Molecules*, 23(12).

Ajuwon, O.R., Marnewick, J.L. & Davids, L.M. 2015. Rooibos (Aspalathus linearis) and its Major Flavonoids — Potential Against Oxidative Stress-Induced Conditions. In *Basic Principles and Clinical Significance of Oxidative Stress*. InTech: 171–218.

Akbari, B., Tavandashti, M.P. & Zandrahimi, M. 2011. Particle size characterization of nanoparticles- a practicalapproach. *Iranian Journal of Materials Science and Engineering*, 8(2): 48–56.

Akinfenwa, A.O., Abdul, N.S., Docrat, F.T., Marnewick, J.L., Luckay, R.C. & Hussein, A.A. 2021. Cytotoxic effects of phytomediated silver and gold nanoparticles synthesised from rooibos (Aspalathus linearis), and aspalathin. *Plants*, 10(11).

Al-sanea, M.M. & Gamal, M. 2022. Critical analytical review : Rare and recent applications of refractive index detector in HPLC chromatographic drug analysis. *Microchemical Journal*, 178(February): 1–11.

Alai, G. 2023. Raynals , an online tool for the analysis of dynamic light scattering research papers. , 79: 673–683.

Alam, M.N., Chatterjee, A., Das, S., Batuta, S., Mandal, D. & Begum, N.A. 2015. Burmese grape fruit juice can trigger the “logic gate”-like colorimetric sensing behavior of Ag nanoparticles towards toxic metal ions. *RSC Advances*, 5(30): 23419–23430. http://dx.doi.org/10.1039/C4RA16984K.

Alam, N., Das, S., Batuta, S. & Mandal, D. 2016. Green-nanochemistry for safe environment : bio-friendly synthesis of fluorescent monometallic (Ag and Au) and bimetallic (Ag / Au alloy) nanoparticles having pesticide sensing activity. *Journal of Nanostructure in Chemistry*, 6(4): 373–395.

Aldawsari, H.M., Singh, S., Alhakamy, N.A., Bakhaidar, R.B., Halwani, A.A. & Badr-eldin, S.M. 2021.

Gum Acacia Functionalized Colloidal Gold Nanoparticles of Letrozole as Biocompatible Drug Delivery Carrier for Treatment of Breast Cancer. *Pharmaceutics*, 13(1554): 1–12.

Ali, Z.A., Yahya, R., Sekaran, S.D. & Puteh, R. 2016a. Green Synthesis of Silver Nanoparticles Using Apple Extract and Its Antibacterial Properties S. C. Potter, ed. *Advances in Materials Science and Engineering*, 2016: 4102196.

Ali, Z.A., Yahya, R., Sekaran, S.D. & Puteh, R. 2016b. Green Synthesis of Silver Nanoparticles Using Apple Extract and Its Antibacterial Properties S. C. Potter, ed. *Advances in Materials Science and Engineering*, 2016: 4102196. https://doi.org/10.1155/2016/4102196.

Alia, K.B., Nadeem, H., Rasul, I., Azeem, F., Hussain, S., Siddique, M.H., Muzammil, S., Riaz, M. & Nasir, S. 2019. Separation and Purification of Amino Acids BT - Applications of Ion Exchange Materials in Biomedical Industries. In Inamuddin, ed. Cham: Springer International Publishing: 1–11.

Alirezalu, K., Pateiro, M., Yaghoubi, M., Alirezalu, A., Peighambardoust, S.H. & Lorenzo, J.M. 2020. Phytochemical constituents, advanced extraction technologies and techno-functional properties of selected Mediterranean plants for use in meat products. A comprehensive review. *Trends in Food Science & Technology*, 100: 292–306.

Aljohani, F.S., Hamed, M.T., Bakr, B.A., Shahin, Y.H., Abu-Serie, M.M., Awaad, A.K., El-Kady, H. & Elwakil, B.H. 2022. In vivo bio-distribution and acute toxicity evaluation of greenly synthesized ultra-small gold nanoparticles with different biological activities. *Scientific reports*, 12(1): 6269.

Alkilany, A.M. & Murphy, C.J. 2010. Toxicity and cellular uptake of gold nanoparticles: what we have learned so far? *Journal of Nanoparticle Research*, 12: 2313–2333. https://api.semanticscholar.org/CorpusID:6564704.

Alruqi, S.S., AL-Thabaiti, S.A. & Khan, Z. 2019. Iron-nickel bimetallic nanoparticles: Surfactant assisted synthesis and their catalytic activities. *Journal of Molecular Liquids*, 282: 448–455. https://www.sciencedirect.com/science/article/pii/S0167732218355338.

Altammar, K.A. 2023. A review on nanoparticles: characteristics, synthesis, applications, and challenges. *Frontiers in Microbiology*, 14(April): 1–20.

Álvarez-Chimal, R. & Arenas-Alatorre, J.Á. 2023. Green Synthesis of Nanoparticles: A biological Approach. In *Advances in Green Chemistry*. 1–19.

Amina, S.J. & Guo, B. 2020. A review on the synthesis and functionalization of gold nanoparticles as a drug delivery vehicle. *International Journal of Nanomedicine*, 15: 9823–9857.

Amina, S.J. & Guo, B. 2023. A Review on the Synthesis and Functionalization of Gold Nanoparticles as a Drug Delivery Vehicle A Review on the Synthesis and Functionalization of Gold Nanoparticles as a Drug Delivery Vehicle.

Amini, S.M. 2019. Preparation of antimicrobial metallic nanoparticles with bioactive compounds. *Materials Science & Engineering C*, 103(January): 109809.

Anadozie, S.O., Adewale, O.B., Sibuyi, N.R.S., Fadaka, A.O., Isitua, C.C., Davids, H. & Roux, S. 2023. One-pot synthesis , characterisation and biological activities of gold nanoparticles prepared using aqueous seed extract of Garcinia kola. *Process Biochemistry*, 128(January): 49–57.

Anandgaonker, P., Kulkarni, G., Gaikwad, S. & Rajbhoj, A. 2019. Synthesis of TiO2 nanoparticles by electrochemical method and their antibacterial application. *Arabian Journal of Chemistry*, 12(8): 1815–1822.

Anshup, A., Venkataraman, J.S., Subramaniam, C., Kumar, R.R., Priya, S.M.V., Kumar, T.R.S., Omkumar, R. V, John, A. & Pradeep, T. 2005. Growth of gold nanoparticles in human cells. *Langmuir : the ACS journal of surfaces and colloids*, 21 25: 11562–11567.

Appa, R.M., Raghavendra, P., Lakshmidevi, J., Naidu, B.R., Sarma, L.S. & Venkateswarlu, K. 2021. Structure controlled Au@Pd NPs/rGO as robust heterogeneous catalyst for Suzuki coupling in biowaste-derived water extract of pomegranate ash. *Applied Organometallic Chemistry*, 35(5): e6188.

Apte, M., Girme, G., Bankar, A., RaviKumar, A. & Zinjarde, S. 2013. 3, 4-dihydroxy-L-phenylalanine-derived melanin from Yarrowia lipolytica mediates the synthesis of silver and gold nanostructures. *Journal of Nanobiotechnology*, 11(1): 2. https://doi.org/10.1186/1477-3155-11-2.

Arnida, Malugin, A. & Ghandehari, H. 2010. Cellular uptake and toxicity of gold nanoparticles in prostate cancer cells: a comparative study of rods and spheres. *Journal of applied toxicology : JAT*, 30(3): 212–217. http://europepmc.org/abstract/MED/19902477.

Askin Celik, T. & Aslantürk, Ö. 2013. Investigation of antioxidant, cytotoxic and apoptotic activities of the extracts from tubers of Asphodelus aestivus Brot. *African journal of pharmacy and pharmacology*, 7: 610–621.

Aslantürk, Ö.S. 2018. In vitro cytotoxicity and cell viability assays: principles, advantages, and disadvantages. *Genotoxicity-A predictable risk to our actual world*, 2: 64–80.

Aslantürk, Ö.S. & K, T.A.Ş.K.I.N.Ç.E.L.İ. 2013. Antioxidant , cytotoxic and apoptotic activities of extracts from medicinal plant Euphorbia platyphyllos L . *Journal of Medicinal Plants Research*,

7(19): 1293–1304.

Atapattu, S.N., Poole, C.F. & Praseuth, M.B. 2016. System maps for retention of small neutral compounds on a superficially porous particle column in reversed-phase liquid chromatography. *Journal of chromatography. A*, 1468: 250–256.

Au, L., Lim, B., Colletti, P., Jun, Y.-S. & Xia, Y. 2010. Synthesis of Gold Microplates Using Bovine Serum Albumin as a Reductant and a Stabilizer. *Chemistry – An Asian Journal*, 5(1): 123–129.

Augustine, R., Hasan, A., Primavera, R., Wilson, R.J., Thakor, A.S. & Kevadiya, B.D. 2020. Cellular uptake and retention of nanoparticles: Insights on particle properties and interaction with cellular components. *Materials Today Communications*, 25: 101692.

Ayyıldız, M.F., Karaman, D.N., Kartoğlu, B., Şaylan, M., Chormey, D.S. & Bakırdere, S. 2023. A simple microwave-assisted synthesis of cobalt ferrite nanoparticles and its application for the determination of lead ions in rooibos (Aspalathus linearis) tea. *Food Chemistry*, 429: 136862. https://www.sciencedirect.com/science/article/pii/S0308814623014802.

Baba, H., Ohtsuka, Y., Haruna, H., Lee, T., Nagata, S., Maeda, M., Yamashiro, Y. & Shimizu, T. 2009. Studies of anti-inflammatory effects of Rooibos tea in rats. *Pediatrics International*, 51(5): 700–704. https://doi.org/10.1111/j.1442-200X.2009.02835.x.

Badeggi, U.M., Ismail, E., Adeloye, A.O., Botha, S., Badmus, J.A., Marnewick, J.L., Cupido, C.N. & Hussein, A.A. 2020. Green synthesis of gold nanoparticles capped with procyanidins from leucosidea sericea as potential antidiabetic and antioxidant agents. *Biomolecules*, 10(3).

Badeggi, U.M., Omoruyi, S.I., Ismail, E., Africa, C., Botha, S. & Hussein, A.A. 2022. Characterization and Toxicity of Hypoxoside Capped Silver Nanoparticles. *Plants*, 11(8).

Baig, R.B.N. & Varma, R.S. 2012. Alternative energy input: Mechanochemical, microwave and ultrasound-assisted organic synthesis. *Chemical Society Reviews*, 41(4): 1559–1584.

Bansal, M. 2023. Organic Chemistry Organic Spectroscopy : Principles of Organic Spectroscopy. *Journal of Medicinal and Organic Chemistry*, 6(3): 65–67.

Barbafieri, M. & Giorgetti, L. 2016. Contaminant bioavailability in soil and phytotoxicity/genotoxicity tests in Vicia faba L.: a case study of boron contamination. *Environmental Science and Pollution Research*, 23(23): 24327–24336.

Barretto, R.P.J. & Schnitzer, M.J. 2012. In vivo optical microendoscopy for imaging cells lying deep within live tissue. *Cold Spring Harbor Protocols*, 7(10): 1029–1034.

Barua, S. & Mitragotri, S. 2014. Challenges associated with Penetration of Nanoparticles across Cell and Tissue Barriers: A Review of Current Status and Future Prospects. *Nano today*, 9(2): 223–243.

Baudot, C., Tan, C.M. & Kong, J.C. 2010. FTIR spectroscopy as a tool for nano-material characterization. *Infrared Physics and Technology*, 53(6): 434–438. http://dx.doi.org/10.1016/j.infrared.2010.09.002.

Bayda, S., Adeel, M., Tuccinardi, T., Cordani, M. & Rizzolio, F. 2020. The history of nanoscience and nanotechnology: From chemical-physical applications to nanomedicine. *Molecules*, 25(1): 1–15.

Bednarska, K. & Fecka, I. 2022. Aspalathin and Other Rooibos Flavonoids Trapped α-Dicarbonyls and Inhibited Formation of Advanced Glycation End Products In Vitro. *International Journal of Molecular Sciences*, 23(23).

de Beer, D., Miller, N. & Joubert, E. 2017. Production of dihydrochalcone-rich green rooibos (Aspalathus linearis) extract taking into account seasonal and batch-to-batch variation in phenolic composition of plant material. *South African Journal of Botany*, 110: 138–143.

Behera, A., Mittu, B., Padhi, S., Patra, N. & Singh, J. 2020. *Bimetallic nanoparticles: Green synthesis, applications, and future perspectives*. Elsevier Inc. http://dx.doi.org/10.1016/B978-0-12-821354-4.00025-X.

Berridge, M. V, Herst, P.M. & Tan, A.S.B.T.-B.A.R. 2005. Tetrazolium dyes as tools in cell biology: New insights into their cellular reduction. In Elsevier: 127–152.

Berta, L., Coman, N.-A., Rusu, A. & Tanase, C. 2021. A Review on Plant-Mediated Synthesis of Bimetallic Nanoparticles, Characterisation and Their Biological Applications. *Materials (Basel, Switzerland)*, 14(24).

Bhattacharya, R. & Mukherjee, P. 2008. Biological properties of “naked” metal nanoparticles. *Advanced Drug Delivery Reviews*, 60(11): 1289–1306. http://www.sciencedirect.com/science/article/pii/S0169409X08000975.

Bhol, P., Bhavya, M.B., Swain, S., Saxena, M. & Samal, A.K. 2020. Modern Chemical Routes for the Controlled Synthesis of Anisotropic Bimetallic Nanostructures and Their Application in Catalysis. *Frontiers in chemistry*, 8: 357.

Bin, P., Huang, R. & Zhou, X. 2017. Oxidation Resistance of the Sulfur Amino Acids: Methionine and Cysteine L. Zhai, ed. *BioMed Research International*: 9584932.

Biswal, A.K. & Misra, P.K. 2020. Biosynthesis and characterization of silver nanoparticles for prospective application in food packaging and biomedical fields. *Materials Chemistry and Physics*, 250: 123014.

Bitwell, C., Indra, S. Sen, Luke, C. & Kakoma, M.K. 2023. A review of modern and conventional extraction techniques and their applications for extracting phytochemicals from plants. *Scientific African*, 19: e01585.

Blom van Staden, A., Kovacs, D., Cardinali, G., Picardo, M., Lebeko, M., Khumalo, N.C., Ray, S.S. & Lall, N. 2021. Synthesis and characterization of gold nanoparticles biosynthesised from Aspalathus linearis (Burm.f.) R.Dahlgren For progressive macular hypomelanosis. *Journal of Herbal Medicine*, 29(May): 100481.

Bolaños, K., Kogan, M.J. & Araya, E. 2019. Capping gold nanoparticles with albumin to improve their biomedical properties. *International journal of nanomedicine*, 14: 6387–6406.

Bondonno, N.P., Lewis, J.R., Blekkenhorst, L.C., Bondonno, C.P., Shin, J.H., Croft, K.D., Woodman, R.J., Wong, G., Lim, W.H., Gopinath, B., Flood, V.M., Russell, J., Mitchell, P. & Hodgson, J.M. 2020. Association of flavonoids and flavonoid-rich foods with all-cause mortality: The Blue Mountains Eye Study. *Clinical nutrition (Edinburgh, Scotland)*, 39(1): 141–150.

Boomi, P., Poorani, G.P., Palanisamy, S., Selvam, S., Ramanathan, G., Ravikumar, S., Barabadi, H., Prabu, H.G., Jeyakanthan, J. & Saravanan, M. 2019. Evaluation of Antibacterial and Anticancer Potential of Polyaniline-Bimetal Nanocomposites Synthesized from Chemical Reduction Method. *Journal of Cluster Science*, 30(3): 715–726.

Bossier, G.C. 1962. Spectrometric Identification of Organic Compounds. *Journal of Chemical Education*, 39: 546–553.

Bouziani, A. & Yahya, M. 2021. Mass Spectrometry Coupled with Chromatography toward Separation and Identification of Organic Mixtures. In K. F. Mendes, R. N. de Sousa, & K. C. Mielke, eds. Rijeka: IntechOpen: Ch. 24.

Bratovcic, A. 2019. Different Applications of Nanomaterials and Their Impact on the Environment. *International Journal of Material Science and Engineering*, 5: 1–7.

Brodusch, N., Brahimi, S. V., Barbosa De Melo, E., Song, J., Yue, S., Piché, N. & Gauvin, R. 2021. Scanning Electron Microscopy versus Transmission Electron Microscopy for Material Characterization: A Comparative Study on High-Strength Steels. *Scanning*, 2021.

Buckner, C.A., Lafrenie, R.M., Dénommée, J.A., Caswell, J.M., Want, D.A., Gan, G.G., Leong, Y.C., Bee, P.C., Chin, E., Teh, A.K.H., Picco, S., Villegas, L., Tonelli, F., Merlo, M., Rigau, J., Diaz, D., Masuelli, M., Korrapati, S., Kurra, P., Puttugunta, S., Picco, S., Villegas, L., Tonelli, F., Merlo, M., Rigau, J., Diaz, D., Masuelli, M., Tascilar, M., de Jong, F.A., Verweij, J. & Mathijssen, R.H.J. 2019.

Cell Division, Cytotoxicity, and the Assays Used in the Detection of Cytotoxicity Erman. *Intech*, 11: 1–20.

Buffat, P.A. 2003. Electron diffraction and HRTEM studies of multiply-twinned structures and dynamical events in metal nanoparticles: facts and artefacts. *Materials Chemistry and Physics*, 81(2): 368–375. http://www.sciencedirect.com/science/article/pii/S0254058403000245.

Bugaev, A.L., Polyakov, V.A., Tereshchenko, A.A., Isaeva, A.N., Skorynina, A.A., Kamyshova, E.G., Budnyk, A.P., Lastovina, T.A. & Soldatov, A. V. 2018. Chemical synthesis and characterization of Pd/SiO2: The effect of chemical reagent. *Metals*, 8(2): 26–29.

Carpen, L.G., Acasandrei, M.A., Acsente, T., Matei, E., Lungu, I. & Dinescu, G. 2023. In vitro analysis of the cytotoxic effect of two different sizes ITER-like tungsten nanoparticles on human dermal fibroblasts. *Heliyon*, 9(3): e13849.

Castillo, R.R., Lozano, D., González, B., Manzano, M., Izquierdo-Barba, I. & Vallet-Regí, M. 2019. Advances in mesoporous silica nanoparticles for targeted stimuli-responsive drug delivery: an update. *Expert Opinion on Drug Delivery*, 16(4): 415–439. https://doi.org/10.1080/17425247.2019.1598375.

Cele, T. 2020. Preparation of Nanoparticles. In S. M. Avramescu, K. Akhtar, I. Fierascu, S. B. Khan, F. Ali, & A. M. Asiri, eds. Rijeka: IntechOpen: Ch. 2.

Cen, H. & Chen, Z. 2021. Amide functionalized graphene oxide as novel and effective corrosion inhibitor of carbon steel in CO2-saturated NaCl solution. *Colloids and Surfaces A: Physicochemical and Engineering Aspects*, 615: 126216.

Chahardoli, A., Karimi, N. & Fattahi, A. 2018. Nigella arvensis leaf extract mediated green synthesis of silver nanoparticles: Their characteristic properties and biological efficacy. *Advanced Powder Technology*, 29(1): 202–210.

Chai, J., Li, F., Hu, Y., Zhang, Q., Han, D. & Niu, L. 2011. Hollow flower-like AuPd alloy nanoparticles: One step synthesis, self-assembly on ionic liquid-functionalized graphene, and electrooxidation of formic acid. *Journal of Materials Chemistry*, 21(44): 17922–17929.

Chakraborty, S. & Panigrahi, P.K. 2020. Stability of nanofluid: A review. *Applied Thermal Engineering*, 174(April).

Chaudhary, S.K., Sandasi, M., Makolo, F., van Heerden, F.R. & Viljoen, A.M. 2021. Aspalathin: a rare dietary dihydrochalcone from Aspalathus linearis (rooibos tea). *Phytochemistry Reviews*, 20(6): 1161–1192.

Chen, T., Foo, C. & Tsang, S.C.E. 2021. Interstitial and substitutional light elements in transition metals for heterogeneous catalysis. *Chemical Science*, 12(2): 517–532.

Chen, X.-Y., Han, J.-X., Liu, Y.-S., Hajiakber, A. & Yuan, T. 2018. Chemical constituents from traditional Uighur herbal medicine Elaeagnus angustifolia flowers. *Zhongguo Zhongyao Zazhi*, 43(9): 1749–1753. https://www.scopus.com/inward/record.uri?eid=2-s2.0-85049395801&partnerID=40&md5=abd449d841b2c69c9c51f8585707d185.

Cheney, R.H. & Scholtz, E. 1963. Rooibos Tea , a South African Contribution to World Beverages Published by : Springer on behalf of New York Botanical Garden Press Stable URL : https://www.jstor.org/stable/4252443 Rooibos Tea , A South African Contribution to , World Beverages1. *Economic Botany*, 17(3): 186–194.

Chenthamara, D., Subramaniam, S., Ramakrishnan, S.G., Krishnaswamy, S., Essa, M.M., Lin, F.-H. & Qoronfleh, M.W. 2019. Therapeutic efficacy of nanoparticles and routes of administration. *Biomaterials Research*, 23(1): 20. https://doi.org/10.1186/s40824-019-0166-x.

Cherian, T., Maity, D., Kumar, R.T.R., Balasubramani, G., Ragavendran, C., Yalla, S., Mohanraju, R. & Peijnenburg, W.J.G.M. 2022. Green Chemistry Based Gold Nanoparticles Synthesis Using the Marine Bacterium Lysinibacillus odysseyi PBCW2 and Their Multitudinous Activities.

Chevallier, V., Zoller, M., Kochanowski, N., Andersen, M.R., Workman, C.T. & Malphettes, L. 2021. Use of novel cystine analogs to decrease oxidative stress and control product quality. *Journal of Biotechnology*, 327: 1–8.

Chowdhury, R., Mollick, M.M.R., Biswas, Y., Chattopadhyay, D. & Rashid, M.H. 2018. Biogenic synthesis of shape-tunable Au-Pd alloy nanoparticles with enhanced catalytic activities. *Journal of Alloys and Compounds*, 763: 399–408.

Christian Ebere, E., Obinna Isiuku, B. & Andrew Wirnkor, V. 2019. Applications of Column, Paper, Thin Layer and Ion Exchange Chromatography in Purifying Samples: Mini Review. *SF Journal of Pharmaceutical and Analytical Chemistry*, 2(2): 1–6. https://www.researchgate.net/publication/337275127.

Ciumărnean, L., Milaciu, M. V, Runcan, O., Vesa, Ștefan C., Răchișan, A.L., Negrean, V., Perné, M.-G., Donca, V.I., Alexescu, T.-G., Para, I. & Dogaru, G. 2020. The Effects of Flavonoids in Cardiovascular Diseases. *Molecules*, 25(18).

Clayton, K.N., Salameh, J.W., Wereley, S.T. & Kinzer-Ursem, T.L. 2016. Physical characterization of nanoparticle size and surface modification using particle scattering diffusometry. *Biomicrofluidics*,

10(5): 1–14. http://dx.doi.org/10.1063/1.4962992.

Clichici, S. & Filip, A. 2015. In vivo Assessment of Nanomaterials Toxicity. In *Nanomaterials - Toxicity and Risk Assessment*. InTech.

Clogston, J.D. & Patri, A.K. 2011. Zeta potential measurement. *Methods in molecular biology (Clifton, N.J.)*, 697: 63–70.

Colon Hidalgo, D., Elajaili, H., Suliman, H., George, M.P., Delaney, C. & Nozik, E. 2022. Metabolism, Mitochondrial Dysfunction, and Redox Homeostasis in Pulmonary Hypertension. *Antioxidants*, 11(2).

Cortie, M.B. & McDonagh, A.M. 2011. Synthesis and optical properties of hybrid and alloy plasmonic nanoparticles. *Chemical reviews*, 111(6): 3713–3735.

Crozier, A., Jaganath, I.B. & Clifford, M.N. 2009. Dietary phenolics: chemistry, bioavailability and effects on health. *Natural Product Reports*, 26(8): 1001–1043. http://dx.doi.org/10.1039/B802662A.

Cui, L., Lu, H. & Lee, Y.H. 2018. Challenges and emergent solutions for LC-MS/MS based untargeted metabolomics in diseases. *Mass Spectrometry Reviews*, 37(6): 772–792. https://doi.org/10.1002/mas.21562.

Damiani, E., Carloni, P., Rocchetti, G., Senizza, B., Tiano, L., Joubert, E., de Beer, D. & Lucini, L. 2019. Impact of Cold versus Hot Brewing on the Phenolic Profile and Antioxidant Capacity of Rooibos (Aspalathus linearis) Herbal Tea. *Antioxidants*, 8(10).

Danaei, M., Dehghankhold, M., Ataei, S., Hasanzadeh Davarani, F., Javanmard, R., Dokhani, A., Khorasani, S. & Mozafari, M.R. 2018. Impact of Particle Size and Polydispersity Index on the Clinical Applications of Lipidic Nanocarrier Systems. *Pharmaceutics*, 10(2).

Das, M. & Dasgupta, D. 1998. Pseudo-affinity column chromatography based rapid purification procedure for T7 RNA polymerase. *Preparative biochemistry & biotechnology*, 28(4): 339–348.

Dauthal, P. & Mukhopadhyay, M. 2016. Noble Metal Nanoparticles: Plant-Mediated Synthesis, Mechanistic Aspects of Synthesis, and Applications. *Industrial & Engineering Chemistry Research*, 55(36): 9557–9577.

Davies, K.M., Jibran, R., Zhou, Y., Albert, N.W., Brummell, D.A., Jordan, B.R., Bowman, J.L. & Schwinn, K.E. 2020. The Evolution of Flavonoid Biosynthesis: A Bryophyte Perspective. *Frontiers in plant science*, 11: 7.

Deiana, D., Verdaguer-Casadevall, A., Malacrida, P., Stephens, I.E.L., Chorkendorff, I., Wagner, J.B. &

Hansen, T.W. 2015. Determination of Core–Shell Structures in Pd-Hg Nanoparticles by STEM-EDX. *ChemCatChem*, 7(22): 3748–3752. https://doi.org/10.1002/cctc.201500791.

Devi, H.S., Boda, M.A., Shah, M.A., Parveen, S. & Wani, A.H. 2019. Green synthesis of iron oxide nanoparticles using Platanus orientalis leaf extract for antifungal activity. , 8(1): 38–45.

Dias, M.C., Pinto, D.C.G.A. & Silva, A.M.S. 2021. Plant flavonoids: Chemical characteristics and biological activity. *Molecules*, 26(17): 1–16.

Dikshit, P.K., Kumar, J., Das, A.K., Sadhu, S., Sharma, S., Singh, S., Gupta, P.K. & Kim, B.S. 2021. Green Synthesis of Metallic Nanoparticles: Applications and Limitations. *Catalysts* , 11(8).

Ding, Y., Fan, F., Tian, Z. & Wang, Z.L. 2010. Atomic Structure of Au−Pd Bimetallic Alloyed Nanoparticles. *Journal of the American Chemical Society*, 132(35): 12480–12486.

Dlamini, N.G., Basson, A.K., Srirama, V. & Pullabhotla, R. 2023. Synthesis and Characterization of Various Bimetallic Nanoparticles and Their Application. : 1–24.

Dmitriev, R.I. 2017. *Multi-Parametric Live Cell Microscopy of 3D Tissue Models*.

Doudna, C., Bertino, M., Pillalamarri, S., Blum, F. & Tokuhiro, A. 2011. Radiolytic Synthesis of Bimetallic Ag−Pt Nanoparticles with a High Aspect Ratio. *Journal of Physical Chemistry B - J PHYS CHEM B*, 107: 6.

Duan, H., Wang, D. & Li, Y. 2015. Green chemistry for nanoparticle synthesis. *Chemical Society Reviews*, 44(16): 5778–5792. http://dx.doi.org/10.1039/C4CS00363B.

Duan, M., Jiang, L., Zeng, G., Wang, D., Tang, W., Liang, J., Wang, H., He, D., Liu, Z. & Tang, L. 2020. Bimetallic nanoparticles / metal-organic frameworks : Synthesis , applications and challenges. , 19.

Duschek, L., Kükelhan, P., Beyer, A., Firoozabadi, S., Oelerich, J.O., Fuchs, C., Stolz, W., Ballabio, A., Isella, G. & Volz, K. 2019. Composition determination of semiconductor alloys towards atomic accuracy by HAADF-STEM. *Ultramicroscopy*, 200: 84–96. https://www.sciencedirect.com/science/article/pii/S0304399118302705.

Dutta, D., Chattopadhyay, A. & Sankar Ghosh, S. 2016. Cationic BSA Templated Au–Ag Bimetallic Nanoclusters As a Theranostic Gene Delivery Vector for HeLa Cancer Cells. *ACS Biomaterials Science & Engineering*, 2(11): 2090–2098.

Dykman, L.A. & Khlebtsov, N.G. 2014. Uptake of Engineered Gold Nanoparticles into Mammalian Cells. *Chemical Reviews*, 114(2): 1258–1288. https://doi.org/10.1021/cr300441a.

Ebad-Sichani, S., Sharafi-Badr, P., Hayati, P. & Soltanian-Fard, M.J. 2023. Nano-Fabrication Methods. In

P. D. R. Sahu, ed. Rijeka: IntechOpen: Ch. 3.

Eisenbrand, G., Pool-Zobel, B., Baker, V., Balls, M., Blaauboer, B.J., Boobis, A., Carere, A., Kevekordes, S., Lhuguenot, J.-C., Pieters, R. & Kleiner, J. 2002. Methods of in vitro toxicology. *Food and Chemical Toxicology*, 40(2): 193–236.

Elbagory, A., Meyer, M., Cupido, C. & Hussein, A.A. 2017. Inhibition of bacteria associated with wound infection by biocompatible green synthesized gold nanoparticles from South African plant extracts. *Nanomaterials*, 7(12).

Elbagory, A.M., Cupido, C.N., Meyer, M. & Hussein, A.A. 2016. Large scale screening of southern African plant extracts for the green synthesis of gold nanoparticles using microtitre-plate method. *Molecules*, 21: 1–20.

Elbagory, A.M., Hussein, A.A. & Meyer, M. 2019. The in vitro immunomodulatory effects of gold nanoparticles synthesized from hypoxis hemerocallidea aqueous extract and hypoxoside on macrophage and natural killer cells. *International Journal of Nanomedicine*, 14: 9007–9018.

Elbaum, M., Seifer, S., Houben, L., Wolf, S.G. & Rez, P. 2021. Toward Compositional Contrast by Cryo-STEM. *Accounts of Chemical Research*, 54(19): 3621–3631.

Elisha, I.L. & Viljoen, A. 2021. Trends in Rooibos Tea (Aspalathus linearis) research (1994–2018): A scientometric assessment. *South African Journal of Botany*, 137: 159–170. https://doi.org/10.1016/j.sajb.2020.10.004.

Elnaker, N.A., Daou, M., Ochsenkühn, M.A., Amin, S.A., Yousef, A.F. & Yousef, L.F. 2021. A metabolomics approach to evaluate the effect of lyophilization versus oven drying on the chemical composition of plant extracts. *Scientific Reports*, 11.

Enea, M., Pereira, E., Costa, J., Soares, M.E., Dias da Silva, D., Bastos, M. de L. & Carmo, H.F. 2021. Cellular uptake and toxicity of gold nanoparticles on two distinct hepatic cell models. *Toxicology in vitro : an international journal published in association with BIBRA*, 70: 105046.

Epure, A., Oniga, I., Benedec, D., Hanganu, D., Gheldiu, A.M., Toiu, A. & Vlase, L. 2019. Chemical analysis and antioxidant activity of some rooibos tea products. *Farmacia*, 67(6): 963–966.

Evstigneeva, R.P. & Pchelkin, V.P. 2003. Catalytic and Biological Activity of Organic Complexes of Precious Metals (A Review). *Pharmaceutical Chemistry Journal*, 37(11): 573–577.

Fageria, P., Uppala, S., Nazir, R., Gangopadhyay, S., Chang, C.-H., Basu, M. & Pande, S. 2016. Synthesis of Monometallic (Au and Pd) and Bimetallic (AuPd) Nanoparticles Using Carbon Nitride

(C(3)N(4)) Quantum Dots via the Photochemical Route for Nitrophenol Reduction. *Langmuir : the ACS journal of surfaces and colloids*, 32(39): 10054–10064.

Fahmy, S.A., Fawzy, I.M., Saleh, B.M., Issa, M.Y., Bakowsky, U. & Azzazy, H.M.E.S. 2021. Green synthesis of platinum and palladium nanoparticles using Peganum harmala L. Seed alkaloids: Biological and computational studies. *Nanomaterials*, 11(4): 1–15.

Fan, L., Ji, X., Lin, G., Liu, K., Chen, S., Ma, G., Xue, W., Zhang, X. & Wang, L. 2021. Green synthesis of stable platinum nanoclusters with enhanced peroxidase-like activity for sensitive detection of glucose and glutathione. *Microchemical Journal*, 166: 106202. https://www.sciencedirect.com/science/article/pii/S0026265X21002861.

Fang, C., Ma, Z., Chen, L., Li, H., Jiang, C. & Zhang, W. 2019. Biosynthesis of gold nanoparticles, characterization and their loading with zonisamide as a novel drug delivery system for the treatment of acute spinal cord injury. *Journal of Photochemistry and Photobiology B: Biology*, 190: 72–75.

Fantoukh, O.I., Dale, O.R., Parveen, A., Hawwal, M.F., Ali, Z., Manda, V.K., Khan, S.I., Chittiboyina, A.G., Viljoen, A. & Khan, I.A. 2019. Safety Assessment of Phytochemicals Derived from the Globalized South African Rooibos Tea (Aspalathus linearis) through Interaction with CYP, PXR, and P-gp. *Journal of Agricultural and Food Chemistry*, 67(17): 4967–4975.

Fantoukh, O.I., Wang, Y., Parveen, A., Hawwal, M.F. & Ali, Z. 2022. Chemical Fingerprinting Profile and Targeted Quantitative Analysis of Chemical Fingerprinting Profile and Targeted Quantitative Analysis of Phenolic Compounds from Rooibos Tea (Aspalathus linearis) and Dietary Supplements Using. *Separations*, 9(159): 1–13.

Fayaz, A.M., Girilal, M., Venkatesan, R. & Kalaichelvan, P.T. 2011. Colloids and Surfaces B : Biointerfaces Biosynthesis of anisotropic gold nanoparticles using Maduca longifolia extract and their potential in infrared absorption. *Colloids and Surfaces B: Biointerfaces*, 88: 287–291.

Feng, J., Ma, C., Miedziak, P.J., Edwards, J.K., Brett, G.L., Li, D., Du, Y., Morgan, D.J. & Hutchings, G.J. 2013. Au–Pd nanoalloys supported on Mg–Al mixed metal oxides as a multifunctional catalyst for solvent-free oxidation of benzyl alcohol. *Dalton Transactions*, 42(40): 14498–14508.

Feng, W., Li, M., Hao, Z. & Zhang, J. 2020. Analytical Methods of Isolation and Identification. In *Phytochemicals in Human Health*. 1–27.

Fernandes, S.R., Barreiros, L., Oliveira, R.F., Cruz, A., Prudêncio, C., Oliveira, A.I., Pinho, C., Santos, N. & Morgado, J. 2019. Chemistry, bioactivities, extraction and analysis of azadirachtin: State-of-the-art. *Fitoterapia*, 134(October 2018): 141–150. https://doi.org/10.1016/j.fitote.2019.02.006.

Ferrando, R., Jellinek, J. & Johnston, R.L. 2008. Nanoalloys: from theory to applications of alloy clusters and nanoparticles. *Chemical reviews*, 108(3): 845–910.

Ferreyra, M.L.F., Serra, P. & Casati, P. 2021. Recent advances on the roles of flavonoids as plant protective molecules after UV and high light exposure. *Physiologia plantarum*, 173(3): 736–749.

Filipe, V., Hawe, A. & Jiskoot, W. 2010. Critical Evaluation of Nanoparticle Tracking Analysis (NTA) by NanoSight for the Measurement of Nanoparticles and Protein Aggregates. *Pharmaceutical Research*, 27(5): 796–810. https://doi.org/10.1007/s11095-010-0073-2.

Flampouri, E., Imar, S., OConnell, K. & Singh, B. 2019. Spheroid-3D and monolayer-2D intestinal electrochemical biosensor for toxicity/viability testing: Applications in drug screening, food safety, and environmental pollutant analysis. *ACS sensors*, 4(3): 660–669.

Foo, Y.Y., Periasamy, V., Kiew, L.V., Kumar, G.G. & Malek, S.N.A. 2017. Curcuma mangga-mediated synthesis of gold nanoparticles: Characterization, stability, cytotoxicity, and blood compatibility. *Nanomaterials*, 7(6).

Formaggio, D.M.D., de Oliveira Neto, X.A., Rodrigues, L.D.A., de Andrade, V.M., Nunes, B.C., Lopes-Ferreira, M., Ferreira, F.G., Wachesk, C.C., Camargo, E.R., Conceição, K. & Tada, D.B. 2019. In vivo toxicity and antimicrobial activity of AuPt bimetallic nanoparticles. *Journal of Nanoparticle Research*, 21(11): 244.

Franco-Ulloa, S., Tatulli, G., Bore, S.L., Moglianetti, M., Pompa, P.P., Cascella, M. & De Vivo, M. 2020. Dispersion state phase diagram of citrate-coated metallic nanoparticles in saline solutions. *Nature Communications*, 11(1): 5422.

Frank, J., Fukagawa, N.K., Bilia, A.R., Johnson, E.J., Kwon, O., Prakash, V., Miyazawa, T., Clifford, M.N., Kay, C.D., Crozier, A., Erdman, J.W., Shao, A. & Williamson, G. 2020. Terms and nomenclature used for plant-derived components in nutrition and related research: efforts toward harmonization. *Nutrition reviews*, 78(6): 451–458.

Gan, P.P., Ng, S.H., Huang, Y. & Li, S.F.Y. 2012. Green synthesis of gold nanoparticles using palm oil mill effluent (POME): A low-cost and eco-friendly viable approach. *Bioresource Technology*, 113: 132–135. https://www.sciencedirect.com/science/article/pii/S0960852412000211.

Gao, X., Liu, Y., An, Z. & Ni, J. 2021. Active Components and Pharmacological Effects of Cornus officinalis: Literature Review. *Frontiers in pharmacology*, 12: 633447.

Gebreslassie, Y.T. & Gebretnsae, H.G. 2021. Green and Cost-Effective Synthesis of Tin Oxide Nanoparticles: A Review on the Synthesis Methodologies, Mechanism of Formation, and Their

Potential Applications. *Nanoscale Research Letters*, 16(1).

Geng, G., Chen, P., Guan, B., Liu, Y., Yang, C., Wang, N. & Liu, M. 2017. Sheetlike gold nanostructures/graphene oxide composites: Via a one-pot green fabrication protocol and their interesting two-stage catalytic behaviors. *RSC Advances*, 7: 51838–51846.

Ghasemi, M., Turnbull, T., Sebastian, S. & Kempson, I. 2021. The mtt assay: Utility, limitations, pitfalls, and interpretation in bulk and single-cell analysis. *International Journal of Molecular Sciences*, 22(23).

Ghosh, S., Roy, S., Naskar, J. & Kole, R.K. 2020. Process optimization for biosynthesis of mono and bimetallic alloy nanoparticle catalysts for degradation of dyes in individual and ternary mixture. *Scientific Reports*, 10(1): 277. https://doi.org/10.1038/s41598-019-57097-0.

Gilani, A.H., Khan, A., Ghayur, M.N., Ali, S.F. & Herzig, J.W. 2006. Antispasmodic Effects of Rooibos Tea (Aspalathus linearis) is Mediated Predominantly through K+-Channel Activation. *Basic & Clinical Pharmacology & Toxicology*, 99(5): 365–373. https://doi.org/10.1111/j.1742-7843.2006.pto_507.x.

Gilbert, S.M., Oliphant, C.J., Hassan, S., Peille, A.L., Bronsert, P., Falzoni, S., Di Virgilio, F., McNulty, S. & Lara, R. 2019. ATP in the tumour microenvironment drives expression of nfP2X7, a key mediator of cancer cell survival. *Oncogene*, 38(2): 194–208.

Ginwala, R., Bhavsar, R., Chigbu, D.G.I., Jain, P. & Khan, Z.K. 2019. Potential Role of Flavonoids in Treating Chronic Inflammatory Diseases with a Special Focus on the Anti-Inflammatory Activity of Apigenin. *Antioxidants*, 8(2).

Githala, C.K., Raj, S. & Dhaka, A. 2022. Phyto-fabrication of silver nanoparticles and their catalytic dye degradation and antifungal ef fi cacy. *Frontiers in Chemistry*: 1–17.

Grabenauer, M. & Stafford, D.T. 2020. Chromatography. *Principles of Forensic Toxicology: Fifth Edition*: 135–162.

Gu, C., Chen, L., Liu, Y., Zhang, X., Liu, J., Zhang, Q., Wang, C. & Ma, L. 2022. One-pot conversion of biomass-derived levulinic acid to furanic biofuel 2-methyltetrahydrofuran over bimetallic NiCo/γ-Al2O3 catalysts. *Molecular Catalysis*, 524: 112317. https://www.sciencedirect.com/science/article/pii/S2468823122002036.

Guntlin, C.P., Kravchyk, K. V, Erni, R. & Kovalenko, M. V. 2019. Transition metal trifluoroacetates (M = Fe, Co, Mn) as precursors for uniform colloidal metal difluoride and phosphide nanoparticles. *Scientific reports*, 9(1): 6613.

Gurunathan, S., Qasim, M., Park, C.H., Arsalan Iqbal, M., Yoo, H., Hwang, J.H., Uhm, S.J., Song, H., Park, C., Choi, Y., Kim, J.-H. & Hong, K. 2019. Cytotoxicity and Transcriptomic Analyses of Biogenic Palladium Nanoparticles in Human Ovarian Cancer Cells (SKOV3). *Nanomaterials*, 9(5).

Haidar Ahmad, I.A., Chen, W., Halsey, H.M., Klapars, A., Limanto, J., Pirrone, G.F., Nowak, T., Bennett, R., Hartman, R., Makarov, A.A., Mangion, I. & Regalado, E.L. 2019. Multi-column ultra-high performance liquid chromatography screening with chaotropic agents and computer-assisted separation modeling enables process development of new drug substances. *The Analyst*, 144(9): 2872–2880.

Hammami, I., Alabdallah, N.M., jomaa, A. Al & kamoun, M. 2021. Gold nanoparticles: Synthesis properties and applications. *Journal of King Saud University - Science*, 33(7).

Han, G., Li, X., Li, J., Wang, X., Zhang, Y.S. & Sun, R. 2017. Special Magnetic Catalyst with Lignin-Reduced Au-Pd Nanoalloy. *ACS Omega*, 2(8): 4938–4945.

Harish, V., Tewari, D., Gaur, M., Yadav, A.B. & Swaroop, S. 2022. Nanoparticles and Nanostructured Materials : Bioimaging , Biosensing , Drug Delivery , Tissue Engineering , Antimicrobial , and Agro-Food Applications.

Hasan, S. 2014. A Review on Nanoparticles : Their Synthesis and Types. *Research Journal of Recent Sciences Res . J . Recent . Sci . Uttar Pradesh (Lucknow Campus)*, 4(February): 1–3.

Hazarika, M., Borah, D., Bora, P., Silva, A.R. & Das, P. 2017. Biogenic synthesis of palladium nanoparticles and their applications as catalyst and antimicrobial agent. *PLoS ONE*, 12(9): 1–19.

He, F., Ji, H., Feng, L., Wang, Z., Sun, Q., Zhong, C., Yang, D., Gai, S., Yang, P. & Lin, J. 2021. Biomaterials Construction of thiol-capped ultrasmall Au – Bi bimetallic nanoparticles for X-ray CT imaging and enhanced antitumor therapy efficiency. *Biomaterials*, 264(October 2020): 120453.

Heinrich, T., Willenberg, I. & Glomb, M.A. 2012. Chemistry of Color Formation during Rooibos Fermentation. *Journal of Agricultural and Food Chemistry*, 60(20): 5221–5228. https://doi.org/10.1021/jf300170j.

Heuer-Jungemann, A., Feliu, N., Bakaimi, I., Hamaly, M., Alkilany, A., Chakraborty, I., Masood, A., Casula, M.F., Kostopoulou, A., Oh, E., Susumu, K., Stewart, M.H., Medintz, I.L., Stratakis, E., Parak, W.J. & Kanaras, A.G. 2019. The role of ligands in the chemical synthesis and applications of inorganic nanoparticles. *Chemical Reviews*, 119(8): 4819–4880.

Hind, A.R., Bhargava, S.K. & McKinnon, A. 2001. At the solid/liquid interface: FTIR/ATR — the tool of choice. *Advances in Colloid and Interface Science*, 93(1): 91–114.

http://www.sciencedirect.com/science/article/pii/S0001868600000798.

Hoosen, M. 2019. The Effects of Aspalathus linearis (Rooibos Tea) on Nitric Oxide (NO) and Cytokine Activity. *International Journal of Human and Health Sciences (IJHHS)*, 3(3): 150.

Huang, S.-H., Kao, Y.-H., Muller, C.J.F., Joubert, E. & Chuu, C.-P. 2020. Aspalathin-rich green Aspalathus linearis extract suppresses migration and invasion of human castration-resistant prostate cancer cells via inhibition of YAP signaling. *Phytomedicine*, 69: 153210.

Ibrahim, H.M.M. 2015. Green synthesis and characterization of silver nanoparticles using banana peel extract and their antimicrobial activity against representative microorganisms. *Journal of Radiation Research and Applied Sciences*, 8(3): 265–275. https://www.sciencedirect.com/science/article/pii/S1687850715000084.

Idris, Dahir Sagir & Roy, A. 2023. Synthesis of Bimetallic Nanoparticles and Applications—An Updated Review. *Crystals*, 13(4).

Idris, Dahir S & Roy, A. 2023. Synthesis of Bimetallic Nanoparticles and Applications—An Updated Review. *Crystals*, 13(4).

Ijaz, I., Gilani, E., Nazir, A. & Bukhari, A. 2020. Detail review on chemical, physical and green synthesis, classification, characterizations and applications of nanoparticles. *Green Chemistry Letters and Reviews*, 13(3): 223–245. https://doi.org/10.1080/17518253.2020.1802517.

Ikhmayies, S.J. 2014. Characterization of nanomaterials. *Jom*, 66(1): 28–29.

Ikram, M., Javed, B., Raja, N.I. & Mashwani, Z.U.R. 2021. Biomedical potential of plant-based selenium nanoparticles: A comprehensive review on therapeutic and mechanistic aspects. *International Journal of Nanomedicine*, 16: 249–268.

Ingle, K.P., Deshmukh, A.G., Padole, D.A., Dudhare, M.S., Moharil, M.P. & Khelurkar, V.C. 2017. Phytochemicals: Extraction methods, identification and detection of bioactive compounds from plant extracts. *Journal of Pharmacognosy and Phytochemistry*, 6(1): 32–36.

Iqbal, M., Elahi, F., Rehman, A., Wasy Zia, A., Islam, G. ul & Zusheng, Z. 2019. Design and beam dynamics of a Transmission Electron Microscope electron gun assembly. *Vacuum*, 165: 283–289. https://www.sciencedirect.com/science/article/pii/S0042207X19304713.

Ismail, E., Khenfouch, M., Dhlamini, M., Dube, S. & Maaza, M. 2017. Green palladium and palladium oxide nanoparticles synthesized via Aspalathus linearis natural extract. *Journal of Alloys and Compounds*, 695(November): 3632–3638.

Iyer, M., Pal, K. & Upadhye, V. 2023. Phytochemicals and cancer. In S. Pati, T. Sarkar, & D. B. T.-R. F. of P. Lahiri, eds. Elsevier: 295–308.

Jadimurthy, R., Jagadish, S., Nayak, S.C., Kumar, S., Mohan, C.D. & Rangappa, K.S. 2023. Phytochemicals as Invaluable Sources of Potent Antimicrobial Agents to Combat Antibiotic Resistance. *Life*, 13(4): 1–34.

Jain, S. & Mehata, M.S. 2017. Medicinal Plant Leaf Extract and Pure Flavonoid Mediated Green Synthesis of Silver Nanoparticles and their Enhanced Antibacterial Property. *Scientific Reports*, 7(1): 15867.

Jamkhande, P.G., Ghule, N.W., Bamer, A.H. & Kalaskar, M.G. 2019. Metal nanoparticles synthesis: An overview on methods of preparation, advantages and disadvantages, and applications. *Journal of Drug Delivery Science and Technology*, 53: 101174.

Janecek, M. & Kral, R. eds. 2016. Modern Electron Microscopy in Physical and Life Sciences.

Janeiro, R., Flores, R. & Viegas, J. 2021. Refractive index of phosphate-buffered saline in the telecom infrared C + L bands. *OSA Continuum*, 4(12): 3039.

Javed, R., Zia, M., Naz, S., Aisida, S.O., Ain, N. ul & Ao, Q. 2020. Role of capping agents in the application of nanoparticles in biomedicine and environmental remediation: recent trends and future prospects. *Journal of Nanobiotechnology*, 18(1): 1–15.

Jemilugba, O.T., Sakho, E.H.M., Parani, S., Mavumengwana, V. & Oluwafemi, O.S. 2019. Green synthesis of silver nanoparticles using Combretum erythrophyllum leaves and its antibacterial activities. *Colloid and Interface Science Communications*, 31: 100191.

Ji, S., Wang, S., Xu, H., Su, Z., Tang, D., Qiao, X. & Ye, M. 2018. The application of on-line two-dimensional liquid chromatography (2DLC) in the chemical analysis of herbal medicines. *Journal of Pharmaceutical and Biomedical Analysis*, 160: 301–313. https://doi.org/10.1016/j.jpba.2018.08.014.

Jiang, J., Trundle, P., Ren, J., Cheng, Y.-L., Lee, C.-Y., Huang, Y.-L., Buckner, C.A., Lafrenie, R.M., Dénommée, J.A., Caswell, J.M., Want, D.A., Gan, G.G., Leong, Y.C., Bee, P.C., Chin, E., Teh, A.K.H., Picco, S., Villegas, L., Tonelli, F., Merlo, M., Rigau, J., Diaz, D., Masuelli, M., Korrapati, S., Kurra, P., Puttugunta, S., Picco, S., Villegas, L., Tonelli, F., Merlo, M., Rigau, J., Diaz, D., Masuelli, M., Tascilar, M., de Jong, F.A., Verweij, J., Mathijssen, R.H.J., Amin, J., Sharif, M., Gul, N., Kadry, S., Chakraborty, C., Dutt, V., Chandrasekaran, S. & García-Díaz, V. 2019. Natural Products in Drug Discovery. In *Intech*. 57–67.

Jiménez Pérez, Z.E., Mathiyalagan, R., Markus, J., Kim, Y.-J., Kang, H.M., Abbai, R., Seo, K.H., Wang,

D., Soshnikova, V. & Yang, D.C. 2017. Ginseng-berry-mediated gold and silver nanoparticle synthesis and evaluation of their in vitro antioxidant, antimicrobial, and cytotoxicity effects on human dermal fibroblast and murine melanoma skin cell lines. *International Journal of Nanomedicine*, 12: 709–723.

Johal, M.S. & Johnson, L.E. 2018. *Understanding nanomaterials*. CRC Press.

Johnson, R., Beer, D. De, Dludla, P. V., Ferreira, D., Muller, C.J.F. & Joubert, E. 2018. Aspalathin from Rooibos (Aspalathus linearis): A Bioactive C -glucosyl Dihydrochalcone with Potential to Target the Metabolic Syndrome. *Planta Medica*, 84(9–10): 568–583.

Johnson, R., Shabalala, S., Louw, J., Kappo, A.P. & Muller, C.J. 2017. Aspalathin Reverts Doxorubicin-Induced Cardiotoxicity through Increased Autophagy and Decreased Expression of p53/mTOR/p62 Signaling. *Molecules*, 22(10).

De Jong, W.H. & Borm, P.J.A. 2008. Drug delivery and nanoparticles: Applications and hazards. *International Journal of Nanomedicine*, 3(2): 133–149.

Joubert, E. & de Beer, D. 2011. Rooibos (Aspalathus linearis) beyond the farm gate: From herbal tea to potential phytopharmaceutical. *South African Journal of Botany*, 77(4): 869–886. https://www.sciencedirect.com/science/article/pii/S0254629911001086.

Joubert, E., Fouche, G., Vermaak, I., Mulaudzi, N. & Chen, W. 2023. Chapter 5 - Aspalathus linearis. In A. Viljoen, M. Sandasi, G. Fouche, S. Combrinck, & I. B. T.-T. S. A. H. P. Vermaak, eds. Academic Press: 107–152.

Joudeh, N. & Linke, D. 2022. Nanoparticle classification, physicochemical properties, characterization, and applications: a comprehensive review for biologists. *Journal of Nanobiotechnology*, 20(1): 262.

JyothiKumar, A., Kailasnath, M., Simon, J. & Mathew, S. 2019. BSA Stabilized Gold Nanoparticles: Synthesis and Characterization. *Materials Today: Proceedings*, 9: 111–5.

Kalyane, D., Raval, N., Maheshwari, R., Tambe, V., Kalia, K. & Tekade, R.K. 2019. Employment of enhanced permeability and retention effect (EPR): Nanoparticle-based precision tools for targeting of therapeutic and diagnostic agent in cancer. *Materials Science and Engineering: C*, 98: 1252–1276.

Kamiloglu, S., Sari, G., Ozdal, T. & Capanoglu, E. 2020. Guidelines for cell viability assays. *Food Frontiers*, 1(3): 332–349. https://doi.org/10.1002/fft2.44.

Kapara, A., Brunton, V., Graham, D. & Faulds, K. 2020. Investigation of cellular uptake mechanism of functionalised gold nanoparticles into breast cancer using SERS. *Chemical Science*, 11(22): 5819–

5829.

Karmakar, S. 2019. Particle Size Distribution and Zeta Potential Based on Dynamic Light Scattering: Techniques to Characterise Stability and Surface distribution of Charged Colloids Studies on the interaction of antimicrobial peptide with phospholipid membranes. View projec. , (January).

Katwal, R., Kaur, H., Sharma, G., Naushad, M. & Pathania, D. 2015. Electrochemical synthesized copper oxide nanoparticles for enhanced photocatalytic and antimicrobial activity. *Journal of Industrial and Engineering Chemistry*, 31: 173–184. http://www.sciencedirect.com/science/article/pii/S1226086X15003007.

Kawano, A., Nakamura, H., Hata, S., Minakawa, M., Miura, Y. & Yagasaki, K. 2009. Hypoglycemic effect of aspalathin, a rooibos tea component from Aspalathus linearis, in type 2 diabetic model db/db mice. *Phytomedicine*, 16(5): 437–443. https://www.sciencedirect.com/science/article/pii/S0944711308002213.

Kevadiya, B.D., Ottemann, B., Mukadam, I.Z., Castellanos, L., Sikora, K., Hilaire, J.R., Machhi, J., Herskovitz, J., Soni, D. & Hasan, M. 2020. Rod-shape theranostic nanoparticles facilitate antiretroviral drug biodistribution and activity in human immunodeficiency virus susceptible cells and tissues. *Theranostics*, 10(2): 630.

Khalid, M., Saeed-ur-Rahman, Bilal, M. & HUANG, D. feng. 2019. Role of flavonoids in plant interactions with the environment and against human pathogens — A review. *Journal of Integrative Agriculture*, 18(1): 211–230.

Khan, Ibrahim, Saeed, K. & Khan, Idrees. 2019. Nanoparticles: Properties, applications and toxicities. *Arabian Journal of Chemistry*, 12(7): 908–931. https://www.sciencedirect.com/science/article/pii/S1878535217300990.

Khan, S.A., Shahid, S. & Lee, C.-S. 2020. Green Synthesis of Gold and Silver Nanoparticles Using Leaf Extract of Clerodendrum inerme; Characterization, Antimicrobial, and Antioxidant Activities. *Biomolecules*, 10(6).

Khandel, P., Yadaw, R.K., Soni, D.K., Kanwar, L. & Shahi, S.K. 2018. Biogenesis of metal nanoparticles and their pharmacological applications: present status and application prospects. *Journal of Nanostructure in Chemistry*, 8(3): 217–254.

Kharissova, O. V., Kharisov, B.I., González, C.M.O., Méndez, Y.P. & López, I. 2019. *Greener synthesis of chemical compounds and materials*.

Kiani, H.S., Ali, A., Zahra, S., Hassan, Z.U., Kubra, K.T., Azam, M. & Zahid, H.F. 2022. Phytochemical

Composition and Pharmacological Potential of Lemongrass (Cymbopogon) and Impact on Gut Microbiota. *AppliedChem*, 2(4): 229–246.

Kim, E. & Ehrmann, K. 2020. Refractive index of soft contact lens materials measured in packaging solution and standard phosphate buffered saline and the effect on back vertex power calculation. *Contact Lens and Anterior Eye*, 43(2): 123–129.

Kim, J.-Y., Kim, M., Kim, H., Joo, J. & Choi, J.-H. 2003. Electrical and optical studies of organic light emitting devices using SWCNTs-polymer nanocomposites. *Optical Materials*, 21(1): 147–151. https://www.sciencedirect.com/science/article/pii/S0925346702001271.

Koeppen, B.H. & Roux, D.G. 1965. Aspalathin : a novel C-glycosylflavonoid from aspalathus linearis. *Tetrahedron Letters*, 6(39): 3497–3503.

Kolahalam, L.A., Kasi Viswanath, I. V, Diwakar, B.S., Govindh, B., Reddy, V. & Murthy, Y.L.N. 2019. Review on nanomaterials: Synthesis and applications. *Materials Today: Proceedings*, 18: 2182–2190. https://www.sciencedirect.com/science/article/pii/S2214785319325507.

Koparde, A.A., Doijad, R.C. & Magdum, C.S. 2019. Natural Products in Drug Discovery. In S. Perveen & A. Al-Taweel, eds. Rijeka: IntechOpen: Ch. 14.

Kora, A.J. & Rastogi, L. 2018. Green synthesis of palladium nanoparticles using gum ghatti (Anogeissus latifolia) and its application as an antioxidant and catalyst. *Arabian Journal of Chemistry*, 11(7): 1097–1106. https://www.sciencedirect.com/science/article/pii/S1878535215001963.

Koshani, R., Mahdi, S. & Ven, T.G.M. Van De. 2020. Trends in Food Science & Technology Going deep inside bioactive-loaded nanocarriers through Nuclear Magnetic Resonance (NMR) spectroscopy. *Trends in Food Science & Technology*, 101(May): 198–212.

Kowalska, T. & Sajewicz, M. 2022. Thin-Layer Chromatography (TLC) in the Screening of Botanicals–Its Versatile Potential and Selected Applications. *Molecules*, 27(19).

Kowshik, M., Deshmukh, N., Vogel, W., Urban, J., Kulkarni, S. & Paknikar, K. 2002. Microbial Synthesis of Semiconductor CdS Nanoparticles, Their Characterization, and Their Use in the Fabrication of an Ideal Diode. *Biotechnology and Bioengineering*, 78: 583–588.

Krafczyk, N. & Glomb, M.A. 2008. Characterization of Phenolic Compounds in Rooibos Tea. *Journal of Agricultural and Food Chemistry*, 56(9): 3368–3376. https://doi.org/10.1021/jf703701n.

Krakowska-Sieprawska, A., Kiełbasa, A., Rafińska, K., Ligor, M. & Buszewski, B. 2022. Modern Methods of Pre-Treatment of Plant Material for the Extraction of Bioactive Compounds. *Molecules*,

27: 730.

Kruer, T.L., Dougherty, S.M., Reynolds, L., Long, E., De Silva, T., Lockwood, W.W. & Clem, B.F. 2016. Expression of the lncRNA maternally expressed gene 3 (MEG3) contributes to the control of lung cancer cell proliferation by the Rb pathway. *PLoS ONE*, 11(11): 1–17.

Kumar, A. & Dixit, C.K. 2017. Methods for characterization of nanoparticles. In S. Nimesh, R. Chandra, & N. B. T.-A. in N. for the D. of T. N. A. Gupta, eds. Woodhead Publishing: 43–58.

Kumar, A., P, N., Kumar, M., Jose, A., Tomer, V., Oz, E., Proestos, C., Zeng, M., Elobeid, T., K, S. & Oz, F. 2023. Major Phytochemicals: Recent Advances in Health Benefits and Extraction Method. *Molecules (Basel, Switzerland)*, 28(2).

Kumar, I., Mondal, M., Meyappan, V. & Sakthivel, N. 2019. Green one-pot synthesis of gold nanoparticles using Sansevieria roxburghiana leaf extract for the catalytic degradation of toxic organic pollutants. *Materials Research Bulletin*, 117: 18–27. https://www.sciencedirect.com/science/article/pii/S0025540818329234.

Kumar, J.A., Krithiga, T., Manigandan, S., Sathish, S., Renita, A.A., Prakash, P., Prasad, B.S.N., Kumar, T.R.P., Rajasimman, M., Hosseini-Bandegharaei, A., Prabu, D. & Crispin, S. 2021. A focus to green synthesis of metal/metal based oxide nanoparticles: Various mechanisms and applications towards ecological approach. *Journal of Cleaner Production*, 324: 129198.

Kumar, R., Mondal, K., Panda, P.K., Kaushik, A., Abolhassani, R., Ahuja, R., Rubahn, H.-G. & Mishra, Y.K. 2020. Core–shell nanostructures: perspectives towards drug delivery applications. *Journal of Materials Chemistry B*, 8(39): 8992–9027. http://dx.doi.org/10.1039/D0TB01559H.

Kumar, T., Shrivas, K., Kurrey, R., Upadhyay, S., Jangde, R. & Chauhan, R. 2020. Phytochemical screening and determination of phenolics and fl avonoids in Dillenia pentagyna using UV – vis and FTIR spectroscopy. *Spectrochimica Acta Part A: Molecular and Biomolecular Spectroscopy*, 242: 118717.

Kumari, S.C., Dhand, V. & Padma, P.N. 2021. Green synthesis of metallic nanoparticles: a review. *Nanomaterials*: 259–281.

LaCourse, W.R. & LaCourse, M.E. 2023. General instrumentation in HPLC. In *Liquid Chromatography*. Elsevier: 61–73.

Layouni, R., Choudhury, M.H., Laibinis, P.E. & Weiss, S.M. 2020. Thermally Carbonized Porous Silicon for Robust Label-Free DNA Optical Sensing. *ACS Applied Bio Materials*, 3(1): 622–627.

Leary, J.F. ed. 2022. Characterizing Nanoparticles. In *Fundamentals of Nanomedicine*. Cambridge: Cambridge University Press: 122–142.

Lee, J.-C., Lee, K.-Y., Son, Y.-O., Choi, K.-C., Kim, J., Truong, T.T. & Jang, Y.-S. 2005. Plant-originated glycoprotein, G-120, inhibits the growth of MCF-7 cells and induces their apoptosis. *Food and Chemical Toxicology*, 43(6): 961–968.

Lee, K.-B., Solanki, A., Kim, J.D. & Jung, J. 2019. Nanomedicine: dynamic integration of nanotechnology with biomedical science. In *Nanomedicine*. Jenny Stanford Publishing: 1–38.

Lee, W. & Bae, J.-S. 2015. Anti-inflammatory Effects of Aspalathin and Nothofagin from Rooibos (Aspalathus linearis) In Vitro and In Vivo. *Inflammation*, 38(4): 1502–1516. https://doi.org/10.1007/s10753-015-0125-1.

Lee, Y.-R., Jang, M.-S., Cho, H.-Y., Kwon, H.-J., Kim, S. & Ahn, W.-S. 2015. A comparison of synthesis methods. *Chemical Engineering Journal*, 271: 276–280. https://www.sciencedirect.com/science/article/pii/S1385894715003034.

Lee, Y.W., Kim, M., Kim, Z.H. & Han, S.W. 2009. One-Step Synthesis of Au @ Pd Core - Shell Nanooctahedron. , (Iii): 17036–17037.

Lengke, M.F., Fleet, M.E. & Southam, G. 2007. Biosynthesis of Silver Nanoparticles by Filamentous Cyanobacteria from a Silver(I) Nitrate Complex. *Langmuir*, 23(5): 2694–2699. https://doi.org/10.1021/la0613124.

Ley-Ngardigal, S. & Bertolin, G. 2022. Approaches to monitor ATP levels in living cells: where do we stand? *The FEBS Journal*, 289(24): 7940–7969.

Li, G., Zhang, W., Luo, N., Xue, Z., Hu, Q., Zeng, W. & Xu, J. 2021. Bimetallic nanocrystals: Structure, controllable synthesis and applications in catalysis, energy and sensing. *Nanomaterials*, 11(8): 1–37.

Li, H. & Yang, X. 2015. Bovine serum albumin-capped CdS quantum dots as an inner-filter effect sensor for rapid detection and quantification of protamine and heparin. *Analytical Methods*, 7(19): 8445–8452.

Li, L., Li, B., Cheng, D. & Mao, L. 2010. Visual detection of melamine in raw milk using gold nanoparticles as colorimetric probe. *Food Chemistry*, 122(3): 895–900. https://www.sciencedirect.com/science/article/pii/S0308814610003067.

Li, M.-T., Wang, C.-H., Lai, S.-F., Ong, E.B.L., Chen, Y.H., Lin, C.-K., Margaritondo, G. & Hwu, Y. 2015. X-ray irradiation synthesis of PEG-coated Au-Pd nanoparticles. *Nanotechnology*, 26(35): 355601.

https://dx.doi.org/10.1088/0957-4484/26/35/355601.

Li, T., Albee, B., Alemayehu, M., Diaz, R., Ingham, L., Kamal, S., Rodriguez, M. & Whaley Bishnoi, S. 2010. Comparative toxicity study of Ag, Au, and Ag–Au bimetallic nanoparticles on Daphnia magna. *Analytical and Bioanalytical Chemistry*, 398(2): 689–700. https://doi.org/10.1007/s00216-010-3915-1.

Li, T., Wang, B., Ning, J., Li, W., Guo, G., Han, D., Xue, B., Zou, J., Wu, G., Yang, Y., Dong, A. & Zhao, D. 2019. Self-Assembled Nanoparticle Supertubes as Robust Platform for Revealing Long-Term, Multiscale Lithiation Evolution. *Matter*, 1(4): 976–987. https://doi.org/10.1016/j.matt.2019.04.009.

Li, W.-L., Zhang, Y., Liu, H.-B., Sun, Y.-H., Zhou, X.-S. & Qu, H.-B. 2019. Research progress on quality control methods of traditional Chinese medicine glues. *Zhongguo Zhongyao Zazhi*, 44(13): 2748–2752. https://www.scopus.com/inward/record.uri?eid=2-s2.0-85070832575&doi=10.19540%2Fj.cnki.cjcmm.20190321.306&partnerID=40&md5=56e21a1711be17b0fe9676440529e039.

Li, Y. & Jin, R. 2020. Seeing Ligands on Nanoclusters and in Their Assemblies by X-ray Crystallography: Atomically Precise Nanochemistry and Beyond. *Journal of the American Chemical Society*, 142(32): 13627–13644.

Liao, W., Liu, K., Chen, Y., Hu, J. & Gan, Y. 2021. Au–Ag bimetallic nanoparticles decorated silicon nanowires with fixed and dynamic hot spots for ultrasensitive 3D SERS sensing. *Journal of Alloys and Compounds*, 868: 159136. https://www.sciencedirect.com/science/article/pii/S0925838821005430.

Lim, J., Yeap, S.P., Che, H.X. & Low, S.C. 2013. Characterization of magnetic nanoparticle by dynamic light scattering. *Nanoscale Research Letters*, 8(1): 381. https://doi.org/10.1186/1556-276X-8-381.

Lin, Y., Zhou, M., Tai, X., Li, H., Han, X. & Yu, J. 2021. Analytical transmission electron microscopy for emerging advanced materials. *Matter*, 4(7): 2309–2339. https://doi.org/10.1016/j.matt.2021.05.005.

Liu, J., Qiao, S.Z., Hu, Q.H. & (Max) Lu, G.Q. 2011. Magnetic Nanocomposites with Mesoporous Structures: Synthesis and Applications. *Small*, 7(4): 425–443. https://doi.org/10.1002/smll.201001402.

Liu, Z., Fu, R. & Yuying, Y. 2022. Preparation and evaluation of stable nanofluids for heat transfer application. In H. M. B. T.-A. in N. H. T. Ali, ed. Elsevier: 25–57.

Loza, K., Heggen, M. & Epple, M. 2020. Synthesis , Structure , Properties , and Applications of Bimetallic Nanoparticles of Noble Metals. , 1909260.

Lu, H., Wang, J., Wang, T., Zhong, J., Bao, Y. & Hao, H. 2016. Recent Progress on Nanostructures for Drug Delivery Applications C. Brosseau, ed. *Journal of Nanomaterials*, 2016: 5762431.

Lunardi, C.N., Gomes, A.J., Rocha, F.S., De Tommaso, J. & Patience, G.S. 2021. Experimental methods in chemical engineering: Zeta potential. *Canadian Journal of Chemical Engineering*, 99(3): 627–639.

Lyimo, G. V, Ajayi, R.F., Maboza, E. & Adam, R.Z. 2022. A green synthesis of zinc oxide nanoparticles using Musa Paradisiaca and Rooibos extracts. *MethodsX*, 9: 101892. https://www.sciencedirect.com/science/article/pii/S2215016122002710.

Magcwebeba, T., Swart, P., Swanevelder, S., Joubert, E. & Gelderblom, W. 2016. Anti-Inflammatory Effects of Aspalathus linearis and Cyclopia spp. Extracts in a UVB/Keratinocyte (HaCaT) Model Utilising Interleukin-1α Accumulation as Biomarker. *Molecules* , 21(10).

Mahakal, S. & Suse, S. 2020. Amino acid Adapted Metal and Metals Oxides. *International Journal of Engineering Research & Technology*, 9(12): 107–119.

Mahato, N., Sinha, M., Sharma, K., Koteswararao, R. & Cho, M.H. 2019. Modern Extraction and Purification Techniques for Obtaining High Purity Food-Grade Bioactive Compounds and Value-Added Co-Products from Citrus Wastes. *Foods*, 8(11).

Majoumouo, M.S., Sharma, J.R., Sibuyi, N.R.S., Tincho, M.B., Boyom, F.F. & Meyer, M. 2020. Synthesis of Biogenic Gold Nanoparticles from Terminalia mantaly Extracts and the Evaluation of Their In Vitro Cytotoxic Effects in Cancer Cells. *Molecules (Basel, Switzerland)*, 25(19).

Majrashi, T.A., Alshehri, S.A., Alsayari, A., Muhsinah, A. Bin, Alrouji, M., Alshahrani, A.M., Shamsi, A. & Atiya, A. 2023. Insight into the Biological Roles and Mechanisms of Phytochemicals in Different Types of Cancer: Targeting Cancer Therapeutics. *Nutrients*, 15(7).

Malatesta, M. 2021. Transmission Electron Microscopy as a Powerful Tool to Investigate the Interaction of Nanoparticles with Subcellular Structures. *International Journal of Molecular Sciences*, 22: 1–17.

Maleki, S.J., Crespo, J.F. & Cabanillas, B. 2019. Anti-inflammatory effects of flavonoids. *Food Chemistry*, 299: 125124. https://www.sciencedirect.com/science/article/pii/S0308814619312300.

Malik, P., Shankar, R., Malik, V., Sharma, N. & Mukherjee, T.K. 2014. Green Chemistry Based Benign Routes for Nanoparticle Synthesis. http://dx.doi.org/10.1155/2014/302429 10 December 2021.

Mallikarjuna, K., Bathula, C., Dinneswara Reddy, G., Shrestha, N.K., Kim, H. & Noh, Y.Y. 2019. Au-Pd bimetallic nanoparticles embedded highly porous Fenugreek polysaccharide based micro networks for catalytic applications. *International Journal of Biological Macromolecules*, 126: 352–358.

https://doi.org/10.1016/j.ijbiomac.2018.12.137.

Mani, S. & Swargiary, G. 2023. In Vitro Cytotoxicity Analysis: MTT/XTT, Trypan Blue Exclusion. In *Animal Cell Culture: Principles and Practice*. Springer: 267–284.

Marais, C., van Rensburg, W.J., Ferreira, D. & Steenkamp, J.A. 2000. (S)- and (R)-Eriodictyol-6-C-ß-D-glucopyranoside, novel keys to the fermentation of rooibos (Aspalathus linearis). *Phytochemistry*, 55(1): 43–49. https://www.sciencedirect.com/science/article/pii/S0031942200001825.

Marnewick, J., Joubert, E., Joseph, S., Swanevelder, S., Swart, P. & Gelderblom, W. 2005. Inhibition of tumour promotion in mouse skin by extracts of rooibos (Aspalathus linearis) and honeybush (Cyclopia intermedia), unique South African herbal teas. *Cancer Letters*, 224(2): 193–202. https://www.sciencedirect.com/science/article/pii/S0304383504008687.

Marnewick, J.L., Gelderblom, W.C.A. & Joubert, E. 2000. An investigation on the antimutagenic properties of South African herbal teas. *Mutation Research/Genetic Toxicology and Environmental Mutagenesis*, 471(1): 157–166. https://www.sciencedirect.com/science/article/pii/S1383571800001285.

Marques, B.L., Oliveira-Lima, O.C., Carvalho, G.A., de Almeida Chiarelli, R., Ribeiro, R.I., Parreira, R.C., da Madeira Freitas, E.M., Resende, R.R., Klempin, F., Ulrich, H., Gomez, R.S. & Pinto, M.C.X. 2020. Neurobiology of glycine transporters: From molecules to behavior. *Neuroscience and Biobehavioral Reviews*, 118(April): 97–110.

Martirez, J.M.P., Bao, J.L. & Carter, E.A. 2021. First-Principles Insights into Plasmon-Induced Catalysis. *Annual Review of Physical Chemistry*, 72(1): 99–119. https://doi.org/10.1146/annurev-physchem-061020-053501.

Mayedwa, N., Mongwaketsi, N., Khamlich, S., Kaviyarasu, K., Matinise, N. & Maaza, M. 2018. Green synthesis of nickel oxide, palladium and palladium oxide synthesized via Aspalathus linearis natural extracts: physical properties & mechanism of formation. *Applied Surface Science*, 446: 266–272.

Mazhar, T., Shrivastava, V. & Tomar, R.S. 2017. Green Synthesis of Bimetallic Nanoparticles and its Applications : A Review. *Journal of Pharmaceutical Sciences and Research*, 9(2): 102–110.

Mazibuko-Mbeje, S.E., Dludla, P. V, Johnson, R., Joubert, E., Louw, J., Ziqubu, K., Tiano, L., Silvestri, S., Orlando, P., Opoku, A.R. & Muller, C.J.F. 2019. Aspalathin, a natural product with the potential to reverse hepatic insulin resistance by improving energy metabolism and mitochondrial respiration. *PloS one*, 14(5): e0216172.

Mazibuko, S.E., Joubert, E., Johnson, R., Louw, J., Opoku, A.R. & Muller, C.J.F. 2015. Aspalathin

improves glucose and lipid metabolism in 3T3-L1 adipocytes exposed to palmitate. *Molecular Nutrition & Food Research*, 59(11): 2199–2208. https://doi.org/10.1002/mnfr.201500258.

Mazumdar, P. & Chowdhury, D. 2021. *Manual of Laboratory Testing Methods for Dental Restorative Materials*. Wiley.

McGrath, A.J., Chien, Y.H., Cheong, S., Herman, D.A.J., Watt, J., Henning, A.M., Gloag, L., Yeh, C.S. & Tilley, R.D. 2015. Gold over Branched Palladium Nanostructures for Photothermal Cancer Therapy. *ACS Nano*, 9(12): 12283–12291.

Md Ishak, N.A.I., Kamarudin, S.K. & Timmiati, S.N. 2019. Green synthesis of metal and metal oxide nanoparticles via plant extracts: an overview. *Materials Research Express*, 6(11): 112004. https://dx.doi.org/10.1088/2053-1591/ab4458.

Md Salim, R., Asik, J. & Sarjadi, M.S. 2021. Chemical functional groups of extractives, cellulose and lignin extracted from native Leucaena leucocephala bark. *Wood Science and Technology*, 55(2): 295–313.

Meyer, C. & Naicker, K. 2023. Collective intellectual property of Indigenous peoples and local communities: Exploring power asymmetries in the rooibos geographical indication and industry-wide benefit-sharing agreement. *Research Policy*, 52(9): 104851.

Milaneze, B.A., Oliveira, J.P., Augusto, I., Keijok, W.J., Côrrea, A.S., Ferreira, D.M., Nunes, O.C., Gonçalves, R. de C.R., Kitagawa, R.R., Celante, V.G., da Silva, A.R., Pereira, A.C.H., Endringer, D.C., Schuenck, R.P. & Guimarães, M.C.C. 2016. Facile Synthesis of Monodisperse Gold Nanocrystals Using Virola oleifera. *Nanoscale Research Letters*, 11(1): 465. https://doi.org/10.1186/s11671-016-1683-3.

Minal, S.P. & Prakash, S. 2018. Characterization and Nano-Efficacy Study of Palladium Nanoparticles against Larvae of Anopheles stephensi (Liston). *International Journal of Advanced Engineering and Nano Technology*, 3(10): 1–5.

Minal, S.P. & Prakash, S. 2020. Laboratory analysis of Au–Pd bimetallic nanoparticles synthesized with Citrus limon leaf extract and its efficacy on mosquito larvae and non-target organisms. *Scientific Reports*, 10(1): 1–13. https://doi.org/10.1038/s41598-020-78662-y.

Mirzaei, H. & Darroudi, M. 2017. Zinc oxide nanoparticles: Biological synthesis and biomedical applications. *Ceramics International*, 43(1, Part B): 907–914. https://www.sciencedirect.com/science/article/pii/S0272884216318144.

Mittal, S. & Roy, A. 2021. 11 - Fungus and plant-mediated synthesis of metallic nanoparticles and their

application in degradation of dyes. In M. Shah, S. Dave, & J. B. T.-P. D. of D. Das, eds. Elsevier: 287–308.

Modena, M.M., Rühle, B., Burg, T.P. & Wuttke, S. 2019. Nanoparticle Characterization: What to Measure? *Advanced Materials*, 31(32): 1901556. https://doi.org/10.1002/adma.201901556.

Mohan, C.D., Kim, C., Siveen, K.S., Manu, K.A., Rangappa, S., Chinnathambi, A., Alharbi, S.A., Rangappa, K.S., Kumar, A.P. & Ahn, K.S. 2021. Crocetin imparts antiproliferative activity via inhibiting STAT3 signaling in hepatocellular carcinoma. *IUBMB Life*, 73(11): 1348–1362. https://doi.org/10.1002/iub.2555.

Mohan, C.D., Yang, M.H., Rangappa, S., Chinnathambi, A., Alharbi, S.A., Alahmadi, T.A., Deivasigamani, A., Hui, K.M., Sethi, G., Rangappa, K.S. & Ahn, K.S. 2022. 3-Formylchromone Counteracts STAT3 Signaling Pathway by Elevating SHP-2 Expression in Hepatocellular Carcinoma. *Biology*, 11(1).

Mohanpuria, P. & Rana, Æ.N.K. 2008. Biosynthesis of nanoparticles : technological concepts and future applications. *J Nanopart Res*, 10: 507–517.

Momeni, S. & Nabipour, I. 2015. A Simple Green Synthesis of Palladium Nanoparticles with Sargassum Alga and Their Electrocatalytic Activities Towards Hydrogen Peroxide. *Applied Biochemistry and Biotechnology*, 176(7): 1937–1949. https://doi.org/10.1007/s12010-015-1690-3.

Mondal, S., Manna, S.K., Pathak, S., Masum, A. Al & Mukhopadhyay, S. 2019. A colorimetric and "off-on" fluorescent Pd2+ chemosensor based on a rhodamine-ampyrone conjugate: synthesis, experimental and theoretical studies along with in vitro applications. *New Journal of Chemistry*, 43(8): 3513–3519.

Moosavi, M.A., Haghi, A., Rahmati, M., Taniguchi, H., Mocan, A., Echeverría, J., Gupta, V.K., Tzvetkov, N.T. & Atanasov, A.G. 2018. Phytochemicals as potent modulators of autophagy for cancer therapy. *Cancer Letters*, 424: 46–69. https://doi.org/10.1016/j.canlet.2018.02.030.

Morton, J.F. 1983. Rooibos tea,aspalathus linearis, a caffeineless, low-tannin beverage. *Economic Botany*, 37(2): 164–173. https://doi.org/10.1007/BF02858780.

Mousavi-Khattat, M., Keyhanfar, M. & Razmjou, A. 2018. A comparative study of stability, antioxidant, DNA cleavage and antibacterial activities of green and chemically synthesized silver nanoparticles. *Artificial cells, nanomedicine, and biotechnology*, 46(sup3): S1022–S1031.

Mousavi-Kouhi, S.M., Beyk-Khormizi, A., Amiri, M.S., Mashreghi, M. & Taghavizadeh Yazdi, M.E. 2021. Silver-zinc oxide nanocomposite: From synthesis to antimicrobial and anticancer properties.

Ceramics International, 47(15): 21490–21497.

Mthembu, S.X.H., Muller, C.J.F., Dludla, P. V, Madoroba, E., Kappo, A.P. & Mazibuko-Mbeje, S.E. 2021. Rooibos Flavonoids, Aspalathin, Isoorientin, and Orientin Ameliorate Antimycin A-Induced Mitochondrial Dysfunction by Improving Mitochondrial Bioenergetics in Cultured Skeletal Muscle Cells. *Molecules*, 26(20).

Mukadam, I.Z., Machhi, J., Herskovitz, J., Hasan, M., Oleynikov, M.D., Blomberg, W.R., Svechkarev, D., Mohs, A.M., Zhou, Y., Dash, P., McMillan, J., Gorantla, S., Garrison, J., Gendelman, H.E. & Kevadiya, B.D. 2020. Rilpivirine-associated aggregation-induced emission enables cell-based nanoparticle tracking. *Biomaterials*, 231: 119669.

Mukherjee, T.K., Malik, P. & Mukherjee, S. 2023. *Practical Approach to Mammalian Cell and Organ Culture*.

Muller, C.J.F., Joubert, E., Pheiffer, C., Ghoor, S., Sanderson, M., Chellan, N., Fey, S.J. & Louw, J. 2013. Z-2-(β-d-glucopyranosyloxy)-3-phenylpropenoic acid, an α-hydroxy acid from rooibos (Aspalathus linearis) with hypoglycemic activity. *Molecular Nutrition & Food Research*, 57(12): 2216–2222. https://doi.org/10.1002/mnfr.201300294.

Muller, C.J.F., Malherbe, C.J., Chellan, N., Yagasaki, K., Miura, Y. & Joubert, E. 2018. Potential of rooibos, its major C-glucosyl flavonoids, and Z-2-(β-D-glucopyranosyloxy)-3-phenylpropenoic acid in prevention of metabolic syndrome. *Critical Reviews in Food Science and Nutrition*, 58(2): 227–246. https://doi.org/10.1080/10408398.2016.1157568.

Mutha, R.E., Tatiya, A.U. & Surana, S.J. 2021. Flavonoids as natural phenolic compounds and their role in therapeutics: an overview. *Future Journal of Pharmaceutical Sciences*, 7(1): 25.

Nabavi, S.M., Šamec, D., Tomczyk, M., Milella, L., Russo, D., Habtemariam, S., Suntar, I., Rastrelli, L., Daglia, M., Xiao, J., Giampieri, F., Battino, M., Sobarzo-Sanchez, E., Nabavi, S.F., Yousefi, B., Jeandet, P., Xu, S. & Shirooie, S. 2020. Flavonoid biosynthetic pathways in plants: Versatile targets for metabolic engineering. *Biotechnology Advances*, 38(June 2018): 107316.

Nadagouda, M.N. & Varma, R.S. 2008. Green synthesis of silver and palladium nanoparticles at room temperature using coffee and tea extract. *Green Chemistry*, 10(8): 859–862.

Nagore, P., Ghotekar, S., Mane, K., Ghoti, A., Bilal, M. & Roy, A. 2021. Structural Properties and Antimicrobial Activities of Polyalthia longifolia Leaf Extract-Mediated CuO Nanoparticles. *BioNanoScience*, 11(2): 579–589.

Nakamura, Y., Watanabe, S., Miyake, N., Kohno, H. & Osawa, T. 2003. Dihydrochalcones: evaluation as

novel radical scavenging antioxidants. *Journal of agricultural and food chemistry*, 51(11): 3309–3312.

Nakbanpote, W., Ruttanakorn, M., Sukadeetad, K., Sakkayawong, N. & Damrianant, S. 2019. Effects of drying and extraction methods on phenolic compounds and in vitro assays of Eclipta prostrata Linn leaf extracts. *ScienceAsia*, 45: 127.

Narayanan, K.B. & Sakthivel, N. 2010. Biological synthesis of metal nanoparticles by microbes. *Advances in Colloid and Interface Science*, 156(1): 1–13. https://www.sciencedirect.com/science/article/pii/S0001868610000254.

Nasrollahzadeh, M., Sajjadi, M., Sajadi, S.M. & Issaabadi, Z. 2019. Chapter 5 - Green Nanotechnology. In M. Nasrollahzadeh, S. M. Sajadi, M. Sajjadi, Z. Issaabadi, & M. B. T.-I. S. and T. Atarod, eds. *An Introduction to Green Nanotechnology*. Elsevier: 145–198.

Nazemi, E., Aithal, S., Hassen, W.M., Frost, E.H. & Dubowski, J.J. 2015. GaAs/AlGaAs heterostructure based photonic biosensor for rapid detection of Escherichia coli in phosphate buffered saline solution. *Sensors and Actuators B: Chemical*, 207: 556–562.

Nguyen, V.B., Wang, S.-L., Phan, T.Q., Pham, T.H.T., Huang, H.-T., Liaw, C.-C. & Nguyen, A.D. 2023. Screening and Elucidation of Chemical Structures of Novel Mammalian α-Glucosidase Inhibitors Targeting Anti-Diabetes Drug from Herbals Used by E De Ethnic Tribe in Vietnam. *Pharmaceuticals (Basel, Switzerland)*, 16(5).

Nogueira Silva Lima, M.T., Boulanger, E., Tessier, F.J. & Takahashi, J.A. 2022. Hibiscus, Rooibos, and Yerba Mate for Healthy Aging: A Review on the Attenuation of In Vitro and In Vivo Markers Related to Oxidative Stress, Glycoxidation, and Neurodegeneration. *Foods*, 11(12).

Nolan, P., Auer, S., Spehar, A., Elliott, C.T. & Campbell, K. 2019. Current trends in rapid tests for mycotoxins. *Food Additives and Contaminants - Part A Chemistry, Analysis, Control, Exposure and Risk Assessment*, 36(5): 800–814.

Nord, M., Webster, R.W.H., Paton, K.A., McVitie, S., McGrouther, D., MacLaren, I. & Paterson, G.W. 2020. Fast Pixelated Detectors in Scanning Transmission Electron Microscopy. Part I: Data Acquisition, Live Processing, and Storage. *Microscopy and microanalysis : the official journal of Microscopy Society of America, Microbeam Analysis Society, Microscopical Society of Canada*, 26(4): 653–666.

Nozhat, Z., Khalaji, M.S., Hedayati, M. & Kia, S.K. 2021. Different Methods for Cell Viability and Proliferation Assay: Essential Tools in Pharmaceutical Studies. *Anti-Cancer Agents in Medicinal*

Chemistry, 22(4): 703–712.

Nugroho, A., Heryani, H. & Istikowati, W.T. 2020. Quantitative determination of quercitrin and myricitrin in three different parts of Euphorbia hirta as bioflavonoid source for functional food. *IOP Conference Series: Earth and Environmental Science*, 443(1): 1–6.

Okoroh, D., Ozuomba, J., Aisida, S. & Asogwa, P. 2019. Properties of Zinc Ferrite Nanoparticles Due to PVP Mediation and Annealing at 500°C. *Advances in Nanoparticles*, 08: 36–45.

Olajire, A.A. & Mohammed, A.A. 2019. Green synthesis of palladium nanoparticles using Ananas comosus leaf extract for solid-phase photocatalytic degradation of low density polyethylene film. *Journal of Environmental Chemical Engineering*, 7(4): 103270. https://doi.org/10.1016/j.jece.2019.103270.

Olmos, C.M., Chinchilla, L.E., Villa, A., Delgado, J.J., Hungría, A.B., Blanco, G., Prati, L., Calvino, J.J. & Chen, X. 2019. Size, nanostructure, and composition dependence of bimetallic Au–Pd supported on ceria–zirconia mixed oxide catalysts for selective oxidation of benzyl alcohol. *Journal of Catalysis*, 375: 44–55. https://www.sciencedirect.com/science/article/pii/S002195171930209X.

Omolaja, A.A., Pearce, B., Omoruyi, S.I., Badmus, J.A., Ismail, E., Marnewick, J., Botha, S., Benjeddou, M., Ekpo, O.E. & Hussein, A.A. 2021. The potential of chalcone-capped gold nanoparticles for the management of diabetes mellitus. *Surfaces and Interfaces*, 25: 101251. https://www.sciencedirect.com/science/article/pii/S246802302100328X.

Omoruyi, S.I., Akinfenwa, A.O., Ekpo, O.E. & Hussein, A.A. 2023. Aspalathin and linearthin from Aspalathus linearis (Rooibos) protect SH-SY5Y cells from MPP+-induced neuronal toxicity. *South African Journal of Botany*, 157: 53–63.

Orlando, P., Chellan, N., Louw, J., Tiano, L., Cirilli, I., Dludla, P., Joubert, E. & Muller, C.J.F. 2019. Diet-Induced Diabetic Vervet Monkeys. *Molecules*, 24(1713): 1–19.

Ortega, E., Nicholls, D., Browning, N.D. & Jonge, N. De. 2021. High temporal - resolution scanning transmission electron microscopy using sparse - serpentine scan pathways. *Scientific Reports*: 1–9.

Ovais, M., Khalil, A.T., Islam, N.U., Ahmad, I., Ayaz, M., Saravanan, M., Shinwari, Z.K. & Mukherjee, S. 2018. Role of plant phytochemicals and microbial enzymes in biosynthesis of metallic nanoparticles. *Applied Microbiology and Biotechnology*, 102(16): 6799–6814.

Pal, K., Chakroborty, S. & Nath, N. 2022. Limitations of nanomaterials insights in green chemistry sustainable route : Review on novel applications. *De Gruyter*: 951–964.

Pal, Y., Mali, S.N., Kale, S.B. & Pratap, A.P. 2022. Improved adsorptive purification and effective separation of acidic and lactonic sophorolipid biosurfactant. *Journal of the Indian Chemical Society*, 99(11): 100776.

Pandey, R.P., Vidic, J., Mukherjee, R. & Chang, C.M. 2023. Experimental Methods for the Biological Evaluation of Nanoparticle-Based Drug Delivery Risks. *Pharmaceutics*, 15(2): 1–17.

Pandit, C., Roy, A., Ghotekar, S., Khusro, A., Islam, M.N., Emran, T. Bin, Lam, S.E., Khandaker, M.U. & Bradley, D.A. 2022. Biological agents for synthesis of nanoparticles and their applications. *Journal of King Saud University - Science*, 34(3): 101869.

Patra, J.K., Das, G., Fraceto, L.F., Campos, E.V.R., Rodriguez-Torres, M.D.P., Acosta-Torres, L.S., Diaz-Torres, L.A., Grillo, R., Swamy, M.K., Sharma, S., Habtemariam, S. & Shin, H.S. 2018. Nano based drug delivery systems: Recent developments and future prospects. *Journal of Nanobiotechnology*, 16(1): 1–33.

Patra, S., Mukherjee, S., Barui, A.K., Ganguly, A., Sreedhar, B. & Patra, C.R. 2015. Green synthesis, characterization of gold and silver nanoparticles and their potential application for cancer therapeutics. *Materials Science and Engineering: C*, 53: 298–309.

Patri, A.K., Dobrovolskaia, M.A., Stern, S.T. & McNeil, S.E. 2019. Preclinical Characterization of Engineered Nanoparticles Intended for Cancer Therapeutics. In *Nanotechnology for Cancer Therapy*. 105–137.

Patri, A.K., Kukowska-Latallo, J.F. & Baker, J.R. 2005. Targeted drug delivery with dendrimers: Comparison of the release kinetics of covalently conjugated drug and non-covalent drug inclusion complex. *Advanced Drug Delivery Reviews*, 57(15): 2203–2214.

Pattasseril, M.B., Abraham, S., M., F.N., M, A.N., Kto, F. & K., S. 2022. EXTRACTION, ISOLATION AND CHARACTERIZATION OF BIOACTIVE CONSTITUENTS OF MYRISTICA FRAGRANCE HOUTT. *European Journal of Biomedical and Pharmaceutical Scienecs*, 9(7): 380–389.

Payne, J.N., Badwaik, V.D., Waghwani, H.K., Moolani, H. V., Tockstein, S., Thompson, D.H. & Dakshinamurthy, R. 2018. Development of dihydrochalcone-functionalized gold nanoparticles for augmented antineoplastic activity. *International Journal of Nanomedicine*, 13: 1917–1926.

Pedroso-Santana, S. & Fleitas-Salasar, N. 2020. Ionotropic gelation method in the synthesis of nanoparticles / microparticles for biomedical purposes. *Society of Chemical Industry*, 69: 443–447.

Peng, J., Lü, J., Hu, X., Liu, J. & Jiang, G. 2007. Determination of atrazine, desethyl atrazine and

desisopropyl atrazine in environmental water samples using hollow fiber-protected liquid-phase microextraction and high performance liquid chromatography. *Microchimica Acta*, 158(1): 181–186. https://doi.org/10.1007/s00604-006-0692-9.

Perez-campos, R. & Esparza, R. 2017. Study of PtPd Bimetallic Nanoparticles for Fuel Cell Applications. *Materials Research*, (September): 1–9.

Perez de Souza, L., Alseekh, S., Scossa, F. & Fernie, A.R. 2021. Ultra-high-performance liquid chromatography high-resolution mass spectrometry variants for metabolomics research. *Nature Methods*, 18(7): 733–746.

Peters, J.J.P., Mullarkey, T., Hedley, E., Müller, K.H., Porter, A., Mostaed, A. & Jones, L. 2023. Electron counting detectors in scanning transmission electron microscopy via hardware signal processing. *Nature Communications*, 14(1).

Petla, R.K., Vivekanandhan, S. & Misra, M. 2012. Soybean (Glycine max) Leaf Extract Based Green Synthesis of Palladium Nanoparticles. , 2012(January): 14–19.

Pinzaru, I., Coricovac, D., Dehelean, C., Moacă, E.-A., Mioc, M., Baderca, F., Sizemore, I., Brittle, S., Marti, D., Calina, C.D., Tsatsakis, A.M. & Şoica, C. 2018. Stable PEG-coated silver nanoparticles - A comprehensive toxicological profile. *Food and chemical toxicology : an international journal published for the British Industrial Biological Research Association*, 111: 546–556.

Pochapski, D., Santos, C., Wosiak Leite, G., Pulcinelli, S. & Santilli, C. 2021. Zeta Potential and Colloidal Stability Predictions for Inorganic Nanoparticle Dispersions: Effects of Experimental Conditions and Electrokinetic Models on the Interpretation of Results. *Langmuir*, 37.

Pomerantseva, E., Bonaccorso, F., Feng, X., Cui, Y. & Gogotsi, Y. 2019. Energy storage: The future enabled by nanomaterials. *Science (New York, N.Y.)*, 366(6468).

Poole, C.F. 2018. Chromatographic test methods for characterizing alkylsiloxane-bonded silica columns for reversed-phase liquid chromatography. *Journal of Chromatography B*, 1092: 207–219.

Poole, C.F. 2019. Influence of Solvent Effects on Retention of Small Molecules in Reversed-Phase Liquid Chromatography. *Chromatographia*, 82(1): 49–64. http://dx.doi.org/10.1007/s10337-018-3531-3.

Pourhakkak, P., Taghizadeh, M., Taghizadeh, A. & Ghaedi, M. 2021. Chapter 2 - Adsorbent. In M. B. T.-I. S. and T. Ghaedi, ed. *Adsorption: Fundamental Processes and Applications*. Elsevier: 71–210.

Prabha, S., Lahtinen, M. & Sillanpää, M. 2010. Tansy fruit mediated greener synthesis of silver and gold nanoparticles. *Process Biochemistry*, 45: 1065–1071.

Präbst, K., Engelhardt, H., Ringgeler, S. & Hübner, H. 2017. Basic Colorimetric Proliferation Assays: MTT, WST, and Resazurin BT - Cell Viability Assays: Methods and Protocols. In D. F. Gilbert & O. Friedrich, eds. New York, NY: Springer New York: 1–17.

Preuss, H.G. 2020. Sodium, chloride, and potassium. In B. P. Marriott, D. F. Birt, V. A. Stallings, & A. A. B. T.-P. K. in N. (Eleventh E. Yates, eds. Academic Press: 467–484.

Pu, S., Li, J., Sun, L., Zhong, L. & Ma, Q. 2019. An in vitro comparison of the antioxidant activities of chitosan and green synthesized gold nanoparticles. *Carbohydrate Polymers*, 211: 161–172. https://www.sciencedirect.com/science/article/pii/S0144861719301353.

Du Puch, C.B.M., Vanderstraete, M., Giraud, S., Lautrette, C., Christou, N. & Mathonnet, M. 2021. Benefits of functional assays in personalized cancer medicine: More than just a proof-of-concept. *Theranostics*, 11(19): 9538–9556.

Rabiee, N., Bagherzadeh, M., Kiani, M. & Ghadiri, A.M. 2020. Rosmarinus officinalis directed palladium nanoparticle synthesis: Investigation of potential anti-bacterial, anti-fungal and Mizoroki-Heck catalytic activities. *Advanced Powder Technology*, 31(4): 1402–1411. https://doi.org/10.1016/j.apt.2020.01.024.

Rabiei, M., Palevicius, A., Monshi, A., Nasiri, S., Vilkauskas, A. & Janusas, G. 2020. Comparing Methods for Calculating Nano Crystal Size of Natural Hydroxyapatite Using X-Ray Diffraction. *Nanomaterials*, 10(9).

Rahdar, A., Amini, N., Askari, F., Bin, M.A. & Susan, H. 2019. Dynamic light scattering: A useful technique to characterize nanoparticles. *J. Nanoanalysis*, 6(2): 80–89. http://creativecommons.org/licenses/by/4.0/.

Rai, S., Bhujel, R., Biswas, J. & Swain, B.P. 2020. A green approach for synthesis of graphene. *AIP Conference Proceedings*, 2273(1): 50032.

Rajawat, J. & Jhingan, G. 2019. Chapter 1 - Mass spectroscopy. In G. B. T.-D. P. H. for C. B. D. S. Misra, ed. Academic Press: 1–20.

Rajitha, B., Malla, R.R., Vadde, R., Kasa, P., Prasad, G.L.V., Farran, B., Kumari, S., Pavitra, E., Kamal, M.A., Raju, G.S.R., Peela, S. & Nagaraju, G.P. 2021. Horizons of nanotechnology applications in female specific cancers. *Seminars in cancer biology*, 69: 376–390.

Ramalingam, V. 2019. Multifunctionality of gold nanoparticles: Plausible and convincing properties. *Advances in Colloid and Interface Science*, 271: 101989.

Rana, A., Yadav, K. & Jagadevan, S. 2020. A comprehensive review on green synthesis of nature-inspired metal nanoparticles: Mechanism, application and toxicity. *Journal of Cleaner Production*, 272: 122880.

Rane, A.V., Kanny, K., Abitha, V.K. & Thomas, S. 2018. Methods for Synthesis of Nanoparticles and Fabrication of Nanocomposites. In S. Mohan Bhagyaraj, O. S. Oluwafemi, N. Kalarikkal, & S. B. T.-S. of I. N. Thomas, eds. *Micro and Nano Technologies*. Woodhead Publishing: 121–139. https://www.sciencedirect.com/science/article/pii/B9780081019757000051.

Rapachi, D., Peixoto, C.R.D.M., Pavan, F.A. & Gelesky, M.A. 2023. Metallic Nanoparticles Biosynthesized by Phenolic - Rich Extracts : Interaction , Characterization and Application. *Journal of Cluster Science*, 34(6): 2743–2757.

Rautaray, D., Ahmad, A. & Sastry, M. 2003. Biosynthesis of CaCO3 Crystals of Complex Morphology Using a Fungus and an Actinomycete. *Journal of the American Chemical Society*, 125(48): 14656–14657. https://doi.org/10.1021/ja0374877.

Raval, N., Maheshwari, R., Kalyane, D., Youngren-Ortiz, S.R., Chougule, M.B. & Tekade, R.K. 2019. Importance of Physicochemical Characterization of Nanoparticles in Pharmaceutical Product Development. In R. K. B. T.-B. F. of D. D. Tekade, ed. *Advances in Pharmaceutical Product Development and Research*. Academic Press: 369–400.

Ravikumar, H., Chua, B.L., Mah, S.H. & Chow, Y.H. 2022. An Insight into Extraction, Isolation, Identification and Quantification of Bioactive Compounds from Crataegus Monogyna Plant Extract Haripriya. , 10: 327–2022.

Rawat, M. 2016. a Review on Green Synthesis and Characterization of Silver Nanoparticles and Their Applications: a Green Nanoworld. *World Journal of Pharmacy and Pharmaceutical Sciences*, (July): 730–762.

Regmi, R., Gumber, V., Subba Rao, V., Kohli, I., Black, C., Sudakar, C., Vaishnava, P., Naik, V., Naik, R., Mukhopadhyay, A. & Lawes, G. 2011. Discrepancy between different estimates of the hydrodynamic diameter of polymer-coated iron oxide nanoparticles in solution. *Journal of Nanoparticle Research*, 13(12): 6869–6875.

Rehana, D., Mahendiran, D., Kumar, R.S. & Rahiman, A.K. 2017. ScienceDirect Evaluation of antioxidant and anticancer activity of copper oxide nanoparticles synthesized using medicinally important plant extracts. *Biomedicine & Pharmacotherapy*, 89: 1067–1077.

Remita, S., Mostafavi, M. & Delcourt, M.O. 1996. Bimetallic Ag-Pt and Au-Pt aggregates synthesized by

radiolysis. *Radiation Physics and Chemistry*, 47(2): 275–279. http://www.sciencedirect.com/science/article/pii/0969806X9400172G.

Richards, S.A. & Hollerton, J.C. 2023. *Essential practical NMR for organic chemistry*. John Wiley & Sons.

Riss, T.L., Moravec, R.A., Niles, A.L., Duellman, S., Benink, H.A., Worzella, T.J. & Minor, L. 2004. Cell Viability Assays. *Assay Guidance Manual*: 1–31.

Rodríguez-Alonso, E., Vergeldt, F.J. & van der Goot, A.J. 2019. TD-NMR to understand water-binding food properties. *Magnetic Resonance in Chemistry*, 57(9): 603–606.

Rodríguez-Zamora, P., Salazar-Angeles, B., Buendía, F., Cordero-Silis, C., Fabila, J., Bazán-Díaz, L., Fernández-Díaz, L.M., Paz-Borbón, L.O., Díaz, G. & Garzón, I.L. 2020. Revisiting the conformational adsorption of L- and D-cysteine on Au nanoparticles by Raman spectroscopy. *Journal of Raman Spectroscopy*, 51(2): 243–255.

Rouessac, F., Rouessac, A. & Towey, J. 2022. *Chemical Analysis: Modern Instrumentation Methods and Techniques*. Wiley.

Roy, N., Mondal, S., Laskar, R.A., Basu, S., Mandal, D. & Begum, N.A. 2010. Biogenic synthesis of Au and Ag nanoparticles by Indian propolis and its constituents. *Colloids and Surfaces B: Biointerfaces*, 76(1): 317–325. http://www.sciencedirect.com/science/article/pii/S0927776509005736.

Saeed, B.A., Lim, V., Yusof, N.A., Khor, K.Z., Rahman, H.S. & Samad, N.A. 2019. Antiangiogenic properties of nanoparticles: A systematic review. *International Journal of Nanomedicine*, 14: 5135–5146.

Saha, R., Arunprasath, D. & Sekar, G. 2019. Surface enriched palladium on palladium-copper bimetallic nanoparticles as catalyst for polycyclic triazoles synthesis. *Journal of Catalysis*, 377: 673–683.

Sahiner, N., Sagbas, S. & Aktas, N. 2016. Preparation and characterization of monodisperse, mesoporous natural poly(tannic acid)–silica nanoparticle composites with antioxidant properties. *Microporous and Mesoporous Materials*, 226: 316–324.

Sahoo, M., Mansingh, S., Subudhi, S., Mohapatra, P. & Parida, K. 2019. Catalysis Science & Technology A plasmonic AuPd bimetallic nanoalloy decorated over a GO / LDH hybrid nanocomposite via a green reactions : a paradigm shift towards a sustainable. : 4678–4692.

Sajid, M. & Akash, H. 2022. *Essentials of Pharmaceutical Analysis*. Springer Nature Singapore.

Sajjad, S., Leghari, S.A.K., Ryma, N.U.A. & Farooqi, S.A. 2018. Green synthesis of metal-based

nanoparticles and their applications. In *The Macabresque: Human Violation and Hate in Genocide, Mass Atrocity and Enemy-Making*. 23–77.

Sakthivel, N.A., Shabaninezhad, M., Sementa, L., Yoon, B., Stener, M., Whetten, R.L., Ramakrishna, G., Fortunelli, A., Landman, U. & Dass, A. 2020. The Missing Link: Au191(SPh-tBu)66 Janus Nanoparticle with Molecular and Bulk-Metal-like Properties. *Journal of the American Chemical Society*, 142(37): 15799–15814.

Saleem, F., Zhang, Z., Cui, X., Gong, Y., Chen, B., Lai, Z., Yun, Q., Gu, L. & Zhang, H. 2019. Elemental Segregation in Multimetallic Core–Shell Nanoplates. *Journal of the American Chemical Society*, 141(37): 14496–14500.

Saleh, H. & Koller, M. 2018. Introductory Chapter: Principles of Green Chemistry.

Salem, M.A., Souza, L.P. De, Serag, A., Fernie, A.R., Farag, M.A., Ezzat, S.M. & Alseekh, S. 2020. Metabolomics in the Context of Plant Natural Products Research : From Sample Preparation to Metabolite Analysis. : 1–30.

Samari-kermani, M., Jafari, S., Rahnama, M. & Raoof, A. 2021. Ionic strength and zeta potential effects on colloid transport and retention processes. *Colloid and Interface Science Communications*, 42(February): 100389.

Samodien, S., Kock, M. de, Joubert, E., Swanevelder, S. & Gelderblom, W.C.A. 2021. Differential Cytotoxicity of Rooibos and Green Tea Extracts against Primary Rat Hepatocytes and Human Liver and Colon Cancer Cells – Causal Role of Major Flavonoids. *Nutrition and Cancer*, 73(10): 2050–2064.

Sanfilippo, C., Paterna, A., Biondi, D.M. & Patti, A. 2019. Lyophilized extracts from vegetable flours as valuable alternatives to purified oxygenases for the synthesis of oxylipins. *Bioorganic chemistry*, 93: 103325.

Santhiya-Nair, K., Shanmugapriya, Logeiswariy, P., Sreeramanan, S., Shakila, R., Chen, Y., Leong, Y.-H., Karupiah, S. & Sasidharan, S. 2022. Chapter 3 - Purification of herbal biomolecules. In S. C. Mandal, A. K. Nayak, & A. K. B. T.-H. B. in H. A. Dhara, eds. Academic Press: 47–62.

Santoshi kumari, A., Venkatesham, M., Ayodhya, D. & Veerabhadram, G. 2015. Green synthesis, characterization and catalytic activity of palladium nanoparticles by xanthan gum. *Applied Nanoscience (Switzerland)*, 5(3): 315–320.

Sardar, R., Funston, A.M., Mulvaney, P. & Murray, R.W. 2009. Gold nanoparticles: past, present, and future. *Langmuir : the ACS journal of surfaces and colloids*, 25(24): 13840–13851.

Sarfraz, N. & Khan, I. 2021. Plasmonic Gold Nanoparticles (AuNPs): Properties, Synthesis and their Advanced Energy, Environmental and Biomedical Applications. *Chemistry – An Asian Journal*, 16(7): 720–742.

Sargazi, S., Laraib, U., Er, S., Rahdar, A., Hassanisaadi, M., Zafar, M.N., Díez-Pascual, A.M. & Bilal, M. 2022. Application of Green Gold Nanoparticles in Cancer Therapy and Diagnosis. *Nanomaterials*, 12(7).

Sasidharan, S., Chen, Y., Dharmaraj, S. & Karupiah, S. 2011. Extraction , Isolation And Characterization Of Bioactive Compounds From Plants ? Extracts. *Afr J Tradit Complement Altern Med*, 8(1): 1–11.

Sathishkumar, M., Sneha, K., Won, S.W., Cho, C.-W., Kim, S. & Yun, Y.-S. 2009. Cinnamon zeylanicum bark extract and powder mediated green synthesis of nano-crystalline silver particles and its bactericidal activity. *Colloids and surfaces. B, Biointerfaces*, 73(2): 332—338. https://doi.org/10.1016/j.colsurfb.2009.06.005.

Scarano, G. & Morelli, E. 2002. Characterization of cadmium- and lead- phytochelatin complexes formed in a marine microalga in response to metal exposure. *Biometals*, 15(2): 145–151. https://doi.org/10.1023/A:1015288000218.

Schalkwyk, M.S. Van, Windvogel, S. & Strijdom, H. 2020. Rooibos (Aspalathus linearis) protects against nicotine-induced vascular injury and oxidative stress in Wistar rats. *Cardiovascular Journal of Africa*, 31(2): 81–90.

Schilrreff, P. & Alexiev, U. 2022. Chronic Inflammation in Non-Healing Skin Wounds and Promising Natural Bioactive Compounds Treatment. *International Journal of Molecular Sciences*, 23(9).

Sekowski, S., Tomaszewska, E., Ranoszek-Soliwoda, K., Celichowski, G. & Grobelny, J. 2017. Interactions of hybrid gold–tannic acid nanoparticles with human serum albumin. *European Biophysics Journal*, 46: 49–57.

Selvamani, V. 2019. Chapter 15 - Stability Studies on Nanomaterials Used in Drugs. In S. S. Mohapatra, S. Ranjan, N. Dasgupta, R. K. Mishra, & S. B. T.-C. and B. of N. for D. D. Thomas, eds. *Micro and Nano Technologies*. Elsevier: 425–444.

Sengul, A.B. & Asmatulu, E. 2020. Toxicity of metal and metal oxide nanoparticles: a review. *Environmental Chemistry Letters*, 18(5): 1659–1683. https://doi.org/10.1007/s10311-020-01033-6.

Setiawati, A., Candrasari, D., Setyajati, F.E., Prasetyo, V., Setyaningsih, D. & Hartini, Y. 2022. Anticancer drug screening of natural products: In vitro cytotoxicity assays, techniques, and challenges . *Asian Pacific Journal of Tropical Biomedicine*, 12(7): 279.

Shabalala, S.C., Dludla, P. V, Muller, C.J.F., Nxele, X., Kappo, A.P., Louw, J. & Johnson, R. 2019. Aspalathin ameliorates doxorubicin-induced oxidative stress in H9c2 cardiomyoblasts. *Toxicology in Vitro*, 55: 134–139.

Shahjahan, T., Javed, B., Sharma, V. & Tian, F. 2023. pH and NaCl Optimisation to Improve the Stability of Gold and Silver Nanoparticles ' Anti-Zearalenone Antibody Conjugates for Immunochromatographic Assay. *Methods and Protocols*: 1–16.

Shaikh, S.C., Saboo, S.G., Tandale, P.S., Memon, F.S., Tayade, S.D., Haque, M.A. & Khan, S.L. 2021. Pharmaceutical and biopharmaceutical aspects of quantum dots-an overview. *International Journal of Applied Pharmaceutics*, 13(5): 44–53.

Shang, L., Nienhaus, K. & Nienhaus, G.U. 2014. Engineered nanoparticles interacting with cells: size matters. *Journal of nanobiotechnology*, 12: 5.

Shankar, S.S., Rai, A., Ahmad, A. & Sastry, M. 2004. Rapid synthesis of Au, Ag, and bimetallic Au core–Ag shell nanoparticles using Neem (Azadirachta indica) leaf broth. *Journal of Colloid and Interface Science*, 275(2): 496–502. http://www.sciencedirect.com/science/article/pii/S0021979704002607.

Sharma, G., Kumar, A., Naushad, M., Pathania, D. & Sillanpää, M. 2016. Polyacrylamide@Zr(IV) vanadophosphate nanocomposite: Ion exchange properties, antibacterial activity, and photocatalytic behavior. *Journal of Industrial and Engineering Chemistry*, 33: 201–208. http://www.sciencedirect.com/science/article/pii/S1226086X15004566.

Sharma, G., Kumar, A., Sharma, S., Naushad, M., Prakash, R., Alothman, Z.A. & Tessema, G. 2019. Novel development of nanoparticles to bimetallic nanoparticles and their composites : A review. *Journal of King Saud University - Science*, 31(2): 257–269. https://doi.org/10.1016/j.jksus.2017.06.012.

Sharma, G., Kumar, D., Kumar, A., Al-Muhtaseb, A.H., Pathania, D., Naushad, M. & Mola, G.T. 2017. Revolution from monometallic to trimetallic nanoparticle composites, various synthesis methods and their applications: A review. *Materials Science and Engineering: C*, 71: 1216–1230. http://www.sciencedirect.com/science/article/pii/S0928493116320173.

Sharma, J.R., Remaliah, N., Sibuyi, S., Fadaka, A.O., Meyer, S., Madiehe, A.M., Katti, K. & Meyer, M. 2023. applied sciences Anticancer and Drug-Sensitizing Activities of Gold Nanoparticles Synthesized from Cyclopia genistoides (Honeybush) Extracts. *Applied Sciences*: 1 to 16.

Sharma, N.K., Vishwakarma, J., Rai, S., Alomar, T.S., Almasoud, N. & Bhattarai, A. 2022. Green Route Synthesis and Characterization Techniques of Silver Nanoparticles and Their Biological Adeptness.

ACS Omega, 7(31): 27004–27020.

Shen, M.R., He, Y. & Shi, S.M. 2021. Development of chromatographic technologies for the quality control of Traditional Chinese Medicine in the Chinese Pharmacopoeia. *Journal of Pharmaceutical Analysis*, 11(2): 155–162.

Shimamura, N., Miyase, T., Umehara, K., Warashina, T. & Fujii, S. 2006. Phytoestrogens from *Aspalathus linearis*. *Biological and Pharmaceutical Bulletin*, 29(6): 1271–1274.

Shinde, V.T., Garad, R., Jain, S., Manoj, K. & Badal, B. 2023. Column chromatography. *Journal of Chromatography Library*, 11: 2320–2882.

Shu, J., Yuan, J., Xie, S., Yue, R., Zhang, R. & Xu, J. 2022. Robust poly(3,4-ethylenedioxythiophene) granules loaded Cu/Ni-doped Pd catalysts for high-efficiency electrooxidation of ethylene glycol. *Journal of Colloid and Interface Science*, 628: 745–757.

Shulyak, N., Piponski, M., Kovalenko, S., Stoimenova, T.B., Drapak, I., Piponska, M., Rezk, M.R., Abbeyquaye, A.D., Oleshchuk, O. & Logoyda, L. 2021. Chaotropic salts impact in HPLC approaches for simultaneous analysis of hydrophilic and lipophilic drugs. *Journal of separation science*, 44(15): 2908–2916.

Sigma-Aldrich Co. LLC. 2016. *Fundamental techniques in cell culture 3*. 3rd ed.

Silva, I.F., Roy, S., Kumar, P., Chen, Z.W., Teixeira, I.F., Campos-Mata, A., Antônio, L.M., Ladeira, L.O., Stumpf, H.O., Singh, C.V., Teixeira, A.P.C., Kibria, M.G. & Ajayan, P.M. 2023. Nanoengineered Au–carbon nitride interfaces enhance photocatalytic pure water splitting to hydrogen. *Journal of Materials Chemistry A*, 11(43): 23330–23341.

Simmonds, M.S.J. 2001. Importance of flavonoids in insect–plant interactions: feeding and oviposition. *Phytochemistry*, 56(3): 245–252. https://www.sciencedirect.com/science/article/pii/S0031942200004532.

Singh, A., Gautam, P.K., Verma, A., Singh, V., Shivapriya, P.M., Shivalkar, S., Sahoo, A.K. & Samanta, S.K. 2020. Green synthesis of metallic nanoparticles as effective alternatives to treat antibiotics resistant bacterial infections: A review. *Biotechnology reports (Amsterdam, Netherlands)*, 25: e00427.

Singh, R. & Bhateria, R. 2021. Core–shell nanostructures: a simplest two-component system with enhanced properties and multiple applications. *Environmental Geochemistry and Health*, 43(7): 2459–2482.

Singh, R., Nawale, L., Arkile, M., Wadhwani, S., Shedbalkar, U., Chopade, S., Sarkar, D. & Chopade, B.A. 2016. Phytogenic silver, gold, and bimetallic nanoparticles as novel antitubercular agents. *International journal of nanomedicine*, 11: 1889–1897.

Singletary, M., Hagerty, S., Muramoto, S., Daniels, Y., MacCrehan, W.A., Stan, G., Lau, J.W., Pustovyy, O., Globa, L., Morrison, E.E., Sorokulova, I. & Vodyanoy, V. 2017. PEGylation of zinc nanoparticles amplifies their ability to enhance olfactory responses to odorant. *PLOS ONE*, 12(12): e0189273.

Sivamaruthi, B.S., Ramkumar, V.S., Archunan, G., Chaiyasut, C. & Suganthy, N. 2019. Biogenic synthesis of silver palladium bimetallic nanoparticles from fruit extract of Terminalia chebula – In vitro evaluation of anticancer and antimicrobial activity. *Journal of Drug Delivery Science and Technology*, 51: 139–151. https://www.sciencedirect.com/science/article/pii/S1773224719301790.

Skoog, D.A., Holler, F.J. & Crouch, S.R. 2019. *Principles of Instrumental Analysis*. Cengage Learning; 6 edition.

Slater, T.J.A., Janssen, A., Camargo, P.H.C., Burke, M.G., Zaluzec, N.J. & Haigh, S.J. 2016. STEM-EDX tomography of bimetallic nanoparticles: A methodological investigation. *Ultramicroscopy*, 162: 61–73.

Sohrabi, F., Saeidifard, S., Ghasemi, M., Asadishad, T., Hamidi, S.M. & Hosseini, S.M. 2021. *Role of plasmonics in detection of deadliest viruses: a review*. Springer Berlin Heidelberg.

Soltys, L., Olkhovyy, O., Tatarchuk, T. & Naushad, M. 2021. Green Synthesis of Metal and Metal Oxide Nanoparticles: Principles of Green Chemistry and Raw Materials. *Magnetochemistry* , 7(11).

Son, M.J., Minakawa, M., Kazumi, Y. & Miura, Y. 2013. Aspalathin improves hyperglycemia and glucose intolerance in obese diabetic ob/ob mice. *European Journal of Nutrition*, 52(6): 1607–1619. https://www.deepdyve.com/lp/springer-journals/aspalathin-improves-hyperglycemia-and-glucose-intolerance-in-obese-QnlloAI0XB.

Son, Y.-O., Kim, J., Lim, J.-C., Chung, Y., Chung, G.-H. & Lee, J.-C. 2003. Ripe fruits of Solanum nigrum L. inhibits cell growth and induces apoptosis in MCF-7 cells. *Food and Chemical Toxicology*, 41(10): 1421–1428.

Sonbol, H., Ameen, F., AlYahya, S., Almansob, A. & Alwakeel, S. 2021. Padina boryana mediated green synthesis of crystalline palladium nanoparticles as potential nanodrug against multidrug resistant bacteria and cancer cells. *Scientific reports*, 11(1): 5444.

Song, H.M., Anjum, D.H., Sougrat, R., Hedhili, M.N. & Khashab, N.M. 2012. Hollow Au@Pd and Au@Pt core–shell nanoparticles as electrocatalysts for ethanol oxidation reactions. *Journal of*

Materials Chemistry, 22(48): 25003–25010.

Song, J.Y. & Kim, B.S. 2008. Rapid biological synthesis of silver nanoparticles using plant leaf extracts. *Bioprocess and Biosystems Engineering*, 32(1): 79. https://doi.org/10.1007/s00449-008-0224-6.

Song, J.Y., Kwon, E.-Y. & Kim, B.S. 2009. Biological synthesis of platinum nanoparticles using Diopyros kaki leaf extract. *Bioprocess and Biosystems Engineering*, 33(1): 159. https://doi.org/10.1007/s00449-009-0373-2.

Sorensen, M.J., Anderson, B.G. & Kennedy, R.T. 2020. Liquid chromatography above 20,000 PSI. *TrAC Trends in Analytical Chemistry*, 124: 115810. https://www.sciencedirect.com/science/article/pii/S0165993619306235.

Sosa, I.O., Noguez, C. & Barrera, R.G. 2003. Optical Properties of Metal Nanoparticles with Arbitrary Shapes. *The Journal of Physical Chemistry B*, 107(26): 6269–6275. https://doi.org/10.1021/jp0274076.

South African Rooibos Council. 2022. *Rooibos Industry Information Sheet*.

Souza, C.D. De, Nogueira, B.R. & Rostelato, M.E.C.M. 2019. Review of the methodologies used in the synthesis gold nanoparticles by chemical reduction. *Journal of Alloys and Compounds*, 798: 714–740.

Sozer, N. & Kokini, J.L. 2009. Nanotechnology and its applications in the food sector. *Trends in Biotechnology*, 27(2): 82–89.

Spangenberg, B., Poole, C.F. & Weins, C. 2011. *Quantitative thin-layer chromatography: A practical survey*.

Srinoi, P., Chen, Y.-T., Vittur, V., Marquez, M. & Lee, T. 2018. Bimetallic Nanoparticles: Enhanced Magnetic and Optical Properties for Emerging Biological Applications. *Applied Sciences*, 8(7): 1106. http://www.mdpi.com/2076-3417/8/7/1106 30 June 2020.

Stahl, E. 1970. *Thin-Layer Chromatography*. 2nd Editio. Berlin: John Wiley & Sons, Ltd. https://doi.org/10.1002/star.19700221110.

Stanciu, S.G., Tranca, D.E., Zampini, G., Hristu, R., Stanciu, G.A., Chen, X., Liu, M., Stenmark, H.A. & Latterini, L. 2022. Scattering-type Scanning Near-Field Optical Microscopy of Polymer-Coated Gold Nanoparticles. *ACS Omega*, 7: 11353–11362. https://api.semanticscholar.org/CorpusID:247691027.

Stander, M.A., Van Wyk, B.-E., Taylor, M.J.C. & Long, H.S. 2017. Analysis of Phenolic Compounds in Rooibos Tea (Aspalathus linearis) with a Comparison of Flavonoid-Based Compounds in Natural

Populations of Plants from Different Regions. *Journal of Agricultural and Food Chemistry*, 65(47): 10270–10281. https://doi.org/10.1021/acs.jafc.7b03942.

Steckiewicz, K.P., Barcinska, E., Malankowska, A., Zauszkiewicz–Pawlak, A., Nowaczyk, G., Zaleska-Medynska, A. & Inkielewicz-Stepniak, I. 2019. Impact of gold nanoparticles shape on their cytotoxicity against human osteoblast and osteosarcoma in in vitro model. Evaluation of the safety of use and anti-cancer potential. *Journal of Materials Science: Materials in Medicine*, 30(2): 22. https://doi.org/10.1007/s10856-019-6221-2.

Stefaniak, K. & Masek, A. 2021. Green Copolymers Based on Poly(Lactic Acid)—Short Review. *Materials*, 14(18).

Stéphane, F., Jules, B., Batiha, G., Ali, I. & Bruno, L. 2021. Extraction of Bioactive Compounds from Medicinal Plants and Herbs. In *Natural Medicinal Plants*. 1–40.

Stipanuk, M.H., Dominy Jr., J.E., Lee, J.-I. & Coloso, R.M. 2006. Mammalian Cysteine Metabolism: New Insights into Regulation of Cysteine Metabolism. *The Journal of Nutrition*, 136(6): 1652S-1659S.

Su, J.F., Kuan, W.-F., Liu, H. & Huang, C.P. 2019. Mode of electrochemical deposition on the structure and morphology of bimetallic electrodes and its effect on nitrate reduction toward nitrogen selectivity. *Applied Catalysis B: Environmental*, 257: 117909. https://www.sciencedirect.com/science/article/pii/S0926337319306551.

Su, S. & Kang, P.M. 2020. Systemic review of biodegradable nanomaterials in nanomedicine. *Nanomaterials*, 10(4): 1–20.

Sujitha, M. V & Kannan, S. 2013. Green synthesis of gold nanoparticles using Citrus fruits (Citrus limon, Citrus reticulata and Citrus sinensis) aqueous extract and its characterization. *Spectrochimica Acta Part A: Molecular and Biomolecular Spectroscopy*, 102: 15–23.

Sultana, S., Alzahrani, N., Alzahrani, R., Alshamrani, W., Aloufi, W., Ali, A., Najib, S. & Siddiqui, N.A. 2020. Stability issues and approaches to stabilised nanoparticles based drug delivery system. *Journal of Drug Targeting*, 28(5): 468–486.

Sundarapandi, M., Shanmugam, S. & Ramaraj, R. 2019. Synthesis and Catalytic Activities of Metal Shells (Monolayer, Bilayer, and Alloy Layer)-Coated Gold Octahedra toward Catalytic Reduction of Nitroaromatics. *The Journal of Physical Chemistry C*, 123(34): 21066–21075.

Sunkar, S., Ranimol, G., Nellore, J., Nachiyar, C.V., Namasivayam, S.K.R. & Renugadevi, K. 2022. Extraction and Purification of Bioactive Ingredients from Natural Products. In *Handbook of*

Nutraceuticals and Natural Products. 221–257. https://doi.org/10.1002/9781119746843.ch23.

Syed, R.A. 2023. VCU Scholars Compass Investigation of factors affecting reverse-phase high performance liquid chromatography Investigation of factors affecting reverse-phase high performance liquid chromatography.

Sytwu, K., Vadai, M. & Dionne, J.A. 2019. Bimetallic nanostructures: combining plasmonic and catalytic metals for photocatalysis. *Advances in Physics: X*, 4(1): 1619480.

Tamang, H.K., Stringham, E.N. & Tourdot, B.E. 2023. Platelet Functional Testing Via High-Throughput Microtiter Plate-Based Assays. *Current Protocols*, 3(2): e668.

Tan, Y.N., Lee, J.Y. & Wang, D.I.C. 2010. Uncovering the Design Rules for Peptide Synthesis of Metal Nanoparticles. *Journal of the American Chemical Society*, 132(16): 5677–5686.

Tanaka, N. 2015. Basics of STEM. In T. Nobuo, ed. *Scanning transmission electron microscopy of nanomaterials: Basics of Imaging and Analysis*. London: Imperial College Press: 77–78.

Tang, Y., Liu, Y., He, G., Cao, Y., Bi, M., Song, M. & Yang, P. 2021. Comprehensive Analysis of Secondary Metabolites in the Extracts from Different Lily Bulbs and Their Antioxidant Ability. *Antioxidants*, 10(1634): 1–16.

Thakkar, K.N., Mhatre, S.S. & Parikh, R.Y. 2010. Biological synthesis of metallic nanoparticles. *Nanomedicine: Nanotechnology, Biology and Medicine*, 6(2): 257–262. http://www.sciencedirect.com/science/article/pii/S1549963409001154.

Thota, S. & Crans, D. 2018. *Metal Nanoparticles: Synthesis and Applications in Pharmaceutical Sciences*.

Tian, B. & Liu, J. 2020. Resveratrol: a review of plant sources, synthesis, stability, modification and food application. *Journal of the Science of Food and Agriculture*, 100(4): 1392–1404. https://doi.org/10.1002/jsfa.10152.

Tiwari, D.K., Behari, J. & Sen, P. 2008. Time and dose-dependent antimicrobial potential of Ag nanoparticles synthesized by top-down approach. *Current Science*, 95(5): 647–655.

Tobin, J. 2018. Rooibos fermentation-Characterising phenolic changes using chemometric analysis and kinetic modelling by. , (March): 141.

Tohamy, H.-A.S., El-Sakhawy, M. & Kamel, S. 2021. Carboxymethyl Cellulose-Grafted Graphene Oxide/Polyethylene Glycol for Efficient Ni(II) Adsorption. *Journal of Polymers and the Environment*, 29(3): 859–870.

Tomaszewska, E., Soliwoda, K., Kadziola, K., Tkacz-Szczesna, B., Celichowski, G., Cichomski, M.,

Szmaja, W. & Grobelny, J. 2013. Detection Limits of DLS and UV-Vis Spectroscopy in Characterization of Polydisperse Nanoparticles Colloids W. W. Yu, ed. *Journal of Nanomaterials*, 2013: 313081. https://doi.org/10.1155/2013/313081.

Turunc, E., Binzet, R., Gumus, I., Binzet, G. & Arslan, H. 2017. Green synthesis of silver and palladium nanoparticles using Lithodora hispidula (Sm .) Griseb . (Boraginaceae) and application to the electrocatalytic reduction of hydrogen peroxide. *Materials Chemistry and Physics*, 202: 310–319.

Tyagi, H., Kushwaha, A., Kumar, A. & Aslam, M. 2014. pH-dependent synthesis of stabilized gold nanoparticles using ascorbic acid. *International Journal of Nanoscience*, 10: 857–860.

Ullah, A., Munir, S., Badshah, S.L., Khan, N., Ghani, L., Poulson, B.G., Emwas, A.-H. & Jaremko, M. 2020. Important Flavonoids and Their Role as a Therapeutic Agent. *Molecules (Basel, Switzerland)*, 25(22).

Unruh, D.K. & Forbes, T.Z. 2019. X-ray diffraction techniques. *Analytical geomicrobiology: a handbook of instrumental techniques*: 215–237.

Vaghela, H., Shah, R. & Pathan, A. 2019. Palladium Nanoparticles Mediated Through Bauhinia variegata: Potent In vitro Anticancer Activity Against MCF-7 Cell Lines and Antimicrobial Assay. *Current Nanomaterials*, 3(3): 168–177.

Valentín-Pérez, Á., Rosa, P., Hillard, E.A. & Giorgi, M. 2022. Chirality determination in crystals. *Chirality*, 34(2): 163–181.

Vaou, N., Stavropoulou, E., Voidarou, C., Tsigalou, C. & Bezirtzoglou, E. 2021. Towards Advances in Medicinal Plant Antimicrobial Activity: A Review Study on Challenges and Future Perspectives. *Microorganisms*, 9(10).

Vasiljevic, Z.Z., Dojcinovic, M.P., Krstic, J.B., Ribic, V., Tadic, N.B., Ognjanovic, M., Auger, S., Vidic, J. & Nikolic, M.V. 2020. Synthesis and antibacterial activity of iron manganite (FeMnO3) particles against the environmental bacterium Bacillus subtilis. *RSC Advances*, 10(23): 13879–13888. http://dx.doi.org/10.1039/D0RA01809K.

Veisi, H., Tamoradi, T., Karmakar, B., Mohammadi, P. & Hemmati, S. 2019. In situ biogenic synthesis of Pd nanoparticles over reduced graphene oxide by using a plant extract (Thymbra spicata) and its catalytic evaluation towards cyanation of aryl halides. *Materials Science and Engineering C*, 104(June): 109919.

Velpula, S., Beedu, S.R. & Rupula, K. 2021. Bimetallic nanocomposite (Ag-Au, Ag-Pd, Au-Pd) synthesis using gum kondagogu a natural biopolymer and their catalytic potentials in the degradation of 4-

nitrophenol. *International Journal of Biological Macromolecules*, 190(August): 159–169. https://doi.org/10.1016/j.ijbiomac.2021.08.211.

Venkatesham, M., Ayodhya, D., Madhusudhan, A., Babu, N.V. & Veerabhadram, G. 2012. A novel green one-step synthesis of silver nanoparticles using chitosan: catalytic activity and antimicrobial studies. *Applied Nanoscience*, 4: 113–119.

Vilchis-nestor, A.R., Sánchez-mendieta, V., Camacho-lópez, Marco A, Gómez-espinosa, R.M., Camacho-lópez, Miguel A & Arenas-alatorre, J.A. 2008. Solventless synthesis and optical properties of Au and Ag nanoparticles using Camellia sinensis extract. *Materals Letters*, 62: 3103–3105.

Vilela, D., González, M.C. & Escarpa, A. 2012. Sensing colorimetric approaches based on gold and silver nanoparticles aggregation: Chemical creativity behind the assay. A review. *Analytica Chimica Acta*, 751: 24–43. https://www.sciencedirect.com/science/article/pii/S0003267012012731.

Villate, A., San Nicolas, M., Gallastegi, M., Aulas, P.-A., Olivares, M., Usobiaga, A., Etxebarria, N. & Aizpurua-Olaizola, O. 2021. Review: Metabolomics as a prediction tool for plants performance under environmental stress. *Plant science : an international journal of experimental plant biology*, 303: 110789.

Vogt, C., Wondergem, C.S. & Weckhuysen, B.M. 2023. Ultraviolet-Visible (UV-Vis) Spectroscopy BT - Springer Handbook of Advanced Catalyst Characterization. In I. E. Wachs & M. A. Bañares, eds. Cham: Springer International Publishing: 237–264. https://doi.org/10.1007/978-3-031-07125-6_11.

Vriendt, Y. De. 2020. *Development of a primary rabbit enterocyte cell culture for the in vitro cultivation of Rabbit Haemorrhagic Disease Virus and Rabbit Haemorrhagic Disease Virus 2*.

Vuolo, M.M., Lima, V.S. & Maróstica Junior, M.R. 2019. Chapter 2 - Phenolic Compounds: Structure, Classification, and Antioxidant Power. In M. R. S. B. T.-B. C. Campos, ed. Woodhead Publishing: 33–50. https://www.sciencedirect.com/science/article/pii/B9780128147740000025.

Wang, B.-J., Huang, S.-H., Kao, C.-L., Muller, C.J.F., Wang, Y.-P., Chang, K.-H., Wen, H.-C., Yeh, C.-C., Shih, L.-J., Kao, Y.-H., Huang, S.-P., Li, C.-Y. & Chuu, C.-P. 2022. Aspalathus linearis suppresses cell survival and proliferation of enzalutamide-resistant prostate cancer cells via inhibition of c-Myc and stability of androgen receptor. *PLOS ONE*, 17(7): e0270803.

Wang, K., Liu, Y., Jin, X. & Chen, Z. 2019. Characterization of iron nanoparticles/reduced graphene oxide composites synthesized by one step eucalyptus leaf extract. *Environmental Pollution*, 250: 8–13.

Wang, S.P., Wang, W.J., Tan, Z.L., Liu, G.W., Zhou, C.F. & Yin, M.J. 2019. Effect of traditional Chinese medicine compounds on rumen fermentation, methanogenesis and microbial flora in vitro. *Animal*

Nutrition, 5(2): 185–190.

Wang, Z. & Bai, X. 2020. One-pot synthesis of bio-supported Pd nanoparticles by using clove leaf and their catalytic performance for Suzuki coupling reaction. *Journal of Molecular Structure*, 1219: 128538.

Wang, Z., Song, Y., Zou, J., Li, L., Yu, Y. & Wu, L. 2018. The cooperation effect in the Au–Pd/LDH for promoting photocatalytic selective oxidation of benzyl alcohol. *Catalysis Science & Technology*, 8(1): 268–275. http://dx.doi.org/10.1039/C7CY02006F.

Wei, G., Zhou, H., Liu, Z. & Li, Z. 2005. A simple method for the preparation of ultrahigh sensitivity surface enhanced Raman scattering (SERS) active substrate. *Applied Surface Science*, 240(1): 260–267. https://www.sciencedirect.com/science/article/pii/S0169433204010700.

Wicaksono, W.P., Kadja, G.T.M., Amalia, D., Uyun, L., Rini, W.P., Hidayat, A., Fahmi, R.L., Nasriyanti, D., Leun, S.G.V., Ariyanta, H.A. & Ivandini, T.A. 2020. A green synthesis of gold–palladium core–shell nanoparticles using orange peel extract through two-step reduction method and its formaldehyde colorimetric sensing performance. *Nano-Structures and Nano-Objects*, 24: 1–9. https://doi.org/10.1016/j.nanoso.2020.100535.

Wilson, N.L.W. 2005. Cape Natural Tea Products and the U.S. Market: Rooibos Rebels Ready to Raid. *Applied Economic Perspectives and Policy*, 27(1): 139–148. https://doi.org/10.1111/j.1467-9353.2005.00213.x.

Wu, M.-L., Chen, D.-H. & Huang, T.-C. 2001. Synthesis of Au/Pd Bimetallic Nanoparticles in Reverse Micelles. *Langmuir*, 17(13): 3877–3883.

Xiao, Q., Sarina, S., Jaatinen, E., Jia, J., Arnold, D.P., Liu, H. & Zhu, H. 2014. Efficient photocatalytic Suzuki cross-coupling reactions on Au–Pd alloy nanoparticles under visible light irradiation. *Green Chemistry*, 16(9): 4272–4285. http://dx.doi.org/10.1039/C4GC00588K.

Xu, Y.-M., Tan, H.W., Zheng, W., Liang, Z.-L., Yu, F.-Y., Wu, D.-D., Yao, Y., Zhong, Q.-H., Yan, R. & Lau, A.T.Y. 2019. Cadmium telluride quantum dot-exposed human bronchial epithelial cells: a further study of the cellular response by proteomics. *Toxicology Research*, 8(6): 994–1001.

Xue, W., Zhang, G. & Zhang, D. 2011. A sensitive colorimetric label-free assay for trypsin and inhibitor screening with gold nanoparticles. *Analyst*, 136(15): 3136–3141. http://dx.doi.org/10.1039/C1AN15224F.

Yang, G., Chen, D., Lv, P., Kong, X., Sun, Y., Wang, Z., Yuan, Z., Liu, H. & Yang, J. 2016. Core-shell Au-Pd nanoparticles as cathode catalysts for microbial fuel cell applications. *Scientific Reports*, 6(July):

1–9.

Yang, P., Li, Z., Yang, Y., Li, R., Qin, L. & Zou, Y. 2022. Effects of Electron Microscope Parameters and Sample Thickness on High Angle Annular Dark Field Imaging. *Scanning*, 2022: 8503314.

Yang, X., Li, Q., Wang, H., Huang, J., Lin, L., Wang, W., Sun, D., Su, Y., Opiyo, J.B., Hong, L., Wang, Y., He, N. & Jia, L. 2010. Green synthesis of palladium nanoparticles using broth of Cinnamomum camphora leaf. *Journal of Nanoparticle Research*, 12(5): 1589–1598.

Yaqoob, A.A., Khan, R.M.R. & Saddique, A. 2019. Review article on applications and classification of gold nanoparticles. *Int. J. Res*, 6(7).

Yasothamani, V. & Vivek, R. 2020. Biosynthesis of Nanoparticles for Cancer Therapeutic Applications. In *Biological Synthesis of Nanoparticles and their Applications*. 105–115.

Yeshi, K., Crayn, D., Ritmejerytė, E. & Wangchuk, P. 2022. Plant Secondary Metabolites Produced in Response to Abiotic Stresses Has Potential Application in Pharmaceutical Product Development. *Molecules*, 27(1).

Ying, S., Guan, Z., Ofoegbu, P.C. & Clubb, P. 2022. Environmental Technology & Innovation Green synthesis of nanoparticles : Current developments and limitations. *Environmental Technology & Innovation*, 26: 102336.

Yu, J., Yin, Y. & Huang, W. 2023. Engineered interfaces for heterostructured intermetallic nanomaterials. *Nature Synthesis*, 2(8): 749–756. https://doi.org/10.1038/s44160-023-00289-4.

Yuan, C.-G., Huo, C., Yu, S. & Gui, B. 2017. Biosynthesis of gold nanoparticles using Capsicum annuum var. grossum pulp extract and its catalytic activity. *Physica E: Low-dimensional Systems and Nanostructures*, 85: 19–26.

Yun, K., Nam, H.-S. & Kim, S. 2020. Categorization of atomic mixing patterns in bimetallic nanoparticles by the energy competition. *Physical Chemistry Chemical Physics*, 22(15): 7787–7793.

Yusuf, A., Almotairy, A.R.Z., Henidi, H., Alshehri, O.Y. & Aldughaim, M.S. 2023. Nanoparticles as Drug Delivery Systems: A Review of the Implication of Nanoparticles’ Physicochemical Properties on Responses in Biological Systems. *Polymers*, 15(7).

Zamora-Justo, J.A., Abrica-González, P., Vázquez-Martínez, G.R., Muñoz-Diosdado, A., Balderas-López, J.A. & Ibáñez-Hernández, M. 2019. Polyethylene Glycol-Coated Gold Nanoparticles as DNA and Atorvastatin Delivery Systems and Cytotoxicity Evaluation A. R. Barron, ed. *Journal of Nanomaterials*, 2019: 5982047.

Zhan, F., Yin, J., Zhang, A., Zhou, J., Wang, M. & Jiao, T. 2020. Controllable morphology and highly efficient catalytic performances of Pd–Cu bimetallic nanomaterials prepared via seed-mediated co-reduction synthesis. *Applied Surface Science*, 527: 146719. https://www.sciencedirect.com/science/article/pii/S0169433220314768.

Zhan, G., Huang, J., Du, M., Abdul-rauf, I., Ma, Y. & Li, Q. 2011. Green synthesis of Au – Pd bimetallic nanoparticles : Single-step bioreduction method with plant extract. *Materials Letters*, 65(19–20): 2989–2991. http://dx.doi.org/10.1016/j.matlet.2011.06.079.

Zhang, H., He, H., Song, W. & Zheng, L. 2023. Pre-Harvest UVB Irradiation Enhances the Phenolic and Flavonoid Content, and Antioxidant Activity of Green- and Red-Leaf Lettuce Cultivars. *Horticulturae*, 9(6).

Zhang, P. & Zhang, W. 2018. Introduction of Bimetallic Nanostructures. In *Bimetallic Nanostructures: Shape-Controlled Synthesis for Catalysis, Plasmonics, and Sensing Applications*. John Wiley & Sons, Inc: 3–22.

Zhao, S., Gao, Y., Tan, J., Zhu, Y., Ying, X., Zhang, M., Yu, X. & You, B. 2019. Facile synthesis and antibacterial applications of cuprous oxide/bovine serum albumin hierarchical nanocomposite particles. *SN Applied Sciences*, 1(8): 917.

Zhao, Y., Zhang, Y., Zhang, J., Zhang, X. & Yang, G. 2020. Molecular Mechanism of Autophagy : Its Role in the Therapy of Alzheimer ' s Disease. *Current Neuropharmacology*: 720–739.

Zheng, J., Li, S., Ma, X., Chen, F., Wang, A., Chen, J. & Feng, J. 2014. Green synthesis of core e shell gold e palladium @ palladium nanocrystals dispersed on graphene with enhanced catalytic activity toward oxygen reduction and methanol oxidation in alkaline media. *Journal of Power Sources*, 262: 270–278.

Zhou, S., Zhao, M., Yang, T.-H. & Xia, Y. 2019. Decahedral nanocrystals of noble metals: Synthesis, characterization, and applications. *Materials Today*, 22: 108–131.

Zhu, Y., Wu, J., Chen, M., Liu, X., Xiong, Y., Wang, Y., Feng, T., Kang, S. & Wang, X. 2019. Recent advances in the biotoxicity of metal oxide nanoparticles: Impacts on plants, animals and microorganisms. *Chemosphere*, 237: 124403.

Zorkipli, N.N.M., Kaus, N.H.M. & Mohamad, A.A. 2016. Synthesis of NiO Nanoparticles through Sol-gel Method. *Procedia Chemistry*, 19: 626–631. https://www.sciencedirect.com/science/article/pii/S187661961600108X.

Zuñiga-Martínez, B.S., Domínguez-Avila, J.A., Robles-Sánchez, R.M., Ayala-Zavala, J.F., Villegas-

Ochoa, M.A. & González-Aguilar, G.A. 2022. Agro-Industrial Fruit Byproducts as Health-Promoting Ingredients Used to Supplement Baked Food Products. *Foods*, 11(20).

8. Appendices

Appendix 1: Hydrodynamic sizes, polydispersity index (PDI), and Zeta Potential (mV) of monometallic and bimetallic nanoparticles obtained through the DLS technique

Samples	Hydrodynamic Sizes (nm)	Polydispersity index (PDI)	Zeta Potential (mV)
GR-AuNPs	47.91	0.383	-24.3
GR-PdNPs	272.9	0.385	-19.6
GR-Au-PdNPs	80.03	0.362	-18.2
Asp-AuNPs	53.94	0.296	-27.1
Asp-Pd NPs	72.11	0.252	-24.0
Asp-Au-PdNPs	42.28	0.381	-21.7

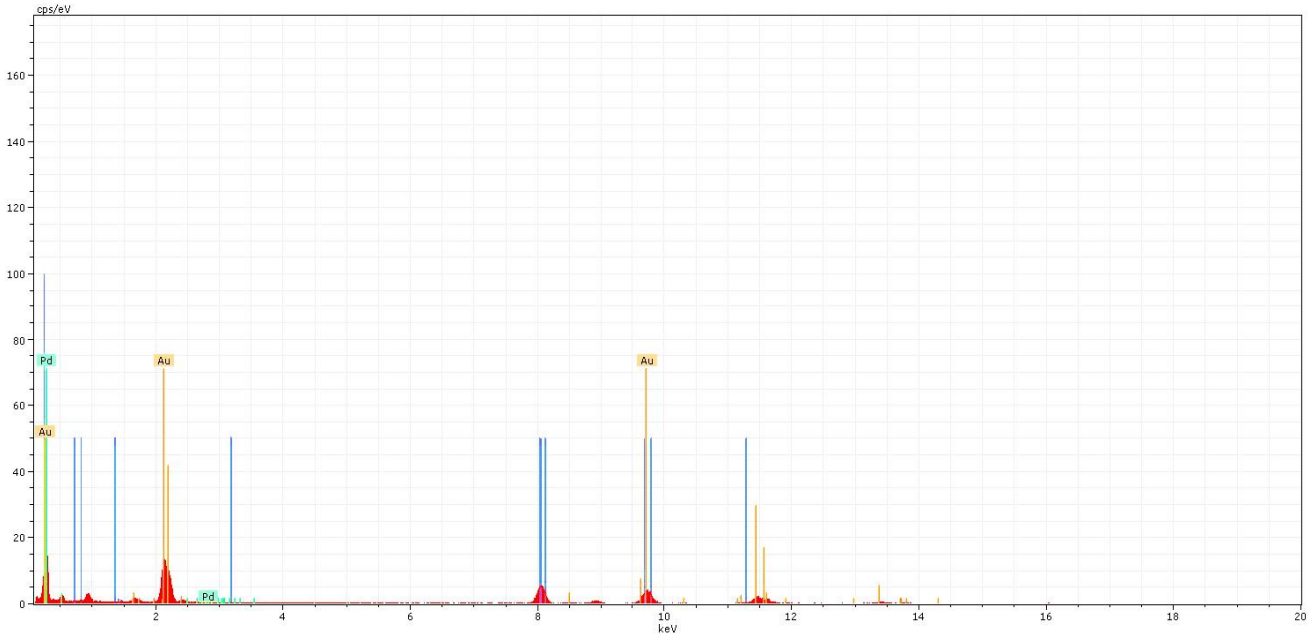

Appendix 2: Energy Dispersive X-ray (EDX) Spectroscopy analysis of Au-Pd bimetallic nanoparticles, synthesized employing GR plant extract, confirmed the presence of both Au and Pd metals

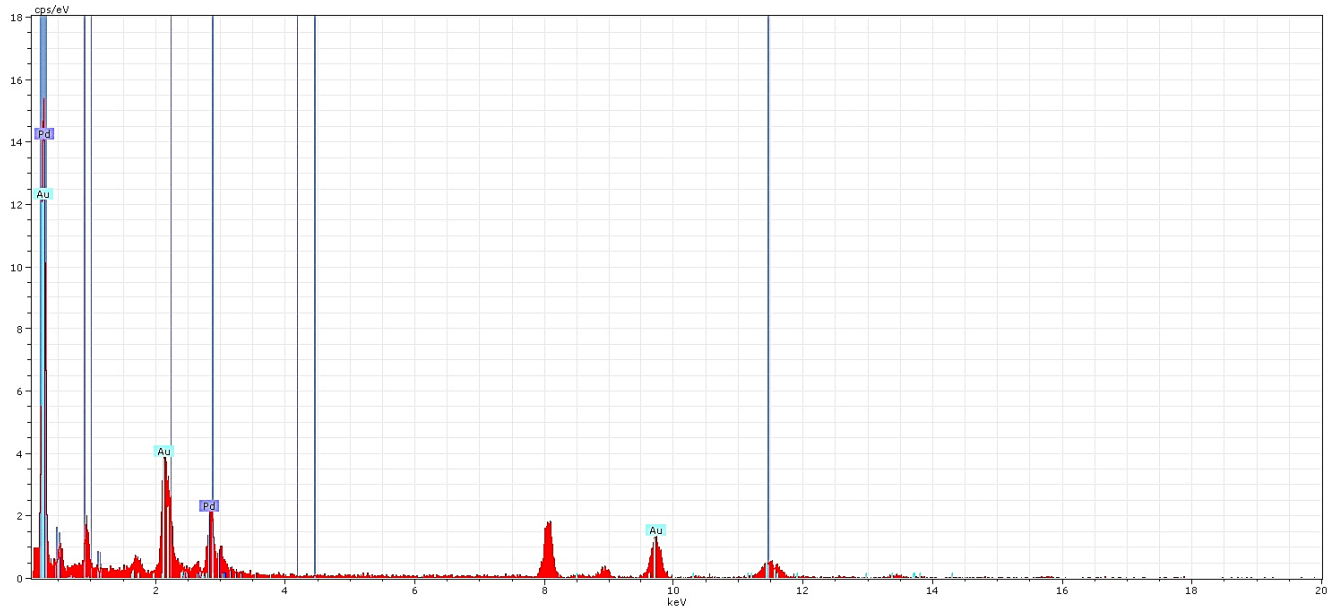

Appendix 3: EDX spectrum of Au-Pd bimetallic nanoparticles, synthesized from the ASP compound, clearly indicates the presence of both Au and Pd metals

8.1. Addendum: Conference(s)

8th International Conference on Nanoscience and Nanotechnology in Africa (NanoAfriaca 2022) "Green synthesis and characterization of Au-Pd bimetallic nanoparticles using *Aspalathus linearis"* Naledi D. Seatle, Enas Ismail, Akeem O. Akinfenwa, and Ahmed A. Hussein (Poster presentation).